New chemistry of 1,1′-bis(*o*-carborane)

Gobika Sivasubramaniam

Submitted for the degree of Doctor of Philosophy at Heriot-Watt University, on completion of research in the School of Engineering and Physical Sciences.

December 2011

I hereby declare that the work presented in this thesis was carried out by myself at Heriot-Watt University, Edinburgh, except where due acknowledgement is made, and has not been submitted for any other degree.

Gobika Sivasubramaniam (Candidate)

Prof. Alan. J. Welch

Date

ABSTRACT

Chapter 1 presents the most relevant literature in the fields of borane, carborane and metallacarborane chemistry, providing the reader with an overview of these topics. In the later part the focus changes to 1,1′-bis(*o*-carborane).

Chapter 2 describes the attempted two electron reduction/metallation and single cage decapitation/metallation chemistry of 1,1′-bis(*o*-carborane). Also described are the analysis of two dimensional ^{11}B-^{11}B correlation spectra of all the products and the calculation of weighted average ^{11}B chemical shifts of the individual cage components of these products which are discussed with respect to the parent compound.

Chapter 3 describes the double cage decapitation of 1,1′-bis(*o*-carborane) with excess KOH and metallation with {(arene)Ru} and {CpCo} fragments at room temperature. Metallation with {(arene)Ru} resulted in two products whereas metallation with {CpCo} yielded the same two structure types plus a third product. Also discussed are the room temperature isomerisations observed.

Chapter 4 reports the double cage decapitation of 1,1′-bis(*o*-carborane) and metallation with {(dmpe)Ni} fragments, and discusses diastereoisomers obtained for the first time. Also discussed are the methylation of 1,1′-bis(*o*-carborane) and the results obtained from decapitation followed by deprotonation and metallation of this.

Chapter 5 gives full details of the experimental procedures undertaken and also provides spectroscopic and analytical data for all new compounds reported herein.

Appendix 1 provides details of the crystal structure determinations of the compounds synthesised.

Appendix 2 (provided on compact disk) gives the appropriate crystallographic files in RTF and CIF format.

ACADEMIC REGISTRY
Research Thesis Submission

Name*:*	Gobika Sivasubramaniam		
School/PGI:	EPS		
Version: *(i.e. First, Resubmission, Final)*	First	Degree Sought (Award **and** Subject area)	PhD Chemistry

Declaration

In accordance with the appropriate regulations I hereby submit my thesis and I declare that:

1) the thesis embodies the results of my own work and has been composed by myself
2) where appropriate, I have made acknowledgement of the work of others and have made reference to work carried out in collaboration with other persons
3) the thesis is the correct version of the thesis for submission and is the same version as any electronic versions submitted*.
4) my thesis for the award referred to, deposited in the Heriot-Watt University Library, should be made available for loan or photocopying and be available via the Institutional Repository, subject to such conditions as the Librarian may require
5) I understand that as a student of the University I am required to abide by the Regulations of the University and to conform to its discipline.

* *Please note that it is the responsibility of the candidate to ensure that the correct version of the thesis is submitted.*

Signature of Candidate*:*		Date:	

Submission

Submitted By *(name in capitals):*	Gobika Sibasubramaniam
Signature of Individual Submitting:	
Date Submitted:	

For Completion in the Student Service Centre (SSC)

Received in the SSC by *(name in capitals):*			
Method of Submission *(Handed in to SSC; posted through internal/external mail):*			
*E-thesis Submitted (**mandatory for final theses)***			
Signature:		Date:	

Acknowledgements

I would like to take this opportunity to express my heartfelt thanks to Professor Alan J Welch for his excellent supervision, immaculate guidance and above all for his incredible patient throughout my research study in his group. This thesis would not have been possible without him.

I owe my deepest gratitude to Dr David Ellis who has made available his support in number of ways throughout this project. I have been lucky to work with someone so friendly.

I would also like to extend my sincere thanks to the ORSAS for funding.

It is my pleasure to thank all of the Boron Group members who made an excellent working environment and helped to make my time at Heriot-Watt an award winning experience. Special thanks go to Peter, Hugo, Brain, Ross, Amilia, Greg and Lisa who created a comfort zone for me in the Lab.

I am grateful to the following people who made this project meaningful. Dr Georgina Rosair for crystallography, Dr AlanBoyd for NMR Spectra, Christina Graham for elemental analysis, Dr David McKay for his computational contribution and University of Edinburgh for mass spectrometry.

I would also like to thank all my family members for their unconditional emotional support, especially my husband, son and mum. They have always been there for me and I am really grateful.

Table of Contents

Abbreviations

MeI	methyl iodide
THF	tetrahydrofuran
[O]	oxidation
Cp	cyclopentadienyl C_5H_5
C-C	carbon-carbon
C-B	carbon-boron
B-B	boron-boron
TLC	thin layer chromatography
NMR	nuclear magnetic resonance
p-cymene, cymene	1-methyl-4-isopropylbenzene $C_{10}H_{14}$
40-60 petroleum ether	fraction of petroleum ether boiling between 40 and 60°C
COSY	correlation spectroscopy
BTMA	benzyltrimethylammonium $[C_6H_5CH_2N(CH_3)_3]^+$
Me	methyl
hrs	hours
DCM	dichloromethane
n-BuLi	*n*-butyllithium $[C_4H_9]Li$
ppm	parts per million
Å	Angstrom 1×10^{-10} m
dmpe	dimethylphosphinoethane $(CH_3)_2PCH_2CH_2P(CH_3)_2$
ph	phenyl
MHz	megahertz
δ	chemical shift
m	multiplet
s	singlet
MS	mass spectroscopy
EI	electron ionisation
mg	milligrams
d	doublet
t	triplet
br. s	broad singlet
mL	millilitre

Abbreviations for specific compounds

1 1-(1′-1′,2′-*closo*-$C_2B_{10}H_{11}$)-3-(η-cymene)-3,1,2-*closo*-$RuC_2B_9H_{10}$

2 1-(1′-1′,2′-*closo*-$C_2B_{10}H_{11}$)-3-(η-benzene)-3,1,2-*closo*-$RuC_2B_9H_{10}$

3 1-(1′-1′,2′-*closo*-$C_2B_{10}H_{11}$)-3-(η-C_5H_5)-3,1,2-*closo*-$CoC_2B_9H_{10}$

4 [BTMA][7-(1′-1′,2′-*closo*-$C_2B_{10}H_{11}$)-7,8-*nido*-$C_2B_9H_{11}$]

5 [$HNMe_3$][7-(1′-1′,2′-*closo*-$C_2B_{10}H_{11}$)-7,8-*nido*-$C_2B_9H_{11}$]

6 8-(1′-1′,2′-*closo*-$C_2B_{10}H_{11}$)-2-(η-C_5H_5)-2,1,8-*closo*-$CoC_2B_9H_{10}$

7 [Cp_2Co][7-(1′-1′,2′-*closo*-$C_2B_{10}H_{11}$)-7,8-*nido*-$C_2B_9H_{11}$]

8 [BTMA]$_2$[7-(7′-7′,8′-*nido*-$C_2B_9H_{11}$)-7,8-*nido*-$C_2B_9H_{11}$]

9 [$HNMe_3$]$_2$[7-(7′-7′,8′-*nido*-$C_2B_9H_{11}$)-7,8-*nido*-$C_2B_9H_{11}$]

10 [(*S*)-$CH_3NC_5H_4$-$C_4H_7NCH_3$]$_2$[7-(7′-7′,8′-*nido*-$C_2B_9H_{11}$)-7,8-*nido*-$C_2B_9H_{11}$]

11 8-(8′-2′-(η-C_5H_5)-2′,1′,8′-*closo*-$CoC_2B_9H_{10}$)-2-(η-C_5H_5)-*closo*-2,1,8-$CoC_2B_9H_{10}$

12 1-(8′-2′-(η-C_5H_5)-2′,1′,8′-*closo*-$CoC_2B_9H_{10}$)-3-(η-C_5H_5)-*closo*-3,1,2-$CoC_2B_9H_{10}$ (form α)

13 1-(8′-2′-(η-C_5H_5)-2′,1′,8′-*closo*-$CoC_2B_9H_{10}$)-3-(η-C_5H_5)-*closo*-3,1,2-$CoC_2B_9H_{10}$ (form β)

14 1-(8′-2′-(η-$C_{10}H_{14}$)-2′,1′,8′-*closo*-$RuC_2B_9H_{10}$)-3-(η-$C_{10}H_{14}$)-*closo*-3,1,2-$RuC_2B_9H_{10}$ (form α)

15 1-(8′-2′-(η-$C_{10}H_{14}$)-2′,1′,8′-*closo*-$RuC_2B_9H_{10}$)-3-(η-$C_{10}H_{14}$)-*closo*-3,1,2-$RuC_2B_9H_{10}$ (form β)

16 1-3′-(dmpe)-(1′-3′,1′,2′-*closo*-$NiC_2B_9H_{10}$)-3-(dmpe)-3,1,2-*closo*-$NiC_2B_9H_{10}$ (*racemic*)

17 1-3′-(dmpe)-(1′-3′,1′,2′-*closo*-$NiC_2B_9H_{10}$)-3-(dmpe)-3,1,2-*closo*-$NiC_2B_9H_{10}$ (*meso*)

18 2,2′-$(CH_3)_2$-1,1′-bis-(*o*-carborane)

19 1-(1′-1′,2′-$C_2B_{10}H_{11}$-2′-CH_3)-2-(dmpe)-7-CH_3-2,1,7-$NiC_2B_9H_{10}$

CHAPTER 1

Introduction

1.1 Boron

Boron was discovered in 1808 by J. L. Thenard and J. L. Gay-Lussac in Paris, France, and Sir Humphry Davy in London, UK[1]. The name is derived from Arabic 'buraq'. It is the element next to carbon and in group 13 of the periodic table with the ground state valence electronic configuration $2s^2\ 2p^1$.

It shows borderline properties between metals and non metals. Pure boron is a dark powder and its compounds are important in many industries such as glass, detergent manufacture and agriculture. It is an essential mineral for plants.

Boron is the only light element with two abundant naturally occurring isotopes ^{10}B and ^{11}B with abundance 19.8% and 80.2% respectively. ^{10}B has an exceptionally high cross section for the capture of thermal neutrons which leads to the application of boron neutron capture therapy (BNCT) in the treatment of cancer. This process is based on the following nuclear reaction.

$$^{10}B + {}^{1}n \rightarrow {}^{4}He + {}^{7}Li + 2.79\ MeV$$

It is the only element other than carbon that exhibits an extensive series of molecular hydrides. There are many boron containing cluster compounds available in the literature, and it remains an expanding field.

1.2 Boron hydrides

The simplest compounds of boron are the boron hydrides, composed of boron and hydrogen, and these are also called boranes. In the periodic table boron forms the most molecular hydrides other than carbon. Boron hydrides are based on polyhedral clusters of boron atoms and these borane clusters are characterised by triangular faces, and such polyhedra are known as deltahedra.

In 1912[2] Alfred Stock first synthesised and characterised a series of boranes from B_2H_6 to $B_{10}H_{14}$ which fall into the two distinctive series of B_nH_{n+4} and B_nH_{n+6}. The simplest boron hydride is not BH_3 because it has two electrons fewer than required to satisfy the octet rule. This led to the concept of the electron deficient three-centre, two-electron bond developed by Longuet-Higgins[3] in 1949.

Therefore the simplest boron hydride is B_2H_6 and the stoichiometry is similar to C_2H_6. However B_2H_6 has insufficient electrons to form 2-center, 2-electron bonds between every adjacent pair of atoms therefore the boranes are said to be 'electron deficient' and this means that the bonding in B_2H_6 and C_2H_6 must be different.

The crystal structure of B_2H_6[4] (Fig 1.1) was confirmed few years later by Lipscomb by *X*-ray diffraction studies. The basket-like structure of the much larger boron hydride, decaborane, $B_{10}H_{14}$[5] (Fig 1.2) was characterised in the 1950s.

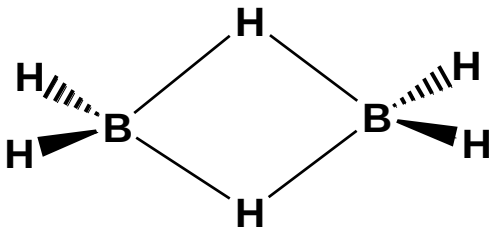

Fig 1.1 The structure of B_2H_6

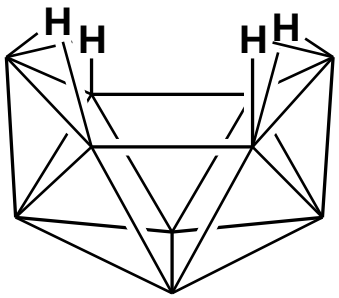

Fig 1.2 The structure of decaborane

Longuet-Higgins[6] used molecular orbital (MO) calculations to predict the geometry of the 12- vertex $[B_{12}H_{12}]^{2-}$ as icosahedral in 1954, (Fig 1.3) and in 1960 Hawthorne and Pitochelli[7] confirmed the closed polyhedral structure of this dianionic species by isolating it initially as the triethylammonium salt followed by the addition of potassium hydroxide in boiling water in order to isolate the product as the potassium salt.

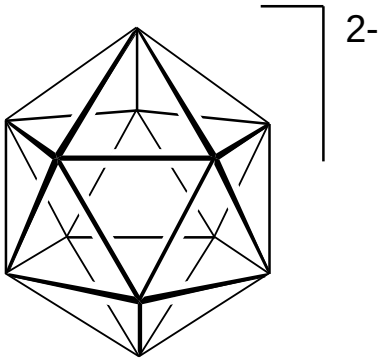

Fig 1. 3 Structure of $[B_{12}H_{12}]^{2-}$

1.3 Bonding theories

Various attempts were made to find a bonding scheme to predict borane structures. Lipscomb extended the 3-centre, 2-electron model proposed by Longuet-Higgins and developed styx[8] rules in order to develop a general method. He used a combination of *s* 3-center, 2-electron BHB, *t* 3-center, 2-electron BBB, *y* 2-centre, 2-electron BB and *x* endo 2-centre, 2-electron BH bonds to explain some borane structures.

This theory is acceptable for the smaller boranes but when trying to explain structures of larger boron hydrides it breaks down.

A superior approach to understanding the bonding in delocalised cluster molecules was provided by Wade and extended by Mingos. Wade's rules[9] which were developed in 1971 have advantages over the *styx* method because they are quicker and easier to apply, have a firm basis in molecular orbital theory and are also applicable to heteroboranes and other clusters such as heavy main group clusters or low valency transition metal clusters. These are electron counting rules and are used to predict structures based on polyhedra in which every face is triangular.

The total number of framework bonding electron pairs must be calculated in order to predict the structure. For a main group atom the number of skeletal framework electrons provided is calculated by the following equation:

$s = v + x - 2$ (1)

v = number of valence electrons from the vertex atom

x = number of electrons from exopolyhedral groups or atoms

s and x are not the same as *s* and *x* in *styx*.

The individual s values for each cluster vertex are then summed to give the number of electrons available for bonding within the cage structure; dividing this value by two gives the total number of electron pairs that contribute to the overall shape. This is called the number of Polyhedral Skeletal Electron Pairs (PSEPs). This number of PSEPs, in conjunction with the number of vertices (n) gives the overall shape of the clusters as follows:

Number of SEPs	Geometrical pattern	
(n+1)	closo	closed parent polyhedron
(n+2)	nido	open polyhedron – one vertex removed
(n+3)	arachno	open polyhedron – two adjacent vertices removed
(n+4)	hypho	open polyhedron – three adjacent vertices removed

The nido geometry is formed by the removal of highest connected vertex from the closo polyhedron and the arachno geometry is created by removal of the highest connected open face vertex from the nido structure or removal of two adjacent vertices from the closo structure.

The Wade-Williams-Rudolph structural matrix (Fig 1.4)[10] shows the geometrical relationships between the parent polyhedra and the fragments of closo, nido and arachno cage structures. This structural relationship exists due to the constant number of shape determining skeletal electrons.

Closo n-vertex polyhedra require (n+1) PSEPs to fill (n+1) skeletal BMOs
Nido n-vertex polyhedra require (n+2) PSEPs to fill (n+2) skeletal BMOs
Arachno n-vertex polyhedra require (n+3) PSEPs to fill (n+3) skeletal BMOs
Hypho n-vertex polyhedra require (n+4) PSEPs to fill (n+4) skeletal BMOs

From the above equation (1), each {BH} vertex contributes two electrons for the polyhedral bonding. Therefore the total number of electrons available for the skeletal bonding in $[B_{12}H_{12}]^{2-}$ can be obtained by the addition of electrons coming from 12{BH} units (2×12 = 24) and electrons from the dinegative charge. This gives twenty six electrons or thirteen pairs for a 12 vertex molecule. Therefore $[B_{12}H_{12}]^{2-}$ adopts a closo geometry.

For a transition metal vertex $s = v + x - 12$ (for 18e species) (2)

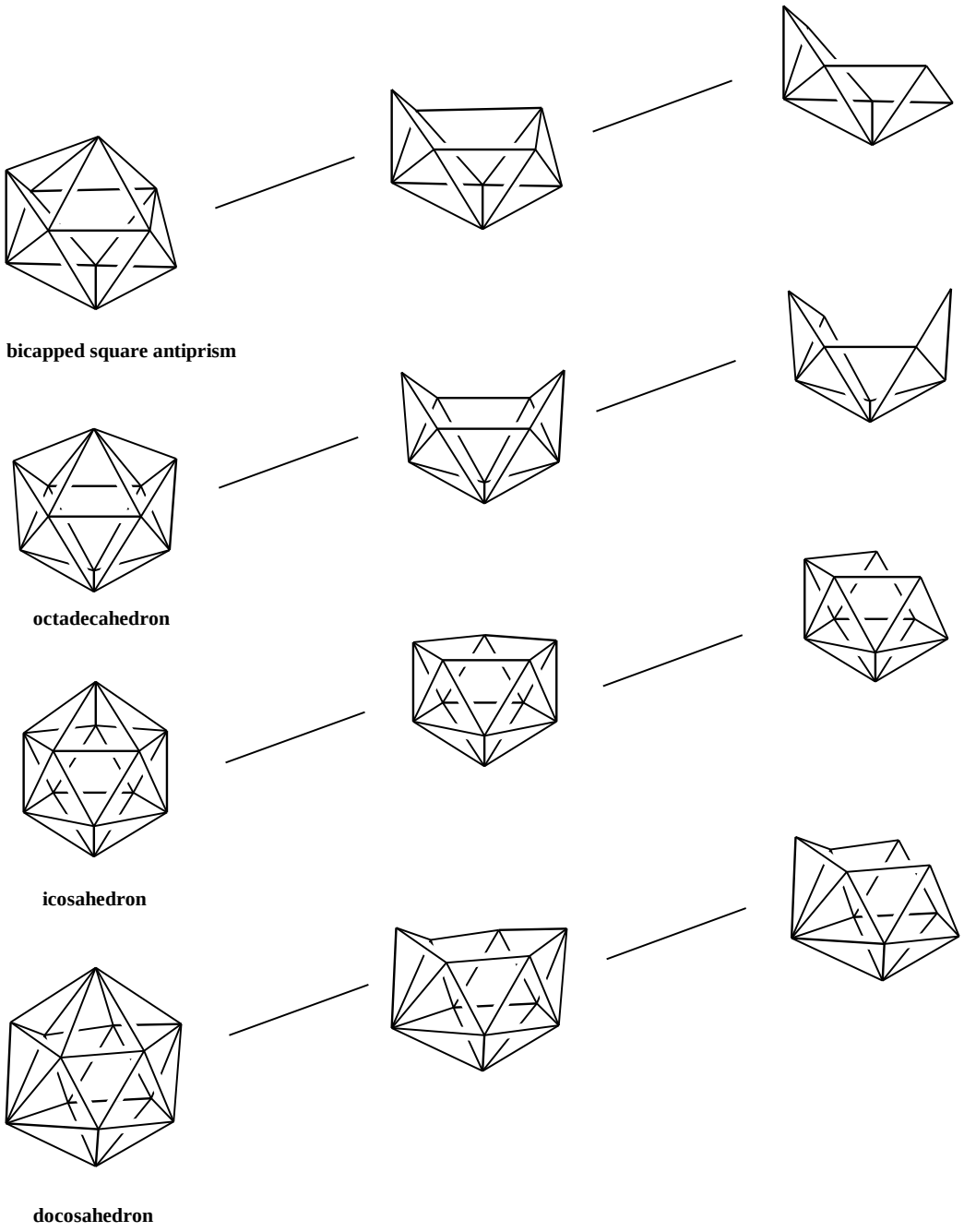

Fig 1.4 Part of the Wade-Williams-Rudolph Structural Matrix

1.4 Boron cages

Closo boron cage structures containing only boron and hydrogen atoms have the general formula $[B_nH_n]^{2-}$. At the present the known boranes have vertices between 5 and 12 and the most stable structure is $[B_{12}H_{12}]^{2-}$ in which the cage contains 12 vertices. It is very difficult to expand a 12-vertex boron cage because it contains a doubly negative charge. In order to expand we should make the cage neutral.

The structure of $[B_{12}H_{12}]^{2-}$ (Fig 1.3) is that of an icosahedron where all the boron atoms occupy a degree-5 vertex. In boranes with more than 12 vertices there are necessarily some degree-6 vertices but the {BH} fragment does not have sufficiently diffuse orbitals for this therefore it destabilizes the cage; the vertices that are differing from degree-5 are known as defective. In order to optimise the stability of structures containing more than 12 vertices the defective vertices must be minimised in number and must also be isolated from each other as much as possible[11].

At present clusters with ≥ 13 vertices are not known for boranes but they are known for carboranes (see 1.5). The reason for this is that carboranes are neutral due to the two carbon atoms and therefore easier to expand. For boranes the 12-vertex to 13-vertex synthetic barrier has presently not been overcome and so the icosahedral 12-vertex $[B_{12}H_{12}]^{2-}$ ion remains the largest known discrete borane cluster.

Calculations carried out by Schleyer in 1998[12] on cumulative BH addition energies revealed that 13-vertex, 14-vertex and 15-vertex boranes are thermodynamically unstable with respect to $[B_{12}H_{12}]^{2-}$ (Fig 1.5). The endothermic step from $[B_{12}H_{12}]^{2-}$ to $[B_{13}H_{13}]^{2-}$ is particularly unfavourable; this is because each boron atom is degree-5 in $[B_{12}H_{12}]^{2-}$ whereas in $[B_{13}H_{13}]^{2-}$, as noted above, some of the vertices are degree-6 vertices, which make the cage unstable.

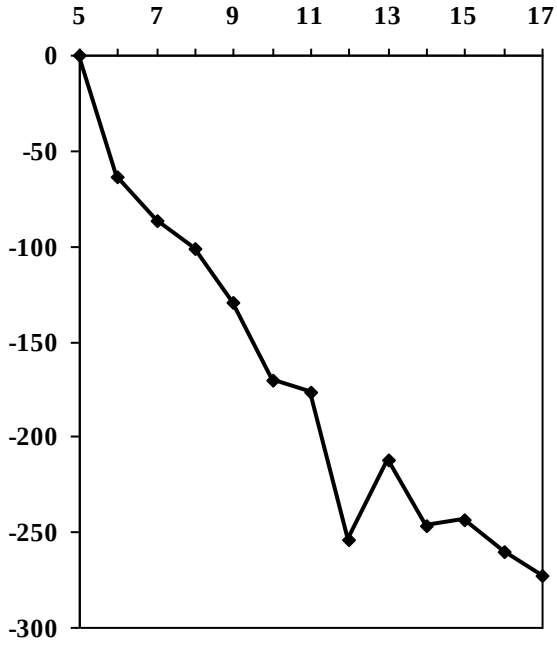

Fig 1.5 Plot of cumulative BH addition energy (kcal mol^{-1}) vs n for $[B_nH_n]^{2-}$

However formation of larger boranes such as $[B_{16}H_{16}]^{2-}$ and $[B_{17}H_{17}]^{2-}$ are exothermic processes because degree-6 vertices are avoided in these species, resulting in more stable boranes (Fig 1.6).

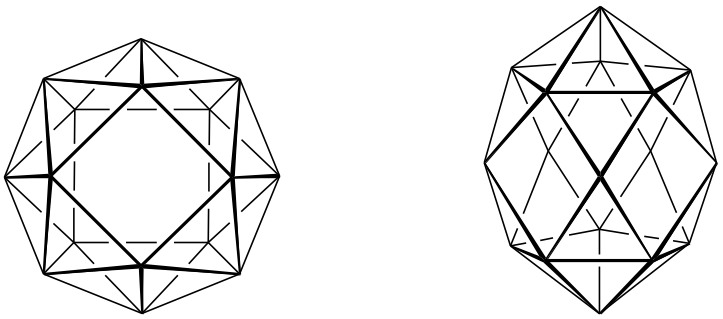

Fig 1.6 Predicted structures of $[B_{16}H_{16}]^{2-}$ and $[B_{17}H_{17}]^{2-}$

1.5 Carboranes

A polyhedral borane with one or more carbon atom(s) incorporated into the structural framework is called a carborane (Fig 1.7). Carboranes are composed of boron, carbon and hydrogen and when closo have the general formula $C_2B_{n-2}H_n$ (n = 5 to 14).

A borane can be converted into a carborane by replacing two $\{BH\}^-$ fragments with two {CH} fragments due to the fragments being both isoelectronic and isolobal. This means that both fragments possess similar frontier molecular orbital (FMO) properties including energy, symmetry, extents in space and electron occupation. Therefore replacing two $\{BH\}^-$ units with two {CH} units results in a neutral compound with the general formula $C_2B_{n-2}H_n$.

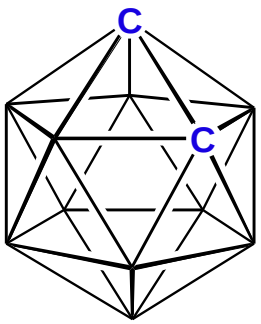

Fig 1.7 The structure of 1,2-*closo*-carborane

The charge distribution predicts sites of electrophilic and nucleophilic substitution. Nucleophilic attack occurs in a polyhedral carborane at boron closest to the carbon, while electrophilic attack is preferred at boron furthest away from carbon.

The first reported carborane was 1,2-*closo*-$C_2B_{10}H_{12}$. Like the 12-vertex borane this cage is based on an icosahedron in which two of the boron atoms have been replaced by two carbon atoms. The neutral icosahedral analogue of $[B_{12}H_{12}]^{2-}$ was prepared by Heying in 1963[13] by inserting acetylene into decaborane in the presence of a Lewis base which acts as a catalyst (Fig 1.8). The base allows formation of the arachno species from the nido decaborane, opening up the borane to allow easier insertion of the alkyne.

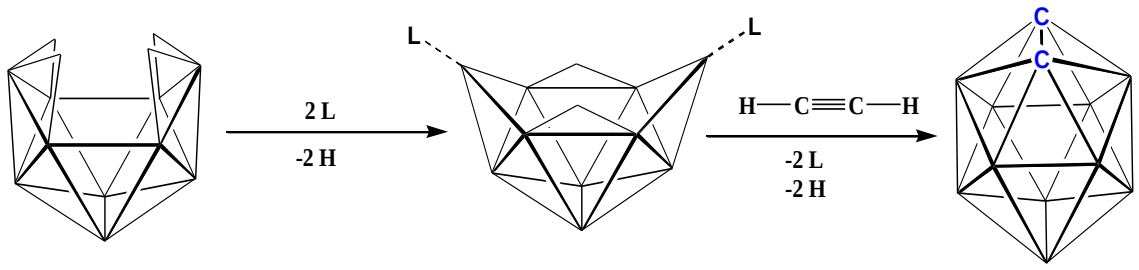

Fig 1.8 Carborane synthesis where L is a Lewis base

Three types of reaction are particularly important with the closo carboranes:

1. Removal of hydrogen and introduction of various functional groups at the cage carbon atoms and the boron atoms.
2. Deboronation by adding strong bases and metallation with suitable metal fragments.
3. Polyhedral expansion with Na/Li metal in the presence of naphthalene followed by recapitation with suitable metal fragments or boron fragments.

1.5.1 Deprotonation

In 1,2-*closo*-$C_2B_{10}H_{12}$, carbon atoms are more electronegative compared to the boron atoms and as a result the hydrogen atoms attached to the carbon atoms are comparatively acidic, therefore can be removed easily. The vast majority of the derivatized carboranes are prepared by lithiation of the carbon followed by reaction with organic halides.

Deprotonation of the carbon CH units using an alkyllithium reagent, followed by the addition of electrophiles such as alkyl halide or aryl halide can result in carbon substituted products. Depending on the stoichiometry either mono or di substituted carboranes can be prepared. For example the dilithiated carborane can undergo substitution reaction with carboxyl group[14] and silyl group[15] to yield the useful C-substituted carboranes 1,2-$(COOH)_2$-1,2-*closo*-$C_2B_{10}H_{10}$ and 1,2-$(Me_2SiCl)_2$-1,2-*closo*-$C_2B_{10}H_{10}$ (Fig 1.9) respectively.

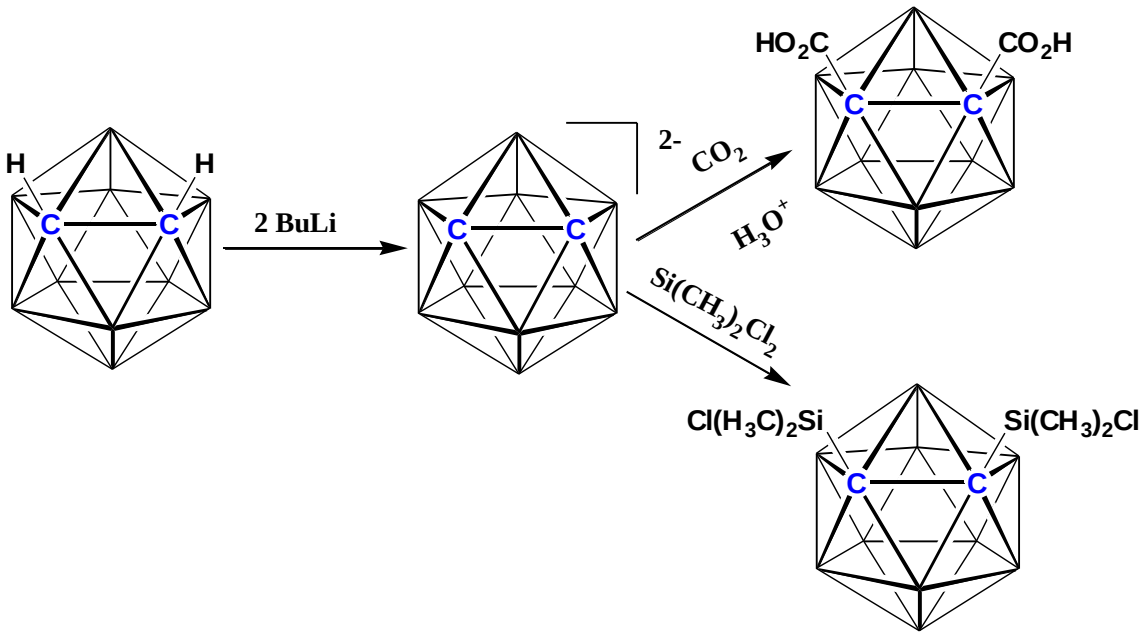

Fig 1.9 Substitution of H atoms on carbon cage atoms

The removal of hydrogen and methylation of the boron BH units in icosahedral carboranes is possible under Friedel-Crafts conditions[16]. In the presence of excess MeI and $AlCl_3$ *ortho*-carborane was methylated at every B atom except B3 and B6, giving an octa-methyl derivative (Fig 1.10) in high yield. These reaction conditions can be applicable to the meta and para carboranes as well[16].

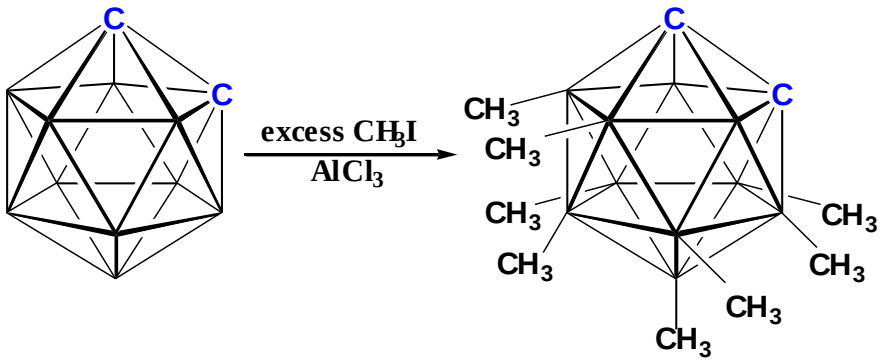

Fig 1.10 Substitution of H atoms on boron atoms

1.5.2 Decapitation and recapitation

The presence of relatively electronegative carbon atoms in 1,2-*closo*-$C_2B_{10}H_{12}$ induces a slight positive charge on the boron atoms adjacent to both carbon atoms within the cluster which makes them open to nucleophilic attack. The addition of strong base such as KOH/EtOH affords decapitation at the B3/B6 position (Fig 1.11) since these are the most electron deficient boron atoms in the carborane cage.

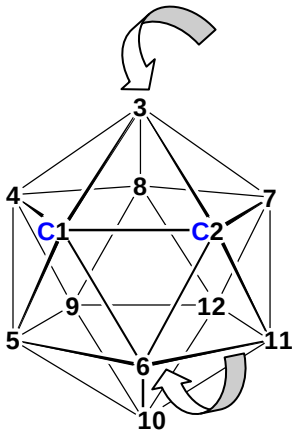

Fig 1.11 Decapitation at B3/B6 position

The degradation of the icosahedral *ortho*-carborane, 1,2-*closo*-$C_2B_{10}H_{12}$, by KOH in MeOH was first reported by Hawthorne and co-workers in 1964[17]. The decapitation produced, on work up, a 11-vertex nido carborane anion, [7,8-*nido*-$C_2B_9H_{12}$]$^-$ which contains an endo proton associated with the open face of the nido cage.

The endo proton is relatively acidic compare to the other protons so we can easily remove it by adding butyllithium to produce the dicarbollide anion $[C_2B_9H_{11}]^{2-}$, which is a very important starting material for the synthesis of a wide range of 12-vertex metallacarboranes. More generally, it can be reacted with {B-R} or {M-L} fragments in order to recapitate the icosahedral geometry (Fig 1.12)[18].

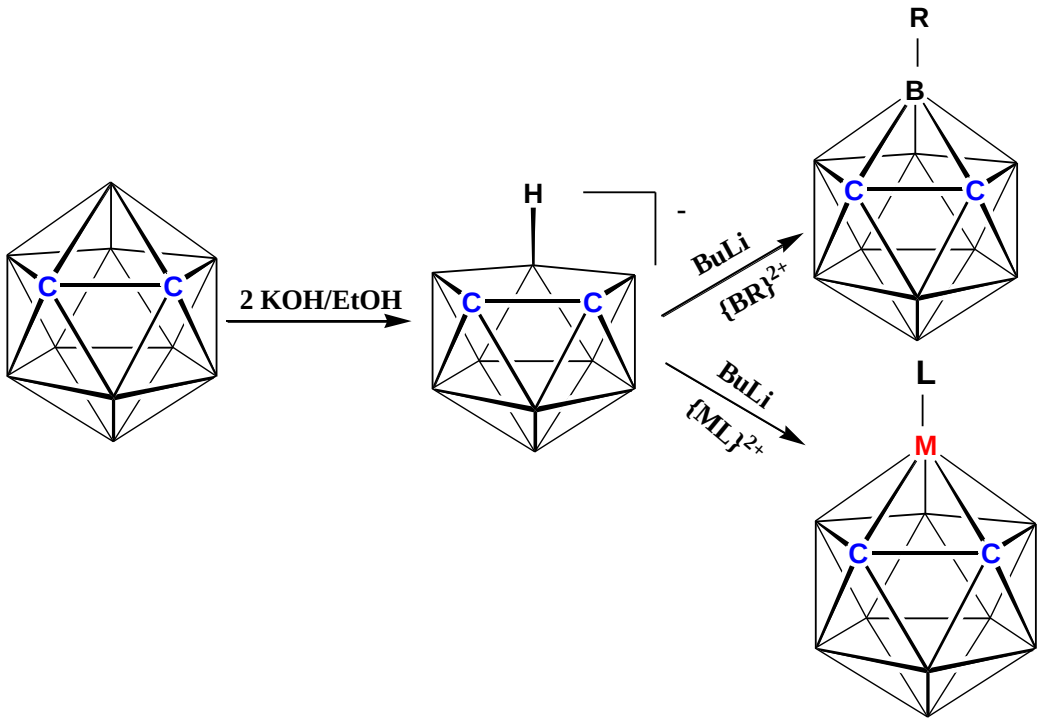

Fig 1.12 Decapitation followed by recapitation

The decapitation reaction of *meta*-carborane, 1,7-*closo*-$C_2B_{10}H_{12}$, takes place similarly to *ortho*-carborane. Upon the addition of strong base in ethanol to *meta*-carborane it is degraded to the *nido*-dianion [7,9-*nido*-$C_2B_9H_{11}]^{2-}$. However, the decapitation of *para*-carborane is ineffective in this way because no boron is adjacent to both carbons.

In 1982 Hawthorne and co-workers reported a way to deboronate *para*-carboarane in high yield. The decapitation by refluxing KOH/18-crown-6 in benzene resulted in a *nido*-dianion, [2,9-*nido*-$C_2B_9H_{11}]^{2-}$, whose structure is that of an icosahedron with one vertex removed[19]. This is the only so far known thermally stable anion which has only one of the two carbons in the open face.

However, the deboronation with alcoholic KOH pathway is not suitable for carborane derivatives which contain functional groups susceptible to the attack of a strong base or nucleophile[20].

The conditions needed to form the nido carborane from closo carborane depend upon the nature of substitutions. For example, closo carborane having basic or strongly electron withdrawing substituents such as nitro derivatives, esters and halo derivatives on one of the carbon atoms can be readily converted to nido carborane even in the presence of water at room temperature[21].

1.5.3 Cage expansion

Cage expansion is used to produce supraicosahedral metallacarboranes and supraicosahedral carboranes which have one vertex more than the parent carborane. The polyhedral expansion is generally performed as a reduction followed by either metallation or capitation. The reduction chemistry of closo carborane is now well established and reported by several workers[22,23].

The reduction process is usually carried out by using Na or Li in degassed THF and it transforms the closo structure into an open nido structure. If the cage carbon atoms are initially adjacent to each other then they are separate following the reduction step. The metallation process is carried out by the addition of transition metal fragments which are isolobal to the {BH} fragment and the recapitation is carried out by the addition of a {BR} fragment.

The reduction of 1,2-*closo*-$C_2B_{10}H_{12}$ produced [7,9-*nido*-$C_2B_{10}H_{12}$]$^{2-}$ which on oxidation yields the starting material, 1,2-*closo*-$C_2B_{10}H_{12}$, and similarly the reduction of 1,7-*closo*-$C_2B_{10}H_{12}$ produced [7,9-*nido*-$C_2B_{10}H_{12}$]$^{2-}$ which on oxidation converts to 1,2-*closo*-$C_2B_{10}H_{12}$[24,25]. The oxidation of the [7,10-*nido*-$C_2B_{10}H_{12}$]$^{2-}$ ion produced from 1,12-*closo*-$C_2B_{10}H_{12}$ yields 1,7-*closo*-$C_2B_{10}H_{12}$[25] (Fig 1.13).

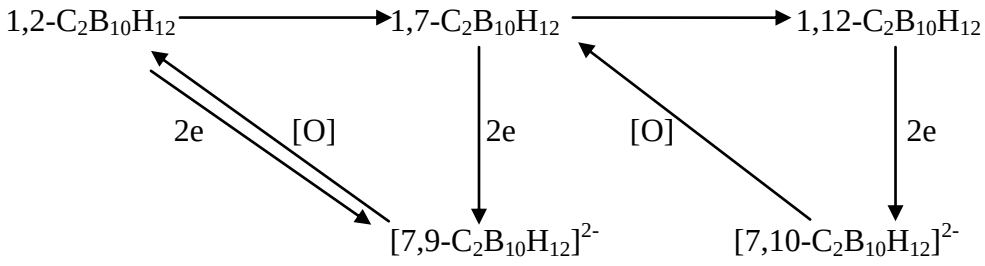

Fig 1.13 Reduction and oxidation of carboranes

Cage expansion is generally easier with a metal atom because the formation of a 13-vertex cage produces a degree six vertex which is unfavoured for boron atoms as their frontier orbitals are not diffuse enough to sit easily on a six atom open face. On the other hand transition metals have more diffuse orbitals that are more compatible therefore a metal is more likely to stabilize the degree six vertices (Fig 1.14).

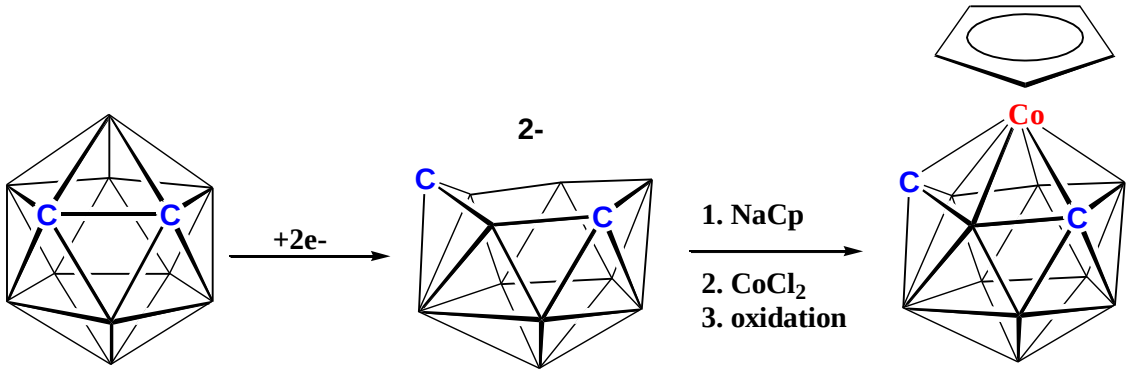

Fig 1.14 Process of reduction followed by metallation with {CoCp}

1.6 Nomenclature

The nomenclature and numbering schemes for boranes and heteroboranes are peculiar to them[26]. For the icosahedral *closo*-boranes and similar structures the numbering starts at an atom located on the highest order axis of symmetry and the first ring of belt atoms is numbered clockwise. When moving from one belt to the other belt, a boron-boron connectivity is crossed.

Icosahedral *closo*-heteroboranes are labelled in the same way, however the heteroatoms are given the lowest possible numbers and priority is given first to carbon atom then the metal vertex has the next lowest number. For a nido or other open cage structure, the boron vertex opposite to the open face takes the lowest number and the other vertices are labelled in the same manner as closo compounds (Fig 1.15).

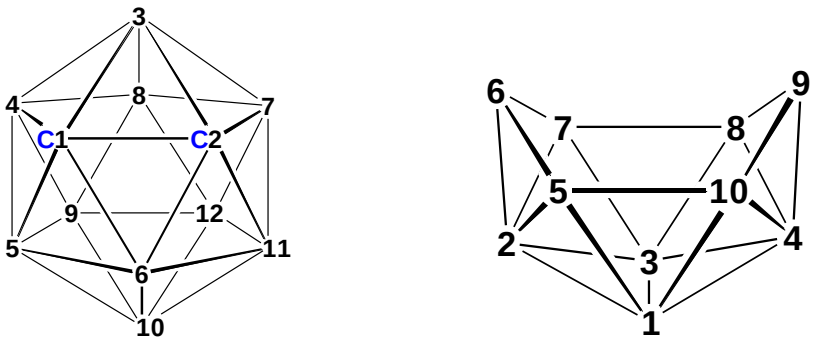

Fig 1.15 Numbering of closo and nido cages

For the neutral molecules, a Greek prefix shows the number of boron atoms and the suffix '-ane' is followed by the number of hydrogen atoms shown in brackets e.g. B_5H_9 is called pentaborane(9). If the molecule is an anion the number of hydrogen atoms is given first, followed by the number of boron atoms and the suffix '-ate' is used to show that it is anionic with the charge given in brackets at the end e.g. $[B_3H_8]^-$ is called octahydrotriborate(-1).

1.7 Polyhedral rearrangement

Three isomers are possible for icosahedral carboranes depending on the positions of the two CH vertices, specifically 1,2- (ortho) , 1,7- (meta) and 1,12- (para). A characteristic feature of the closo carboranes is their thermal isomerisation involving intramolecular rearrangement of the cage skeleton. Thermodynamic stability of these isomers increases with the increasing distance between the two negatively charged carbon atoms.

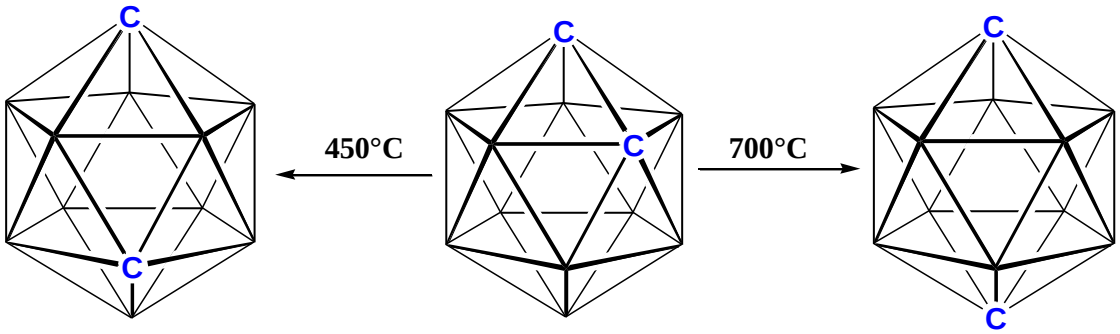

1,7-*closo*-$C_2B_{10}H_{12}$ 1,2-*closo*-$C_2B_{10}H_{12}$ 1,12-*closo*-$C_2B_{10}H_{12}$

Fig 1.16 Thermal isomerisation of carborane

Fig 1.16 shows that icosahedral 1,2-*closo*-$C_2B_{10}H_{12}$ undergoes thermal rearrangement at 450^oC to give 1,7-*closo*-$C_2B_{10}H_{12}$ and similarly at 700^oC to give 1,12-*closo*-$C_2B_{10}H_{12}$[27]. The precise mechanism of isomerisation of carborane has not been established due to the high temperatures required for the conversion to occur preventing the isolation of intermediates.

There are several mechanisms proposed for the isomerisation of icosahedral *closo* carboranes. The first is Lipscomb's 'diamond-square-diamond' mechanism[28] (Fig 1.17) in which a common edge between two adjacent triangular faces is broken and then replaced by a new bond between the two other vertices, which is perpendicular to the lost bond. The first and the last structures have edge-fused triangles, while the middle structure has a square face.

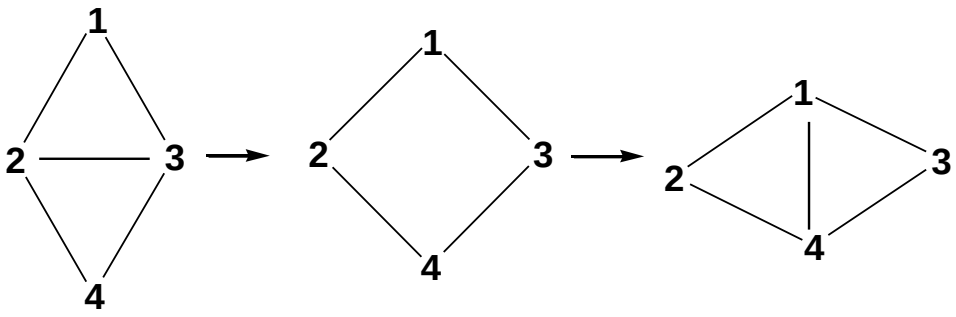

Fig 1.17 A single Diamond-Square Diamond process

In 1966 Lipscomb attempted to rationalise the isomerisation process when he proposed a hextuple DSD process via a cuboctahedral intermediate (Fig 1.18) which plays a key role in the rearrangements of deltahedral clusters. This mechanism can explains the transformation of 1,2-*closo*-$C_2B_{10}H_{12}$ to the 1,7-*closo*-$C_2B_{10}H_{12}$ isomer but it failed to explain the conversion to the 1,12-*closo*-$C_2B_{10}H_{12}$ isomer starting from either the 1,2-*closo*-$C_2B_{10}H_{12}$ or the 1,7-*closo*-$C_2B_{10}H_{12}$ isomers, and as a result this theory was modified to allow triangular face rotation (TFR) in the intermediate[29].

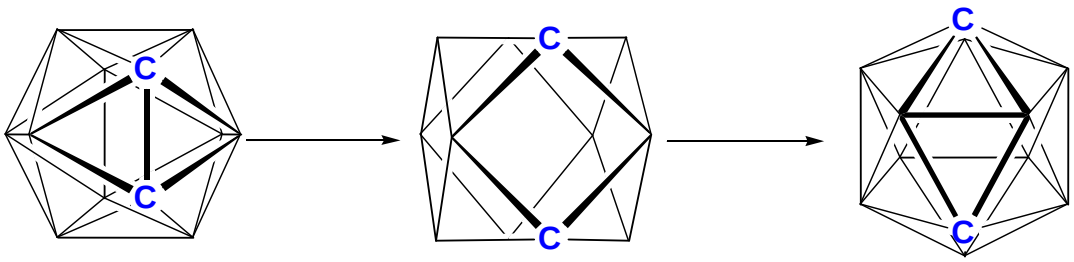

1,2-*closo*-$C_2B_{10}H_{12}$ cuboctahedral intermediate 1,12-*closo*-$C_2B_{10}H_{12}$

Fig 1.18 Hextuple-concerted DSD process via cuboctahedral intermediate

The triangular face rotation is a simple isomerisation mechanism involving the 120^o rotation of a single three atom face on the surface of the polyhedron. This isomerisation technique can easily explain the conversion of 1,2-*closo*-$C_2B_{10}H_{12}$ to the 1,7-isomer followed by conversion to the 1,12-isomer (Fig 1.19).

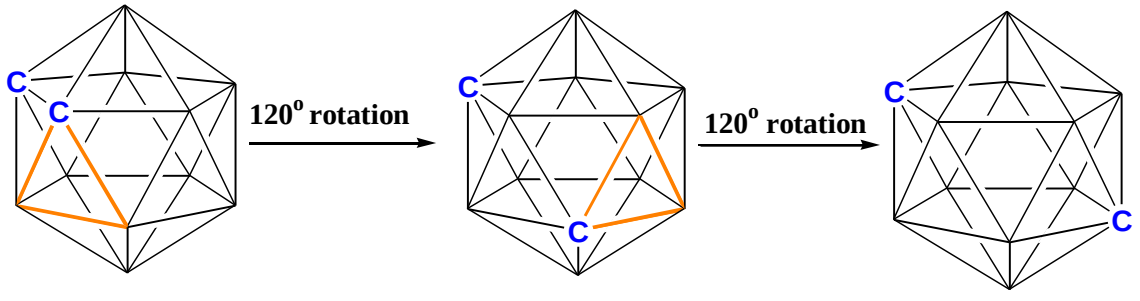

1,2-*closo*-$C_2B_{10}H_{12}$ 1,7-*closo*-$C_2B_{10}H_{12}$ 1,12-*closo*-$C_2B_{10}H_{12}$

Fig 1.19 Isomerisation by Triangular Face Rotation

Through the pentagonal face rotation mechanism proposed by Dvorak[30] could be explained the isomerisation of 1,2-*closo*-$C_2B_{10}H_{12}$ to 1,7-*closo*-$C_2B_{10}H_{12}$ and 1,12-*closo*-$C_2B_{10}H_{12}$ (Fig 1.20). In this mechanism a whole belt of atoms rotates relative to the other. However, this leads to breakage of too many connectivites, consequently large energy barriers would need to be overcome and due to this reason the mechanism is considered unlikely[31].

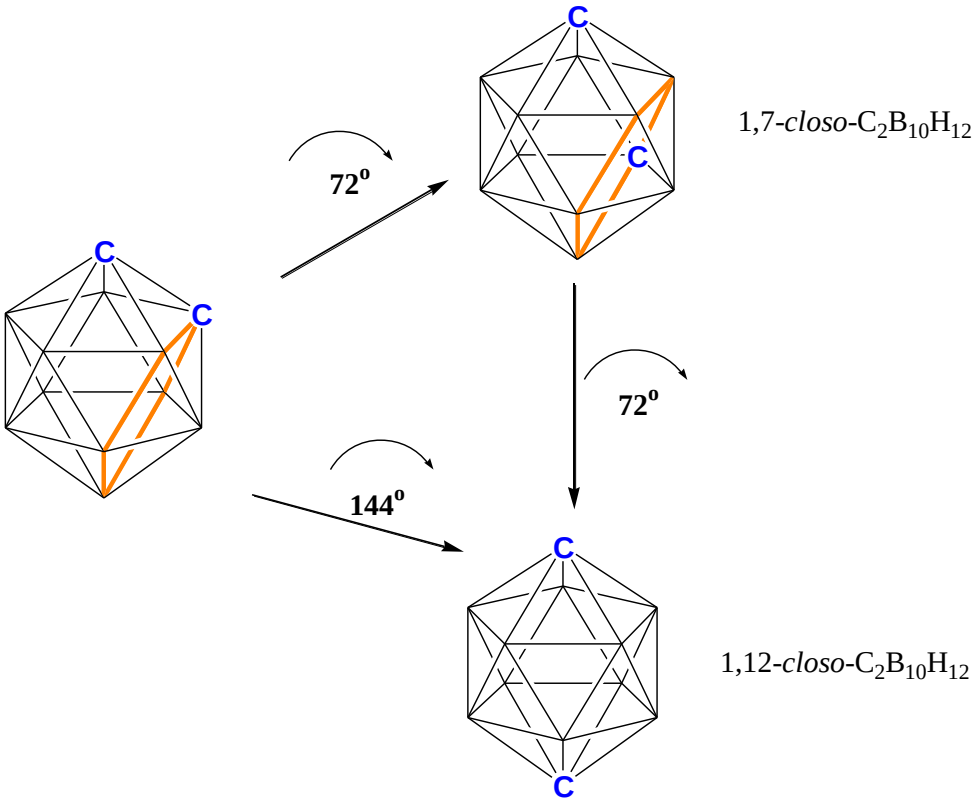

Fig 1.20 Isomerisation by Pentagonal Face Rotation

1.8 Icosahedral metallacarboranes

In 1965, Hawthorne reported the first metallacarboranes in which one[32] or both[33] of the $[C_5H_5]^-$ rings of ferrocene were replaced by $[C_2B_9H_{11}]^{2-}$. The work done by Hawthorne recognised the relationship between the cyclopentadienide anion, $[C_5H_5]^-$, and the five atom open face of the dicarbollide dianion, $[C_2B_9H_{11}]^{2-}$ (Fig 1.21). This led to the analogues of metallocene sandwich compounds.

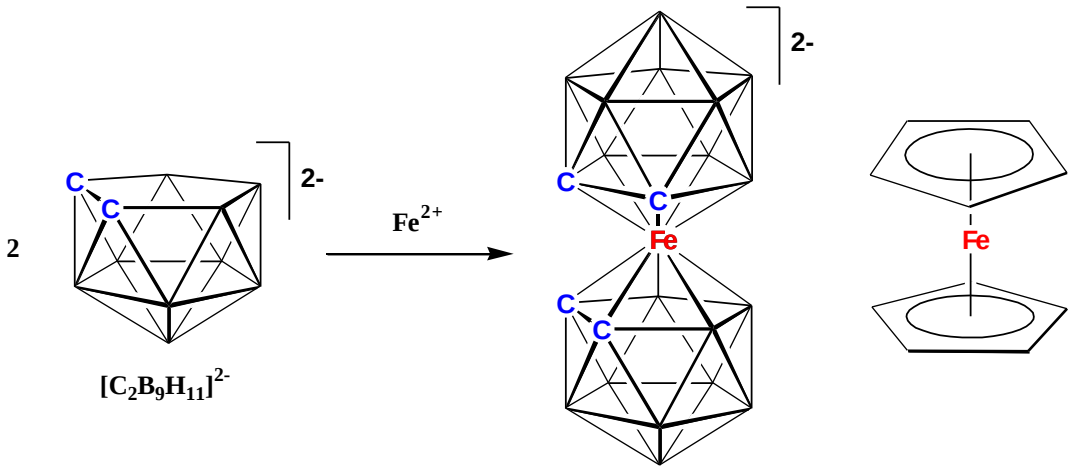

Fig 1.21 Synthesis of bis(dicarbollide) iron and analogous ferrocene

The *closo*-$[Fe(C_2B_9H_{11})_2]^{2-}$ and other transition metal dicarbollide complexes in general are found to be more stable than the corresponding metallocene analogues. This is due to the fact that the frontier molecular orbitals are more favourably orientated to bind to a metal as they point inwards, due to the inclination of exo hydrogen atoms (Fig 1.22). Therefore the orbital overlap is greater compared to cyclopentadienide, in which the orbitals lie parallel to each other.

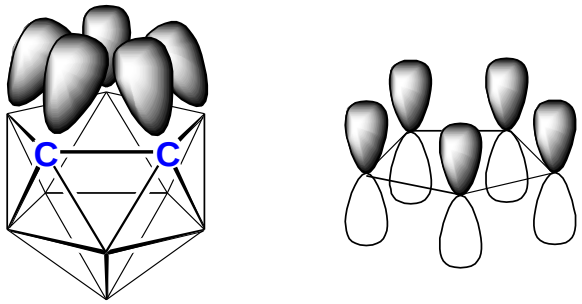

Fig 1.22 Orientation of frontier orbitals on open face of dicarbollide and Cp anions

The dicarbollide anion has been used to form metallacarboranes with a wide range of transition metals. There are now many hundreds of metallacarboranes synthesised since they were first reported by Hawthorne and co-workers[32, 33, 34].

The most commonly studied metallacarboranes are those with an icosahedral $MC_2B_9H_{11}$ cage, which can form nine isomers (Fig 1.23) and most of these isomers are very difficult to make. These nine isomers can be divided into three main groups, ortho, meta and para according to the relative positions of the carbon atoms.

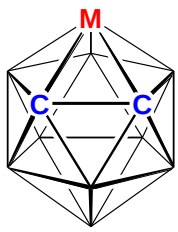

3,1,2-*closo*-$MC_2B_9H_{11}$

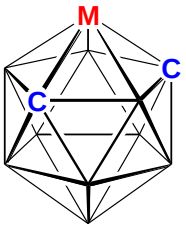

2,1,7-*closo*-$MC_2B_9H_{11}$

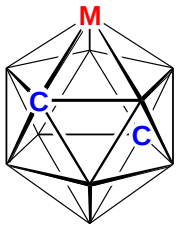

2,1,12-*closo*-$MC_2B_9H_{11}$

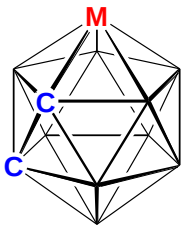

4,1,2-*closo*-$MC_2B_9H_{11}$

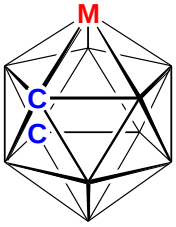

2,1,8-*closo*-$MC_2B_9H_{11}$

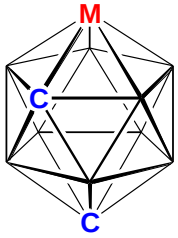

2,1,9-*closo*-$MC_2B_9H_{11}$

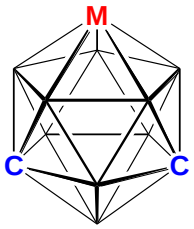

9,1,7-*closo*-$MC_2B_9H_{11}$

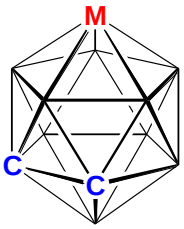

8,1,2-*closo*-$MC_2B_9H_{11}$

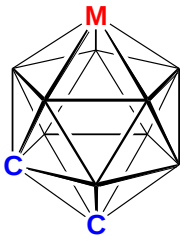

9,1,2-*closo*-$MC_2B_9H_{11}$

Fig 1.23 The nine isomeric structures of icosahedral metallacarboranes

From these 3,1,2-*closo*-$MC_2B_9H_{11}$, 4,1,2-*closo*-$MC_2B_9H_{11}$, 8,1,2-*closo*-$MC_2B_9H_{11}$ and 9,1,2-*closo*-$MC_2B_9H_{11}$ isomers are categorised as ortho and 2,1,7-*closo*-$MC_2B_9H_{11}$, 2,1,8-*closo*-$MC_2B_9H_{11}$, 2,1,9-*closo*-$MC_2B_9H_{11}$ and 9,1,7-*closo*-$MC_2B_9H_{11}$ are categorised as meta. Only one type of para metallacarborane is available, which is 2,1,12-*closo*-$MC_2B_9H_{11}$.

The 3,1,2-*closo*-$MC_2B_9H_{11}$ 2,1,7-*closo*-$MC_2B_9H_{11}$ and 2,1,12-*closo*-$MC_2B_9H_{11}$ isomers can be formed by the removal of one of the boron vertices from the *ortho*-$C_2B_{10}H_{12}$, *meta*-$C_2B_{10}H_{12}$ and *para*-$C_2B_{10}H_{12}$ isomers of carborane respectively with a nucleophile, followed by the addition of a suitable metal fragment. The other isomers shown in Fig 23 are formed by the isomerisation of the first three isomers; from these only the 4,1,2-*closo*-$MC_2B_9H_{11}$, 2,1,8-*closo*-$MC_2B_9H_{11}$, 9,1,7-*closo*-$MC_2B_9H_{11}$ and 2,1,9-*closo*-$MC_2B_9H_{11}$ isomers have been synthesised and characterised[35].

In 1993 the Welch group demonstrated that severely overcrowded transition metal metallacarboranes can undergo 1,2→1,7 isomerisation at low temperature[36] and in 1997 reported the unexpected isolation of an intermediate in an icosahedral-to-icosahedral rearangement[37] (Fig 1.24). Low temperature isomerisation opens up the possibility of experimental study of the mechanism.

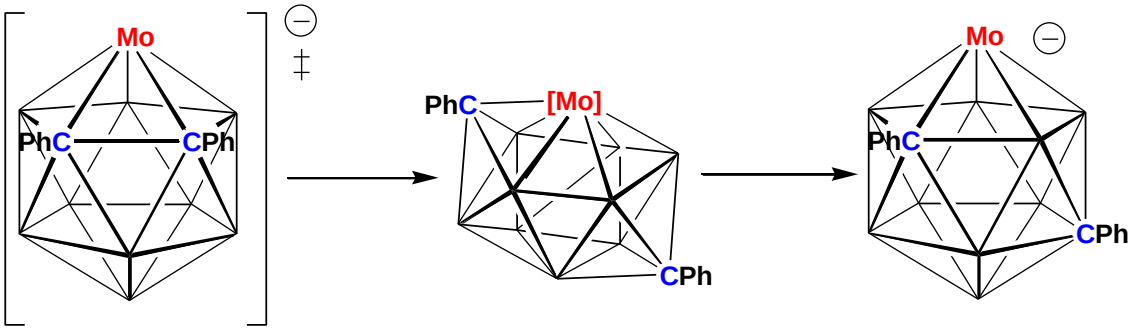

Fig 1.24 Isomerisation through a nonicosahedral intermediate

1.9 Supraicosahedral metallacarboranes

In 1971 Hawthorne reported the first supraicosahedral metallacarborane, 4-Cp-4,1,6-*closo*-$CoC_2B_{10}H_{12}$, which was prepared using the polyhedral expansion method[38]. As already noted, in general polyhedral expansion involves the opening of a closed cluster via chemical reduction followed by treatment with a suitable metal fragment to form a new closed cluster with one vertex more than the parent *closo*-carborane.

The majority of these structures exhibit docosahedral geometry, the most common isomer being the 4-L-4,1,6-*closo*-$MC_2B_{10}H_{12}$. The cage is fluxional in solution exchanging enantiomers (Fig 1.25) and the lowest energy process has been proved computationally to be a double diamond-square-diamond mechanism [23, 38].

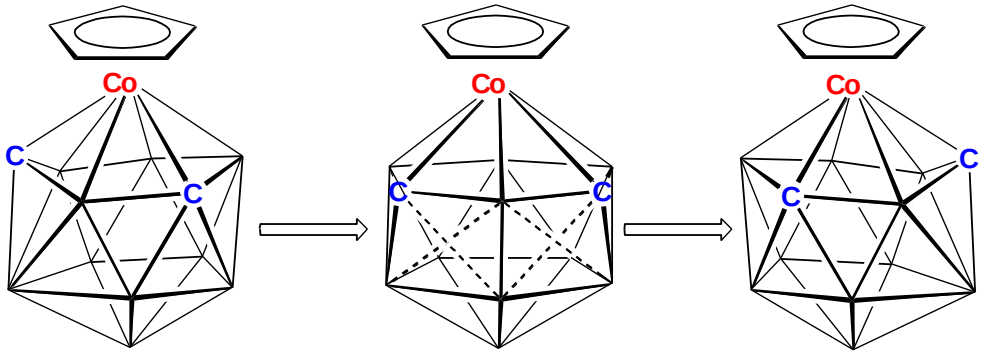

Fig 1.25 Cage fluctionality within 4,1,6-*closo*-$CoC_2B_{10}H_{12}$

Skeletal rearrangements of most of the metallacarboranes generally occurred at low temperatures compared to rearrangements of carboranes. Thermal isomerisation of the 13-vertex metallacarborane with {CpCo} as the metal fragment was reported in 1971 by Hawthorne[39] and with {Cp*Co} by Welch in 2002[40].

It was reported that the isomerisation of the 4-Cp-4,1,6-*closo*-$CoC_2B_{10}H_{12}$ occurred first by reflux in hexane at 69°C to produce 4-Cp-4,1,8-*closo*-$CoC_2B_{10}H_{12}$, followed by reflux in benzene at 80°C to give 4-Cp-4,1,12-*closo*-$CoC_2B_{10}H_{12}$. The red-orange 4,1,12-*closo*-$CoC_2B_{10}H_{12}$ isomer is the thermodynamically most stable isomer whereas the red 4,1,6-*closo*-$CoC_2B_{10}H_{12}$ is the kinetically stable isomer (Fig 1.26).

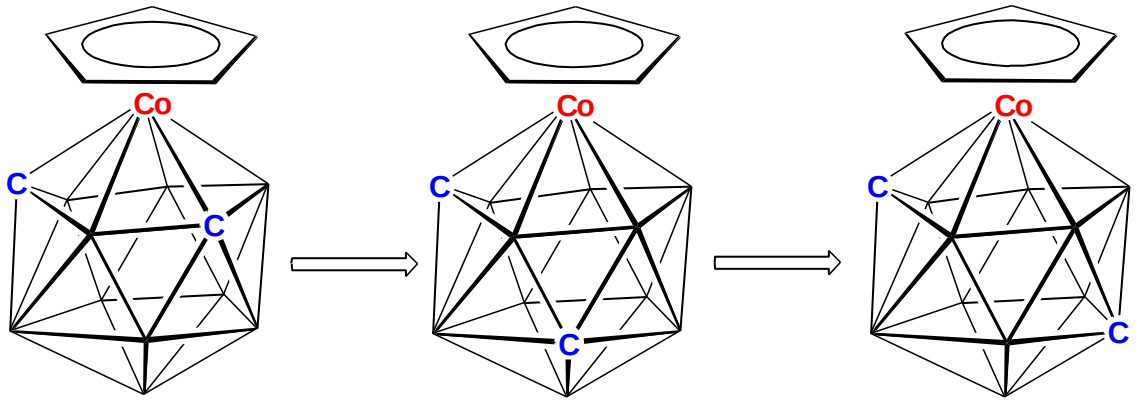

Fig 1.26 Thermal isomerisations in supraicosahedral metallacarboranes

The supraicosahedral metallacarborane is not only possible with transition metal fragments but also possible with p block elements. The first synthesis by reduction with Na metal followed by reaction with $SnCl_2$ and crystallographic characterisation of such a species was carried out by the Welch group in 2002[41] and incorporated Sn as the metal vertex. The analogous compound with methyl groups replacing the hydrogens attached to cage carbon atoms was also synthesized (Fig 1.27).

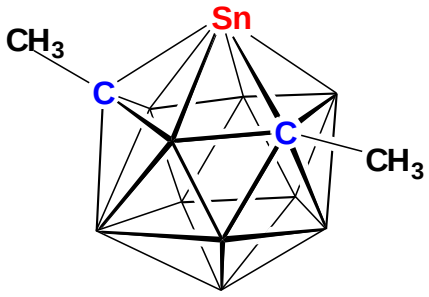

Fig 1.27 Structure of 1,6-$(CH_3)_2$-4,1,6-*closo*-$SnC_2B_{10}H_{10}$

In addition supraicosahedral metallacarboranes can form sandwich type complexes. The first sandwich type complex, $[4,4\text{-}M\text{-}(1,6\text{-}closo\text{-}C_2B_{10})_2]^{n-}$ (n=1 where M is Co(III) and n=2 where M is Fe(II) and Ni(II)) was synthesised by Hawthorne in 1973[23]. This was prepared by reduction of 1,2-*closo*-$C_2B_{10}H_{12}$ to the *nido*-complex, followed by subsequent metallation with the suitable metal fragment (Fig 1.28). The $[4,4\text{-}M\text{-}(1,10\text{-}closo\text{-}C_2B_{10})_2]^{n-}$ (n=1 where M is Co(III) and n=2 where M is Fe(II), Ni(II) and Ti(II)) was isolated by Welch in 2008[42], and was formed by reduction of 1,12-*closo*-$C_2B_{10}H_{12}$ in Na/liquid ammonia, followed by metallation.

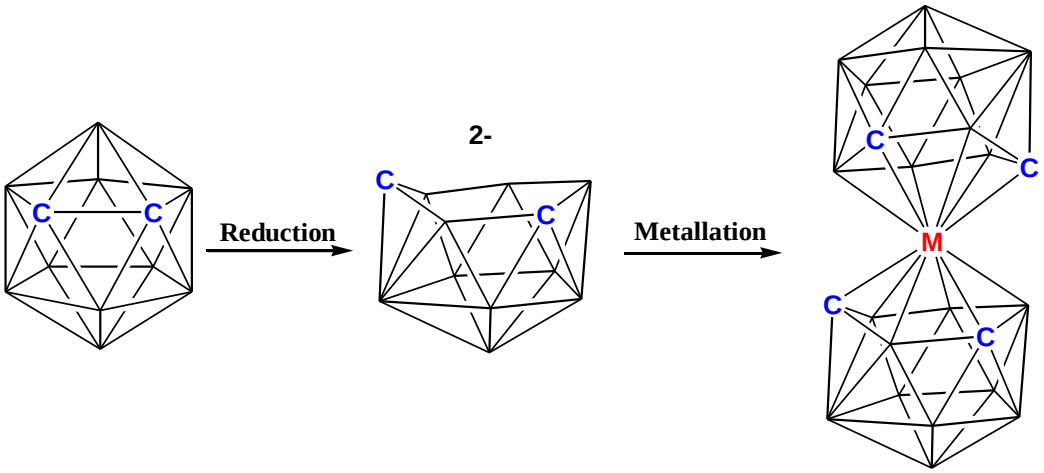

Fig 1.28 Supraicosahedral sandwich type complex

However, work done by Xie in 2001[43] described the formation of [4,4-*M*-(1,2-*closo*-$C_2B_{10}H_{10}R)_2]^{3-}$ where M is potassium. This was achieved by tethering the carbon atoms to avoid separation on reduction.

To date there are many metallacarboranes containing more than 12-vertices reported by several workers, but the most impressive structure is that of a 15-vertex metallacarborane first reported by the Welch group[44].

The reduction of *o*-$C_2B_{10}H_{12}$ or *m*-$C_2B_{10}H_{12}$ and *p*-$C_2B_{10}H_{12}$ yields the [7,9-*nido*-$C_2B_{10}H_{12}]^{2-}$ and [7,10-*nido*-$C_2B_{10}H_{12}]^{2-}$ species respectively. The metallation of [7,9-*nido*-$C_2B_{10}H_{12}]^{2-}$ and [7,10-*nido*-$C_2B_{10}H_{12}]^{2-}$ results in the kinetically most stable 13-vertex isomers 4,1,6-*closo*-MC_2B_{10} and 4,1,10-*closo*-MC_2B_{10} respectively.

The thermodynamically most stable isomer 4,1,12-*closo*-MC_2B_{10} is obtained by heating of 4,1,6-*closo*-MC_2B_{10} or 4,1,10-*closo*-MC_2B_{10} isomers. The thermal rearrangement of these metallacarboranes from 4,1,6-*closo*-MC_2B_{10} occurs in two steps via 4,1,8-*closo*-MC_2B_{10} species whereas the isomerisation from 4,1,10-*closo*-MC_2B_{10} to 4,1,12-*closo*-MC_2B_{10} occurs in a single-step[45] (Fig 1.29).

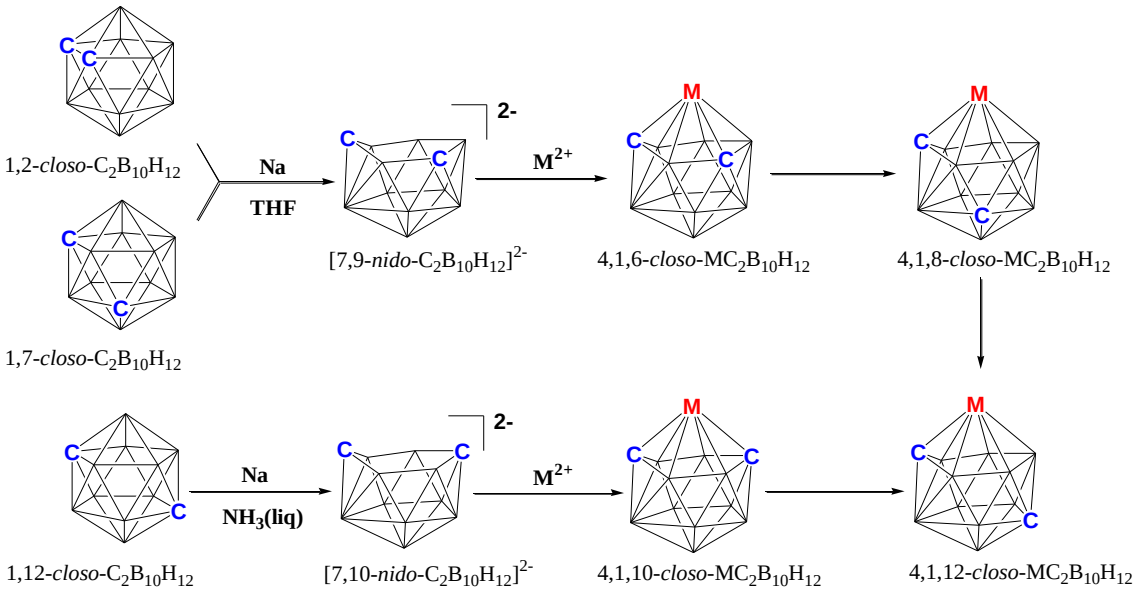

Fig 1.29 Reduction, metallation and isomerisation of MC_2B_{10} species

1.10 1,1′-bis(*o*-carborane)

One of the most fertile areas of heteroborane chemistry is that of metallacarboranes, and as noted above these molecules are generally prepared from *closo*-carboranes by either reduction followed by metallation (cage expansion) or by deboronation followed by metallation (size retention).

Single cage carborane chemistry is well explored as noted above however the analogous double-cage carborane (biscarborane) chemistry is not fully explored due to the previous inefficient synthesis of the starting material.

There are three major biscarboranes, 1,1′-bis(*o*-carborane) (two *o*-carborane cages are connected through a C-C linkage at the 1,1′ positions), 1,1′-bis(*m*-carborane) (two *m*-carborane cages are connected through a C-C linkage at the 1,1′ positions) and 1,1′-bis(*p*-carborane) (two *p*-carborane cages are connected through a C-C linkage at 1,1′ positions) (Fig 1.30).

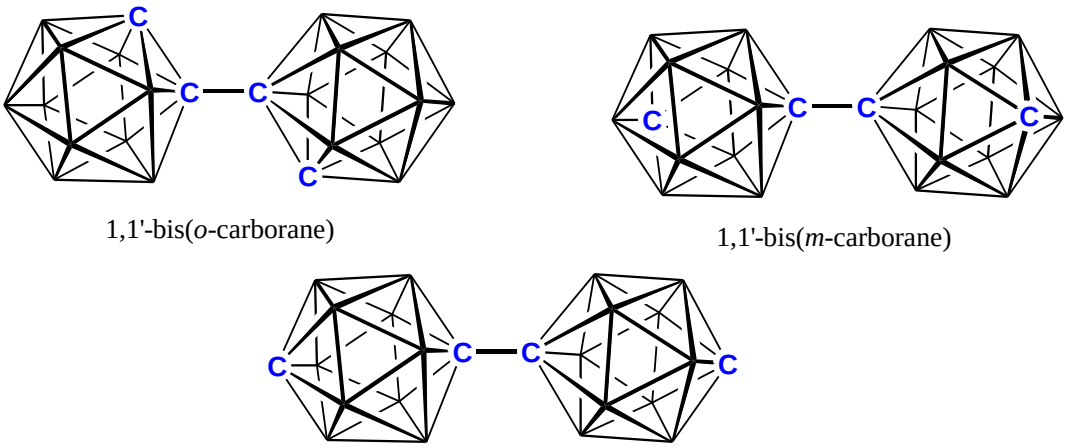

Fig 1.30 Major isomers of biscarborane

Currently, 12-vertex/12-vertex metallacarborane/carborane species derived from 1,1′-bis(*o*-carborane), 1,1′-bis(*m*-carborane) and 1,1′-bis(*p*-carborane) and 12-vertex/12-vertex metallacarborane/metallacarborane species derived from 1,1′-bis(*m*-carborane) and 1,1′-bis(*p*-carborane) are unknown and, as noted above, this may be due to the previously inefficient synthesis of these biscarboranes.

In 1964 Hawthorne first reported the synthesis of 1,1′-bis(*o*-carborane) in 21% overall yield by reacting bisacetonitrile decaborane with diacetylene at reflux temperature[46] (Fig 1.31).

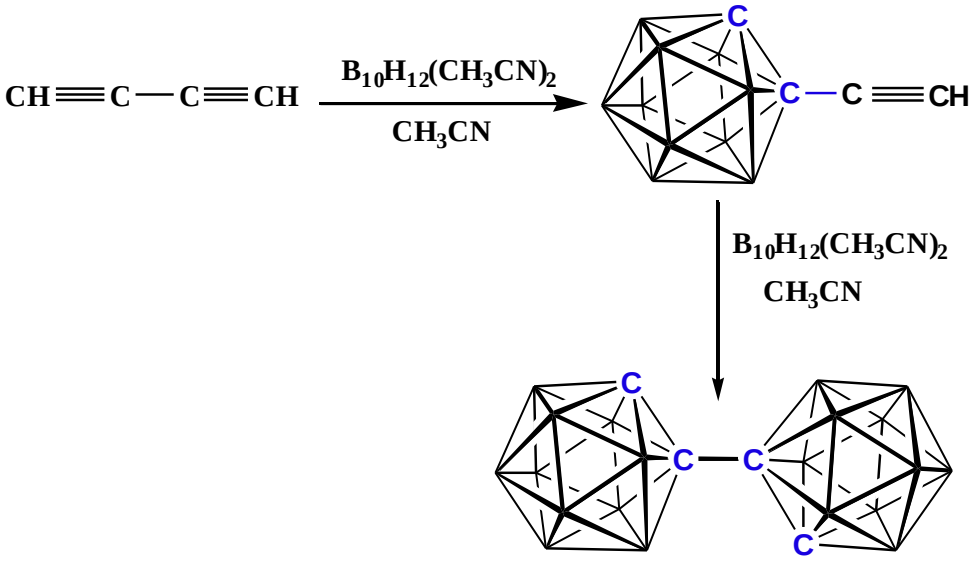

Fig 1.31 Preparation of 1,1′-bis(*o*-carborane) in early 1960's

Hawthorne reported an improved synthesis of 1,1′-bis(*o*-carborane) in 1973 in 37.5% overall yield by replacing $B_{10}H_{12}.2S(CH_2CH_3)_2$ for $B_{10}H_{12}.2CH_3CN$ and reducing the temperature to -25˚C in order to minimize the loss of diacetylene[47] (Fig 1.32).

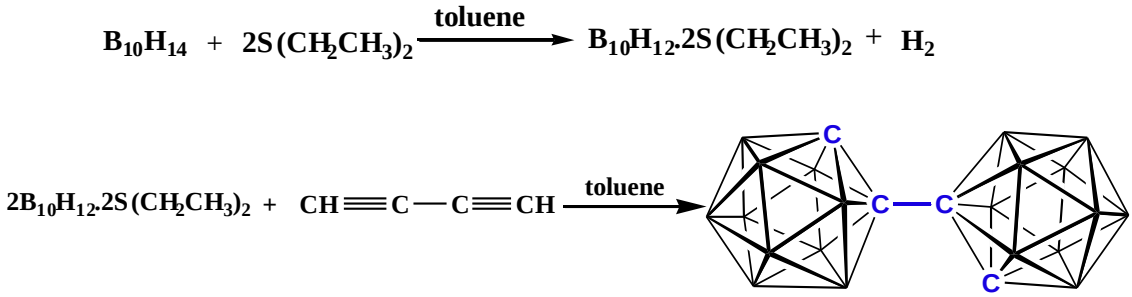

Fig 1.32 Improved synthesis of 1,1′-bis(*o*-carborane) by Hawthorne

Later, using $CuCl_2$, Hawthorne coupled two *o*-carborane molecules to produce a mixture of 1,1′-bis(*o*-carborane), 1,3′-bis(*o*-carborane) and 1,4′-bis(*o*-carborane) (Fig 1.33) in 31% overall yield with respect to dilithio(*o*-carborane) as starting material[48]. Hawthorne then repeated the same procedure except that monolithio(*o*-carborane) was used as the starting material instead of dilithio(*o*-carborane) and the yield was then improved to 45%[48].

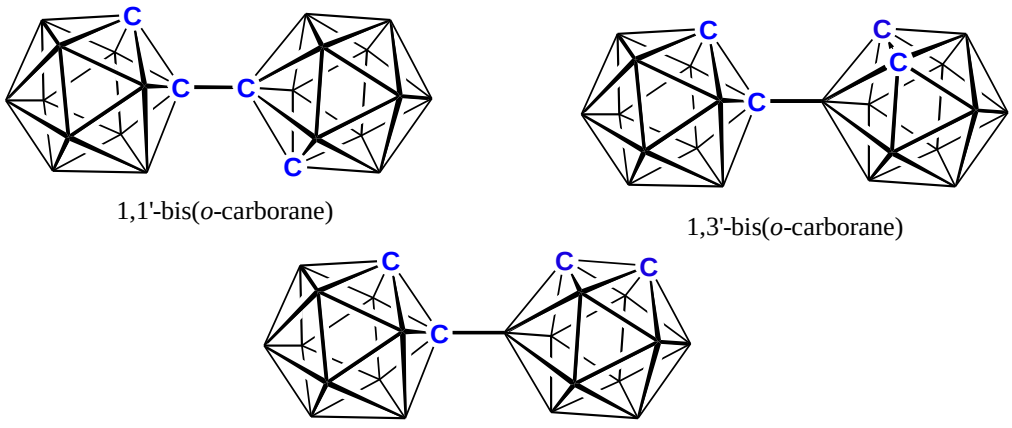

Fig 1.33 Different isomers of bis(*o*-carborane)

However, in 2008 Xie developed a new method to synthesise 1,1′-bis(*o*-carborane) in high yield[49] (83%) (Fig 1.34) by using CuCl instead of $CuCl_2$ in order to avoid C-B and B-B coupled isomeric products. Coupling efficiency depends on reaction conditions such as donor solvent and the copper salt involved. In the intermediate step each Cu atom is σ-bound to the cage carbon atom and η^3-bound to a toluene molecule[49].

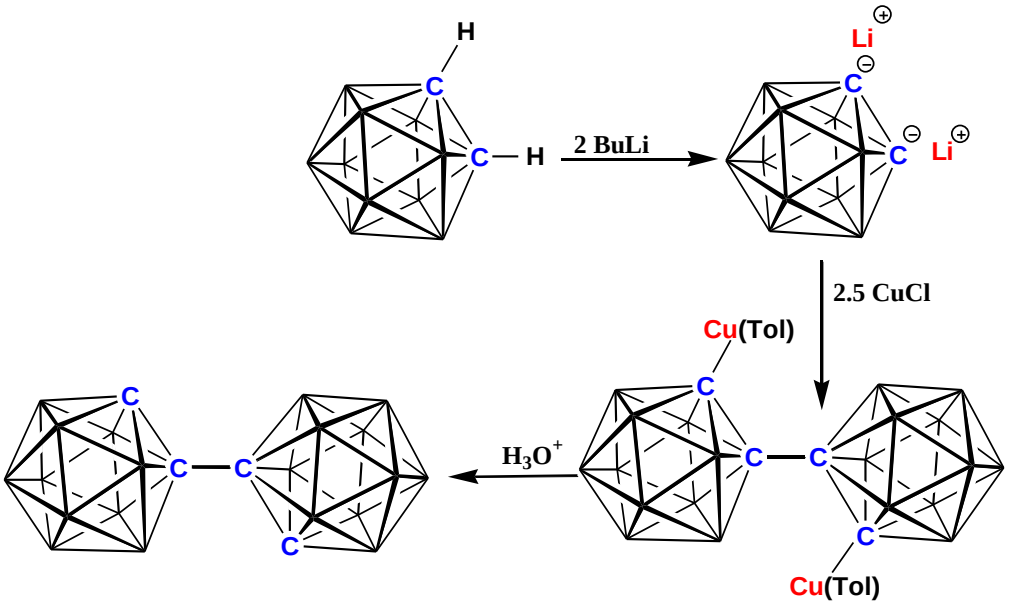

Fig 1.34 Synthesis of 1,1′-bis(*o*-carborane) in high yield

The improved synthesis of 1,1′-bis(*o*-carborane) reported by Xie opens up the possibility of exploring the derivative chemistry of this molecule. This should be worthwhile for a number of reasons, including interest in such species in homogeneous catalysis and as potential new agents for boron-neutron capture therapy.

In 1971 Hawthorne reported that double deprotonated 1,1′-bis(*o*-carborane) acts as a chelating agent with transition metal ions[50] (Fig 1.35).

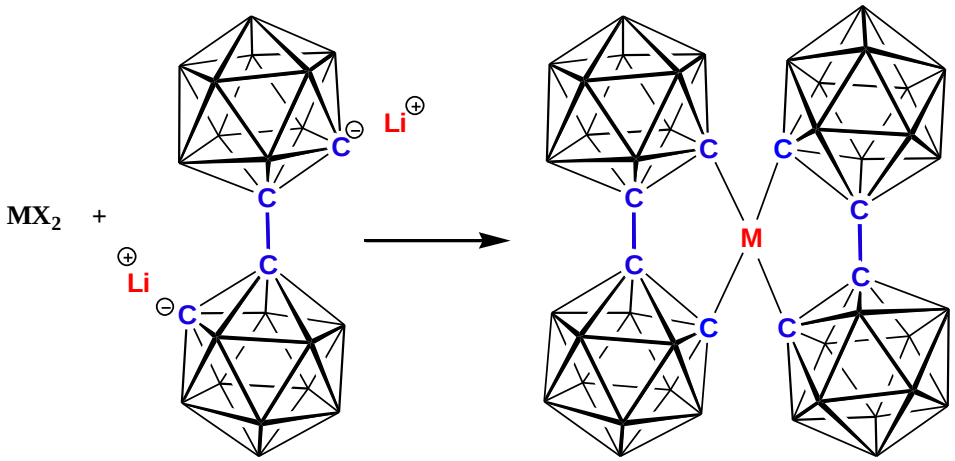

Fig 1.35 **Structural representation of 1,1′-bis(*o*-carborane) acting as a chelating agent (M stands for Co(II), Ni(II), Cu(II) and Cu(III) and X stands for Cl and Br)**

There are three major types of reaction possible with 1,1′-bis(*o*-carborane) based on similar chemistry for *o*-carborane.

1. Removal of hydrogen and introduction of various functional groups at the cage carbon atoms or the boron atoms distant from carbon.
2. Deboronation of either one or both cages by adding strong base followed by metallation or capitation.
3. Polyhedral expansion by reduction with Na/Li metal in the presence of naphthalene of either one or both cages followed by the metallation or capitation.

1.10.1 Removal of hydrogen and methylation

Similarly to *o*-carborane, the removal of hydrogen from 1,1′-bis(*o*-carborane) can be carried out in two ways. Deprotonation and alkylation of the carbon atom in 1,1′-bis(*o*-carborane) can be carried out by the addition of alkyllithium reagent followed by the addition of alkyl halide to yield the carbon substituted product, and this was first reported by Hawthorne in 1964[46] (Fig 1.36).

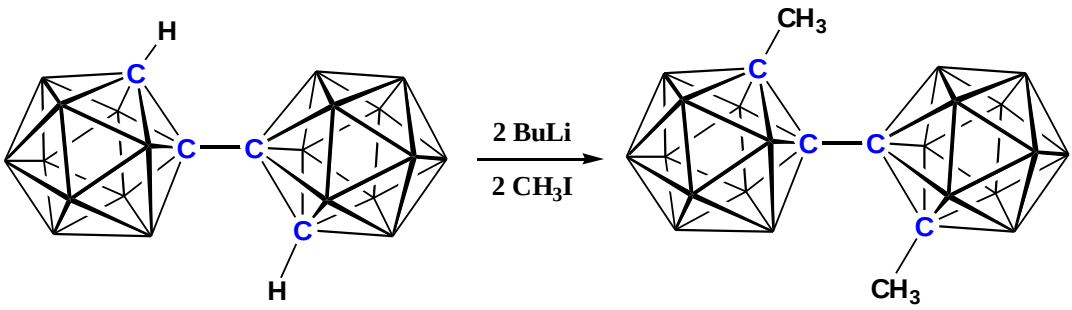

Fig 1.36 Substitution of H atoms on 1,1′-bis(*o*-carborane) cage carbon atoms

Removal of hydrogen and methylation of the boron atoms distant from CH in 1,1′-bis(*o*-carborane) are possible with Friedal-Craft reagents (Fig 1.37). Octamethylated derivatives of 1,1′-bis(*o*-carborane) resulted from the use of excess MeI/$AlCl_3$[16].

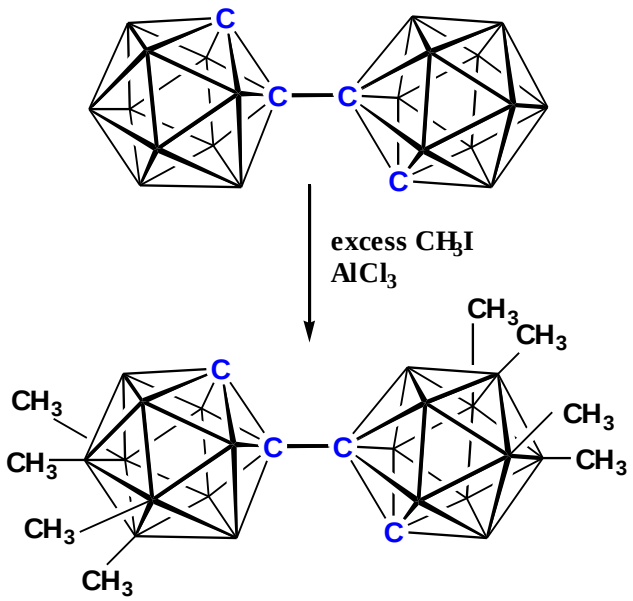

Fig 1.37 Substitution of H atoms on boron atoms in 1,1′-bis(*o*-carborane)

1.10.2 Decapitation of 1,1′-bis(*o*-carborane)

The decapitations of a single cage and both cages were reported by Hawthorne in 1971 (Fig 1.38) and the products were initially isolated as $[Cs]^+$ followed by [alkyl ammonium]$^+$ salts[51] but were not characterised crystallographically. In principle, following deprotonation, these decapitated products could be metallated to yield either the single cage metallated or doubly metallated products.

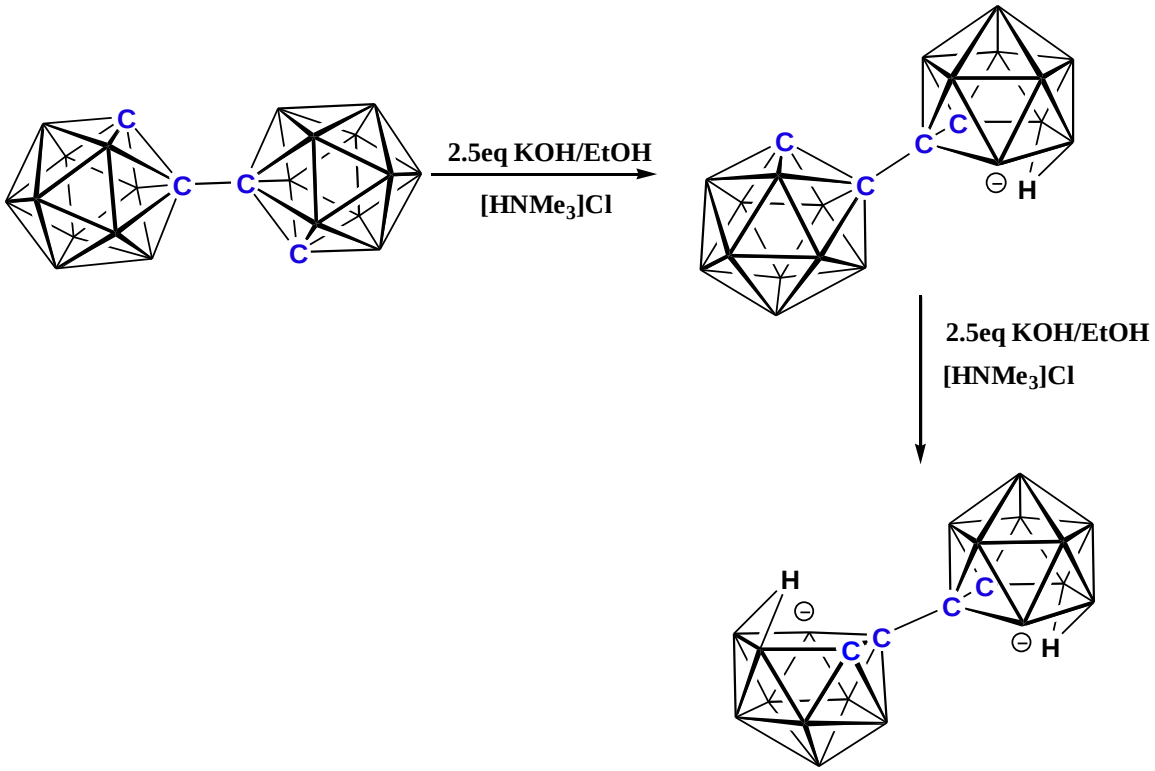

Fig 1.38 Stepwise single and double decapitation of 1,1′-bis(*o*-carborane)

The decapitation reaction of the second cage of [7-(1′-1′,2′-*closo*-$C_2B_{10}H_{11}$)-7,8-*nido*-$C_2B_9H_{11}$]$^-$ is possible in either B3 or B6 position (Fig 1.39) therefore it is possible to get *racemic* and *meso* diastereoisomers.

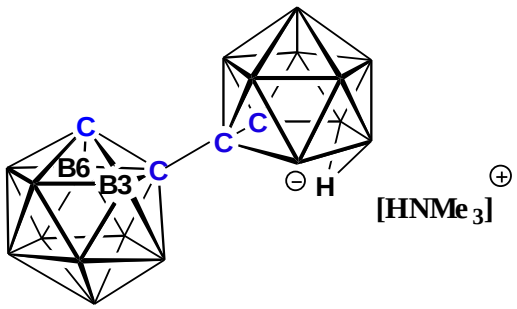

Fig 1.39 Decapitation of the closo cage in [7-(1′-1′,2′-*closo*-$C_2B_{10}H_{11}$)-7,8-*nido*-$C_2B_9H_{11}$]$^-$

As far as we know, there are no results reported for the metallation of a single cage. However in 1985 Hawthorne reported the formation of complex new bimetallic rhodacarborane products using [Rh(COD)(PEt_3)Cl][52] but there is no evidence given for diastereoisomers. The reaction was carried out by the addition of [Rh(COD)(PEt_3)Cl] to a THF solution of Cs_2[7-(7′,8′-*nido*-$C_2B_9H_{11}$)-7,8-*nido*-$C_2B_9H_{11}$] and heating to reflux for two days.

1.10.3 Reduction and metallation of 1,1′-bis(*o*-carborane)

The attempt made by Hawthorne and co-workers in 1990 to reduce a single cage by the addition of two electrons was unsuccessful. The anion isolated as the $[PPh_3Me]^+$ salt has two partially open CBCB faces[53].

However, the two electron reduction with Na in THF followed by sequestration with 15-crown-5 ether yielded a different product in the *X*-ray diffraction study. One of the two carborane polyhedra has a partially opened four atom face similar to the $[PPh_3Me]^+$ salt but the other cage has a five atom CBCBB face[54] which is more open.

The four electron reduction followed by protonation of 1,1′-bis(*o*-carborane) yields [μ-$_{9,10}$-CH-(μ-$_{9',10'}$-CH-*nido*-7′-$CB_{10}H_{11}$)-*nido*-7-$CB_{10}H_{11}$]$^{2-}$ and this anion is most likely the result of protonation of the anion $[(C_2B_{10}H_{11})_2]^{4-}$ followed by movement of the linking C atoms to bridging positions above nido 11-vertex cages[54].

However, the reduction of 1,1′-bis(*o*-carborane) with an excess of Li in degassed THF followed by metallation with [Ru(*p*-cymene)Cl_2]$_2$ interestingly affords an unexpected compound[55]. Instead of each cage being capped by the metal, an exotic “flyover” type complex was produced.

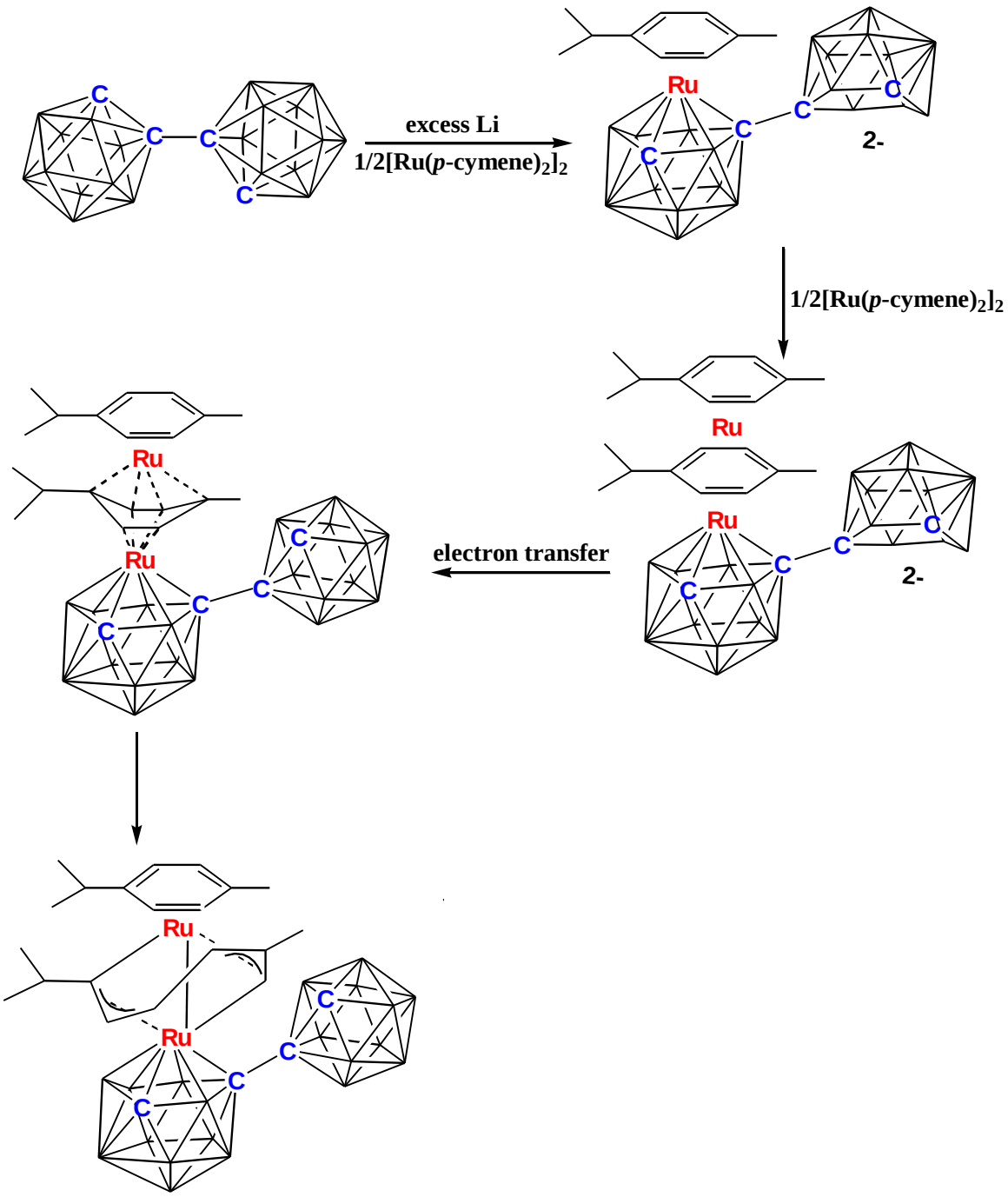

Fig 1.40 Proposed mechanism for the formation of fly-over complex

The most interesting feature of this complex is that the formation involves the breaking of an aromatic C-C bond at room temperature, which is usually a very high energy process[55] (Fig 1.40) .

The reduction of 1,1′-bis(*o*-carborane) with excess Li in degassed THF in the presence of naphthalene followed by metallation with NaCp/$CoCl_2$ has shown that the double polyhedral expansion of 1,1′-bis(*o*-carborane) is possible in the same way as for mono-carborane. This yielded the first supraicosahedral bis(heteroborane), afforded as a mixture of diastereoisomers[56] (Fig 1.41).

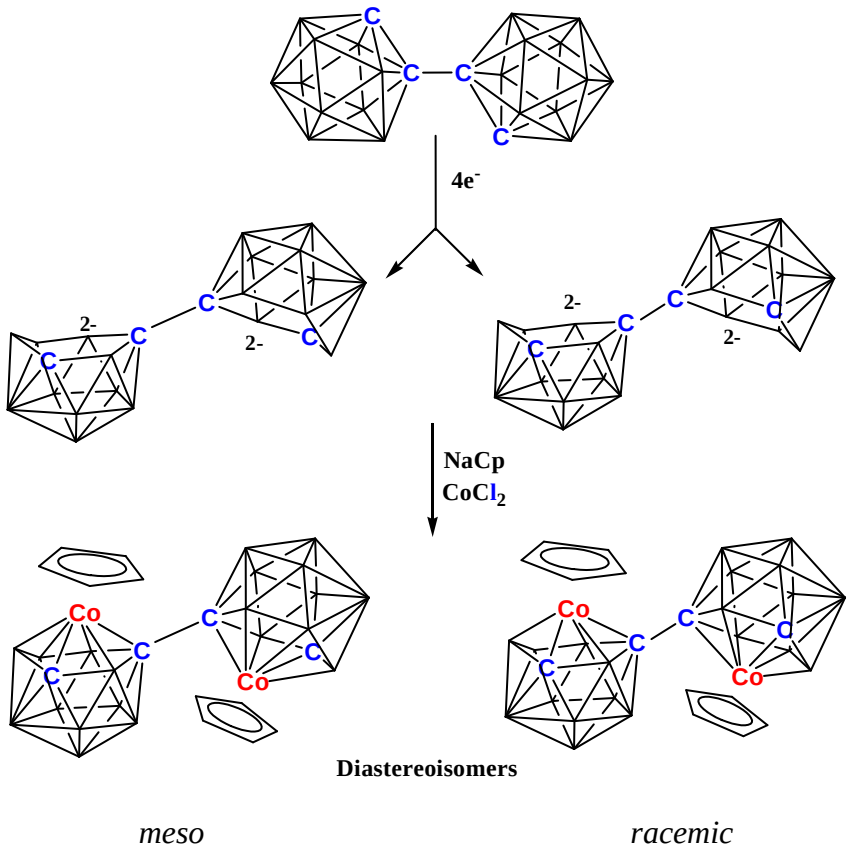

Fig 1.41 Formation of diastereoisomers during reduction and metallation of 1,1′-bis(*o*-carborane)

.

1.11 Scope of Thesis

Chapter 1 introduces the field of boranes, carboranes and metallacarboranes including a discussion of the variety of isomerisation mechanisms proposed for 12-vertex heteroboranes. In the latter part of this chapter the focus changes to the synthesis of biscarboranes and the research done so far with 1,1′-bis(*o*-carborane).

Chapter 2 describes the two electron reduction and attempted polyhedral expansion by metallation of 1,1′-bis(*o*-carborane). The polyhedral expansion was not successful, however, although 12-vertex/12-vertex metallacarboranes/carboranes are isolated for the first time. In an attempt to increase yields single cage decapitation followed by metallation was performed. Metallation with {(arene)Ru} fragments yielded the same products as reduction and metallation however, metallation with {CpCo} yielded a different product. Two dimensional ^{11}B-^{11}B correlation spectra were analysed in order to identify the individual resonances due to carborane and metallacarborane cages. This allowed the weighted average ^{11}B chemical shifts, $<\delta^{11}B>$ to be calculated for each carborane cage and metallacarborane cage and the results obtained are discussed in relation to the parent compounds.

Chapter 3 describes the double decapitation of 1,1′-bis(*o*-carborane) in good yield in short time and introduces the possibility of diastereoisomers, although as salts these cannot be separated. The doubly metallated derivatives of 1,1′-bis(*o*-carborane) and their interesting and varied isomeric forms are described. It is found that metallation with {(arene)Ru} fragments resulted in two products in which one cage is isomerised (2′,1′,8′-) and the other is not (3,1,2-). Metallation with {CpCo} yielded the same two structure types plus a third product with both cages isomerised (2,1,8- and 2′,1′,8′-).

Chapter 4 examines the double decapitation of 1,1′-bis(*o*-carborane) followed by metallation with $\{(dmpe)Ni\}^{2+}$. This work yielded the first examples of 12-vertex/12-vertex 3,1,2-$MC_2B_9H_{10}$/3,1,2-$MC_2B_9H_{10}$ species, afforded as *racemic* and *meso* diastereoisomers. Methylation at carbon of 1,1′-bis(*o*-carborane) was carried out, followed by decapitation and metallation with $\{(dmpe)Ni\}^{2+}$. Interestingly, only single cage decapitation and metallation occurred and an unprecedented low temperature 2,1,7- isomerisation was observed.

Chapter 5 gives full details of the synthetic experiments undertaken and the characterisation of products by mass spectrometry, microanalysis, NMR spectroscopies and *X*-ray diffraction studies.

1.12 References:

1.1. J. Daintith, Dictionary of Chemistry, 3rd Edition, Oxford University Press, 1986.

1.2. A. Stock, *Hydrides of Boron and Silicon*, Cornell University Press, Ithaca, New York, 1933.

1.3. H. C. Longuet-Higgins, *J. Chim. Phys*., 1949, **46**, 268.

1.4. H. W. Smith and W. N. Lipscomb, *J. Chem. Phys*., 1965, **43**, 1060.

1.5. J. S. Kasper, C. M. Lucht and D. Harker, *Acta Crystallogr*., 1950, **3**, 436.

1.6. H. C. Longuet-Higgins and M. de V. Roberts, *Proc. Roy. Soc*., 1954, **A224**, 336; 955, **A230**, 110.

1.7. A. R. Pitochelli and M. F. Hawthorne, *J. Am. Chem. Soc*., 1960, **82**, 3228.

1.8. W. N. Lipscomb, *Boron Hydrides*, W. A. Benjamin Inc., New York, 1963.

1.9. K. Wade, *J. C. S. Chem. Commun*., 1971, 792.

1.10. R. E. Williams, *Inorg. Chem.*, 1971, **10**, 210; *Adv. Inorg. Chem. Radiochem*., 1976, **18**, 66.

1.11. R. B. King, *J. Organometal. Chem.*, 2007, **692**, 1773.

1.12. P. von R. Schleyer, K. Najafian and A. M. Mebel, *Inorg. Chem.*, 1998, **37**, 6765.

1.13. T. L. Heying, J. W. Ager Jnr, S. L. Clark, D. J. Mangold, H. L. Goldstein, M. L. Hillman, R. J. Polak and J. W. Szymanski, *Inorg. Chem*., 1963, **2**, 1089.

1.14. T. L. Heying, J. W. Ager Jnr, S. L. Clark, R. P. Alexander, S. Papetti, J. A. Reid and S. I. Trotz, *Inorg. Chem*., 1963, **2**, 1097.

1.15. S. Pepetti and T. L. Heying, *Inorg. Chem*., 1963, **2**, 1105.

1.16. A. Herzog, A. Maderna, G. N. Harakas, C. B. Knobler and M. F. Hawthorne, *Chem. Eur. J*., 1999, **5**, 1212.

1.17. R. A. Wiesboeck and M. F. Hawthorne, *J. Am. Chem. Soc*., 1964, **86**, 1642.

1.18. (a) J. S. Roscoe, S. Kongpricha and S. Papetti, *Inorg. Chem.*, 1970, **9**, 1561; (b) M. F. Hawthorne and P. A. Wegner, *J. Am. Chem. Soc.*, 1968, **90**, 896.

1.19. D. C. Busby and M. F. Hawthorne, *Inorg. Chem*., 1982, **21**, 4101.

1.20. M. A. Fox, W. R. Gill, P. L. Herbatson, J. A. H. Macbride and K. Wade, *Polyhedron*, 1996, **15**, 565.

1.21. (a) C. L. Powell, M. Schulze, S. J. Black, A. S. Thompson and M. D. Threadgill, *Tetrahedron Lett*., 2007, **48**, 1251; (b) A. F Armstrong and J. F. Valliant, *Dalton Trans*., 2007, 4243.

1.22. G. B. Dunks, R. J. Wiersema and M. F. Hawthorne, *J. Am. Chem. Soc*., 1973, **95**, 3174.

1.23. D. F. Dustin, G. B. Dunks and M. F. Hawthorne, *J. Am. Chem. Soc*., 1973, **95**, 1109.

1.24. (a) L. Zakharkin, V. Kalinin and L. Podvisotskaya, *Izv. Akad. Nauk SSSR, Ser. Khimi*., 1967, 2310; (b) L. Zakharkin, V. Kalinin and L. Podvisotskaya, *Izv. Akad. Nauk SSSR, Ser. Khim*., 1967, **16**, 2212.

1.25. (a) L. Zakharkin and V. Kalinin, *Izv. Akad. Nauk SSSR, Ser. Khim*., 1969, 194; (b) V. Stanko, Yu. V. Gol'typain and V. Brattsev, *Zh. Obsch. Khim*., 1969, **39**, 1175.

1.26. R. Adams, *Inorg. Chem*., 1963, **2**, 1087.

1.27. S. Papetti and T. L. Heying, *J. Am. Chem. Soc.*, 1964, **86**, 2295.

1.28. W. N. Lipscomb, *Science*, 1966, **153**, 373.

1.29. H. D. Kaesz, R. Bau, H. A. Beall and W. N. Lipscomb, *J. Am. Chem. Soc*., 1967, **89**, 4219.

1.30. D. Grafstein and J. Dvorak, *Inorg. Chem*., 1963, **17**, 1128.

1.31. M. J. S. Dewar and M. L. McKee, *Inorg. Chem*., 1978, **17**, 1569.

1.32. M. F. Hawthorne and R. L. Pilling, *J. Am. Chem. Soc*., 1965, **87**, 3987.

1.33. M. F. Hawthorne, D. C. Young and P. A. Wegner, *J. Am. Chem. Soc*., 1965, **87**, 1818.

1.34. M. F. Hawthorne and T. D. Andrews, *Chem. Commun*., 1965, 443.

1.35. (a) R. M. Garrioch, P. Kuballa, K. S. Low, G. M. Rosair and A. J. Welch, *J. Organomet. Chem.*, 1999, **575**, 57; (b) S. Robertson, R. M. Garrioch, D. Ellis, T. D. McGrath, B. E. Hodson, G. M. Rosair and A. J. Welch, *Inorg. Chim. Acta*, 2005, **358**, 1485; (c) M. K. Kaloustain, R. J. Wiersema and M. F. Hawthorne, *J. Am. Chem. Soc.*, 1972, **94**, 6679.

1.36. D. R. Baghurst, R. C. B. Copley, H. Fleisher, D. M. P. Mingos, G. O. Kyd, L. J. Yellowless, A. J. Welch, T. R. Spalding and D. O'Connell, *J. Organometal. Chem.*, 1993, **447**, C14.

1.37. S. Dunn, G. M. Rosair, Rh. Ll. Thomas, A. S. Weller and A. J. Welch, *Angew. Chem. Int. Ed. Engl.*, 1997, **36**, 645.

1.38. A. Burke, D. Ellis, D. Ferrer, D. L. Ormsby, G. M. Rosair and A. J. Welch, *Dalton Trans*., 2005, 1716.

1.39. G. B. Dunks, M. M. McKown and M. F. Hawthorne, *J. Am. Chem. Soc.*, 1971, **93**, 2541.

1.40. A. Burke, R. McIntosh, D. Ellis, G. M. Rosair and A. J. Welch, *Collect. Czech. Chem. Commun.*, 2002, **67**, 991.

1.41. N. M. M. Wilson, D. Ellis, A. S. F. Boyd, B. T. Giles, S. A. Macgregor, G. M. Rosair and A. J. Welch, *Chem. Commun.*, 2002, 464.

1.42. D. Ellis, R. D. McIntosh, S. Esquirolea, C. Vinas, G. M. Rosair, F. Teixidor and A. J. Welch, *Dalton Trans.*, 2008, 1009.

1.43. G. Zi, H. W. Li and Z. Xie, *Chem. Commun.*, 2001, 1110.

1.44. R. D. McIntosh, D. Ellis, G. M. Rosair and A. J. Welch, *Angew. Chem. Int. Ed.*, 2006, **45**, 4313.

1.45. D. Ellis, M. E. Lopez, R. D. McIntosh, G. M. Rosair, A. J. Welch, and R. Quenardelle, *Chem. Commun.*, 2005, 1348.

1.46. J. A. Dupont and M. F. Hawthorne, *J. Am. Chem. Soc*., 1964, **86**, 1643.

1.47. T. E. Paxon, K. P. Callahan and M. F. Hawthorne, *Inorg. Chem.*, 1973**, 12**, 708.

1.48. X. Yang, W. Jiang, C. B. Knobler, M. D. Mortimer and M. F. Hawthorne, *Inorg. Chim. Acta*, 1995, **240**, 371.

1.49. S. Ren and Z. Xie, *Organometallics.*, 2008, **27**, 5167.

1.50. D. A. Owen and M. F. Hawthorne, *J. Am. Chem. Soc*., 1971, **93**, 873.

1.51. D. A. Owen, J. W. Wiggins and M. F. Hawthorne, *Inorg. Chem*., 1971, **10**, 1304

1.52. P. E. Behnken, T. B. Marder, R. T. Baker, C. B. Knobler, M. R. Thompson and M. F. Hawthorne, *J. Am. Chem. Soc*., 1985**, 107**, 933.

1.53. T. D. Getman, C. B. Knobler and M. F. Hawthorne, *J. Am. Chem. Soc*., 1990, **112**, 4593.

1.54. T. D. Getman, C. B. Knobler and M. F. Hawthorne, *Inorg. Chem*., 1992, **31**, 101.

1.55. D. Ellis, D. McKay, S. A. Macgregor, G. M. Rosair and A. J. Welch, *Angew. Chem. Int. Ed*., 2010, **49**, 4943.

1.56. D. Ellis, G. M. Rosair and A. J. Welch, *Chem. Commun.*, 2010, **46**, 7394.

CHAPTER 2

Single cage metallation of 1,1′-bis(o-carborane)

2.1 Introduction

The ultimate goal of the project is to synthesise larger polyhedra with a greater number of vertices *via* the polyhedral expansion method. Successful reduction occurs when the reduced nido species is stabilised by the presence of cage carbon atoms in the six atom open face.

It is well known that two electron reduction of 12-vertex icosahedral *ortho*-carborane is carried out by the addition of sodium in degassed THF to afford the 12-vertex nido di-anion [7,9-*nido*-$C_2B_{10}H_{12}$]$^{2-}$. This can then be metallated with suitable metal fragments to yield a 13-vertex supraicosahedral metallacarborane $MC_2B_{10}H_{12}$ (Fig 2.1)[1]. Transition metal fragments which are isolobal to the {BH} including {(arene)Ru} and {CpCo} are used to metallate the nido cage.

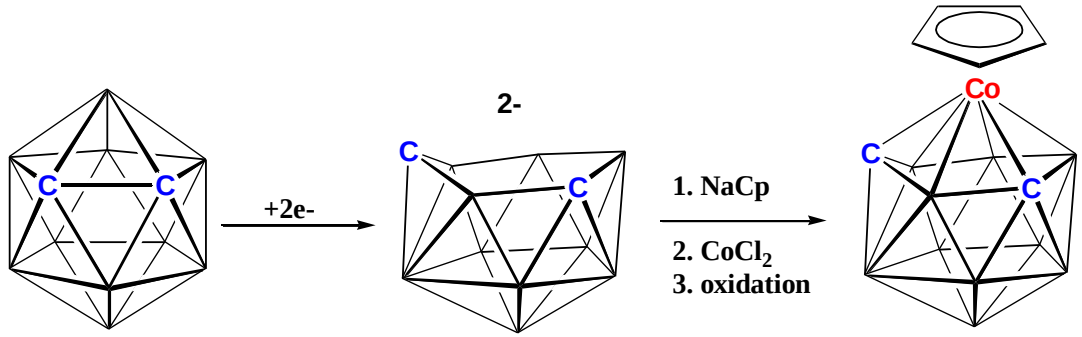

Fig 2.1 Reduction and metallation process of 1,2-*closo*-carborane

Initially in *ortho*-carborane both carbon atoms are next to each other, but after the reduction they are separated by a boron vertex and therefore the metallacarborane that is isolated after the metallation should have a 4-L-4,1,6-*closo*-$MC_2B_{10}H_{12}$ geometry.

The reduction chemistry of 1,1′-bis(*o*-carborane) is an interesting area of study because it consists of two *ortho*-carborane polyhedral cages connected through a carbon-carbon sigma bond. Few relevant results are published so far and this may be due to the previously inefficient synthesis of 1,1′-bis(*o*-carborane). The breakthrough procedure was first reported by Zie and co-workers in 2008 in 83% yield[2] by using CuCl instead of the $CuCl_2$ used by Hawthorne[3] in order to avoid the C-B and B-B coupled isomeric products.

The reduction chemistry of 1,1′-bis(*o*-carborane) was first reported by Hawthorne and co-workers in 1990[4]. The reduction can be carried out by the addition of either two electrons or four electrons in order to reduce a single cage or both cages respectively. The metallation of these reduced species would then result in supraicosahedral bis(heteroboranes).

However the two electron reduction of 1,1′-bis(*o*-carborane) with sodium naphthalenide in degassed THF followed by work up resulted in a 12-vertex/12-vertex $[C_2B_{10}H_{11}]^-$-$[C_2B_{10}H_{11}]^-$ species with an inversion center in the middle of carbon-carbon sigma bond (1.377(4) Å)[4] instead of *nido*-$[C_2B_{10}H_{11}]^{2-}$/*closo*-$[C_2B_{10}H_{11}]$. Thus instead of adding two electrons to a single cage one electron was added to each cage. As far as we know there is no metallation chemistry established so far for the two electron reduced species by other workers.

The four electron reduction of 1,1′-bis(*o*-carborane) with sodium naphthalenide in degassed THF followed by protonation yields [μ-$_{9,10}$-CH-(μ-$_{9',10'}$-CH-*nido*-7′-$CB_{10}H_{11}$)-*nido*-7-$CB_{10}H_{11}]^{2-}$ which formed by the protonation of the anion $[(C_2B_{10}H_{11})_2]^{4-}$[5].

The four electron reduction of 1,1′-bis(*o*-carborane) with excess lithium naphthalenide in degassed THF followed by the metallation with $[Ru(p\text{-cymene})Cl_2]_2$ resulted in a fly-over bridge compound[6] and the mechanism of this species was discussed in chapter 1.

The first supraicosahedral bis(heteroborane) from reduction of 1,1′-bis(*o*-carborane) followed by metallation with {CpCo} fragments was reported by Welch group in 2010 and was afforded as interesting *racemic* and *meso* isomers[7]. As already noted the analogous reaction with $[Ru(p\text{-cymene})Cl_2]_2$ resulted in a carbon-carbon bond cleavage on a reduced biscarborane and only one of the cages was expanded. This is most likely due to the fact that the $\{Ru(p\text{-cymene})\}^{2+}$ is much larger than $\{CoCp\}^{2+}$ therefore there is not enough space for a fragment to co-ordinate to both cages.

It is well known that the decapitation reaction of 1,2-*closo*-carborane is carried out by the addition of KOH/EtOH giving a $[7,8\text{-}nido\text{-}C_2B_9H_{11}]^{2-}$[8] species (Fig 2.2). The degraded product can be metallated with a metal fragment to achieve a metallacarborane with the same number of vertices as the original carborane.

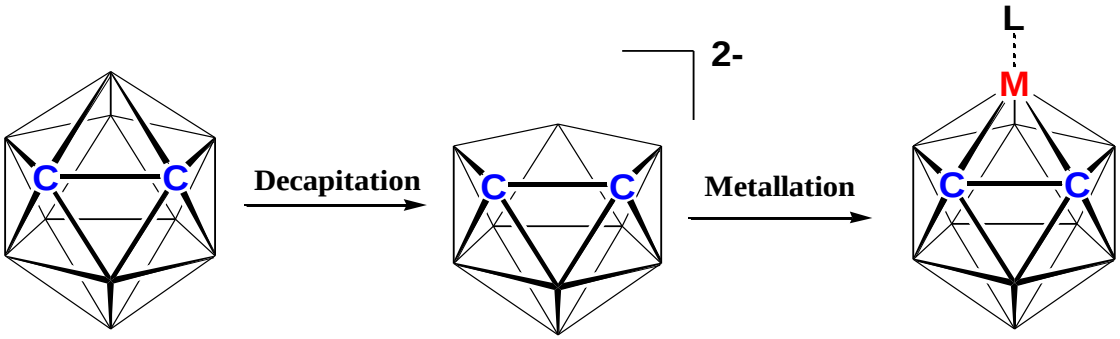

Fig 2.2 Decapitation and metallation process of 1,2-*closo*-carborane

The same type of reaction is possible with 1,1′-bis(*o*-carborane). The selective degradation of 1,1′-bis(*o*-carborane) to form $[7\text{-}(1'\text{-}1',2'\text{-}closo\text{-}C_2B_{10}H_{11})\text{-}7,8\text{-}nido\text{-}C_2B_9H_{11}]^-$[9] can be achieved by the addition of 2.5 equivalents of KOH/EtOH to 1,1′-bis(*o*-carborane) and heating under reflux for several hours.

However, as far as we are aware no metallation chemistry of $[7\text{-}(1'\text{-}1',2'\text{-}closo\text{-}C_2B_{10}H_{11})\text{-}7,8\text{-}nido\text{-}C_2B_9H_{11}]^-$ species has been established so far, and again this may be due to the previously inefficient synthesis of the starting material.

In this chapter are described the syntheses and the complete characterisation of the first examples of 12-vertex/12-vertex metallacarborane/carborane species 1-(1′-1′,2′-*closo*-$C_2B_{10}H_{11}$)-3-(η-cymene)-3,1,2-*closo*-$RuC_2B_9H_{10}$, 1-(1′-1′,2′-*closo*-$C_2B_{10}H_{11}$)-3-(η-benzene)-3,1,2-*closo*-$RuC_2B_9H_{10}$ and 1-(1′-1′,2′-*closo*-$C_2B_{10}H_{11}$)-3-(η-C_5H_5)-3,1,2- *closo*-$CoC_2B_9H_{10}$ resulting from the two electron reduction of 1,1′-bis(*o*-carborane) followed by metallation.

In order to improve yields the single cage degradation and metallation reaction was carried out with {(arene)Ru} and {CpCo} fragments at room temperature. This chapter also includes the results of room temperature isomerisation during metallation with the {CpCo} fragment.

2.2 Preparation of 1-(1′-1′,2′-*closo*-$C_2B_{10}H_{11}$)-3-(η-cymene)-3,1,2-*closo*-$RuC_2B_9H_{10}$ (1)

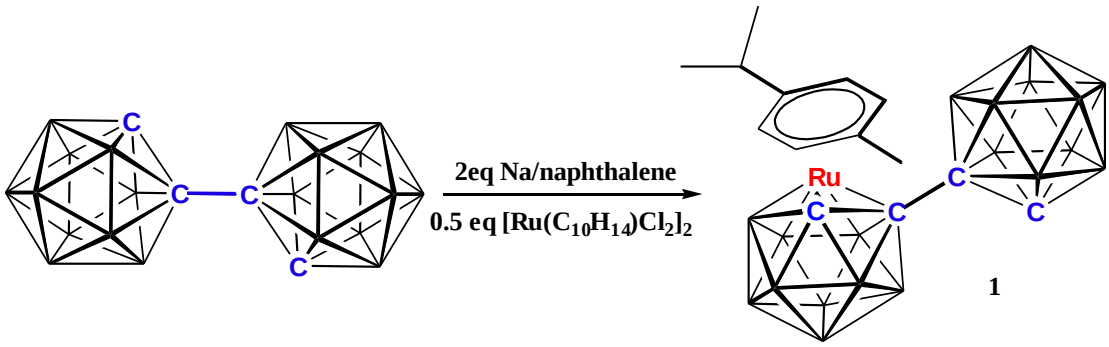

1

Stoichiometric two electron reduction of 1,1′-bis(*o*-carborane) with sodium naphthalenide in degassed THF was carried out at -78^{0}C followed by stirring overnight at room temperature. The resulting orange solution was then treated with 0.5 equivalents of [Ru(*p*-cymene)Cl_2]$_2$ in degassed THF at -78^{0}C followed by stirring overnight at room temperature. The crude mixture was filtered, evaporated, dissolved in DCM, filtered again through Celite® and following preparative TLC found to afford, surprisingly, a 12-vertex/12-vertex ruthenacarborane/carborane species instead of a 13-vertex/12-vertex ruthenacarborane/carborane species, in 2-3% yield.

The yellow product obtained by TLC was fully characterised by mass spectrometry, microanalysis, ^{1}H and ^{11}B NMR spectroscopies and *X*-ray crystallography.

Mass spectrometry of compound **1** shows the parent ion to have a mass of 510.3 with a broad heteroborane envelope from 503.3 to 514.3 whilst elemental analysis was in good agreement with the values expected for $C_{14}H_{35}B_{19}Ru$.

In the ^{1}H NMR spectrum of compound **1** the four H atoms of the *p*-cymene ring appear as a multiplet between δ 6.45 ppm and δ 6.25 ppm. Two singlets at δ 4.65 ppm (1H) and δ 4.30 ppm (1H) are assigned to the two protons of the cages. The apparent septet at δ 3.05 ppm (1H), the singlet at δ 2.50 ppm (3H) and multiplet at δ 1.40 (6H) ppm are assigned to the C*H*$(CH_3)_2$, C*H*$_3$ and CH(C*H*$_3$)$_2$ groups of the *p*-cymene ligand respectively.

$^{11}B\{^{1}H\}$ NMR spectroscopy revealed twelve resonances at δ 2.07, -0.42, -3.19, -3.94, -4.86, -7.92, -8.75, -9.66, -11.05, -13.21, -14.58 and -17.79 in the relative ratio 1:1:1:1:1:3:2:2:2:2:1:2.

X-ray diffraction quality yellow plates of compound **1** were grown by vapour diffusion of a DCM solution and 40-60 petroleum ether at room temperature. An *X*-ray diffraction study confirmed compound **1** to be 1-(1′-1′,2′-*closo*-$C_2B_{10}H_{11}$)-3-(η-cymene)-3,1,2-*closo*-$RuC_2B_9H_{10}$ (Fig 2.3). The *p*-cymene ligand attached to metal in the first cage is bent towards B7 and B8 and away from the second cage by 16.04^0 with respect to the planer B5 ring B5-B6-B11-B12-B9 to minimize steric hindrance. This is the first reported example of a icosahedral bis(heteroborane) derived from 1,1′-bis(*o*-carborane).

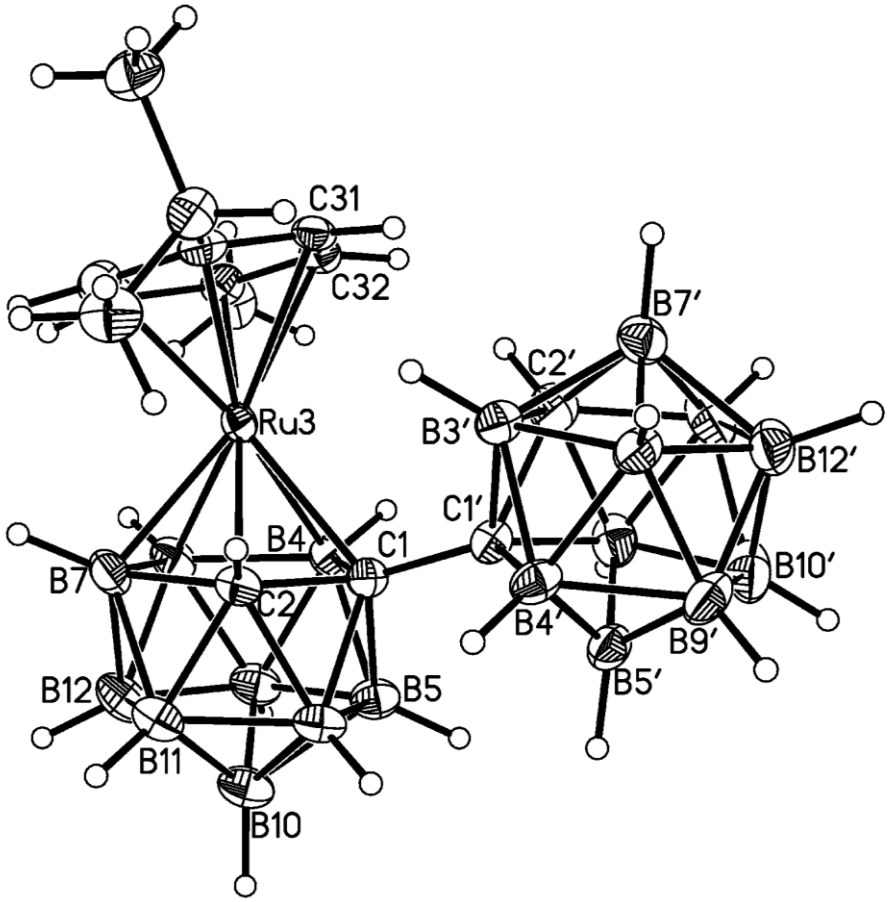

Fig 2.3 Structure of 1-(1′-1′,2′-*closo*-$C_2B_{10}H_{11}$)-3-(η-cymene)-3,1,2-*closo*-$RuC_2B_9H_{10}$

In the solid state the cages of compound **1** have approximately icosahedral geometry with degree five vertices occupied by all the atoms in both cages. Ru3 is capping the upper belt of the metallacarborane cage. The carbon atoms in the metallacarborane cage remain adjacent to the metal and each other. The ruthenacarborane and carborane cages are connected *via* C1 and C1′ atoms.

The longest B-B connectivity in the ruthenacarborane cage is 1.827(4) Å between B7-B8 while the shortest one is between B6-B11 with a length of 1.749(5) Å. The ruthenium to carbon distances are 2.212(3) Å to C2 and 2.272(3) Å to C1 and Ru3-B7, Ru3-B4 and Ru3-B8 distances are 2.203(3) Å, 2.212(3) Å and 2.220(3) Å respectively.

X-ray diffraction study and mass spectrometry clearly shows that the compound is a single cage metallated 12-vertex/12-vertex derivative of 1,1′-bis(*o*-carborane). Therefore in order to discover if the surprising result of a 12-vertex/12-vertex metallacarborane/carborane was the result of steric crowding we repeated the experiment with $[Ru(C_6H_6)Cl_2]_2$ and $NaCp/CoCl_2$.

2.3 Preparation of 1-(1′-1′,2′-*closo*-$C_2B_{10}H_{11}$)-3-(η-benzene)-3,1,2-*closo*-$RuC_2B_9H_{10}$ (2)

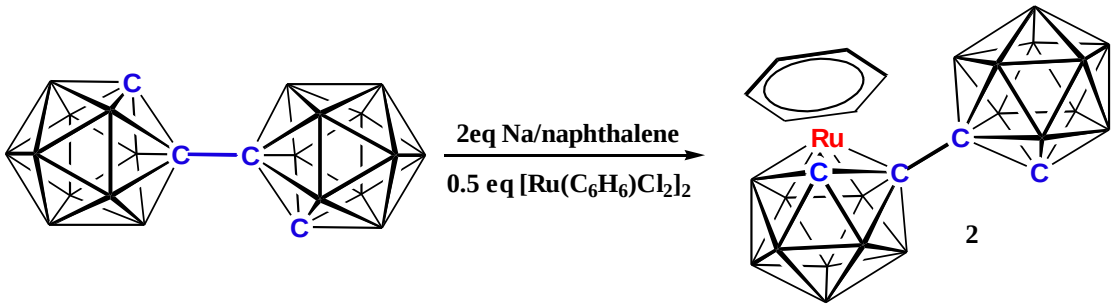

2

Compound **2** was prepared by treatment of a degassed THF solution of 1,1′-bis(*o*-carborane) with two equivalents of sodium naphthalenide in degassed THF at -78^{0}C and then stirred overnight at room temperature. Addition of the orange solution to $[Ru(C_6H_6)Cl_2]_2$ in degassed THF at -78^{0}C resulted in a dark brown suspension which was then stirred overnight at room temperature. The solvent was removed *in vacuo* and the resulting brown solid was dissolved in DCM and filtered through Celite®.

The yellow product is formed in 2-3% yield after work up involving preparative TLC and crystallisation from diffusion of a $CDCl_3$ solution and 40-60 petroleum ether at room temperature. However the two electron reduction once again affords a 12-vertex/12-vertex ruthenacarborane/carborane species. The product was then fully characterised by mass spectrometry, microanalysis, ^{1}H and ^{11}B NMR spectroscopies and *X*-ray diffraction study.

Mass spectrometry of compound **2** shows the parent ion to have a mass of 454.3 with a broad heteroborane envelope from 448.3 to 458.3 whilst elemental analysis gave results close to those calculated for $C_{10}H_{27}B_{19}Ru$.

^{1}H NMR spectroscopy consists of one resonance of intensity six at δ 6.60 ppm which assigned to the C_6H_6 ligand and two different signals of intensity one at δ 4.65 ppm and δ 4.60 ppm corresponding to CH_{cage}.

^{11}B{^{1}H} NMR spectroscopy consists of twelve signals at δ 1.67, 0.09, -3.17, -3.85, -6.28, -7.83, -8.79, -9.25, -11.13, -13.19, -14.67 and -17.83 ppm with integrals in the relative ratio 1:1:1:1:1:3:2:2:2:2:1:2.

An *X*-ray diffraction study reveals the molecular structure of compound **2** to be 1-(1′-1′,2′-*closo*-$C_2B_{10}H_{11}$)-3-(η-C_6H_6)-3,1,2-*closo*-$RuC_2B_9H_{10}$ (Fig 2.4). Both adjacent carbon atoms and the metal form one triangular face in the metallacarborane icosahedron and we observe that the C_6H_6 ligand attached to the ruthenium metal is bent away (similar to the situation in **1**) from the carborane cage by 16.30° with respect to the lower pentagonal belt of the metallacarborane cage B5-B6-B11-B12-B9.

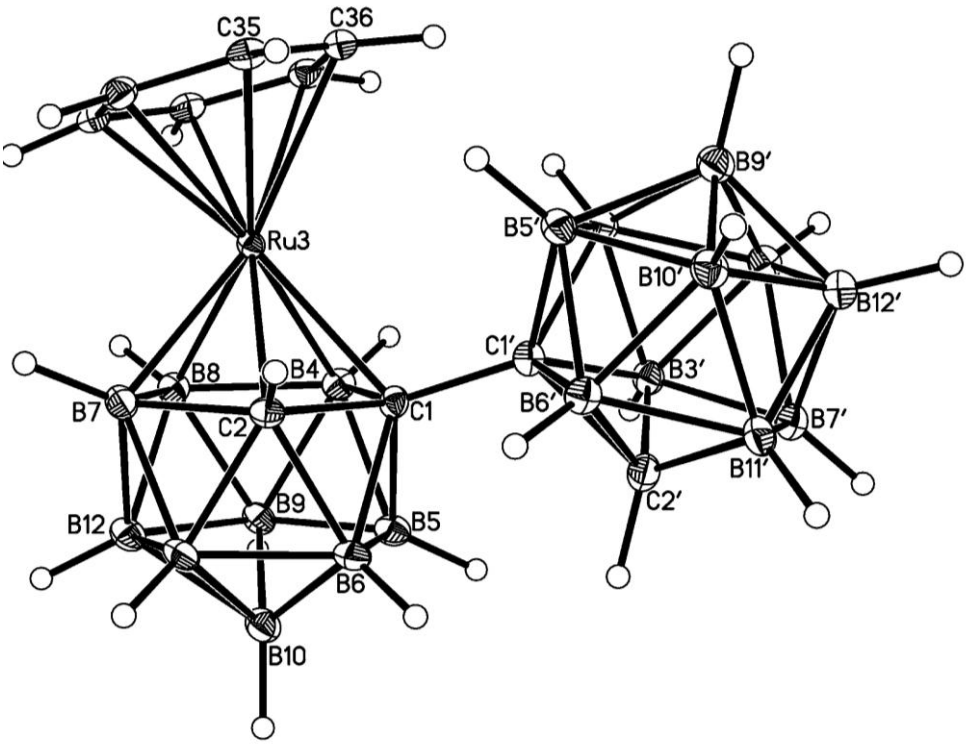

Fig 2.4 Molecular structure of 1-(1′-1′,2′-*closo*-$C_2B_{10}H_{11}$)-3-(η-C_6H_6)-3,1,2-*closo*-$RuC_2B_9H_{10}$

2.4 Preparation of 1-(1′-1′,2′-*closo*-$C_2B_{10}H_{11}$)-3-(η-C_5H_5)-3,1,2-*closo*-$CoC_2B_9H_{10}$ (3)

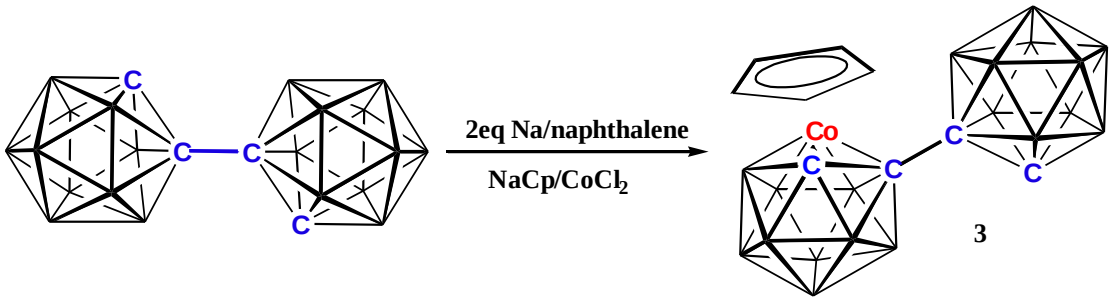

Two electron reduction of 1,1′-bis(*o*-carborane) with sodium in degassed THF in the presence of naphthalene followed by the addition of excess $NaCp/CoCl_2$ in degassed THF at -78°C results in a dark brown suspension which was stirred overnight, then subjected to aerial oxidation and filtration, followed by preparative thin layer chromatography to give an orange coloured 12-vertex/12-vertex cobaltacarborane/carborane in 3.8% yield.

Cp^-, $[C_4B_{19}H_{22}]^{2-}$ and Co^{2+} initially produces an anionic 19 electron species which is, on oxidation, converted to the neutral 18 electron product. This argument is consistent with experimental observation. On application to a TLC plate the neutral species will move whereas the anionic intermediate will remain with the base line of the plate thus limiting the yield of product obtained. Therefore, prior oxidation of Co^{II} to Co^{III} is an important step in the synthesis of cyclopentadienyl cobaltacarboranes.

The product was purified by preparative thin layer chromatography and fully characterised by mass spectrometry, microanalysis, ^1H and ^{11}B NMR spectroscopies and single-crystal *X*-ray diffraction study.

Mass spectrometry of compound **3** shows the parent ion to have a mass of 399.2 with a broad heteroborane envelope from 395.3 to 401.3. Unfortunately elemental analysis was never in good agreement with the expected values for $C_9H_{26}B_{19}Co$ even following repeated crystallization.

^{1}H NMR spectroscopy reveals one resonance at δ 6.10 ppm of relative intensity five which is assigned to the C_5H_5 ligand and two different signals of intensity one at δ 4.75 ppm and δ 4.65 ppm corresponding to CH_{cage}.

$^{11}B\{^{1}H\}$ NMR spectroscopy consists of thirteen signals at δ 5.28, 0.87, -2.50, -3.51, -4.21, -5.32, -8.40, -9.60, -10.44, -11.75, -12.86, -15.07 and -16.41 ppm with integrals in the ratio 1:1:1:2:1:1:2:3:2:1:2:1:1.

X-ray quality single crystals of orange compound 1-(1′-1′,2′-*closo*-$C_2B_{10}H_{11}$)-3-(η-C_5H_5)-3,1,2-*closo*-$CoC_2B_9H_{10}$ (**3**) (Fig 2.5) were obtained by vapour diffusion of a CH_2Cl_2 solution and 40-60 petroleum ether at room temperature.

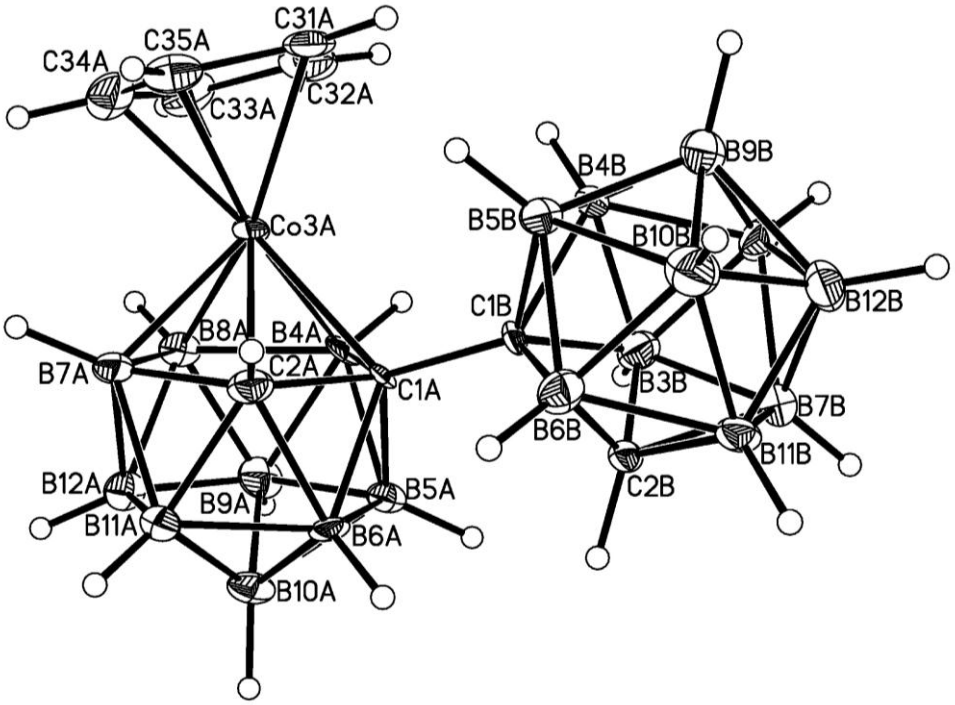

Fig 2.5 Molecular structure of 1-(1′-1′,2′-*closo*-$C_2B_{10}H_{11}$)-3-(η-C_5H_5)-3,1,2-*closo*-$CoC_2B_9H_{10}$

The crystal structure revealed the presence of two crystallographically independent molecules **(3AB** and **3CD)** (Fig 2.6) in the asymmetric fraction of the unit cell. We observe that the C_5H_5 ligand is bent away from the carborane cage with respect to the lower pentagonal belt of the cobaltacarborane cage, B5-B6-B11-B12-B9 by 16.43° and 16.26° respectively. This is similar to the situation in compounds **1** and **2**.

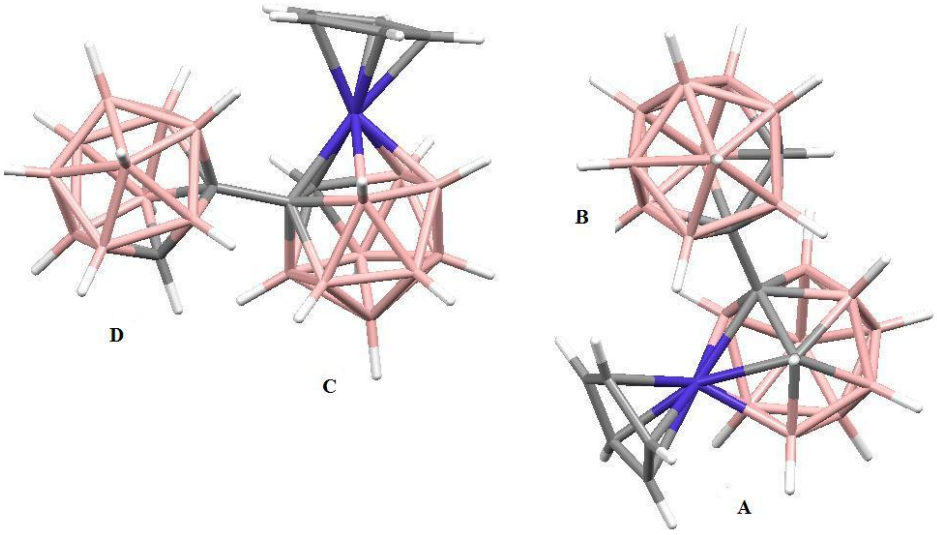

Fig 2.6 Two independent molecules in the asymmetric fraction of the unit cell

In the solid state the molecules of compounds **3AB** and **3CD** are linked icosahedra with degree five vertices occupied by all the atoms in the cobaltacarborane and carborane cages.

The longest connectivities in the metallacarborane cages are formed by the Co3 atom, and range from 2.118(11) Å to 2.072(12) Å in **3AB** and 2.118(11) Å to 2.043(11) Å in **3CD.** The bond lengths in the cobaltacarborane cage are comparable in both molecules except for C1-B4 and B4-B8 which are 1.750(16) Å and 1.827(19) Å in **3AB** and 1.667(16) Å and 1.740(2) Å in **3CD**.

2.5 Discussion

The compounds 1-(1′-1′,2′-*closo*-$C_2B_{10}H_{11}$)-3-(η-cymene)-3,1,2-*closo*-$RuC_2B_9H_{10}$ (**1**), 1-(1′-1′,2′-*closo*-$C_2B_{10}H_{11}$)-3-(η-C_6H_6)-3,1,2-*closo*-$RuC_2B_9H_{10}$ (**2**) and 1-(1′-1′,2′-*closo*-$C_2B_{10}H_{11}$)-3-(η-C_5H_5)-3,1,2-*closo*-$CoC_2B_9H_{10}$ (**3**) were synthesised by two electron reduction of 1,1′-bis(*o*-carborane) with sodium naphthalenide in degassed THF followed by metallation at room temperature with {(arene)Ru}fragments for compounds **1** and **2** and with the {CpCo} fragment for compound **3**. All three compounds were fully characterised by mass spectrometry, elemental analysis, ^{1}H NMR spectroscopy, ^{11}B NMR spectroscopy and *X*-ray diffraction studies.

Mass spectrometry and *X*-ray diffraction studies of compound **1** confirmed that the two electron reduction followed by metallation affords a 12-vertex/12-vertex metallacarborane/carborane species instead of a 13-vertex/12-vertex metallacarborane/carborane species.

The experiment was repeated with $[Ru(C_6H_6)Cl_2]_2$ and $NaCp/CoCl_2$ in order to discover if the surprising result of a 12-vertex/12-vertex metallacarborane/carborane was the result of steric crowding. However compounds **2** and **3** once again proved that the two electron reduction of 1,1′-bis(*o*-carborane) results in a decapitation product rather than an expansion product.

As noted in the introduction (**2.1**) the reason behind this is most likely due to the fact that stoichiometric two electron reduction does not take place on a single cage. In 1,1′-bis(*o*-carborane) the cages are connected through a carbon-carbon sigma bond and therefore, during the two electron reduction, rather than reducing a single cage the two electrons will distribute themselves in both cages, and both cages are partially opened so we end up with $[C_2B_{10}H_{11}]^-/[C_2B_{10}H_{11}]^-$ species.

Therefore we can come to the conclusion that cage expansion is not possible with only 2 electrons and instead we find the unexpected deboronation. Compounds **1**, **2** and **3** are the first reported example of a 12-vertex/12-vertex metallacarborane/carborane species synthesised from 1,1′-bis(*o*-carborane).

2.5.1 NMR spectroscopic studies

All the compounds, 1-(1′,2′-*closo*-$C_2B_{10}H_{11}$)-3-(η-$C_{10}H_{14}$)-3,1,2-*closo*-$RuC_2B_9H_{10}$ (**1**), 1-(1′,2′-*closo*-$C_2B_{10}H_{11}$)-3-(η-C_6H_6)-3,1,2-*closo*-$RuC_2B_9H_{10}$ (**2**) and 1-(1′,2′-*closo*-$C_2B_{10}H_{11}$)-3-(η-C_5H_5)-3,1,2-*closo*-$CoC_2B_9H_{10}$ (**3**) in this chapter are characterised by ^1H and $^{11}B\{^1H\}$ NMR spectroscopies.

The species 3-(η-$C_{10}H_{14}$)-3,1,2-*closo*-$RuC_2B_9H_{11}$[10] is C_s symmetric in solution because the *p*-cymene ligand attached to the metal appears as a doublet for $CH(CH_3)_2$ and septet for $CH(CH_3)_2$. However, in compound **1** the *p*-cymene ligand attached to the metal displays a multiplet for $CH(CH_3)_2$ and apparent septet for $CH(CH_3)_2$ (this may be due to the coincidence of 2 quartets). This implies that both CH_3 groups attached to the CH group are not magnetically equivalent therefore the ^1H NMR confirms the overall asymmetry of compound **1**. In compounds **2** and **3** the ligands display only one resonance due to the symmetric C_6H_6 and C_5H_5 ring respectively and this observation clearly indicates the free rotation of these rings in solution.

Compound	**C*H*cage**
1,2-*closo*-carborane	4.44
1,1′-bis(*o*-carborane)	5.02
3-(η-$C_{10}H_{14}$)-3,1,2-*closo*-$RuC_2B_9H_{11}$[11]	3.95
1-(1′-1′,2′-*closo*-$C_2B_{10}H_{11}$)-3-(η-$C_{10}H_{14}$)-3,1,2-*closo*-$RuC_2B_9H_{10}$ (**1**)	4.65, 4.30
1-(1′-1′,2′-*closo*-$C_2B_{10}H_{11}$)-3-(η-C_6H_6)-3,1,2-*closo*-$RuC_2B_9H_{10}$ (**2**)	4.65, 4.60
1-(1′-1′,2′-*closo*-$C_2B_{10}H_{11}$)-3-(η-C_5H_5)-3,1,2-*closo*-$CoC_2B_9H_{10}$ (**3**)	4.65, 4.75

Table 2.1 CH_{cage} signals

In compound **1** the CH_{cage} resonances are shifted to lower frequencies compared to that in 1,1′-bis(*o*-carborane) and from the data in table 2.1 we can confidently suggest that the singlet at δ 4.30 ppm is due to the metallacarborane {3,1,2-$RuC_2B_9H_{10}$} fragment and at δ 4.65 ppm is due to the carborane {1′,2′-$C_2B_{10}H_{11}$} fragment with respect to the CH_{cage} chemical shifts in 1,2-*closo*-carborane[11] and 3-(η-$C_{10}H_{14}$)-3,1,2-*closo*-$RuC_2B_9H_{11}$[11]. But in compounds **2** and **3** the CH_{cage} signals are much closer to each other therefore it is very difficult to assign them.

The weighted average ^{11}B NMR chemical shifts of 1,2-*closo*-carborane, 1,1′-bis(*o*-carborane) and its metallacarboranes derivatives, 1-(1′-1′,2′-*closo*-$C_2B_{10}H_{11}$)-3-(η-$C_{10}H_{14}$)-3,1,2-*closo*-$RuC_2B_9H_{10}$ (**1**), 1-(1′-1′,2′-*closo*-$C_2B_{10}H_{11}$)-3-(η-C_6H_6)-3,1,2-*closo*-$RuC_2B_9H_{10}$ (**2**) and 1-(1′-1′,2′-*closo*-$C_2B_{10}H_{11}$)-3-(η-C_5H_5)-3,1,2-*closo*-$CoC_2B_9H_{10}$ (**3**) are given in table 2.2.

Compound	**Ratio**	**$<\delta^{11}B>$**
1,2-*closo*-carborane	2:2:4:2	-10.9
1,1′-bis(*o*-carborane)	2:2:6:6:4	-9.1
Compound (**1**)	1:1:1:1:1:3:2:2:2:2:1:2	-8.9
Compound (**2**)	1:1:1:1:1:3:2:2:2:2:1:2	-8.9
Compound (**3**)	1:1:1:2:1:1:2:3:2:1:2:1:1	-7.8

Table 2.2 $<\delta^{11}B>$ values for carboranes and metallacarboranes

The $^{11}B\{^1H\}$ NMR spectra of compounds **1** and **2** consist of twelve resonances in the ratio 1:1:1:1:1:3:2:2:2:2:1:2 and of compound **3** thirteen resonances in the relative ratio 1:1:1:2:1:1:2:3:2:1:2:1:1. Since **1**, **2** and **3** cannot possess anything other than C_1 symmetry this must be due to coincidence of some of the peaks.

The weighted average $^{11}B\{^1H\}$ chemical shift, $<\delta^{11}B>$, of 1,1′-bis(*o*-carborane) (-9.1 ppm) is deshielded compared to the equivalent value in 1,2-*closo*-carborane (-10.9 ppm). This may be due to the result of replacing an H substitution with a carborane cage which is more electron withdrawing than H.

Similarly, the weighted average chemical shifts of 12-vertex/12-vertex metallacarborane/carborane imply that replacing a boron atom of 1,1′-bis(*o*-carborane) with an {(arene)Ru} fragment shifts the spectra to higher frequencies and with a {CpCo} fragment the spectra are shifted to even higher frequencies. This suggests that the {CpCo} fragment has a more deshielding effect than the {(arene)Ru} fragment but that both are deshielding compared to {BH}.

The two dimensional $^{11}B\{^{1}H\}$-$^{11}B\{^{1}H\}$ correlation spectrum of compound **2** (Fig 2.7) was easily interpreted in terms of resonances which correspond to the metallacarborane and carborane cages individually, and the results obtained from this are summarised in a stick diagram (Fig 2.8) in which red and blue implies $\{RuC_2B_9\}$ and $\{C_2B_{10}\}$ fragments respectively.

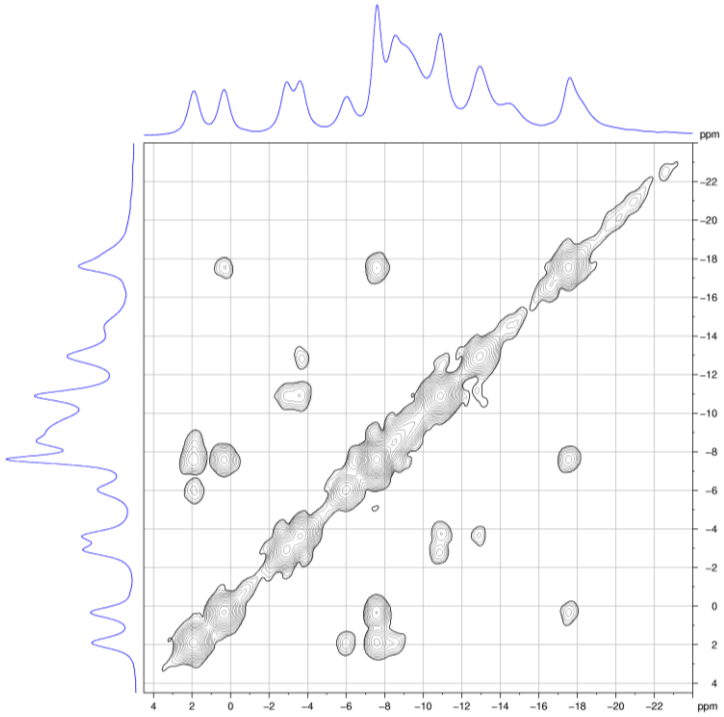

Fig 2.7 $^{11}B\{^{1}H\}$-$^{11}B\{^{1}H\}$ of compound 2

From the two dimensional $^{11}B\{^{1}H\}$-$^{11}B\{^{1}H\}$ correlation spectrum of compound **2** we can deduce that resonances at δ 1.67 (1B), 0.09 (1B),-6.28 (1B) -7.84 (3B), -8.79 (1B) and -17.83 (2B) resonances are due to the $\{RuC_2B_9\}$ fragment while those at δ -3.17 (1B), -3.85 (1B), -8.79 (1B), -9.25 (sh., 2B), -11.13 (2B), -13.19 (2B) and -14.67 (1B) are due to the $\{C_2B_{10}\}$ fragment.

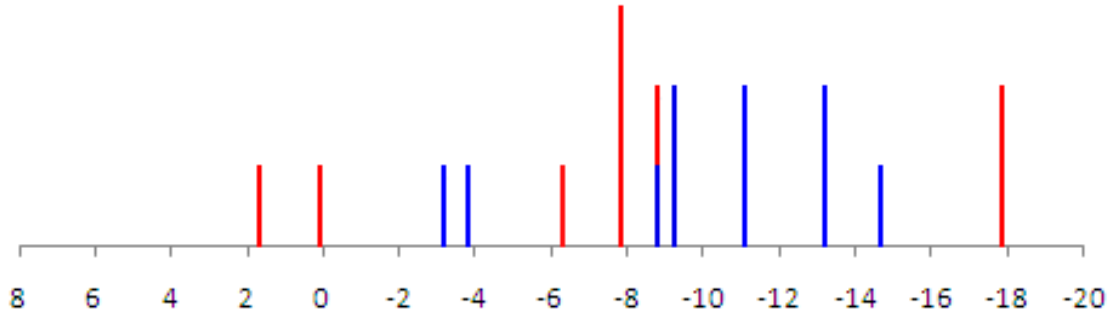

Fig 2.8 Stick diagram of the ^{11}B resonances of compound 2

Similarly to compound **2** the ^{11}B resonances of the analogous compound **1** can be assigned, because in both cases they have the same metal and show the same type of $^{11}B\{^{1}H\}$ NMR spectrum. Therefore the resonances at δ 2.07 (1B), -0.42 (1B), -4.86 (1B), -7.92 (3B), -8.75 (sh., 1B) and -17.79 (2B) correspond to the $\{RuC_2B_9\}$ fragment and the peaks at δ -3.19 (1B), -3.94 (1B), -8.75 (sh., 1B), -9.66 (2B), -11.05 (2B), -13.21 (2B) and -14.58 (1B) are assigned to the $\{C_2B_{10}\}$ fragment (Fig 2.9).

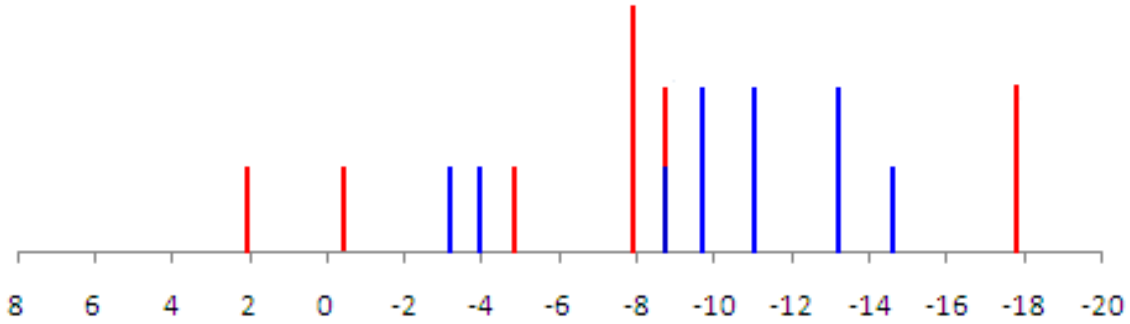

Fig 2.9 Stick diagram of the ^{11}B resonances of compound 1

Similarly to compound **2** the $^{11}B\{^{1}H\}$-$^{11}B\{^{1}H\}$ COSY spectrum of compound **3** was analysed to identify the resonances due to metallacarborane cage and carborane cage. The resonances at δ -15.07 (1B) and -16.41 (1B) ppm are assigned to the cobaltacarborane cage because generally metallacarboranes display a wide range of resonances. The resonance at δ -15.07 couples with 0.87 (1B) and -3.51 (2B) ppm therefore the boron atom at 0.87 and at least one of the boron atoms at -3.51 are assigned to the $\{CoC_2B_9\}$ cage fragment.

The resonance at δ -4.21 (1B) is assigned to the cobaltacarborane cage because it couples with the peak at 0.87 ppm which is part of the $\{CoC_2B_9\}$ cage fragment. The peak at δ -11.75 (1B) is also assigned to the $\{CoC_2B_9\}$ cage fragment because of its coupling with the resonances at δ -4.21 and 0.87 ppm. The resonance at δ -4.21 also couples to 5.28 and -5.32 couples to that at 5.28 therefore the resonances at δ 5.28 and -5.32 ppm are also due to the cobaltacarborane cage.

As with the resonance at -3.51 at least one of the boron atoms at δ -8.40 ppm is assigned to cobaltacarborane cage due to the coupling observed with the peak at 5.28. There are only nine boron atoms in the $\{CoC_2B_9\}$ cage fragment therefore only one boron atom from both δ -3.51 and -8.40 ppm are possible for the cobaltacarborane cage.

The resonance at δ -12.86 ppm is coupled with the resonances at δ -10.44 and -3.51 ppm and these resonances are assigned to the carborane cage and therefore there is a coincident present at -3.51 due to carborane and metallacarborane cages. The resonance at δ -10.44 ppm which corresponds to the carborane cage couples with the resonances at δ -3.51 and -2.50 ppm.

There are no couplings observed at δ -9.60 and -8.40 ppm due to carborane cage fragment. However we are confident about the assignment due to $\{CoC_2B_9\}$ cage fragment therefore the resonances at -9.60 (3B) and -8.40 (1B) are assigned to $\{C_2B_{10}\}$ fragment.

Therefore from the analysis of $^{11}B\{^1H\}$-$^{11}B\{^1H\}$ COSY spectrum for compound **3** (overleaf in fig 2.10) we can assign that the peaks at δ 5.28 (1B), 0.87 (1B), -4.21 (1B), -5.32 (1B), -11.75 (1B), -15.07 (1B) and -16.41 (1B) are due to the cobaltacarborane cage while the peaks at δ -2.50 (sh., 1B), -9.60 (3B), -10.44 (2B) and -12.86 (2B) are due to the carborane cage.

The stick diagram in fig 2.11 shows the assignments of $\{CoC_2B_9\}$ (red) and $\{C_2B_{10}\}$ (blue) fragments from the analysis of the two dimensional $^{11}B\{^1H\}$-$^{11}B\{^1H\}$ COSY spectrum.

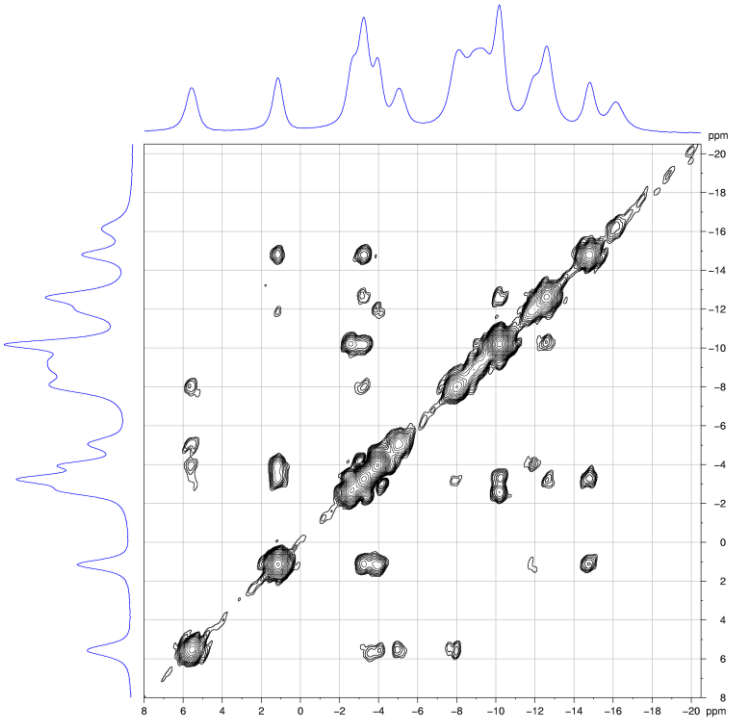

Fig 2.10 $^{11}B\{^{1}H\}$-$^{11}B\{^{1}H\}$ COSY spectrum of compound 3

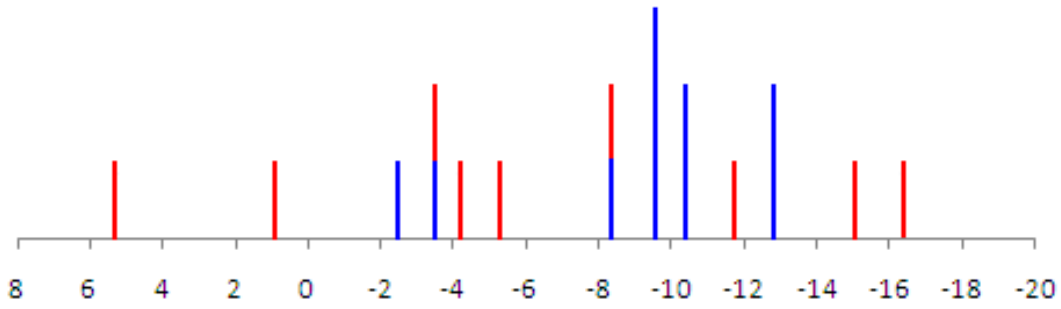

Fig 2.11 NMR stick diagram of the ^{11}B resonances of compound 3

The weighted average ^{11}B chemical shifts (<$\delta^{11}B$>) of 1,2-*closo*-carborane, 1,1′-bis(*o*-carborane), 3-*p*-cymene-3,1,2-*closo*-$RuC_2B_9H_{11}$, 3-Cp-3,1,2-*closo*-$CoC_2B_9H_{11}$ and the individual components of compounds **1**, **2** and **3** are given below in table 2.3 in order to discover how the chemical shifts of the individual components are changed with respect to the parent 1,2-*closo*-carborane and the metallacarborane derivatives[11]. Although the compounds 1,2-*closo*-carborane[12], 1,1′-bis(*o*-carborane)[2], 3-*p*-cymene-3,1,2-*closo*-$RuC_2B_9H_{11}$[10] and 3-Cp-3,1,2-*closo*-$CoC_2B_9H_{11}$[13] have been reported previously we synthesised them again and recorded their ^{11}B NMR spectra in $(CD_3)_2CO$ in order to maintain consistency.

Compound	**<δ^{11}B>**
1,2-*closo*-carborane	-10.9
1,1′-bis(*o*-carborane)	-9.1
3,1,2-*closo*-$RuC_2B_9H_{11}$	-10.5
3,1,2- $RuC_2B_9H_{10}$ (**1**)	-8.1
1′,2′-$C_2B_{10}H_{11}$ (**1**)	-9.8
3,1,2-$RuC_2B_9H_{10}$ (**2**)	-7.9
1′,2′-$C_2B_{10}H_{11}$ (**2**)	-9.8
3,1,2-*closo*-$CoC_2B_9H_{11}$	-8.2
3,1,2-$CoC_2B_9H_{10}$ (**3**)	-6.5
1′,2′-$C_2B_{10}H_{11}$ (**3**)	-9.0

Table 2.3 <δ^{11}B> shifts for conjoined cage compounds and their components

The data in table 2.3 clearly show for compounds **1** and **2** that <δ^{11}B> of both the fragments, {RuC_2B_9} and {C_2B_{10}}, are moved to higher frequencies, by ca. 2.5 ppm and 1.1 ppm respectively, with respect to the single cage components. This is comparable when conjoining two 1,2-*closo*-carboranes to produce 1,1′-bis(*o*-carborane) (<δ^{11}B> moves to high frequency from -10.9 (former) to -9.1 ppm (later)). A similar observation is made for compound **3**. The <δ^{11}B> values of {CoC_2B_9} and {C_2B_{10}} fragments move to higher frequencies, the former by 1.7 ppm and the later by ca. 2.0 ppm.

In all three cases the weighted average chemical shifts in the ^{11}B NMR spectra move to higher frequencies, which implies, overall that the boron nuclei in single cage metallated 1,1′-bis(*o*-carboranes) are deshielded compared to their individual components.

DFT calculations were carried out on 1,2-*closo*-$C_2B_{10}H_{12}$ and 1,1′-bis(*o*-carborane) to support the above results. We are grateful to Dr. D. McKay for these calculations. From these calculations it is clear that there is effectively no preference in 1,1′-bis(*o*-carborane) between conformations with C-C-C-C torsion angles of 108° and 180° (Fig 2.12)[11].

The 108^0 conformation is favoured by 0.2 kcal mol^{-1} in terms of only the electronic energy, whereas if zero point energy is included the 108^0 conformation is preferred by 0.5 kcal mol^{-1} and the energy barrier to free rotation about the C-C′ bond is only ca. 10 kcal mol^{-1}.

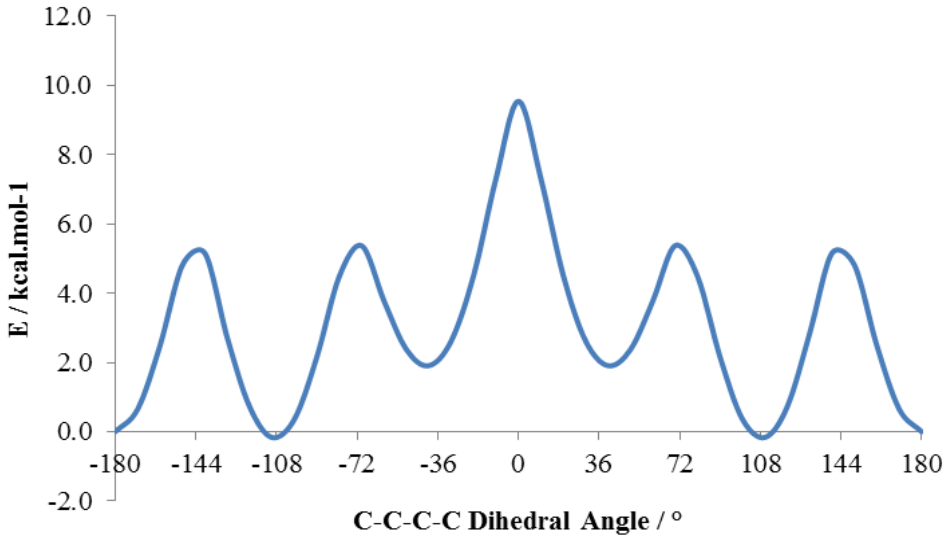

Fig 2.12 Plot of energy vs. dihedral angle for 1,1′-bis(*o*-carborane)

(a) 1,2-*closo*-$C_2B_{10}H_{12}$

Atom	Charge
C1, C2	-0.56
B3, B6	0.13
B4, B5, B7, B11	-0.03
B8, B10	-0.19
B9, B12	-0.17
H1, H2	0.36
H3, H6	0.08
H4, H5, H7, H11	0.10
H8, H10	0.11
H9, H12	0.10

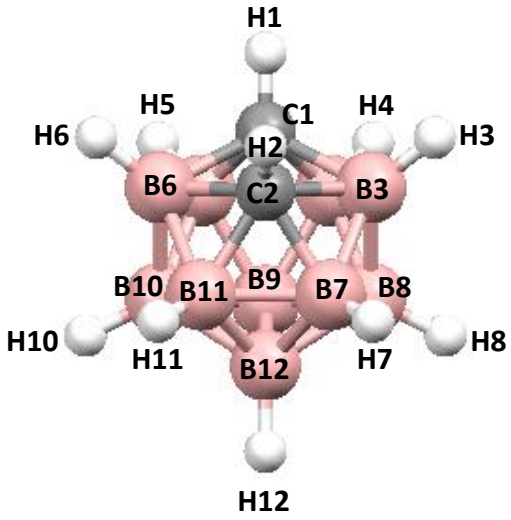

(b) 1,1′-bis(*o*-carborane)

Atom	Charge
C1	-0.31
C2	-0.51
B3, B6	0.15
B4, B5	-0.01
B7, B11	-0.01
B8, B10	-0.18
B9	-0.16
B12	-0.14
H2	0.32
H3, H6	0.08
H4, H5	0.08
H7, H11	0.09
H8, H10	0.10
H9	0.10
H12	0.09

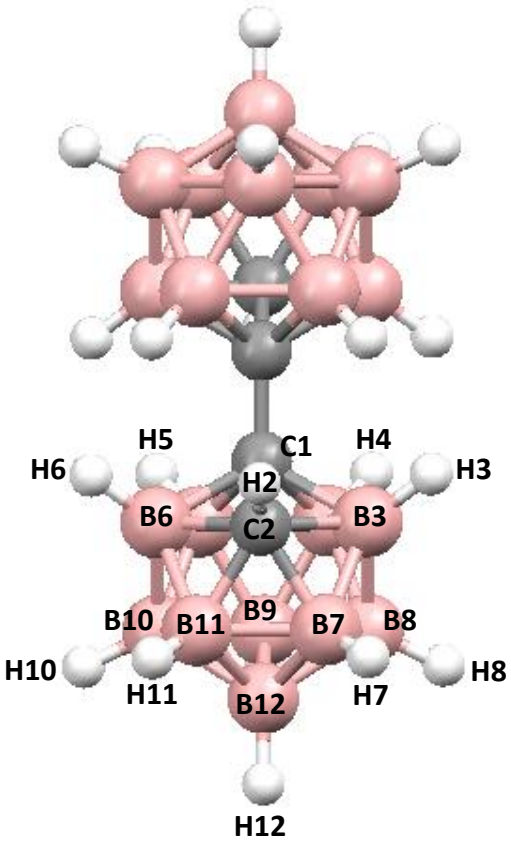

Table 2.4 Natural atomic charges in 1,2-*closo*-$C_2B_{10}H_{12}$ and 1,1′-bis(*o*-carborane) (180° conformation) by DFT calculation.

Table 2.4 gives atomic charges calculated and clearly shows that for 1,2-*closo*-$C_2B_{10}H_{12}$ the C atoms carry a charge of -0.56 and the B atoms an average charge of -0.06. H bonded to C is 0.36 whilst the average charge of H bonded to B is 0.10. In 1,1′-bis(*o*-carborane) the negative charge on both C atoms decreases by 0.25 in C1 and 0.05 in C2. The change is larger in C1 due to the fact that C1 is connected to the {$C_2B_{10}H_{11}$} fragment. The B atoms are also less negative in 1,1′-bis(*o*-carborane) with an average charge -0.04. The remaining C-bonded H atom carries a charge of 0.32 and the average charge on H bound to B is 0.09.

Thus substitution of one of the C-bound H atoms in 1,2-*closo*-$C_2B_{10}H_{12}$ by a {1′,2′-*closo*-$C_2B_{10}H_{11}$} unit causes all the atoms in the original cage to become more positively charged because the $C_2B_{10}H_{11}$ substituent is electron-withdrawing compared to H. At the same time there is an opposite, but smaller, change in the charges on the H atoms bonded to the cage atoms, which become slightly less positively charged.

Overall, it is clear that replacement of H1 (with a charge of 0.36 in 1,2-*closo*-$C_2B_{10}H_{12}$) by an overall electroneutral substituent causes a reduction in negative charge of the original cage. The changes in atomic charges are small in most cases but we believe that it is significant that they can be experimentally reproduced by changes in weighted average chemical shifts. In particular, $<\delta^{11}B>$ represents a convenient measure of monitoring subtle electronic changes in (hetero)carboranes and has proved useful in this respect on several occasions[14].

2.5.2 *X*-ray diffraction studies

X-ray diffraction studies of all three compounds, 1-(1′-1′,2′-*closo*-$C_2B_{10}H_{11}$)-3-(η-$C_{10}H_{14}$)-3,1,2-*closo*-$RuC_2B_9H_{10}$ (**1**), 1-(1′-1′,2′-*closo*-$C_2B_{10}H_{11}$)-3-(η-C_6H_6)-3,1,2-*closo*-$RuC_2B_9H_{10}$ (**2**) and 1-(1′-1′,2′-*closo*-$C_2B_{10}H_{11}$)-3-(η-C_5H_5)-3,1,2-*closo*-$CoC_2B_9H_{10}$ (**3**) confirm that two electron reduction of 1,1′-bis(*o*-carborane) followed by metallation yields an unexpected 12-vertex/12-vertex metallacarborane/carborane species instead of a 13-vertex/12-vertex metallacarborane/carborane species, and that in all three cases the ligand attached to the metal is bent away from the pendant carborane cage to avoid steric hindrance (Fig 2.13).

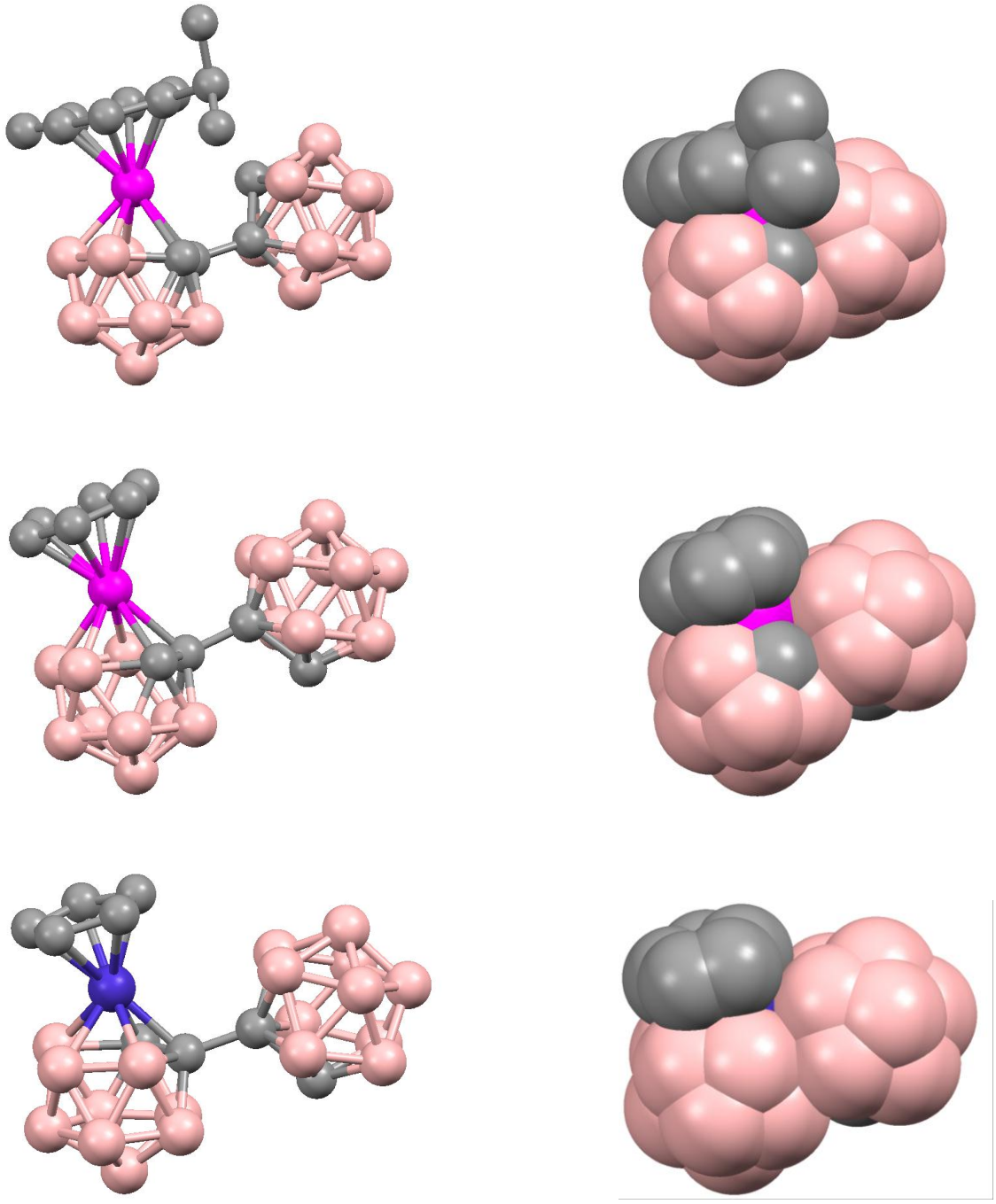

Fig 2.13 Ball and stick and space fill views of compounds 1, 2 and 3

The inclination of the ligand attached to the metal in the cage is quantified by θ. This is defined as the dihedral angle between the least-squares plane through the lower belt of the five B atoms face, B5B6B11B12B9, and the plane through the C atoms in the ring of the ligand. Measured values of θ in metallated 1,2-*closo*-carborane and metallated 1,1′-bis(*o*-carborane) are given in table 2.5.

Compound	**θ**
3-(η-cymene)-3,1,2-*closo*-$RuC_2B_9H_{11}$[10]	3.26
1-(1′-1′,2′-*closo*-$C_2B_{10}H_{11}$)-3-(η-cymene)-3,1,2-*closo*-$RuC_2B_9H_{10}$ (**1**)	16.04
1-(1′-1′,2′-*closo*-$C_2B_{10}H_{11}$)-3-(η-C_6H_6)-3,1,2-*closo*-$RuC_2B_9H_{10}$ (**2**)	16.30
3-(η-C_5H_5)-3,1,2-*closo*-$CoC_2B_9H_{11}$[15]	2.18
1-(1′-1′,2′-*closo*-$C_2B_{10}H_{11}$)-3-(η-C_5H_5)-3,1,2-*closo*-$CoC_2B_9H_{10}$ (**3AB**)	16.43
1-(1′-1′,2′-*closo*-$C_2B_{10}H_{11}$)-3-(η-C_5H_5)-3,1,2-*closo*-$CoC_2B_9H_{10}$ (**3CD**)	16.26

Table 2.5 Dihedral angles in metallated 1,2-*closo*-carborane and metallated 1,1′-bis(*o*-carborane)

The θ values in 12-vertex/12-vertex metallacarborane/carboranes are much greater than those in corresponding 12-vertex metallacarborane species because in all three cases the hydrogen atom attached to carbon 1 in the 12-vertex metallacarborane is replaced by a sterically more crowded carborane cage.

The values of θ do not change when moving from $\{(arene)Ru\}^{2+}$ to $\{CpCo\}^{2+}$ which suggests that the tilting is not influenced by the size of the metal.

Table 2.6 shows by how much each atom in the structure of the individual components of compounds **1**, and **3** has deviated with respect to the parent compounds[10, 15]. The overall deviation is larger in $\{MC_2B_9\}$ fragments compared to the $\{C_2B_{10}\}$ fragments. In $\{MC_2B_9\}$ fragments atoms C1 and M3 deviate more than the other atoms because H on C1 is replaced by a $\{C_2B_{10}\}$ fragment which causes the tilting of the ligand attached to M3.

Compound **1**				Compound **2**			
{RuC_2B_9}	dev.	{C_2B_{10}}	dev.	{RuC_2B_9}	dev.	{C_2B_{10}}	dev.
C1	0.066	C1′	0.051	C1	0.080	C1′	0.058
C2	0.037	C2′	0.056	C2	0.031	C2′	0.022
Ru3	0.082	B3′	0.038	Ru3	0.079	B3′	0.010
B4	0.032	B4′	0.014	B4	0.033	B4′	0.026
B5	0.024	B5′	0.042	B5	0.030	B5′	0.006
B6	0.036	B6′	0.016	B6	0.025	B6′	0.008
B7	0.012	B7′	0.007	B7	0.014	B7′	0.020
B8	0.020	B8′	0.009	B8	0.010	B8′	0.014
B9	0.009	B9′	0.009	B9	0.013	B9′	0.012
B10	0.025	B10′	0.006	B10	0.024	B10′	0.010
B11	0.014	B11′	0.017	B11	0.008	B11′	0.015
B12	0.007	B12′	0.015	B12	0.015	B12′	0.022
overall	0.037	overall	0.029	Overall	0.038	overall	0.023

Compound **3** (**AB**)				Compound **3** (**CD**)			
{CoC_2B_9}	dev.	{C_2B_{10}}	dev.	{CoC_2B_9}	dev.	{C_2B_{10}}	dev.
C1	0.087	C1′	0.059	C1	0.071	C1′	0.066
C2	0.052	C2′	0.015	C2	0.040	C2′	0.022
Co3	0.092	B3′	0.024	Co3	0.089	B3′	0.020
B4	0.029	B4′	0.014	B4	0.075	B4′	0.010
B5	0.014	B5′	0.022	B5	0.043	B5′	0.017
B6	0.047	B6′	0.021	B6	0.027	B6′	0.020
B7	0.024	B7′	0.022	B7	0.025	B7′	0.040
B8	0.016	B8′	0.038	B8	0.026	B8′	0.006
B9	0.021	B9′	0.020	B9	0.013	B9′	0.018
B10	0.015	B10′	0.031	B10	0.040	B10′	0.031
B11	0.033	B11′	0.016	B11	0.021	B11′	0.021
B12	0.020	B12′	0.013	B12	0.020	B12′	0.013
overall	0.045	overall	0.027	Overall	0.047	overall	0.028

Table 2.6 Rms deviations (Å) between the {MC_2B_9}, {C_2B_{10}} or {C_2B_9} "components" of compounds 1-3 and these fragments in single cage reference compounds.

2.5.3 Cage connectivities

The cage connectivity distances of 1-(1′-1′,2′-*closo*-$C_2B_{10}H_{11}$)-3-(η-cymene)-3,1,2-*closo*-$RuC_2B_9H_{10}$ (**1**), 1-(1′-1′,2′-*closo*-$C_2B_{10}H_{11}$)-3-(η-benzene)-3,1,2-*closo*-$RuC_2B_9H_{10}$ (**2**) and 1-(1′-1′,2′-*closo*-$C_2B_{10}H_{11}$)-3-(η-C_5H_5)-3,1,2-*closo*-$CoC_2B_9H_{10}$ (**3AB** and **3CD**) are listed in table 2.7.

The metallated cages of compounds **1** and **2** are icosahedral with Ru3 capping the upper belt of the carborane. In compounds **3AB** and **3CD** the capping is by Co3. The C atoms in the metallacarborane cages are adjacent to the metal atoms and each other. In all four cases the top belt of the metallacarborane cage is connected to the carborane cage through C1 and C1′ with C1-C1′ distances of 1.547(3), 1.550(3), 1.548(13) (**AB**) and 1.554(15) Å (**CD**) respectively; these values are longer than the corresponding distance in 1,1′-bis(*o*-carborane) (1.530(3) Å)[2], again reflecting the steric overcrowding in compounds **1**, **2** and **3**. The longest bonds in the cages are to Ru in **1** and **2** and Co in **3AB** and **3CD**. The shortest bonds are between the C1 and C2 atoms in all four metallacarborane cages.

The M-cage atom connectivities of compound **1** are longer than the corresponding distance of compound **2** except for Ru3-B4. The average M-cage atom distance in compound **1** is 2.224 Å whereas in compound **2** the average distance of 2.216 Å. This may be due to the fact that the size of the ligand which is attached to the Ru metal has reduced when we move from compound **1** to compound **2**.

The average M-cage atom distance of compounds **3AB** and **3CD** are 2.0844 Å in **3AB** and 2.0762 Å in **3CD**, which are shorter than those in compounds **1** and **2**. This is because the second row transition metal has been replaced by a first row transition metal.

The torsion angle M-C-C-C in compounds **2**, **3AB** and **3CD** is $175.9(2)^0$, $179.7(7)^0$ and $176.4(7)^0$ respectively, close to 180°. However in compound **1** the corresponding torsion angle is only 34.7(2)°.

	1	**2**		**1**	**2**
M(3)-B(7)	2.203(3)	2.187(2)	C(1′)-C(2′)	1.669(4)	1.679(3)
M(3)-B(4)	2.212(3)	2.225(2)	C(1′)-B(5′)	1.712(4)	1.717(3)
M(3)-C(2)	2.212(3)	2.192(2)	C(1′)-B(3′)	1.715(4)	1.757(3)
M(3)-B(8)	2.220(3)	2.207(2)	C(1′)-B(4′)	1.731(4)	1.730(3)
M(3)-C(1)	2.272(3)	2.270(2)	C(1′)-B(6′)	1.738(4)	1.747(3)
C(1)-C(1′)	1.547(3)	1.550(3)	C(2′)-B(7′)	1.728(4)	1.705(3)
C(1)-C(2)	1.644(4)	1.661(3)	C(2′)-B(11′)	1.728(5)	1.699(3)
C(1)-B(5)	1.736(4)	1.742(3)	C(2′)-B(6′)	1.728(4)	1.724(3)
C(1)-B(4)	1.747(4)	1.739(3)	C(2′)-B(3′)	1.737(4)	1.722(3)
C(1)-B(6)	1.753(4)	1.768(3)	B(3′)-B(4′)	1.752(4)	1.772(3)
C(2)-B(11)	1.722(4)	1.714(3)	B(3′)-B(8′)	1.757(4)	1.777(3)
C(2)-B(6)	1.746(4)	1.744(3)	B(3′)-B(7′)	1.774(5)	1.795(4)
C(2)-B(7)	1.745(4)	1.747(3)	B(4′)-B(5′)	1.743(5)	1.791(3)
B(4)-B(9)	1.787(4)	1.799(3)	B(4′)-B(8′)	1.774(4)	1.786(3)
B(4)-B(5)	1.799(4)	1.807(3)	B(4′)-B(9′)	1.776(5)	1.788(3)
B(4)-B(8)	1.824(4)	1.835(3)	B(5′)-B(6′)	1.744(5)	1.773(3)
B(5)-B(9)	1.766(5)	1.772(4)	B(5′)-B(9′)	1.746(4)	1.775(3)
B(5)-B(6)	1.767(4)	1.765(4)	B(5′)-B(10′)	1.752(5)	1.777(3)
B(5)-B(10)	1.775(5)	1.777(4)	B(6′)-B(10′)	1.763(5)	1.754(3)
B(6)-B(11)	1.749(5)	1.747(3)	B(6′)-B(11′)	1.780(5)	1.777(3)
B(6)-B(10)	1.755(4)	1.762(3)	B(7′)-B(12′)	1.777(5)	1.783(4)
B(7)-B(12)	1.788(5)	1.780(3)	B(7′)-B(8′)	1.778(5)	1.780(3)
B(7)-B(11)	1.788(5)	1.782(3)	B(7′)-B(11′)	1.788(5)	1.780(4)
B(7)-B(8)	1.827(4)	1.823(3)	B(8′)-B(9′)	1.778(4)	1.779(4)
B(8)-B(9)	1.773(5)	1.789(3)	B(8′)-B(12′)	1.787(5)	1.786(4)
B(8)-B(12)	1.777(4)	1.790(3)	B(9′)-B(12′)	1.775(5)	1.787(4)
B(9)-B(10)	1.777(5)	1.786(4)	B(9′)-B(10′)	1.776(5)	1.794(4)
B(9)-B(12)	1.781(5)	1.784(4)	B(10′)-B(11′)	1.772(6)	1.777(3)
B(10)-B(11)	1.773(5)	1.776(3)	B(10′)-B(12′)	1.790(5)	1.790(4)
B(10)-B(12)	1.775(5)	1.778(4)	B(11′)-B(12′)	1.774(5)	1.784(4)
B(11)-B(12)	1.779(5)	1.776(4)			

	3AB	3CD		3AB	3CD
M(3X)-B(7X)	2.073(14)	2.065(13)	C(1Y)-C(2Y)	1.676(15)	1.676(15)
M(3X)-B(4X)	2.086(14)	2.066(15)	C(1Y)-B(5Y)	1.713(17)	1.714(18)
M(3X)-C(2X)	2.072(12)	2.043(11)	C(1Y)-B(3Y)	1.728(18)	1.782(18)
M(3X)-B(8X)	2.073(13)	2.089(15)	C(1Y)-B(4Y)	1.708(16)	1.734(17)
M(3X)-C(1X)	2.118(11)	2.118(11)	C(1Y)-B(6Y)	1.779(18)	1.709(18)
C(1X)-C(1Y)	1.548(13)	1.554(15)	C(2Y)-B(7Y)	1.717(18)	1.713(18)
C(1X)-C(2X)	1.629(17)	1.676(17)	C(2Y)-B(11Y)	1.696(17)	1.687(18)
C(1X)-B(5X)	1.741(17)	1.744(18)	C(2Y)-B(6Y)	1.724(19)	1.700(2)
C(1X)-B(4X)	1.750(16)	1.667(16)	C(2Y)-B(3Y)	1.705(18)	1.717(18)
C(1X)-B(6X)	1.756(16)	1.774(16)	B(3Y)-B(4Y)	1.760(2)	1.780(2)
C(2X)-B(11X)	1.730(18)	1.719(17)	B(3Y)-B(8Y)	1.800(2)	1.747(18)
C(2X)-B(6X)	1.719(17)	1.744(18)	B(3Y)-B(7Y)	1.780(2)	1.793(18)
C(2X)-B(7X)	1.769(17)	1.758(19)	B(4Y)-B(5Y)	1.770(2)	1.790(2)
B(4X)-B(9X)	1.795(18)	1.761(19)	B(4Y)-B(8Y)	1.802(19)	1.771(19)
B(4X)-B(5X)	1.772(18)	1.792(19)	B(4Y)-B(9Y)	1.760(2)	1.780(2)
B(4X)-B(8X)	1.827(19)	1.740(2)	B(5Y)-B(6Y)	1.788(19)	1.776(19)
B(5X)-B(9X)	1.774(19)	1.750(2)	B(5Y)-B(9Y)	1.770(2)	1.790(2)
B(5X)-B(6X)	1.768(19)	1.780(2)	B(5Y)-B(10Y)	1.820(2)	1.760(2)
B(5X)-B(10X)	1.782(19)	1.782(19)	B(6Y)-B(10Y)	1.770(2)	1.790(2)
B(6X)-B(11X)	1.741(19)	1.750(2)	B(6Y)-B(11Y)	1.780(2)	1.770(2)
B(6X)-B(10X)	1.739(19)	1.779(19)	B(7Y)-B(12Y)	1.750(2)	1.750(2)
B(7X)-B(12X)	1.740(2)	1.780(2)	B(7Y)-B(8Y)	1.790(2)	1.784(18)
B(7X)-B(11X)	1.792(19)	1.800(2)	B(7Y)-B(11Y)	1.780(2)	1.740(2)
B(7X)-B(8X)	1.810(2)	1.830(2)	B(8Y)-B(9Y)	1.770(2)	1.780(2)
B(8X)-B(9X)	1.750(2)	1.770(2)	B(8Y)-B(12Y)	1.770(2)	1.800(2)
B(8X)-B(12X)	1.752(19)	1.780(2)	B(9Y)-B(12Y)	1.800(2)	1.770(2)
B(9X)-B(10X)	1.780(2)	1.810(2)	B(9Y)-B(10Y)	1.790(2)	1.740(2)
B(9X)-B(12X)	1.770(2)	1.770(2)	B(10Y)-B(11Y)	1.770(2)	1.790(2)
B(10X)-B(11X)	1.790(2)	1.760(2)	B(10Y)-B(12Y)	1.770(2)	1.770(2)
B(10X)-B(12X)	1.770(2)	1.780(2)	B(11Y)-B(12Y)	1.770(2)	1.760(2)
B(11X)-B(12X)	1.800(2)	1.770(2)			

Table 2.7 Cage connectivity distances in compounds 1, 2 (upper) and 3 (lower, X implies A and C and Y implies B and D).

2.6 Preparation of [BTMA][7-(1′-1′,2′-*closo*-$C_2B_{10}H_{11}$)-7,8-*nido*-$C_2B_9H_{11}$] (4)

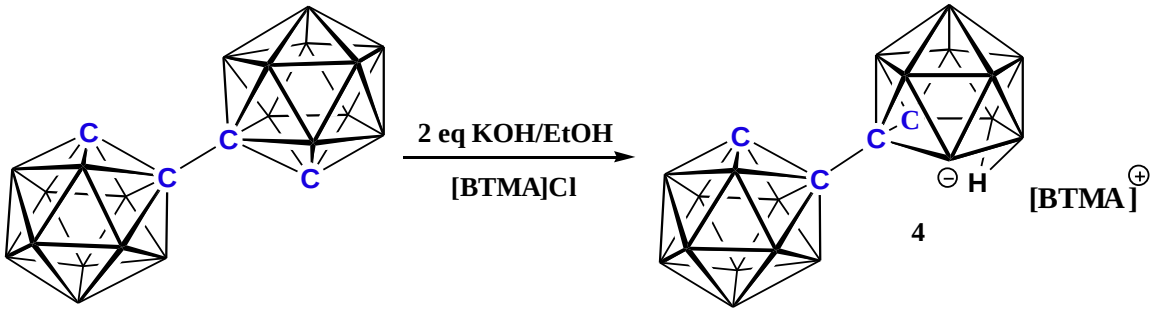

Unfortunately the yields of the 12-vertex/12-vertex metallacarborane/carborane species **1**, **2** and **3** prepared by reduction and metallation were low. In order to improve the yields the more obvious route of decapitation and metallation was attempted instead of reduction and metallation.

As noted above (**2.1**) in 1971 work done by Hawthorne et al described the synthesis of [7-(1′-1′,2′-*closo*-$C_2B_{10}H_{11}$)-7,8-*nido*-$C_2B_9H_{11}$]$^-$ as $[NMe_4]^+$ and Cs^+ salts[9]. The products were characterised by ^{11}B NMR spectroscopy and microanalysis but not by *X*-ray crystallography.

Decapitation of a single cage was carried out by the addition of 2 equivalents of KOH in ethanol and heating to reflux for 4 hrs. The reaction mixture was then cooled to room temperature and $CO_{2(g)}$ was bubbled through the colourless solution in order to remove the excess KOH. After filtration the solvent was removed on a rotary evaporator to yield a colourless oil which was then dissolved in water to yield a clear solution. The white product was isolated as [BTMA][7-(1′-1′,2′-*closo*-$C_2B_{10}H_{11}$)-7,8-*nido*-$C_2B_9H_{11}$] (**4**) in 74% yield by the addition of [BTMA]Cl as an aqueous solution.

The product was fully characterised by microanalysis, ^{1}H and ^{11}BNMR spectroscopies and an *X*-ray diffraction study. Elemental analysis was in good agreement with the values expected for $C_{14}H_{38}B_{19}N$.

The ^{1}H NMR spectrum of salt **4** shows a multiplet centred on δ 7.60 ppm due to the aromatic protons of $[BTMA]^{+}$. Two singlets at δ 4.75 ppm and δ 3.35 ppm correspond to C*H*$_2$ and HN(C*H*$_3$)$_3$ respectively. The signals for the two C_{cage}-*H* appear as singlets at δ 4.35 ppm and δ 1.95 ppm.

The ^{11}B{^{1}H} NMR spectrum of salt **4** consists of eleven signals in the range δ -4.18 to -35.50 ppm with integrals in the ratio 1:1:1:5:2:3:2:1:1:1:1 with the signals at δ -33.15 and δ -35.50 ppm indicating the presence of a nido cage.

X-ray diffraction quality colourless crystals of salt **4** were grown by vapour diffusion of a DCM solution and 40-60 petroleum ether. *X*-ray diffraction analysis revealed that salt **4** has conjoined 11-vertex *nido*-$C_2B_9H_{11}$ and 12-vertex *closo*-$C_2B_{10}H_{11}$ components and, except for C1 and C7′**,** each of the cage atoms is bonded to an exo terminal hydrogen atom (Fig 2.14).

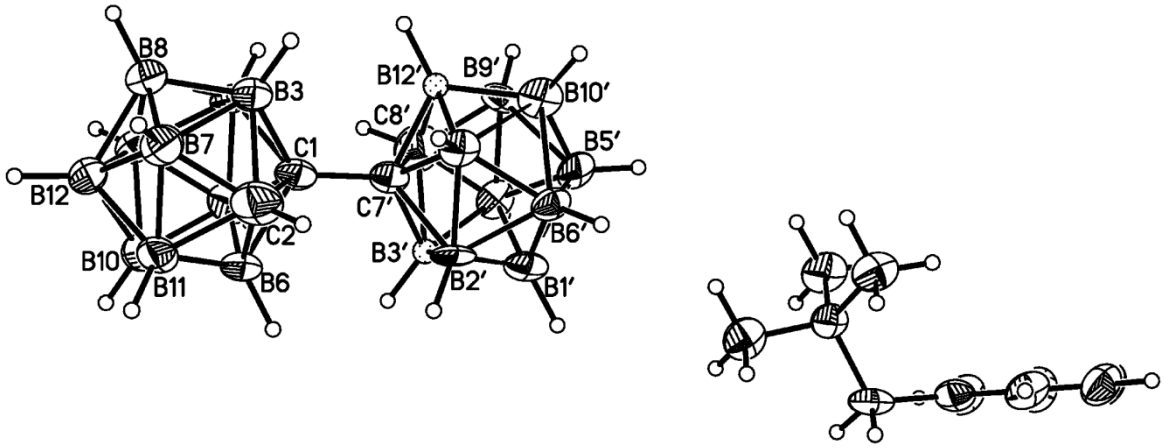

Fig 2.14 Molecular structure of [BTMA][7-(1′-1′,2′-*closo*-$C_2B_{10}H_{11}$)-7,8-*nido*-$C_2B_9H_{11}$)

In the crystal structure the closo cage is ordered but the nido cage is highly disordered between B3′ and B12′. Both the closo and the nido cages are connected through C1-C7′, 1.518(9) Å, which is shorter than that in 1,1′-bis(*o*-carborane) (1.530(3) Å)[2] which implies that salt **4** is less sterically crowded due to the presence of an open cage. The C-C-C-C torsion angle is 177.5^{0}.

2.7 Preparation of [HNMe$_3$][7-(1′-1′,2′-*closo*-$C_2B_{10}H_{11}$)-7,8-*nido*-$C_2B_9H_{11}$] (5)

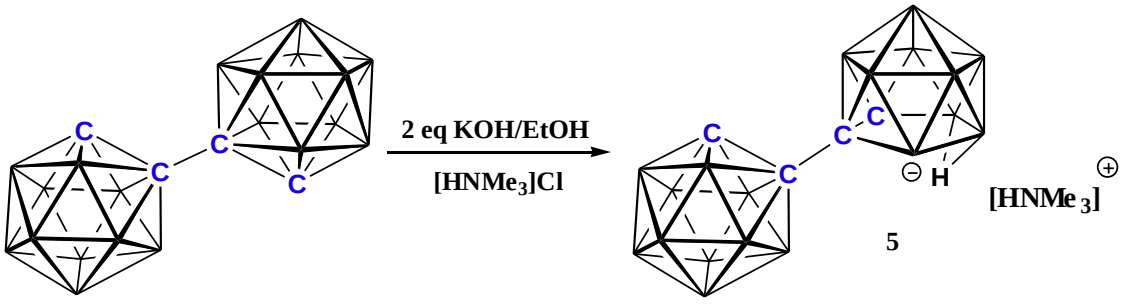

5

The single cage decapitation was carried out exactly as in **2.6** except that the product was isolated as the $[HNMe_3]^+$ salt instead of the $[BTMA]^+$ salt because the $[HNMe_3]^+$ salt is a convenient starting material for the synthesis of MC_2B_9-C_2B_{10} species, in a manner similar to MC_2B_9[16]. The salt [HNMe$_3$][7-(1′-1′,2′-*closo*-$C_2B_{10}H_{11}$)-7,8-*nido*-$C_2B_9H_{11}$] (**5**) was isolated in 79% yield as a white solid.

The salt **5** was fully characterised by microanalysis, ^{11}B NMR and ^{1}H NMR spectroscopies. The elemental analysis was in good agreement with the values expected for $C_7H_{32}B_{19}N$.

^{1}H NMR spectroscopy of salt **5** shows three singlets at δ 4.35 ppm, δ 3.15 ppm and δ 1.95 ppm which correspond to C_{cage}-*H*, HN(C*H*$_3$)$_3$ and C_{cage}-*H* respectively.

^{11}B{^{1}H} NMR spectroscopy of salt **5** consists of the same eleven signals as observed in salt **4** at δ -4.18, - 6.23, -9.03, -10.63, -11.51, -13.73, -17.00, -19.23, -22.90, -33.12 and -35.49 ppm with integrals in the relative ratio 1:1:1:5:2:3:2:1:1:1:1.

Attempts to grow crystals suitable for *X*-ray diffraction were unsuccessful.

2.8 Deprotonation and metallation with [Ru(*p*-cymene)Cl_2]$_2$

The deprotonation of [$HNMe_3$][7-(1′-1′,2′-*closo*-$C_2B_{10}H_{11}$)-7,8-*nido*-$C_2B_9H_{11}$] in THF with *n*-BuLi at reflux temperature followed by the metallation with 0.5 equivalents of [Ru(*p*-cymene)Cl_2]$_2$ in THF yielded a brown suspension which was then dried under *vac-uo*. The resulting brown solid was dissolved in the minimum amount of DCM, filtered through Celite® and subjected to preparative TLC. The isolation of the yellow compound 1-(1′-1′,2′-*closo*-$C_2B_{10}H_{11}$)-3-(η-cymene)-3,1,2-*closo*-$RuC_2B_9H_{10}$ (**1**) was confirmed by -^{11}B NMR and ^{1}H NMR spectroscopies and CHN analysis.

The product was isolated in 7.9% which is better than the reduction and metallation method but not as high as we expected.

2.9 Deprotonation and metallation with [Ru(C_6H_6)Cl_2]$_2$

The deprotonation of [$HNMe_3$][7-(1′-1′,2′-*closo*-$C_2B_{10}H_{11}$)-7,8-*nido*-$C_2B_9H_{11}$] with *n*-BuLi followed by the treatment with 0.5 equivalents of [Ru(C_6H_6)Cl_2]$_2$ was carried out in exactly the same way as **2.8**. Preparative TLC yielded the same yellow compound, 12-vertex/12-vertex ruthenacarborane/carborane (**2**), as obtained by reduction and metallation, this time in 8.8% yield which is once again better than the reduction and metallation but not as high as we expected.

2.10 Preparation of 8-(1′-1′,2′-*closo*-$C_2B_{10}H_{11}$)-2-(η-C_5H_5)-2,1,8-*closo*-$CoC_2B_9H_{10}$ (6) and [Cp_2Co][7-(1′-1′,2′-*closo*-$C_2B_{10}H_{11}$)-7,8-*nido*-$C_2B_9H_{11}$] (7)

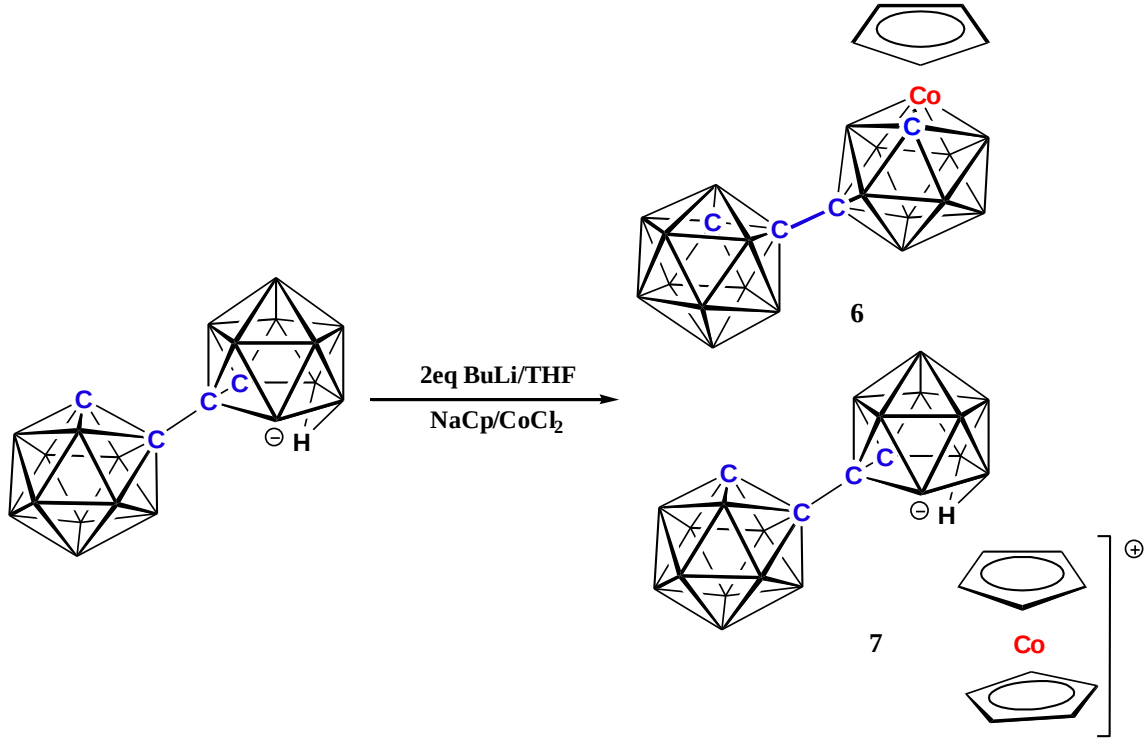

Deprotonation of a THF solution of compound **5** was carried out with n-BuLi at 0°C and the mixture was then heated to reflux for 4 hrs. The mixture was then cooled to 0°C and metallated with NaCp/$CoCl_2$. The resulting dark green suspension was then subjected to aerial oxidation for an hour followed by filtration through silica. The solvent was removed under reduced pressure and the residue was dissolved in DCM and filtered through Celite®.

Preparative TLC with a mixed eluent of CH_2Cl_2-petroleum ether (bp 40-60 °C) (1:1) revealed two different products, 8-(1′-1′,2′-*closo*-$C_2B_{10}H_{11}$)-3-(η-C_5H_5)-2,1,8-*closo*-$CoC_2B_9H_{10}$ (**6**) as the major product with R_f 0.7 in 32% yield and [Cp_2Co][7-(1′-1′,2′-*closo*-$C_2B_{10}H_{11}$)-7,8-*nido*-$C_2B_9H_{11}$] (**7**) with R_f 0.1 in 13% yield.

The compound **6** was fully characterised by mass spectrometry, microanalysis, ^{1}H NMR and ^{11}B NMR spectroscopies and *X*-ray crystallography.

Mass spectrometry of compound **6** shows the parent ion to have a mass of 399.3 with a broad heteroborane envelope from 393.3 to 402.3 while elemental analysis was in good agreement with the values expected for $C_9H_{26}B_{19}Co$.

^{1}H NMR spectroscopy accounted for all the protons of compound **6**. One singlet at δ 5.75 ppm corresponds to the C_5H_5 ligand and two singlets at δ 4.45 ppm and δ 3.15 ppm are assigned to CH_{cage}.

^{11}B{^{1}H} NMR spectroscopy consists of twelve signals in the range δ 1.11 to -18.36 ppm with integrals in the relative ratio 1:2:1:1:1:1:1:6:1:2:1:1. ^{11}B{^{1}H} NMR and ^{1}H NMR spectroscopies of compound **6** suggest that the product obtained from decapitation and metallation is not the same as that from reduction and metallation, viz. compound **3**.

X-ray quality yellow crystals of compound **6** were grown by vapour diffusion of a DCM solution and 40-60 petroleum ether at room temperature. *X*-ray diffraction examination revealed that in solid state compound **6** is 8-(1′-1′,2′-*closo*-$C_2B_{10}H_{11}$)-2-(η-C_5H_5)-2,1,8-*closo*-$CoC_2B_9H_{10}$ (Fig 2.15) which is an isomerisation product of compound **3**.

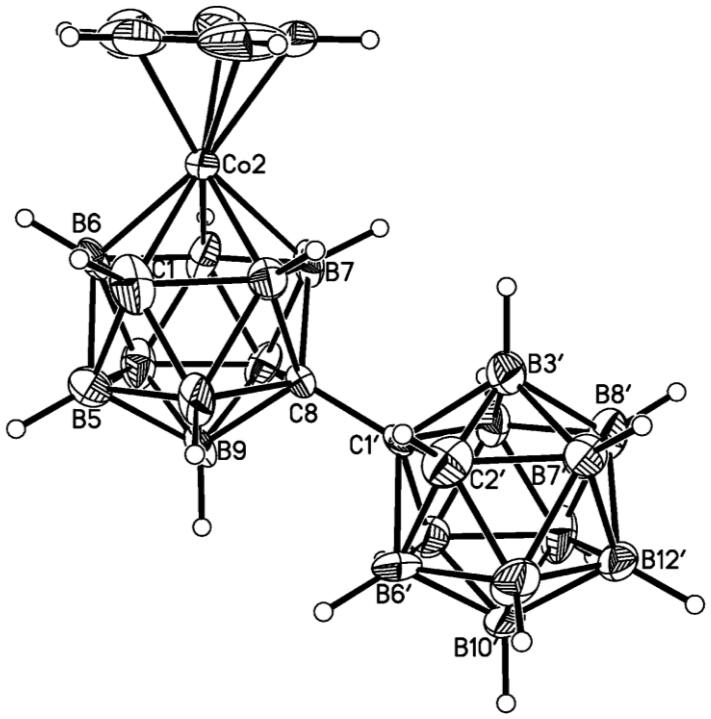

Fig 2.15 Molecular structure of 8-(1′-1′,2′-*closo*-$C_2B_{10}H_{11}$)-2-(η-C_5H_5)-2,1,8-*closo*-$CoC_2B_9H_{10}$

In compound **6** the ligand attached to the metal is bent away from the cage by only 2.11^0 and the C8-C1′ distance is 1.532(16) Å, which is identical to the C1-C1′ distance of 1,1′-bis(*o*-carborane)[2] (1.530(3) Å). These structural features are due to the fact that the carborane cage has moved from 1st position of the cobaltacarborane cage to the 8th position therefore the intramolecular steric crowding has been removed. This is the first example of a 12-vertex/12-vertex 2,1,8-metallacarborane/1′,2′-carborane species.

The metallated cage of **6** is icosahedral with Co2 capping the upper belt of the molecule. The C atoms in the metallacarborane cage are not adjacent to each other. One of them in the upper belt and the other one is in the lower belt and they are separated by 2.684 Å. The bottom belt of the metallacarborane cage is connected to the top belt of the carborane cage through C8 and C1′ atoms. The longest bonds in the molecule are centered on Co, and these lie in the range 2.083(18) Å-2.008(16) Å, and the shortest bond is 1.69(2) Å between the C1 and B4 atoms in the metallacarborane cage.

The salt **7** was fully characterised by microanalysis, ^{1}H and ^{11}B{^{1}H} NMR spectroscopies and *X*-ray crystallography. The elemental analysis was in good agreement with the values expected for $C_{14}H_{32}B_{19}Co$.

^{1}H NMR spectroscopy shows the presence of 10H due to two C_5H_5 groups at δ 5.85 ppm and the CH_{cage} signals appear as singlets at δ 4.35 ppm and δ 1.95 ppm.

^{11}B{^{1}H} NMR spectroscopy of salt **7** consists of eleven signals similar to salts **4** and **5** with integrals in the ratio 1:1:1:5:2:3:2:1:1:1:1 with the signals at δ -33.12 ppm and δ -35.49 ppm confirming the presence of a nido cage.

Pale green crystals were grown from a DCM/40-60 petroleum ether by vapour diffusion and *X*-ray diffraction examination confirmed that in the solid state salt **7** is the cobaltacenium salt of [7-(1′-1′,2′-*closo*-$C_2B_{10}H_{11}$)-7,8-*nido*-$C_2B_9H_{11}$]$^-$ (Fig 2.16).

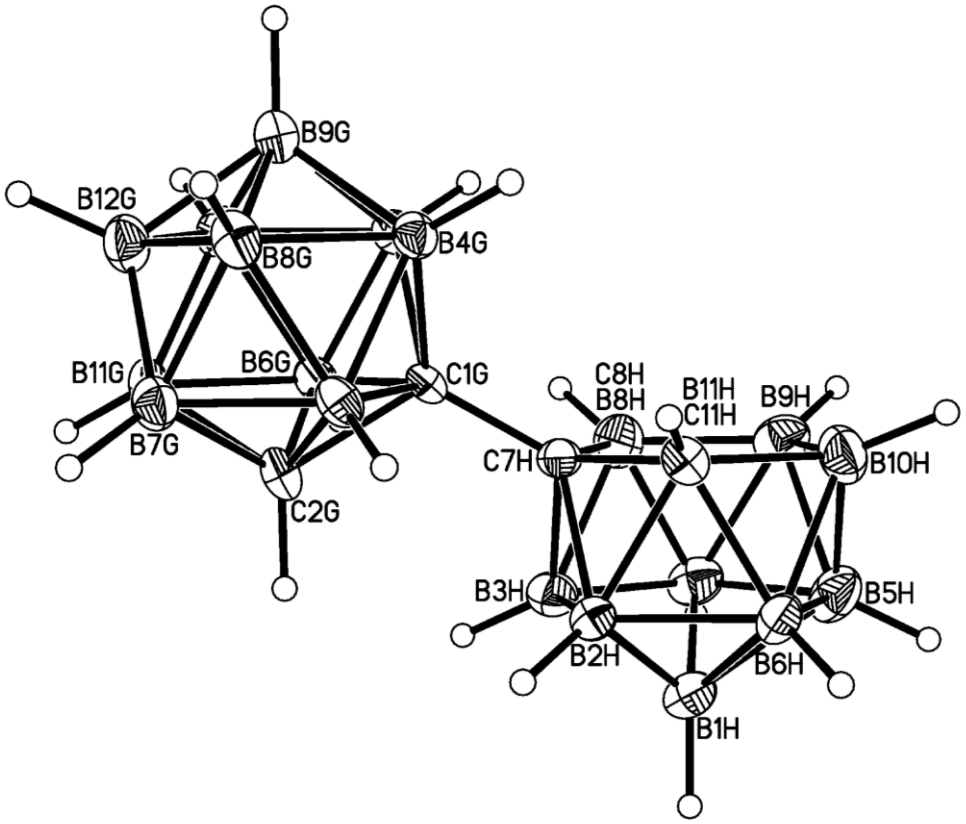

Fig 2.16 Molecular structure of the anion of [Cp_2Co][7-(1′-1′,2′-*closo*-$C_2B_{10}H_{11}$)-7,8-*nido*-$C_2B_9H_{11}$]

The asymmetric fraction of the unit cell of salt **7** has four biscarborane units, **AB**, **CD**, **EF**, **GH** (first letter refers to the C_2B_{10} cage and the second letter to C_2B_9 cage). **AB** and **EF** are similar. **A** and **E** are fully ordered whereas in **B** and **F** there is disorder between two sites B11B and B12B and it was not possible to unambiguously locate the second carbon atom. In **CD** there is disorder in both cages. In the C_2B_{10} cage **C** the non-linking carbon atom is disordered between two sites, C/B2 being 0.51(4)C and 0.49(4)B and B/C4 being 0.51(4)B and 0.49(4)C. In the C_2B_9 cage **D** the non-linking carbon atom is disordered between two sites, C/B8 being 0.61(5)C and 0.39(5)B and B/C11 being 0.61(5)B and 0.39(5)C. In **GH**, the C_2B_{10} cage **G** is fully ordered whereas in the C_2B_9 cage **H** the non-linking carbon atom is disordered between two sites, C/B8 being 0.61(5)C and 0.39(5)B and B/C11 being 0.61(5)B and 0.39(5)C.

2.11 Discussion

As noted above in **2.5** the two electron reduction and metallation of 1, 1′-bis(*o*-carborane) produced unexpected 12-vertex/12-vertex 3,1,2-metallacarborane/1′,2′-carborane species in low yield rather than the expected 13-vertex/12-vertex metallacarborane/carborane species.

In principle there is an alternate way of preparing the above species in better yield by decapitation and metallation rather than reduction and metallation. The single cage decapitation was achieved by reaction with two equivalents of KOH in EtOH and the products were isolated as [BTMA][7-(1′-1′,2′-*closo*-$C_2B_{10}H_{11}$)-7,8-*nido*-$C_2B_9H_{11}$] (**4**) and [$HNMe_3$][7-(1′-1′,2′-*closo*-$C_2B_{10}H_{11}$)-7,8-*nido*-$C_2B_9H_{11}$] (**5**) separately. The salts **4** and **5** were fully characterised by microanalysis, ^1H and ^{11}B NMR spectroscopies and salt **4** was further characterised by *X*-ray diffraction study.

Deprotonation of [$HNMe_3$][7-(1′-1′,2′-*closo*-$C_2B_{10}H_{11}$)-7,8-*nido*-$C_2B_9H_{11}$] (**5**) with *n*-BuLi followed by metallation with {(arene)Ru} fragments at room temperature yielded the same products as observed by reduction and metallation. The yields are improved but not by as much as we expected.

Interestingly, metallation with $\{CpCo\}^{2+}$ at room temperature resulted in two different products which are 8-(1′-1′,2′-*closo*-$C_2B_{10}H_{11}$)-2-(η-C_5H_5)-2,1,8-*closo*-$CoC_2B_9H_{10}$ (**6**) and [Cp_2Co][7-(1′-1′,2′-*closo*-$C_2B_{10}H_{11}$)-7,8-*nido*-$C_2B_9H_{11}$] (**7**). Compound **6** is the first isomerized product observed in the single cage metallation of 1,1′-bis(*o*-carborane), the heteroatom pattern changing from 3,1,2 to 2,1,8 without heating.

It has been already noted that at room temperature two types of isomerisation are possible with 3,1,2-*closo*-$MC_2B_9H_{11}$ species when bulky groups are substituted on the carbon atoms and the ligands attached to the metal are also large (Fig 2.17).

1. 1,2 to 1,2 isomerisation

   In this isomerisation process one of the cage carbon atoms moves to the lower belt of the cage. However, both carbon atoms are still *ortho* to each other. This isomerisation is observed in bis(phosphine)nickelacarborane[17].

2. 1,2 to 1,7 isomerisation

In this process one of the cage carbon atoms migrates to the lower pentagonal belt but now the carbon atoms are not *ortho* to each other. Both of them are separated by a boron-boron connectivity. This is frequently observed with diphenyl substitution on carbon[18].

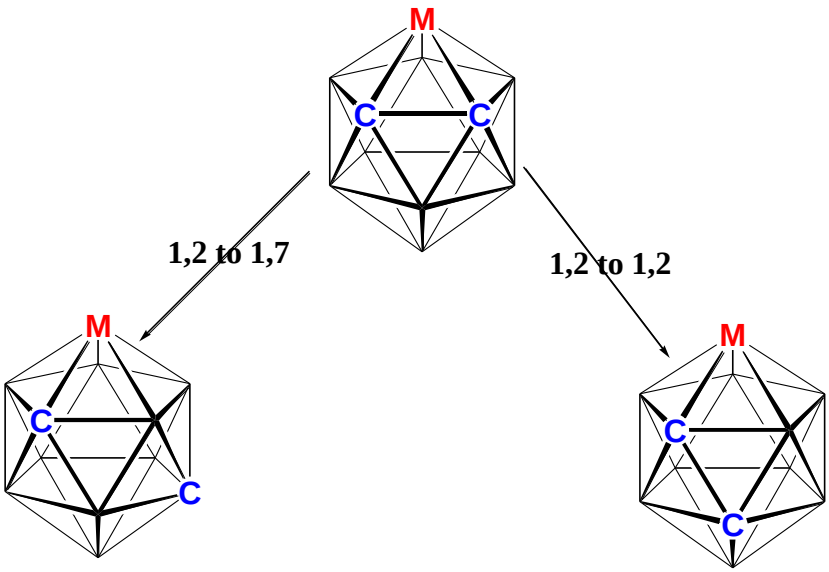

Fig 2.17 Two forms of isomerisation with 3,1,2-*closo*-$MC_2B_9H_{11}$

The similar type of isomerisation obtained at room temperature during the metallation of single cage decapitated 1,1′-bis(*o*-carborane) with the {CpCo} fragment once again suggests that these systems are highly crowded. However, the isomerisation was not observed with the {(arene)Ru} fragment and this may be due to the fact that cobaltacarboranes are more flexible than ruthenacarboranes [19].

To discover if compound **3** forms first and then isomerises to compound **6,** compound **3** was heated under toluene reflux for 48 hrs. Only starting material was isolated by thin layer chromatography and not the expected compound **6**. Therefore it is clear that reduction/metallation and decapitation/metallation follow different pathways. Work is in progress in order to understand these different mechanisms.

In the ^{1}H NMR spectrum of compound **6** there are two signals observed due to C*H*$_{cage}$ at δ 4.45 and 3.15 ppm. It is proposed that the signal at δ 4.45 ppm is assigned to the CH$_{cage}$ of the {C_2B_{10}} fragment whilst that at δ 3.15 ppm is assigned to the CH$_{cage}$ of the {2,1,8-CoC_2B_9} fragment by reference to the individual parent compounds[12, 20].

^{11}B{^{1}H}-^{11}B{^{1}H} COSY spectroscopy of compound **6** (Fig 2.18) allows the peaks due to the carborane and metallacarborane cages to be identified, and these are shown as a stick diagram in fig 2.19 .

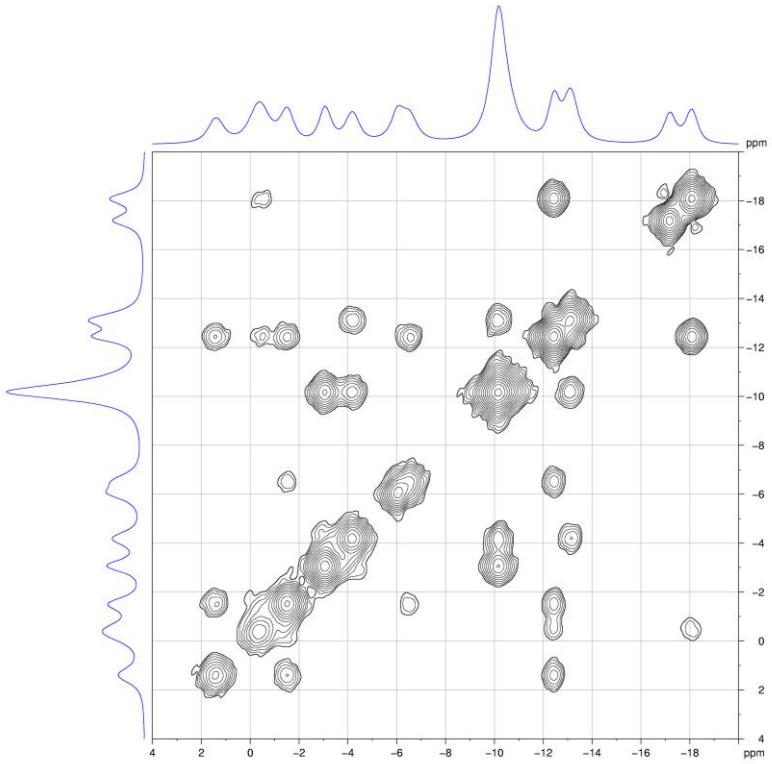

Fig 2.18 ^{11}B{^{1}H}-^{11}B{^{1}H} correlation spectrum of compound 6

The two dimensional ^{11}B{^{1}H}-^{11}B{^{1}H} correlation spectrum of compound **6** clearly shows the resonances for the {2,1,8-CoC_2B_9} fragment are at δ 1.11 (1B), -0.67 (2B), -1.78 (1B), -6.36 (1B), -7.00 (sh., 1B), -12.78 (1B), -17.48 (1B), -18.36 (1B) and those for the {C_2B_{10}} fragment are at -3.36 (1B), -4.46 (1B), -10.46 (6B), -13.36 (2B).

The weighted average chemical shift, $<\delta^{11}B>$, of the individual components, i.e. the {2,1,8-CoC_2B_9} and {C_2B_{10}} fragments, of compound **6** also move to high frequency, by δ 1.7 and 1.2 ppm respectively, with respect to 2-Cp-2,1,8-*closo*-$CoC_2B_9H_{11}$[20] and 1,2-*closo*-carborane[12].

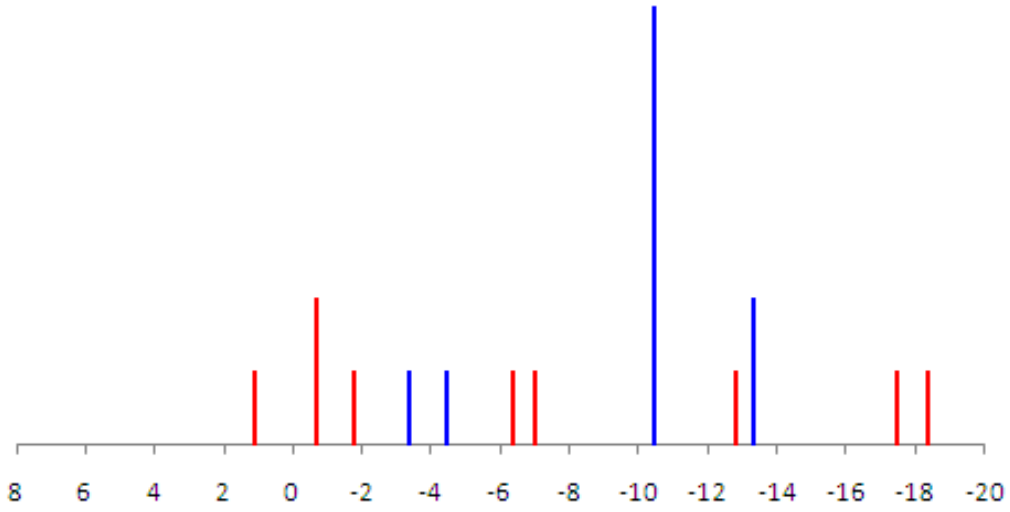

Fig 2.19 Stick diagram of the ^{11}B resonances of compound 6 (metallacarborane shown in red and carborane shown in blue)

In the ^1H NMR spectra of salts **4**, **5** and **7** the CH_{cage} signals are at exactly the same positions, δ 4.35 and 1.95 ppm. From these the signal at δ 4.35 ppm is due to the *closo*-carborane cage, $C_2B_{10}H_{11}$, while the signal at δ 1.95 ppm is due to the *nido*-$C_2B_9H_{11}$ cage, these signals being assigned with respect to those of 1,2-*closo*-carborane[12] and [7,8-*nido*-$C_2B_9H_{12}]^-$[21].

The ^{11}B NMR spectra of salts **4**, **5** and **7** show resonances in the range of δ -4.2 to -35.6 ppm in the relative ratio 1:1:1:5:2:3:2:1:1:1:1. A two dimensional $^{11}B\{^1H\}$-$^{11}B\{^1H\}$ correlation spectrum of salt **7** (Fig 2.20) was obtained in order to identify the signals which corresponds to *closo*-carborane cage, $C_2B_{10}H_{11}$, and *nido*-carborane cage, $C_2B_9H_{10}$, individually. A stick diagram for salts **4**, **5** and **7** is given in fig 2.21 following analysis of the correlation spectrum of salt **7,** with green showing the {C_2B_9} fragment and blue showing the {C_2B_{10}} fragment.

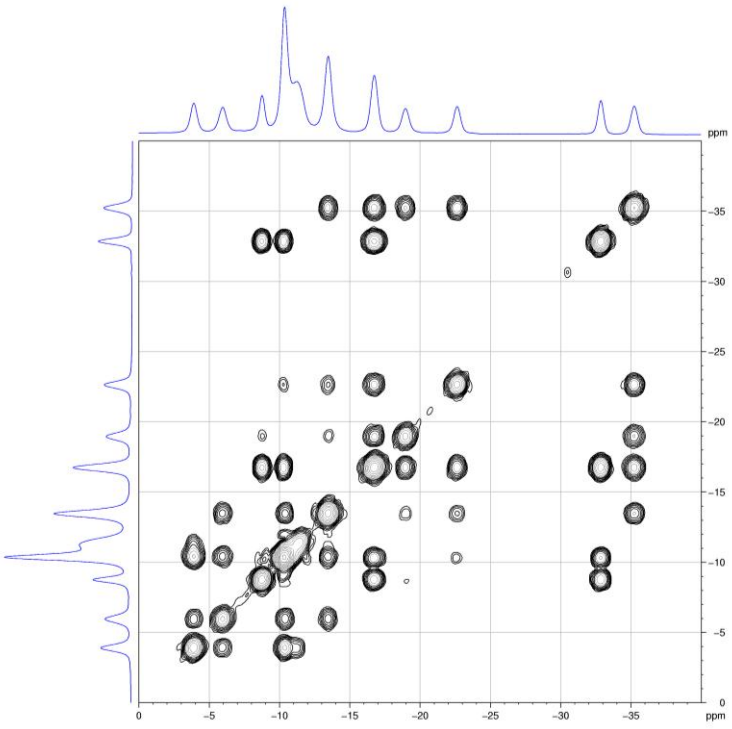

Fig 2.20 $^{11}B\{^{1}H\}$-$^{11}B\{^{1}H\}$ correlation spectrum of salt 7

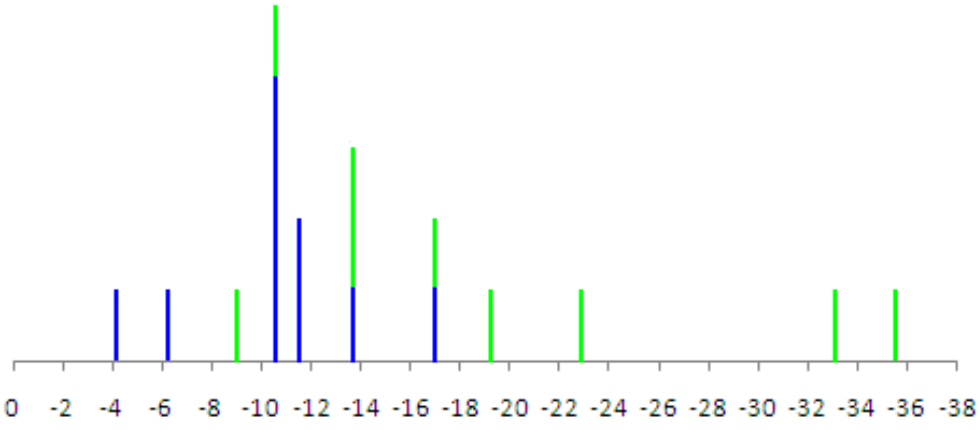

Fig 2.21 Stick diagram of the ^{11}B resonances of salts 4, 5 and 7

The resonances at δ -4.18 (1B), -6.23 (1B), -10.63 (4B), -11.51 (sh., 2B), -13.73 (1B) and -17.00 (1B) are due to the {C_2B_{10}}fragment and the resonances at δ -9.03 (1B), -10.63 (1B), -13.73 (2B), -17.00 (1B) -19.22 (1B), -22.90 (1B), -33.12 (1B), -35.49 (1B) are due to the {C_2B_9} fragment. There are coincidences between resonances of the closo and nido cages at δ 10.63, -13.73 and -17.00. Assignments were made with the help of the spectra of 1,2-*closo*-carborane[12] and [7,8-*nido*-$C_2B_9H_{12}$]$^-$[21].

The weighted average ^{11}B NMR chemical shifts of the individual components, {1′,2′-C_2B_{10}} and {7,8-C_2B_9}, of salts **4**, **5** and **7** both move to higher frequency, by ca. δ 0.2 and 1.6 ppm, with respect to 1,2-*closo*-carborane[12] and [7,8-*nido*-$C_2B_9H_{12}$]$^-$[21].

2.12 Summary

The 2-electron reduction of 1,1′-bis(*o*-carborane) with Na naphthalenide in degassed THF followed by metallation with {(arene)Ru} and {CpCo} fragments surprisingly yielded 1-(1′-1′,2′-*closo*-$C_2B_{10}H_{11}$)-3-(η-cymene)-3,1,2-*closo*-$RuC_2B_9H_{10}$ (**1**), 1-(1′-1′,2′-*closo*-$C_2B_{10}H_{11}$)-3-(η-C_6H_6)-3,1,2-*closo*-$RuC_2B_9H_{10}$ (**2**) and 1-(1′-1′,2′-*closo*-$C_2B_{10}H_{11}$)-3-(η-C_5H_5)-3,1,2-*closo*-$CoC_2B_9H_{10}$ (**3**). *X*-ray diffraction studies and mass spectrometry clearly show that the products obtained are 12-vertex/12-vertex 3,1,2-metallacarborane/1′,2′-carborane and not 13-vertex/12-vertex metallacarborane/1′,2-carborane. In all three cases the ligand attached to the metal is bent away from the carborane cage to avoid intramolecular steric crowding. These are the first examples of single cage metallation of 1,1′-bis(*o*-carborane).

The single cage decapitation of 1,1′-bis(*o*-carborane) was carried out by heating to reflux with two equivalents of KOH in EtOH and the products were isolated as [BTMA][7-(1′-1′,2′-*closo*-$C_2B_{10}H_{11}$)-7,8-*nido*-$C_2B_9H_{11}$] (**4**) and [$HNMe_3$][7-(1′-1′,2′-*closo*-$C_2B_{10}H_{11}$)-7,8-*nido*-$C_2B_9H_{11}$] (**5**) separately. Salt **4** was characterised by *X*-ray crystallography.

Deprotonation of [$HNMe_3$][7-(1′-1′,2′-*closo*-$C_2B_{10}H_{11}$)-7,8-*nido*-$C_2B_9H_{11}$] (**5**) and metallation with {(arene)Ru}$^{2+}$ and {CpCo}$^{2+}$ was attempted in order to improve the yields of compounds **1**-**3**. The yields of ruthenacarboranes **1** and **2** were improved but not by as much as we expected. Interestingly, with {CpCo}$^{2+}$ the product obtained was 8-(1′-1′,2′-*closo*-$C_2B_{10}H_{11}$)-2-(η-C_5H_5)-2,1,8-*closo*-$CoC_2B_9H_{10}$ (**6**) which is not the same as that from reduction/metallation due to the greater flexibility of {CpCo}$^{2+}$ over {(arene)Ru}$^{2+}$. In addition we obtained another product, [Cp_2Co][7-(1′-1′,2′-*closo*-$C_2B_{10}H_{11}$)-7,8-*nido*-$C_2B_9H_{11}$] (**7**). Compound **6** is the first example of a 2,1,8-metallacarborane/1′,2′-carborane species.

^{11}B-^{11}B COSY of all these products, **1**-**7** were analysed and the resonances due to the individual carborane (closo/nido) or metallacarborane cage were identified. Knowing these, the weighted average boron chemical shifts of the individual cage components were calculated and in all cases it is formed that the resonances move to high frequency with respect to their parent compounds. This is because an H atom is replaced by a carborane or metallacarborane cage, both of which are more e-withdrawing than H.

2.13 References

2.1. G. B. Dunks, M. M. McKown and M. F. Hawthorne, *J. Am. Chem. Soc.*, 1971, **93**, 2541.

2.2. S. Ren and Z. Xie, *Organometallics.*, 2008, **27**, 5167.

2.3. X. Yang, W. Jiang, C. B. Knobler, M. D. Mortimer and M. F. Hawthorne, *Inorg. Chim. Acta*., 1995, **240**, 371.

2.4. T. D. Getman, C. B. Knobler and M. F. Hawthorne, *J. Am. Chem. Soc*., 1990, **112**, 4593.

2.5. T. D. Getman, C. B. Knobler and M. F. Hawthorne, *Inorg. Chem*., 1992, **31**, 101.

2.6. D. Ellis, D. Mckay, S. A. Macgregor, G. M. Rosair and A. J. Welch, *Angew. Chem. Int. Ed.*, 2010, **49**, 4943.

2.7. D. Ellis, G. M. Rosair and A. J. Welch, *Chem. Commun.*, 2010, **46**, 7394.

2.8. R. A. Wiesboeck and M.F.Hawthorne, *J. Am. Chem. Soc*., 1964, **86**, 1642.

2.9. D. A. Owen, J. W. Wiggins and M. F. Hawthorne, *Inorg. Chem*., 1971, **10**, 1304.

2.10. M. E. Lopez, M. J. Edie, D. Ellis, A. Horneber, S. A. Macgregor, G. M. Rosair and A. J. Welch, *Chem. Commun.*, 2007, 2243.

2.11. Although the spectra of 1,2-*closo*-carborane and 3-(η-$C_{10}H_{14}$)-3,1,2-*closo*-$RuC_2B_9H_{11}$ have been reported previously[12, 10] we have remeasured them in $(CD_3)_2CO$ for internal consistency.

2.12. M. A. Fox, J. A. K. Howard, A. K. Hughes, J. M. Malget and D. S. Yufit, *Dalton Trans*., 2001, 2263.

2.13. X. L. R. Fontaine, N. N. Greenwood, J. D. Kennedy, K. Nestor and M. Thornton-Pett, *J. Chem. Soc*., *Dalton Trans*., 1990, 681.

2.14. (a) M. E. Lopez, D. Ellis, P. R. Murray, G. M. Rosair, A. J. Welch and L. J. Yellowlees, *Collect. Czech. Chem. Commun.*, 2010, **75**, 853; (b) H. Tricas, M. Colon, D. Ellis, S. A. Macgregor, D. McKay, G. M. Rosair, A. J. Welch, I. V. Glukhov, F. Rossi, F. Laschi and P. Zanello, *Dalton Trans*., 2011, **40**, 4200.

2.15. D. E. Smith and A. J. Welch, *Organometallics*, 1986, **5**, 760.

2.16. D. C. Young, P. A. Wegner and M. F. Hawthorne, *J. Am. Chem. Soc*., 1965, **87**, 1818.

2.17. R. M. Garrich, P. Kuballa, K. S. Low, G. M. Rosair and A. J. Welch, *J. Organomet. Chem*., 1999, **57**, 575.

2.18. D. R. Baghurst, R. C. B. Copley, H. Fleischer, D. M. P. Mingos, G. O. Kyd, L. J. Yellowlees, A. J. Welch, T. R. Spalding and D. O′Connell, *J. Organometal. Chem*., 1993, **447**, C14

2.19. (a) D. Ellis, M. E. Lopez, R. McIntosh, G. M. Rosair, A. J. Welch and R. Quenardelle, *Chem. Commun*., 2005, 1348; (b) S. Zlatogorsky, D. Ellis, G. M. Rosair and A. J. Welch, *Chem. Commun.*, 2007, 2178.

2.20. M. K. Kaloustain, R. J. Wiersema and M. F. Hawthorne, *J. Am. Chem. Soc*., 1972, **94**, 6679.

2.21. J. Buchanan, E. J. M. Hamilton, D. Reed and A. J. Welch, *J. Chem. Soc*., *Dalton Trans*., 1990, 677.

CHAPTER 3

Metallation of both cages of 1,1′-bis(*o*-carborane) with {(arene)Ru} and {CpCo} fragments

3.1 Introduction

The decapitation and metallation chemistry of 1,2-*closo*-carborane is a widely known area of study[1] however the analogous chemistry of 1,1′-bis(*o*-carborane) is not well explored due to its inefficient synthesis. In 1,1′-bis(*o*-carborane) two 1,2-*closo*-carborane cages are connected through a carbon-carbon sigma bond therefore it is possible to degrade either a single cage as noted in chapter 1 or both cages. The degradation reaction of 1,1′-bis(*o*-carborane) of single and both cages is dependent on the number of equivalents of KOH.

In 1971, Hawthorne reported a procedure to synthesise [7-(7′-7′,8′-*nido*-$C_2B_9H_{11}$)-7,8-*nido*-$C_2B_9H_{11}]^{2-}$ by adding 2.5 equivalents of KOH to [7-(1′-1′,2′-*closo*-$C_2B_{10}H_{11}$)-7,8-*nido*-$C_2B_9H_{11}]^-$ species and heated under reflux for 120 hrs[2] (Fig 3.1). The products were precipitated as Cs^+ and $[HNMe_3]^+$ salts and characterised by NMR spectroscopy and microanalysis but the structures were not confirmed by *X*-ray crystallography.

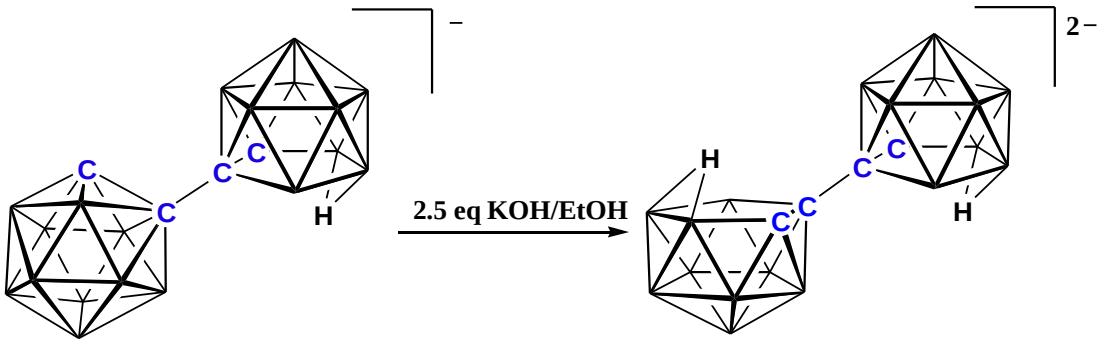

Fig 3.1 **Decapitation of closo cage of [7-(1′-1′,2′-*closo*-$C_2B_{10}H_{11}$)-7,8-*nido*-$C_2B_9H_{11}]^-$**

The decapitation of the second cage in [7-(1′-1′,2′-*closo*-$C_2B_{10}H_{11}$)-7,8-*nido*-$C_2B_9H_{11}$]$^-$ species is possible in either B3 or B6 position (Fig 3.2) therefore it is possible to obtain *racemic* and *meso* diastereoisomers.

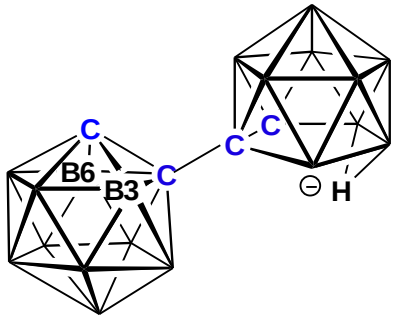

Fig 3.2 Decapitation of the closo cage in [7-(1′-1′,2′-*closo*-$C_2B_{10}H_{11}$)-7,8-*nido*-$C_2B_9H_{11}$]$^-$

The metallation chemistry of the doubly decapitated species, [7-(7′-7′,8′-*closo*-$C_2B_9H_{11}$)-7,8-*nido*-$C_2B_9H_{11}$]$^{2-}$ is not well explored. However, in 1985 Hawthorne reported the formation of new bimetallic rhodacarborane species by the addition of [Rh(COD)(PEt_3)Cl] to a THF solution of Cs_2[7-(7′-7′,8′-*nido*-$C_2B_9H_{11}$)-7,8-*nido*-$C_2B_9H_{11}$] and heating under reflux for two days[3].

In this chapter is described an alternate method of decapitating both cages instead of doing it stepwise as reported by Hawthorne[2] and the isolation of the products by metathesis with [$HNMe_3$]Cl, [BTMA]Cl and [(*S*)-$CH_3NC_5H_4$-$C_4H_7NCH_3$]I individually.

The syntheses and complete characterisation of the compounds, 8-(8′-2′-(η-C_5H_5)-2′,1′,8′-*closo*-$CoC_2B_9H_{10}$)-2-(η-C_5H_5)-2,1,8-*closo*-$CoC_2B_9H_{10}$ (**11**), 8-(8′-2′-(η-C_5H_5)-2′,1′,8′-*closo*-$CoC_2B_9H_{10}$)-3-(η-C_5H_5)-3,1,2-*closo*-$CoC_2B_9H_{10}$ (**12**/**13**) and 8-(8′-2′-(η-$C_{10}H_{14}$)-2′,1′,8′-*closo*-$RuC_2B_9H_{10}$)-3-(η-$C_{10}H_{14}$)-3,1,2-*closo*-$RuC_2B_9H_{10}$ (**14**/**15**) are reported. These compounds were obtained from deprotonation and metallation of [$HNMe_3$]$_2$[7-(7′-7′,8′-$C_2B_9H_{11}$)-7,8-$C_2B_9H_{11}$] (**9**), since [$HNMe_3$]$^+$ is the cation of choice for such reactions[4].

3. 2 Preparation of [BTMA]$_2$[7-(7′,8′-*nido*-$C_2B_9H_{11}$)-7,8-*nido*-$C_2B_9H_{11}$] (8)

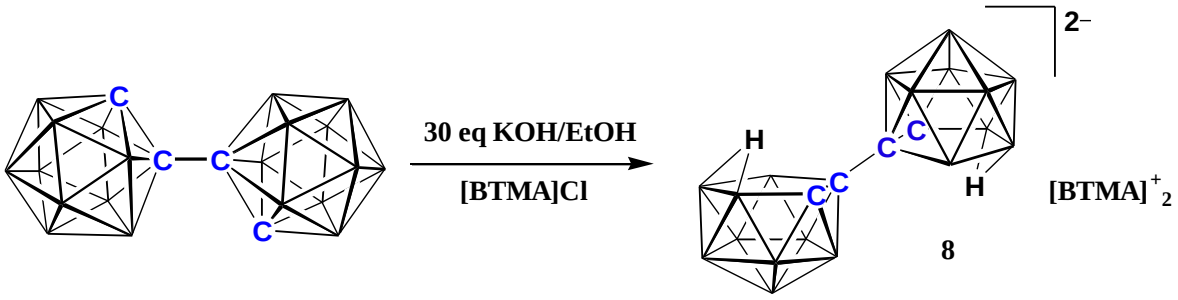

As noted in **3.1** the double decapitation of 1,1′-bis(*o*-carborane) can be carried out selectively by adding 2.5 equivalents of KOH to decapitate single cage followed by the addition of another portion of 2.5 equivalents of KOH in EtOH to heating to reflux for 120 hrs to decapitate both cages.

However, we found an alternate way to synthesise the above product by adding 30 equivalents of KOH in ethanol to 1,1′-bis(*o*-carborane) and heating under reflux for 48 hrs. The reaction mixture was then cooled to room temperature and the excess KOH was removed by passing CO_2(g) through the colourless solution. The white precipitate was filtered off and the solvent was removed under reduced pressure to yield an oil. Water was added to the colourless oil and the solution filtered. [BTMA]Cl was added as an aqueous solution. The resulting white precipitate was filtered off, washed with water and dried under reduced pressure on the vaccuum line.

Salt **8** was fully characterized by microanalysis, ^{1}H and ^{11}B NMR spectroscopies and *X*-ray crystallography. Elemental analysis gave results close to the calculated values for $C_{24}H_{54}B_{18}N_2$.

In the ^{1}H NMR spectrum of salt **8** the multiplet centred on δ 7.58 ppm is assigned to 2C$_6H_5$. The singlet at δ 4.75 ppm is assigned to four protons of 2CH_2 while the singlet at δ 3.30 ppm is assigned to 2N(CH_3)$_3$. The 2CH_{cage} signals were not visible in the spectrum.

$^{11}B\{^{1}H\}$ NMR spectroscopy of salt **8** revealed eleven resonances at δ -11.04, -14.88, -15.90, -17.69, -18.69, -20.50, -21.39, -23.96, -24.66, -33.85 and -36.79 ppm but it was not possible to obtain relative ratios because the spectrum clearly shows the presence of major and minor diastereoisomers (see p108). The signals at δ -33.85 and -36.79 ppm clearly indicate the presence of nido cage.

X-ray quality colourless crystals of salt **8** were grown by vapour diffusion of a THF solution and 40-60 petroleum ether at room temperature and crystallographic study confirmed that salt **8** is $[BTMA]_2[7\text{-}(7'\text{-}7',8'\text{-}\textit{nido}\text{-}C_2B_9H_{11})\text{-}7,8\text{-}\textit{nido}\text{-}C_2B_9H_{11}]$ the anion of which is shown in Fig 3.3.

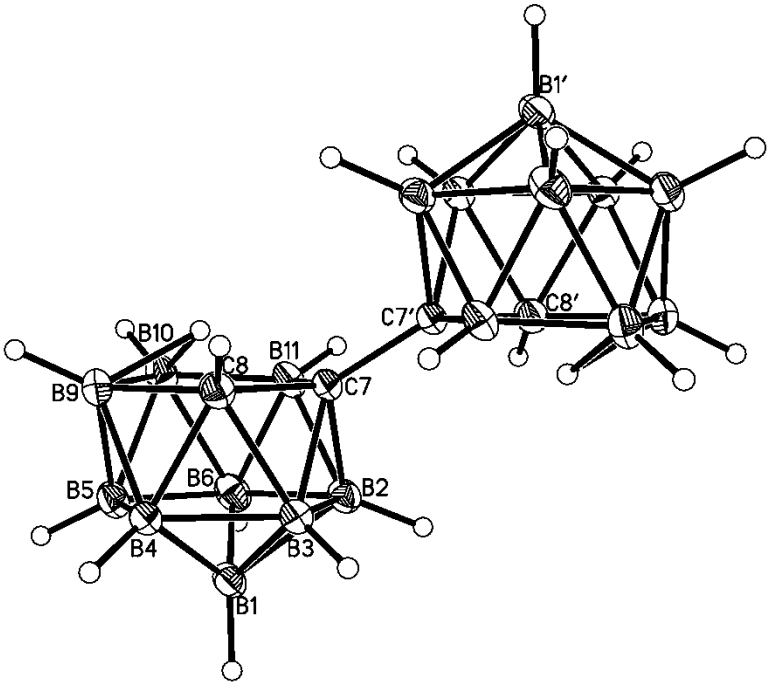

Fig 3.3 Molecular structure of the anion $[7\text{-}(7'\text{-}7',8'\text{-}\textit{nido}\text{-}C_2B_9H_{11})\text{-}7,8\text{-}\textit{nido}\text{-}C_2B_9H_{11}]^{2-}$ (8)

In fig 3.3 two 11-vertex *nido*-$C_2B_9H_{11}$ cages are connected through a C7-C7′ linkage and the other two carbon atoms (C8 and C8′) are trans to each other with a C-C-C-C torsion angle of 180°. There is a centre of inversion present in the middle of C7-C7′ and hence the structure is that of the *meso* diastereoisomer. The C7-C7′ bond distance is 1.515(3) Å, slightly shorter than in 1,1′-bis(*o*-carborane)[5], 1.530(3) Å.

Each of the cage atoms are bonded to an exo terminal hydrogen atom. B9 and B10 in one cage and B9′ and B10′ in the other cage are connected through bridging hydrogen atoms.

Clearly the crystal selected for the *X*-ray study is the *meso* diastereoisomer. However, since ^{11}B NMR spectroscopy of crystals clearly showed the presence of both diastereoisomers (*meso* and *racemic*), simple crystallisation as the $[BTMA]^+$ salt does not allow the isomers to be separated.

3.3 Preparation of $[HNMe_3]_2[7\text{-}(7'\text{-}7',8'\text{-}\textit{nido}\text{-}C_2B_9H_{11})\text{-}7,8\text{-}\textit{nido}\text{-}C_2B_9H_{11}]$ (9)

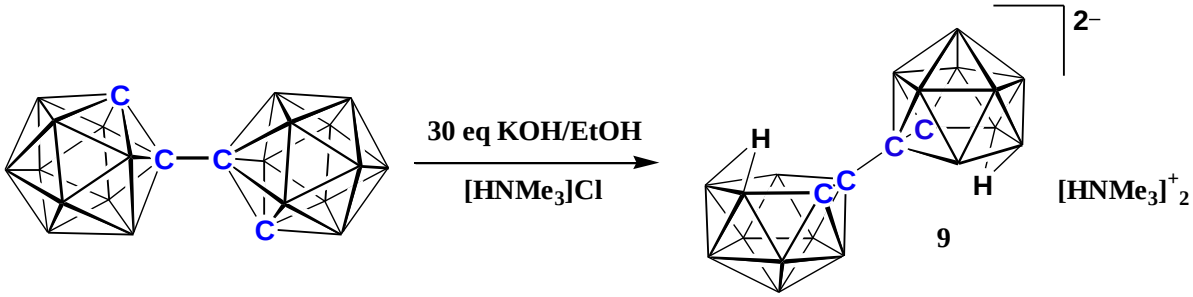

The double decapitation of 1,1′-bis(*o*-carborane) was carried out exactly as same as in **3.2**. Thus 1,1′-bis(*o*-carborane) was dissolved in EtOH and 30 equivalents of KOH were added. The colourless solution was heated under reflux for 48 hrs and cooled to room temperature. $CO_{2(g)}$ was passed through the mixture and the white precipitate was filtered off.

EtOH was removed *in vacuo* to yield an oil which was then dissolved in water and filtered. $[HNMe_3]Cl$ was added as an aqueous solution and the immediate white precipitate was filtered, washed with water and dried under reduced pressure. As noted above $[HNMe_3]_2[7\text{-}(7'\text{-}7',8'\text{-}\textit{nido}\text{-}C_2B_9H_{11})\text{-}7,8\text{-}\textit{nido}\text{-}C_2B_9H_{11}]$ was synthesised because this is a convenient starting material to carry out the deprotonation and metallation[4].

The salt **9** was fully characterised by microanalysis and $^{11}B\{^1H\}$ NMR spectroscopy. Elemental analysis was in good agreement with the calculated values for $C_{10}H_{42}B_{18}N_2$.

$^{11}B\{^1H\}$ NMR spectroscopy of salt **9** revealed eleven resonances at δ -11.10, -14.92, -15.94, -17.74, -18.72, -20.56, -21.40, -23.98, -24.66, -33.89 and -36.83 ppm which are effectively the same ratios as salt **8**. Thus $^{11}B\{^1H\}$ NMR spectroscopy confirmed that the salt **9** contains the $[7\text{-}(7'\text{-}7',8'\text{-}\textit{nido}\text{-}C_2B_9H_{11})\text{-}7,8\text{-}\textit{nido}\text{-}C_2B_9H_{11}]^{2-}$ anion.

3.4 Preparation of [(*S*)-$CH_3NC_5H_4$-$C_4H_7NCH_3$]$_2$[7-(7′-7′,8′-*nido*-$C_2B_9H_{11}$)-7,8-*nido*-$C_2B_9H_{11}$] (10)

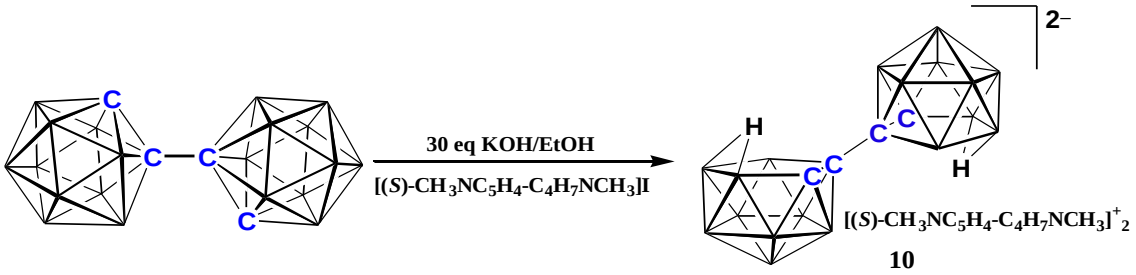

10

The double decapitation of 1,1′-bis(*o*-carborane) was carried out exactly as same as in **3.2** and **3.3** except that after work up [(*S*)-$CH_3NC_5H_4$-$C_4H_7NCH_3$]I was added as an aqueous solution instead of [BTMA]Cl in **3.2** and [$HNMe_3$]Cl in **3.3**. The pale yellow precipitate was filtered, washed with water and dried under reduced pressure.

[(*S*)-$CH_3NC_5H_4$-$C_4H_7NCH_3$]$_2$[7-(7′-7′,8′-*nido*-$C_2B_9H_{11}$)-7,8-*nido*-$C_2B_9H_{11}$] (**10**) was synthesised because the cation, [(*S*)-$CH_3NC_5H_4$-$C_4H_7NCH_3$]$^+$ has a chiral centre therefore we hoped that the *racemic* and *meso* forms of the double decapitated anion could be separated by crystallisation.

The salt **10** was fully characterised by microanalysis, ^{1}H NMR spectroscopy and ^{11}B{^{1}H} NMR spectroscopy. Elemental analysis was in good agreement with the calculated values for $C_{26}H_{56}B_{18}N_4$.

^{1}H NMR spectroscopy displayed singlet, doublet, doublet and triplet signals all with intensities one at δ 8.95, 8.85, 8.55 and 8.05 ppm respectively which correspond to the protons of the NC_5H_4 ring. The singlet with intensity three at δ 4.50 ppm is due to the CH_3 group attached to the NC_5H_4 ring.

Two triplets at δ 3.50 and 3.20 ppm are assigned to the two protons of C_4H_7 and a multiplet at δ 2.25 ppm is due to another two protons from C_4H_7. The singlet at δ 2.10 ppm is assigned to the CH_3 group attached to NC_4H_7 and two multiplets with integrals two at δ 1.80 and one at 1.60 ppm respectively are assigned to the remaining protons of C_4H_7. The details of these assignments will be discussed in **3.7**.

$^{11}B\{^{1}H\}$ NMR spectroscopy of salt **10** revealed eleven resonances at δ -11.04, -14.88, -15.90, -17.69, -18.69, -20.55, -21.39, -23.96, -24.66, -33.85 and -36.79 ppm which are exactly as same as in salts **8** and **9**.

Unfortunately, many attempted crystallisations with various solvent systems such as DCM/40-60 petroleum ether and THF/40-60 petroleum ether by solvent diffusion and vapour diffusion at room temperature as well as at 0° C, and slow evaporation from DCM and THF all failed to afford crystals and resulted instead in a sticky orange product. The reason behind this may be due to the interference of I^-.

3.5 Preparation of 12-v/12-v cobaltacarborane/cobaltacarborane species (11, 12 and 13) from the deprotonation and metallation of [7-(7′-7′,8′-*nido*-$C_2B_9H_{11}$)-7,8-*nido*-$C_2B_9H_{11}$]$^{2-}$

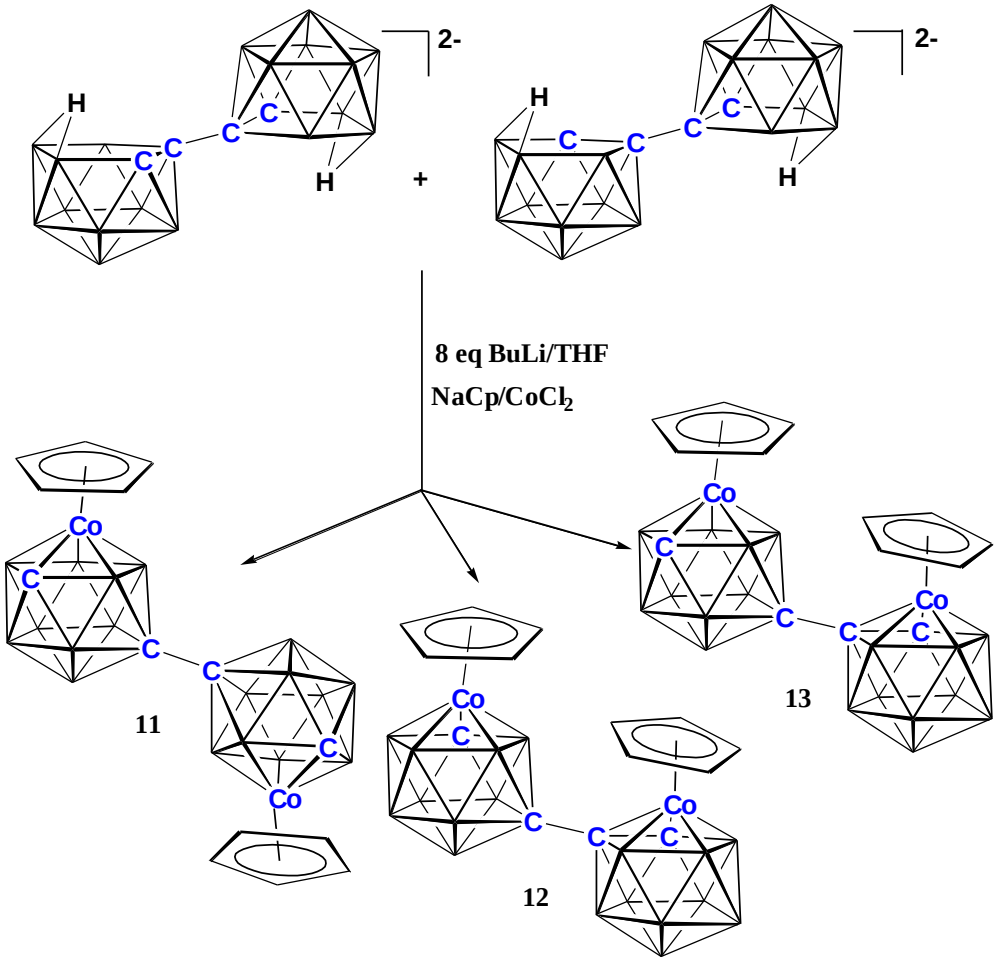

Deprotonation was carried out by the dropwise addition of 8 equivalents of BuLi to a THF solution of $[HNMe_3]_2$[7-(7′-7′,8′-*nido*-$C_2B_9H_{11}$)-7,8-*nido*-$C_2B_9H_{11}$] while cooling at 0°C. Then the mixture was heated under reflux for 4 hrs and cooled to 0°C. Metallation with excess $CoCl_2$/NaCp at 0°C resulted in a dark brown suspension which was then stirred overnight.

The resultant mixture was then subjected to aerial oxidation for an hour followed by filtration through silica and the solvent was removed under reduced pressure. The remaining brown solid was dissolved in DCM, filtered through Celite® and purified by TLC. Preparative TLC with a mixed eluent of DCM and petroleum ether (40-60°C) (1:1) yielded one yellow (compound **11**) and two orange bands (compounds **12** and **13**) with R_f 0.62, 0.56, 0.51 in 3.7%, 2% and 5% yields respectively.

Compound **11** was fully characterised by mass spectrometry, microanalysis, $^{11}B\{^1H\}$ NMR spectroscopy and *X*-ray crystallography.

Mass spectrometry of compound **11** shows the parent ion to have a mass of 510.3 with a broad heteroborane envelope from 503.2 to 514.3 which is consistent with $C_{14}H_{30}B_{18}Co_2$, whilst elemental analysis was in good agreement with the values expected.

In the ^1H NMR spectrum the signals due to C_5H_5 and CH_{cage} were not resolved. However $^{11}B\{^1H\}$ NMR spectroscopy of compound **11** revealed eleven signals at δ 0.22, -1.75, -2.61, -3.15, -6.22, -9.83, -10.49, -12.80, -13.81, -17.40 and -18.67 ppm with integrals in the relative ratio 3:2:1:1:2:2:1:2:1:2:1.

X-ray quality single crystals of yellow compound **11**, 8-(8′-2′-(η-C_5H_5)-2′,1′,8′-*closo*-$CoC_2B_9H_{10}$)-2-(η-C_5H_5)-2,1,8-*closo*-$CoC_2B_9H_{10}$ (Fig 3.4) were obtained by vapour diffusion of a DCM solution and 40-60 petroleum ether at room temperature. This is the third example of a 12-vertex/12-vertex MC_2B_9/MC_2B_9 species. In this compound both cages are isomerised at room temperature.

The *X*-ray diffraction study clearly indicates the presence of a centre of inversion in the middle of C8-C8B and a mirror plane is passing through Co2, B6, B9, C8, C8B, B6B, B9B and Co2B. The atoms C1, C1A, C1B and C1C are treated as 50% B and 50% C character in the crystallographic study. The crystal structure is disordered in the non-linked carbon atoms positions since the metallation was carried out on a mixture of diastereoisomers.

The cages of compound **11** adopt an icosahedral geometry with all atoms in degree five vertices. The dihedral angle between the lower pentagonal belt of the cage and the C_5 plane of the cyclopentadienyl ligand is only 0.48°. Since both cages are connected by a C8-C8B linkage through the bottom belts steric crowding is negligible. The C8-C8B distance of 1.536(3) Å is very close to the value of 1.530(3) Å in 1,1′-bis(*o*-carborane) reported by Xie[5].

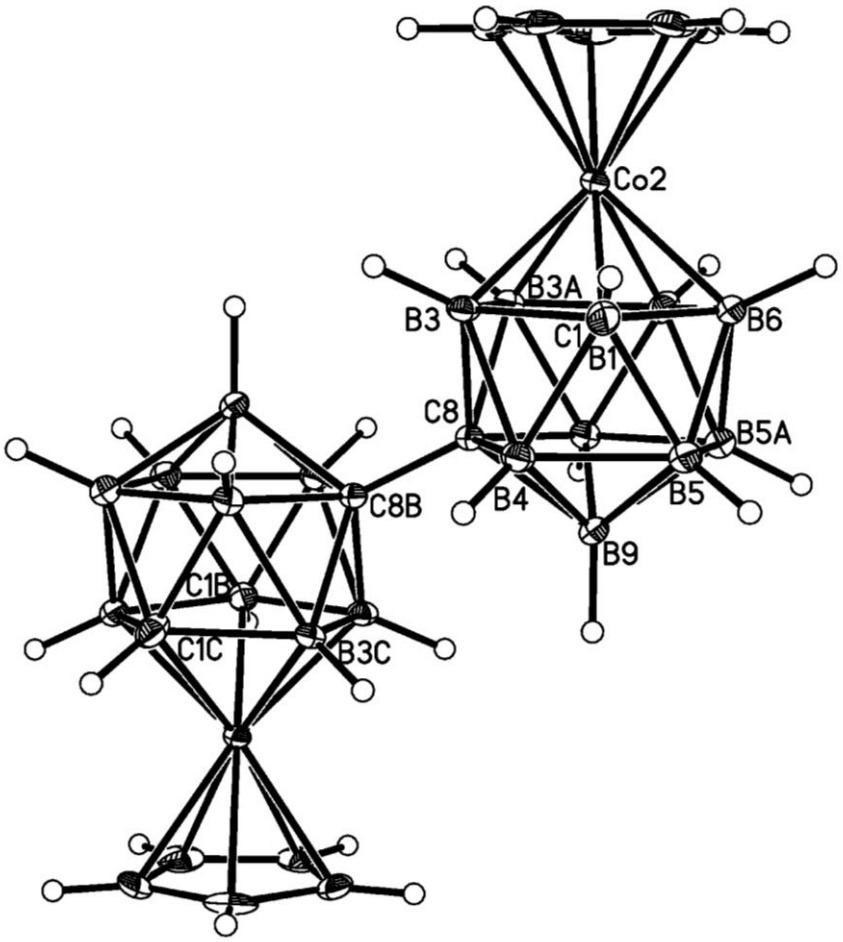

Fig 3.4 Molecular structure of 8-(8′-2′-(η-C_5H_5)-2′,1′,8′-*closo*-$CoC_2B_9H_{10}$)-2-(η-C_5H_5)-2,1,8-*closo*-$CoC_2B_9H_{10}$ (11)

Compound **12** was fully characterised by mass spectrometry, elemental analysis, ^{1}H NMR and $^{11}B\{^{1}H\}$ NMR spectroscopies and *X*-ray crystallography.

Mass spectrometry showed the highest mass envelope to range from 503.2 to 514.2 with the most intense signal at 510.3. Elemental analysis was in good agreement with the expected values for $C_{14}H_{30}B_{18}Co_2$.

^{1}H NMR spectroscopy shows two singlets at δ 6.00 ppm and δ 5.70 ppm which correspond to two different types of C_5H_5 and another two singlets assigned to CH_{cage} protons which appear at δ 4.35 ppm and δ 3.05 ppm.

The $^{11}B\{^{1}H\}$ NMR spectrum consists of ten resonances at δ 4.68, -1.25, -1.62, -4.61, -8.63, -10.64, -12.50, -15.18, -15.79 and -18.27 ppm in the relative ratio 1:4:1:5:1:1:2:1:1:1.

X-ray diffraction-quality orange plates of compound **12** were grown by vapour diffusion of a DCM solution and 40-60 petroleum ether at room temperature and structural study established that the compound is 8-(8′-2′-(η-C_5H_5)-2′,1′,8′-*closo*-$CoC_2B_9H_{10}$)-3-(η-C_5H_5)-3,1,2-*closo*-$CoC_2B_9H_{10}$ (form α) (Fig 3.5). Both cages are capped by Co atoms with degree five vertices occupied by all atoms.

The diffraction study clearly shows that both cages are different, in that one of the cages is 3,1,2 whereas the other cage is isomerised to 2,1,8. The cages are connected through a C1-C8′ linkage with a distance of 1.552(5) Å which is longer than that in 1,1′-bis(*o*-carborane) reported by Xie[5] and similar to that 1-(1′-1′,2′-*closo*-$C_2B_{10}H_{11}$)-3-(η-C_5H_5)-3,1,2-*closo*-$CoC_2B_9H_{10}$ (**3AB** and **3CD**) (1.548(13) (**AB**) and 1.554(15) Å (**CD**) reported in chapter 2[6] (**2.5.3**) which implies that the compound is more sterically crowded than 1,1′-bis(*o*-carborane).

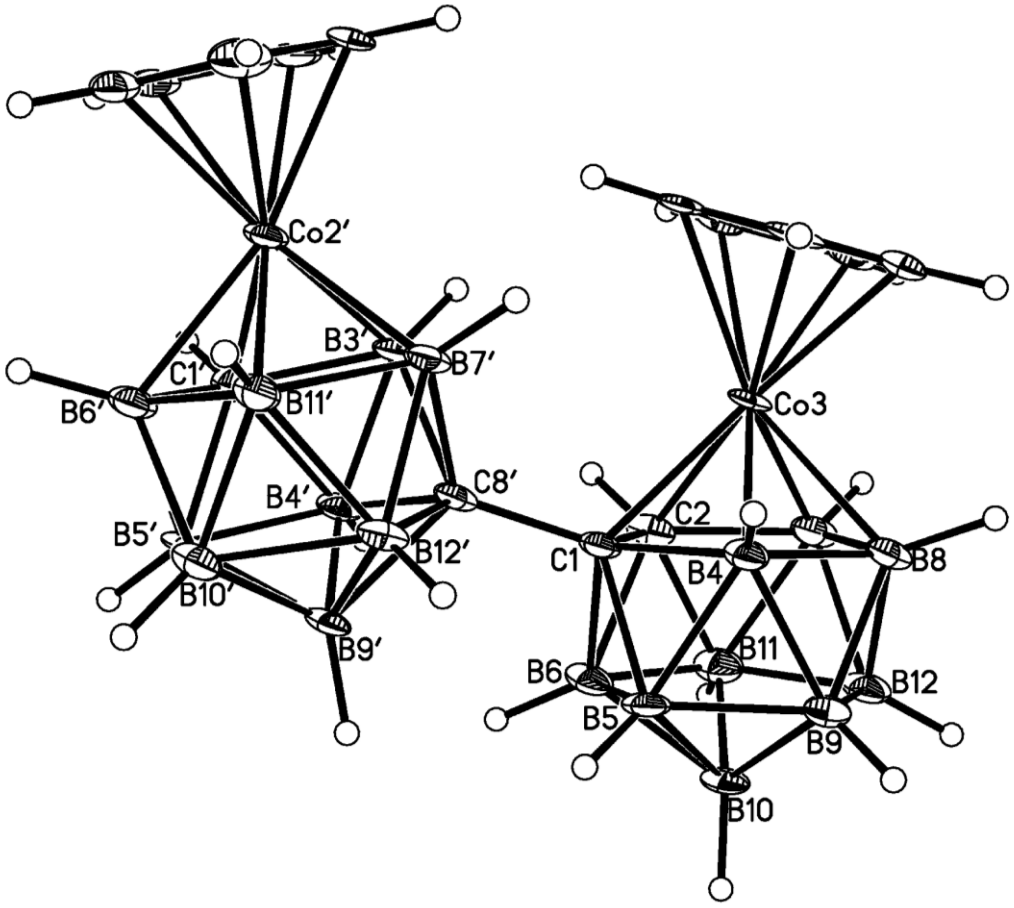

Fig 3.5 Molecular structure of 1-(8′-2′-(η-C_5H_5)-2′,1′,8′-*closo*-$CoC_2B_9H_{10}$)-3-(η-C_5H_5)-3,1,2-*closo*-$CoC_2B_9H_{10}$ (form α, 12)

The dihedral angle between the B_5 (B12-B9-B5-B6-B11) and C_5 (C31-C32-C33-C34-C35) planes of the 3,1,2-CoC_2B_9 cage is 13.57° with the cyclopentadienyl ligand bent away from the 2′,1′,8′-CoC_2B_9 cage and towards the B8 atom. The large tilt angle is due to the bulky cage which is attached to C1. However the dihedral angle between the CB_4 (C8′-B12′-B10′-B5′-B4′) and C_5 (C21′-C22′-C23′-C24′-C25′) planes of the 2′,1′,8′-CoC_2B_9 cage is only 1.54° which implies that this cage is not sterically crowded.

Compound **13** was fully characterised by mass spectrometry, microanalysis, ^{1}H NMR spectroscopy, ^{11}B{^{1}H} NMR spectroscopy and *X*-ray diffraction studies.

Mass spectrometry of compound **13** displayed a peak centred on 510.3 with an envelope from 506.2-514.2 which corresponds to the mass of the parent ion, while elemental analysis was in good agreement with the expected values for $C_{14}H_{30}B_{18}Co_2$.

^{1}H NMR spectroscopy of compound **13** shows two singlets at δ 6.05 ppm and δ 5.70 ppm which correspond to two different types of C_5H_5 and another two singlets at δ 4.35 ppm and δ 3.05 ppm which are due to the CH_{cage} protons. As we expected the C_5H_5 and CH_{cage} signals of compound **13** are essentially the same as those of compound **12**.

^{11}B{^{1}H} NMR spectroscopy consists of nine resonance at δ 4.67, -1.30, -1.62, -4.60, -8.54, -10.83, -12.10, -15.28 and -18.08 ppm in a 1:4:1:5:1:1:1:3:1 relative ratio. The resonances of compound **13** are almost same as those of compound **12** however the relative ratio shows slight variations compared to compound **12** due to accidental coincidence of some of the peaks.

X-ray diffraction quality orange single crystals were grown by vapour diffusion of a DCM solution and 40-60 petroleum ether at room temperature and the study confirmed that compound **13** is 1-(8′-2′-(η-C_5H_5)-2′,1′,8′-*closo*-$CoC_2B_9H_{10}$)-3-(η-C_5H_5)-3,1,2-*closo*-$CoC_2B_9H_{10}$ (form β) (Fig 3.6).

Similarly to compound **12** the diffraction study shows that one of the cages is 3,1,2-CoC_2B_9 whereas the other cage is isomerised to 2′,1′,8′-CoC_2B_9. The cages are connected through a C1-C8′ linkage with a distance of 1.559(5) Å which is longer than that in 1,1′-bis(*o*-carborane) reported by Xie[5] and similar to compound **12**, which implies that the compound is more sterically crowded than 1,1′-bis(*o*-carborane).

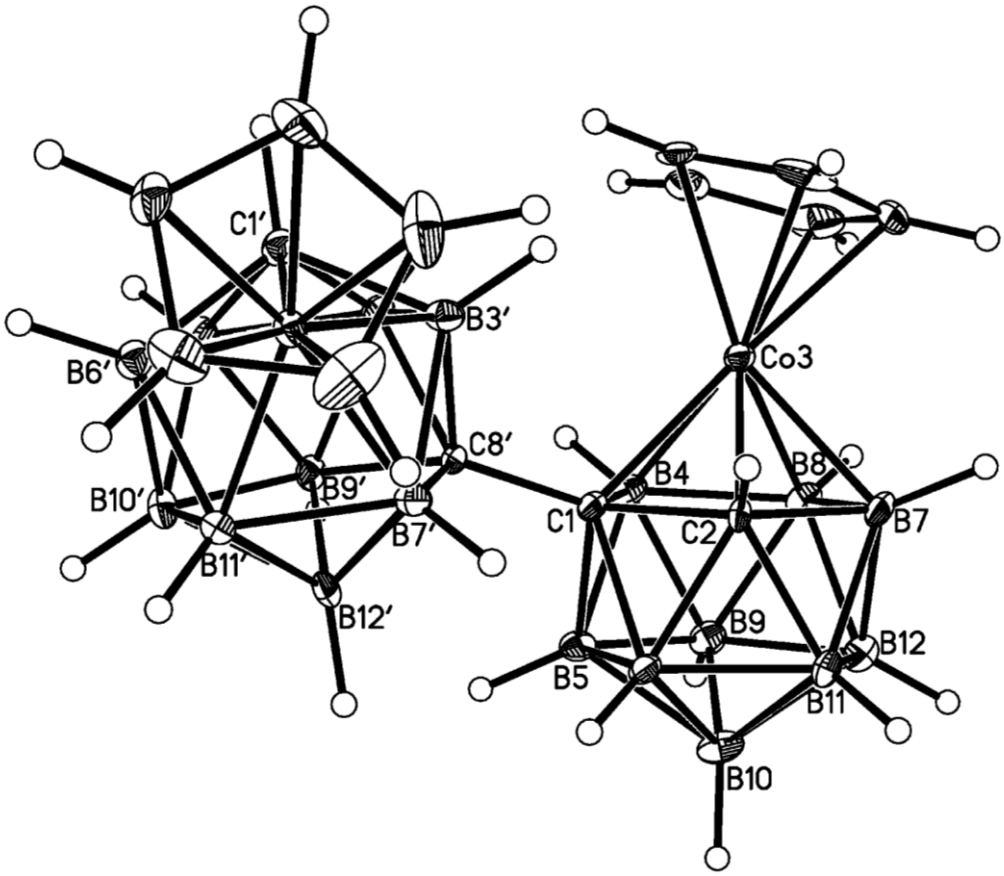

Fig 3.6 Molecular structure of 1-(8′-2′-(η-C_5H_5)-2′,1′,8′-*closo*-$CoC_2B_9H_{10}$)-3-(η-C_5H_5)-3,1,2-*closo*-$CoC_2B_9H_{10}$ (form β, 13)

The C_5H_5 ligand attached to the cobalt in the 3,1,2-$CoC_2B_9H_{10}$ cage is bent away (similar to compound **12**) from the 2′,1′,8′-CoC_2B_9 cage by 15.46° with respect to the lower pentagonal belt to avoid the bulky cage attached to the C1 position. The dihedral angle between the CB_4 and C_5 planes of the 2′,1′,8′-CoC_2B_9 cage is only 2.40° which implies less steric hindrance in the 2′,1′,8′-CoC_2B_9 cage.

The relationship between compounds **12** (form α) and **13** (form β) is that, as can been seen from comparison (Fig 3.7), while one cage (B) is constant the other cage (A) is of opposite handedness. This is due to the fact that metallation with the {CpCo} fragment was carried out on a mixture of *racemic* and *meso* diasterioisomers of [7-(7′-7′,8′-*nido*-$C_2B_9H_{11}$)-7,8-*nido*-$C_2B_9H_{11}$]$^{2-}$.

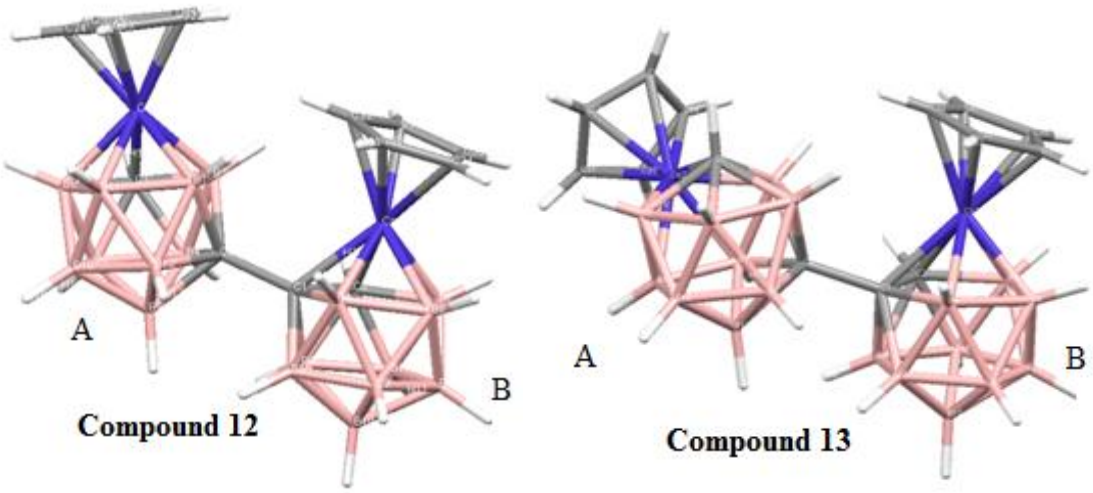

Fig 3.7 Relationship between compounds 12 (form α) and 13 (form β) of 1-(8′-2′-(η-C_5H_5)-2′,1′,8′-*closo*-$CoC_2B_9H_{10}$)-3-(η-C_5H_5)-3,1,2-*closo*-$CoC_2B_9H_{10}$

3.6 Preparation of 12-v/12-v ruthenacarborane/ruthenacarborane species (14 and 15) from deprotonation and metallation of [7-(7′-7′,8′-*nido*-$C_2B_9H_{11}$)-7,8-*nido*-$C_2B_9H_{11}$]$^{2-}$

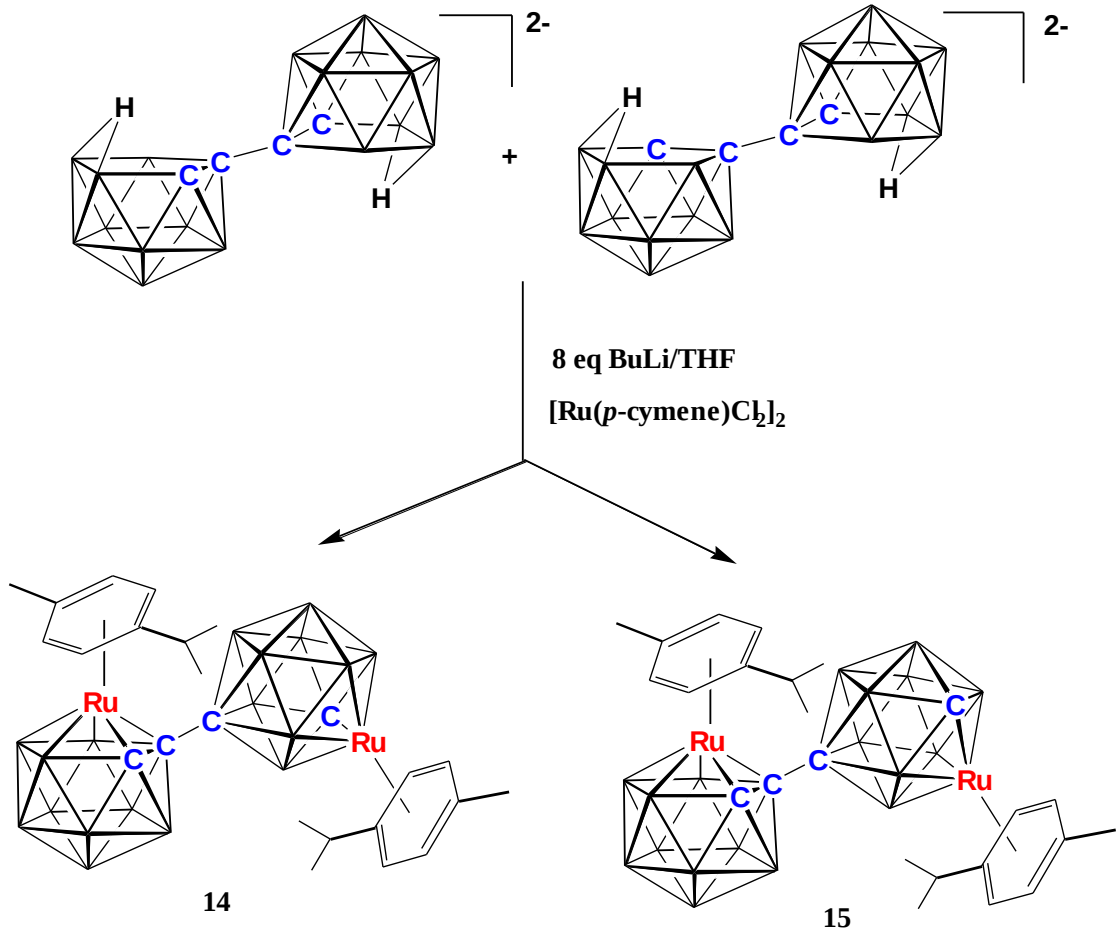

Deprotonation was carried out exactly as same as noted in **3.5** by adding 8 equivalents of BuLi to a THF solution of $[HNMe_3]_2$[7-(7′-7′,8′-*nido*-$C_2B_9H_{11}$)-7,8-*nido*-$C_2B_9H_{11}$] at 0°C. Then the mixture was heated under reflux for 4 hrs and cooled to room temperature. The resultant mixture was treated with a THF suspension of one equivalent of [Ru(*p*-cymene)Cl_2]$_2$ at 0°C and stirred overnight.

The reaction mixture was then filtered through silica and the THF was removed under reduced pressure on the vaccuum line. The resulted brown suspension was dissolved in DCM, filtered through Celite® and then purified by thin layer chromatography. Preparative TLC with mixed eluent of DCM and petroleum ether (40-60°C) (1:1) yielded two yellow products (compounds **14** and **15**) with R_f 0.45 and 0.40 in 2.1% and 10.4% yields respectively.

Compound **14** was fully characterised by mass spectrometry, microanalysis, ^{1}H NMR spectroscopy, ^{11}B{^{1}H} NMR spectroscopy and *X*-ray diffraction study.

Mass spectrometry of compound **14** shows the parent ion to have a mass of 734.3 with a broad heteroborane envelope from 724.3 to 737.3 whilst elemental analysis was in good agreement with the values expected for $C_{24}H_{48}B_{18}Ru_2$.

The ^{1}H NMR spectrum of compound **14** clearly shows that there are two different types of *p*-cymene present. The multiplet centered on δ 6.15 ppm is assigned to eight aromatic protons due to the overlap of two C_6H_4 ligands. The CH_{cage} signals at δ 3.75 ppm and δ 2.75 ppm indicate the presence of two different types of cages.

One septet at δ 3.10 ppm (1H) is assigned to the tertiary H of the *i*-propyl group of one *p*-cymene ligand whereas the other tertiary H of an *i*-propyl group and one of the methyl groups overlap and appear as a multiplet centered on δ 2.85 ppm (4H). The singlet at δ 2.45 ppm (3H) is assigned to the other methyl group and the multiplet centered on δ 1.3 ppm (12H) is assigned to $2CH(CH_3)_2$.

^{11}B{^{1}H} NMR spectroscopy revealed nine resonances at δ 1.33, -0.58, -1.39, -4.15, -8.16, -13.34, -17.09, -18.01 and -21.27 ppm in the relative ratio 1:3:1:2:5:1:3:1:1.

Crystals were grown by vapour diffusion of a DCM solution and 40-60 petroleum ether at room temperature. An *X*-ray diffraction study confirmed the compound is 1-(8′-2′-(η-$C_{10}H_{14}$)-2′,1′,8′-*closo*-$RuC_2B_9H_{10}$)-3-(η-$C_{10}H_{14}$)-3,1,2-*closo*-$RuC_2B_9H_{10}$ (form α) (Fig 3.8).

The top belt of the 3,1,2-$RuC_2B_9H_{10}$ cage is connected to the bottom belt of the 2′,1′,8′-$RuC_2B_9H_{10}$ cage through a C1-C8′ linkage. The atoms C1′ and C8′ in the 2′,1′,8′-$RuC_2B_9H_{10}$ cage are separated by 2.705 Å. It is remarkable that an isomerised (2,1,8-RuC_2B_9) ruthenacarborane has been formed without any heating.

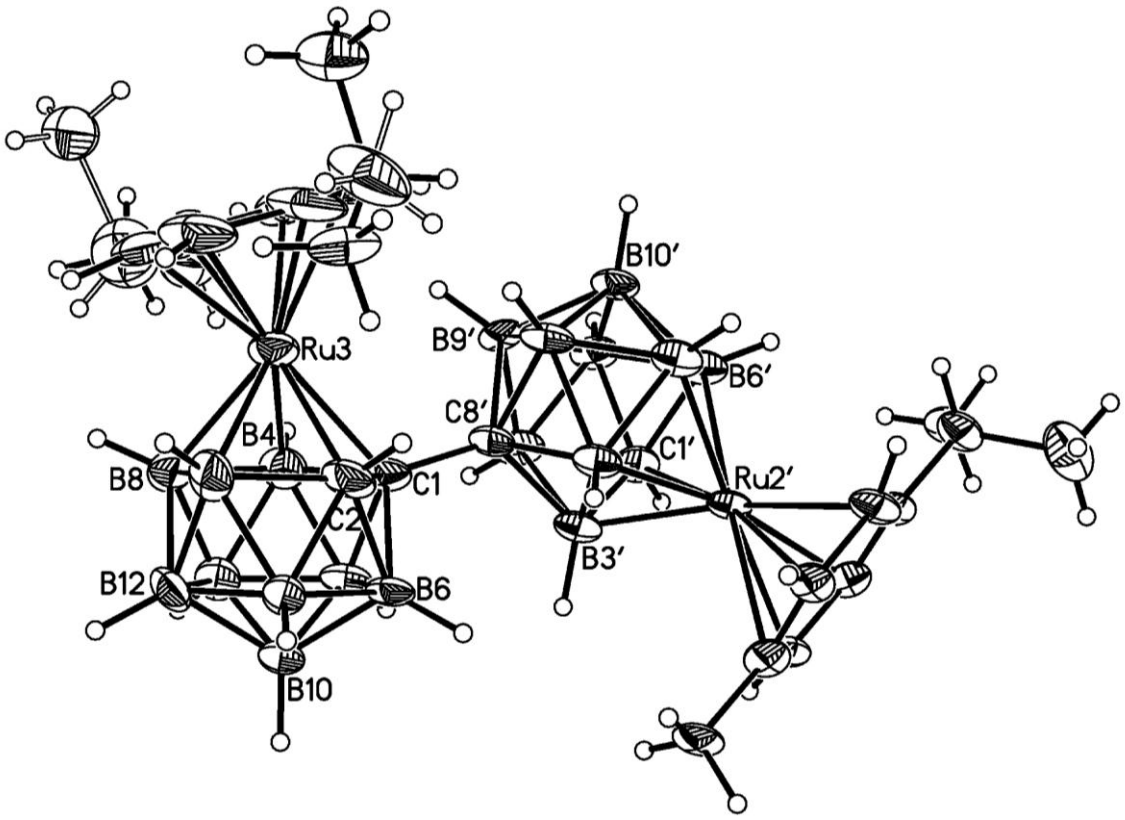

Fig 3.8 Molecular structure of 1-(8′-2′-(η-$C_{10}H_{14}$)-2′,1′,8′-*closo*-$RuC_2B_9H_{10}$)-3-(η-$C_{10}H_{14}$)-3,1,2-*closo*-$RuC_2B_9H_{10}$ (form α, 14)

In the 3,1,2-$RuC_2B_9H_{10}$ cage the dihedral angle between the lower pentagonal belt, B5-B6-B11-B12-B9, and the arene ring of the *p*-cymene, C30-C31-C32-C33-C34-C35, is 17.27° and the distance between C1 and C8′ is 1.561(10) Å, both of which imply that the 3,1,2-$RuC_2B_9H_{10}$ cage is sterically crowded. However the tilt angle of the 2′,1′,8′-$RuC_2B_9H_{10}$ cage is only 2.10°, which is very small compared to that in the 3,1,2-$RuC_2B_9H_{10}$ cage and therefore the primed cage is not sterically crowded.

Compound **15** was fully characterised by mass spectrometry, microanalysis, ^{1}H and $^{11}B\{^{1}H\}$ NMR spectroscopies and *X*-ray diffraction study.

Mass spectrometry of compound **15** displayed a peak of the parent ion centred on 734.3 with a characteristic broad heteroborane envelope from 728.3 to 738.3 whilst elemental analysis was in good agreement with the values expected for $C_{24}H_{48}B_{18}Ru_2$.

The ^{1}H NMR spectrum of compound **15** shows slight variations in the resonances compared to those in compound **14**. The multiplet centered on δ 6.15 ppm is assigned to eight aromatic protons due to the overlap of two C_6H_4 groups of the *p*-cymene ligands. The CH_{cage} signals with integral one at δ 3.95 ppm and δ 2.70 ppm indicate the presence of two different types of cages.

One septet at δ 3.05 ppm (1H) is assigned to the tertiary H atom of the *i*-propyl group of one *p*-cymene ligand whereas the other tertiary H atom and one of the methyl groups overlap and appear as a multiplet centered on δ 2.85 ppm (4H). The singlet and multiplet at δ 2.45 ppm (3H) and δ 1.30 ppm (12H) are assigned to the other CH_3 and $2CH(CH_3)_2$ groups respectively.

$^{11}B\{^{1}H\}$ NMR spectroscopy revealed ten signals at δ 1.38, -0.50, -1.33, -4.42, -5.26, -8.20, -13.56, -16.98, -17.98 and -21.03 ppm in the relative ratio 1:3:1:1:1:5:1:1:3:1.

Yellow *X*-ray diffraction-quality crystals were grown from d_6-acetone by solvent evaporation and confirmed the compound to be 1-(8′-2′-(η-$C_{10}H_{14}$)-2′,1′,8′-*closo*-$RuC_2B_9H_{10}$)-3-(η-$C_{10}H_{14}$)-3,1,2-*closo*-$RuC_2B_9H_{10}$ (form β) (Fig 3.9). Like compounds **12** and **13** the relationship between compounds **14** and **15** is that one cage is the same whilst the other cage is enantiomerically related. As with compound **14** one ruthenacarborane cage has clearly isomerised at room temperature, which is surprising, and presumably the result of severe steric crowding.

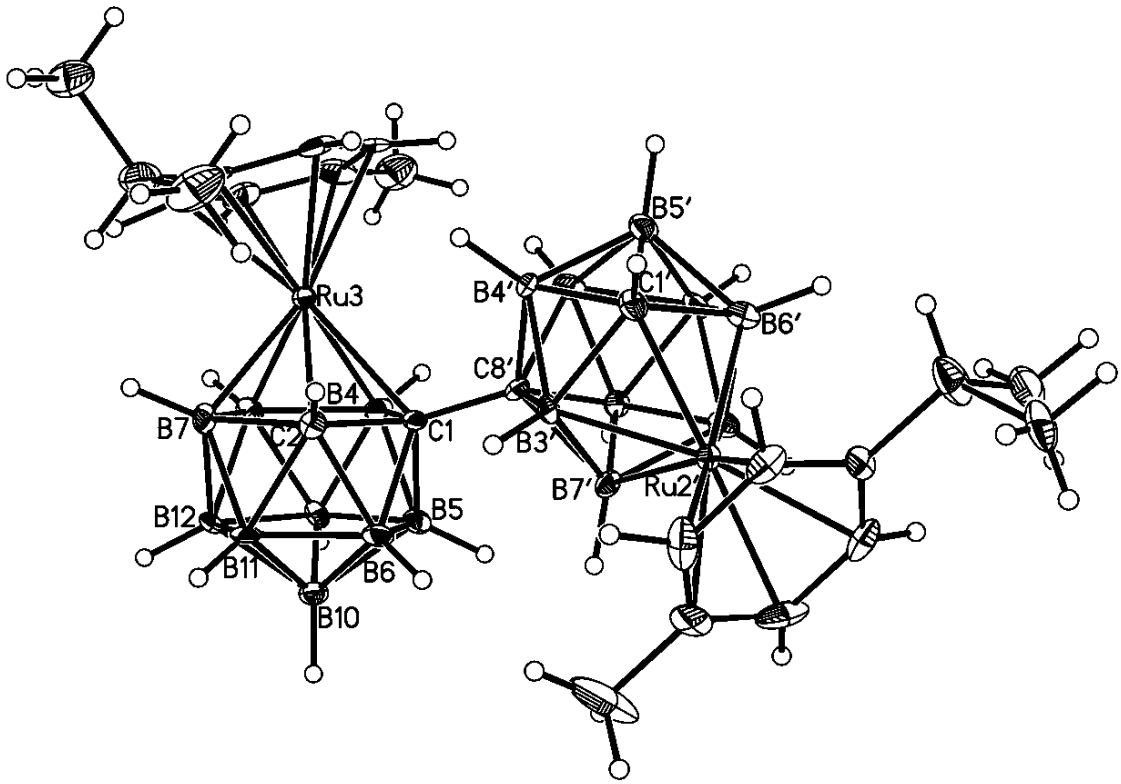

Fig 3.9 Molecular structure of 1-(8′-2′-(η-$C_{10}H_{14}$)-2′,1′,8′-*closo*-$RuC_2B_9H_{10}$)-3-(η-$C_{10}H_{14}$)-3,1,2-*closo*-$RuC_2B_9H_{10}$ (form β, 15)

In compound **15** similarly to compound **14** the *p*-cymene ligand attached to the 3,1,2-$RuC_2B_9H_{10}$ cage is bent away from the 2′,1′,8′-$RuC_2B_9H_{10}$ cage by 17.16° to avoid steric crowding. Both cages are connected through C1 and C8′ with a bond distance of 1.546(8) Å which is slightly shorter than that in compound **14**.

However the *p*-cymene ligand attached to the 2′,1′,8′-$RuC_2B_9H_{10}$ cage is bent away from the 3,1,2-$RuC_2B_9H_{10}$ cage by only 3.04° with respect to the lower pentagonal belt. The reason behind this is due to the fact that the 3,1,2-$RuC_2B_9H_{10}$ cage is connected at C8′ in the lower pentagonal belt of the 2′,1′,8′-$RuC_2B_9H_{10}$ cage therefore the steric strain has been relieved by isomerisation.

3.7 Discussion

This section is mainly focused on the spectroscopic and structural details of the following compounds, $[BTMA]_2[7\text{-}(7'\text{-}7',8'\text{-}\textit{nido}\text{-}C_2B_9H_{11})\text{-}7,8\text{-}\textit{nido}\text{-}C_2B_9H_{11}]$ (**8**), $[HNMe_3]_2[7\text{-}(7'\text{-}7',8'\text{-}\textit{nido}\text{-}C_2B_9H_{11})\text{-}7,8\text{-}\textit{nido}\text{-}C_2B_9H_{11}]$ (**9**), $[(S)\text{-}CH_3NC_5H_4\text{-}C_4H_7NCH_3]_2[7\text{-}(7'\text{-}7',8'\text{-}\textit{nido}\text{-}C_2B_9H_{11})\text{-}7,8\text{-}\textit{nido}\text{-}C_2B_9H_{11}]$ (**10**), $8\text{-}(8'\text{-}2'\text{-}(\eta\text{-}C_5H_5)\text{-}2',1',8'\text{-}\textit{closo}\text{-}CoC_2B_9H_{10})\text{-}2\text{-}(\eta\text{-}C_5H_5)\text{-}2,1,8\text{-}\textit{closo}\text{-}CoC_2B_9H_{10}$ (**11**), $8\text{-}(8'\text{-}2'\text{-}(\eta\text{-}C_5H_5)\text{-}2',1',8'\text{-}\textit{closo}\text{-}CoC_2B_9H_{10})\text{-}3\text{-}(\eta\text{-}C_5H_5)\text{-}3,1,2\text{-}\textit{closo}\text{-}CoC_2B_9H_{10}$ (**12** and **13**) and $8\text{-}(8'\text{-}2'\text{-}(\eta\text{-}C_{10}H_{14})\text{-}2',1',8'\text{-}\textit{closo}\text{-}RuC_2B_9H_{10})\text{-}3\text{-}(\eta\text{-}C_{10}H_{14})\text{-}3,1,2\text{-}\textit{closo}\text{-}RuC_2B_9H_{10}$ (**14** and **15**).

Deprotonation of $[HNMe_3]_2[7\text{-}(7'\text{-}7',8'\text{-}\textit{nido}\text{-}C_2B_9H_{11})\text{-}7,8\text{-}\textit{nido}\text{-}C_2B_9H_{11}]$ (**9**) with n-BuLi followed by metallation with {CpCo} fragments resulted in three different compounds, **11**, **12** and **13**. In compound **11** both cages are isomerised whereas in compounds **12** and **13** only a single cage is isomerised.

However, metallation with {(*p*-cymene)Ru} fragments resulted in only two compounds, **14** and **15**. In both of these compounds only single cage is isomerised whereas the other cage remains non-isomerised at room temperature. A product with both cages isomerised was not obtained as had been with metallation with {CpCo} fragments, which may be due to the fact that {CpCo} is more flexible than {(*p*-cymene)Ru} in metallacarboranes[6,7].

3.7.1 ^{11}B NMR spectroscopy

As noted in **3.1** in 1971 Hawthorne reported the ^{11}B NMR spectrum of salt **9** at 80 MHz[2] which showed only eight resonances and did not indicate the presence of diastereoisomers. $^{11}B\{^1H\}$ NMR spectroscopy of salts **8**, **9** and **10** would have up to nine resonances for either the *racemic* or *meso* form of the diastereoisomer. Interestingly, the $^{11}B\{^1H\}$ NMR spectrum of salts **8**, **9** (Fig 3.10) and **10** revealed eleven resonances. Moreover, eight of these resonances are closely related as major and minor components.

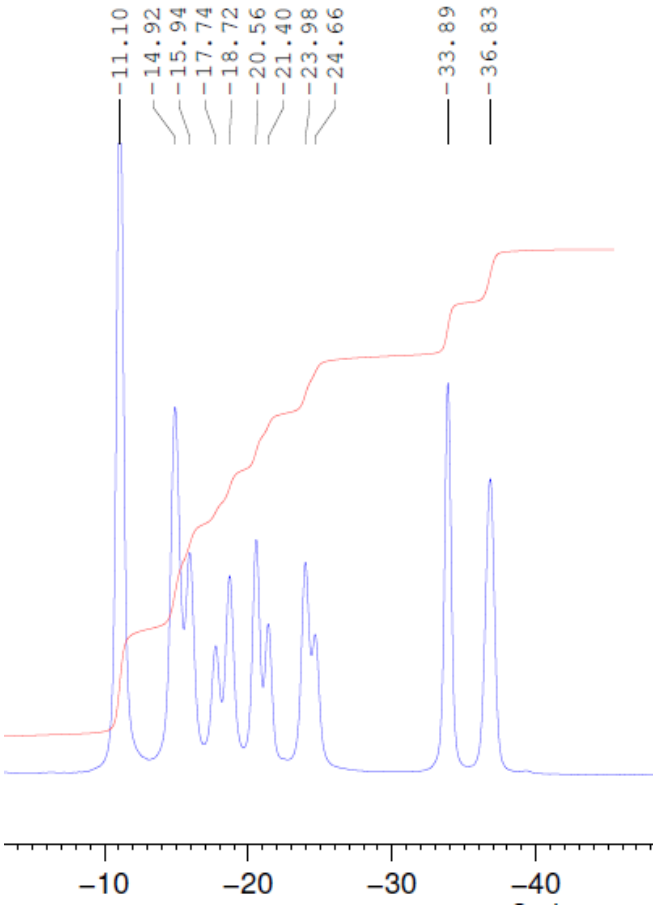

Fig 3.10 **$^{11}B\{^{1}H\}$ NMR spectrum of [7-(7′-7′,8′-*nido*-$C_2B_9H_{11}$)-7,8-*nido*-$C_2B_9H_{11}$]$^{2-}$**

Therefore we can conclude that salts **8**, **9** and **10** exist as mixtures of diastereoisomers, *meso* and *racemic*. The reason behind this may be due to the fact that when the reaction was carried out with excess of KOH it is possible to remove the boron atoms from either the B3 and B6 positions of the closo cage in [7-(1′-1′,2′-*closo*-$C_2B_{10}H_{11}$)-7,8-*nido*-$C_2B_9H_{11}$]$^-$ (fig 3.2) and therefore we isolated mixtures of diastereoisomers. This might not have happened when using 2.5 equivalents of KOH reported by Hawthorne[2] because one of the boron atoms would be slightly more positive than the other boron atom and preferentially removed. Therefore 2.5 equivalents of KOH is not enough to remove the less positive boron atom and results in the isolation of only either the *meso* or *racemic* diasteroisomer.

Unfortunately the crystals of both *meso* and *racemic* diastereoisomers of salt **8** seem to have the same shape and we have no way to separate them to discover which is the major and minor form of product. The crystal that was subjected to *X*-ray diffraction studies was the *meso* form of $[BTMA]_2[7\text{-}(7'\text{-}7',8'\text{-}nido\text{-}C_2B_9H_{11})\text{-}7,8\text{-}nido\text{-}C_2B_9H_{11}]$ and revealed the presence of a centre of inversion in the middle of the C7-C7′ bond.

Therefore salt **10** was synthesised with the hope of separating the isomers and identifying the $^{11}B\{^1H\}$ NMR signals which correspond to *meso* and *racemic* diastereoisomers individually, by crystallising only one isomer due to the presence of a chiral center in the cation, $[(S)\text{-}CH_3NC_5H_4\text{-}C_4H_7NCH_3]^+$.

$[(S)\text{-}CH_3NC_5H_4\text{-}C_4H_7NCH_3]I$ (Fig 3.11) was prepared in 1976 by the addition of iodomethane to (*S*)-nicotine in the presence of glacial acetic acid however the complete characterisation was not reported[8]. Therefore the complete characterisation of this iodide was carried out first.

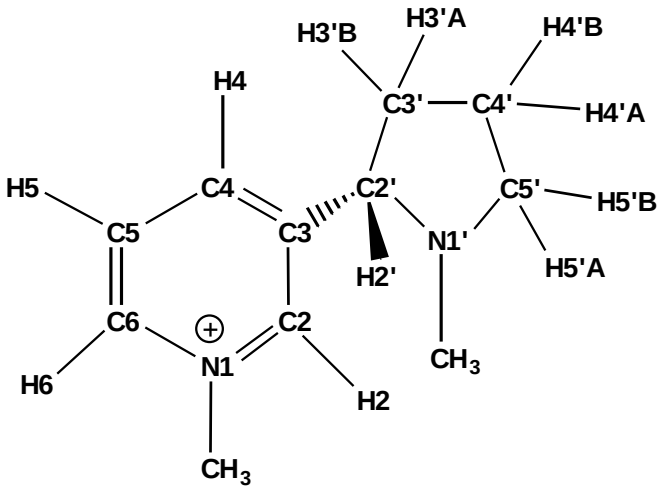

Fig 3.11 Structure of $[(S)\text{-}CH_3NC_5H_4\text{-}C_4H_7NCH_3]^+$

In table 3.1 are the assignments of each carbon and proton of $[(S)\text{-}CH_3NC_5H_4\text{-}C_4H_7NCH_3]^+$ according to ^{13}C, ^{13}C DEPT, two dimensional ^{13}C-^1H HSQC experiment and ^1H NMR spectroscopies.

Assignment	δ(^{13}C) / ppm	δ(^{1}H) / ppm
3	146.6	
6	143.8	9.25
2	143.8	9.10
4	143.8	8.40
5	128.1	8.10
2′	66.7	3.50
5′	56.6	3.15, 2.35
1(CH_3)	49.4	4.65
1′(CH_3)	40.6	2.15
3′	35.6	2.35, 1.65
4′	23.2	1.80

Table 3.1 NMR parameters for [(*S*)-$CH_3NC_5H_4$-$C_4H_7NCH_3$]$^+$

The highest frequency ^{13}C NMR peak at 146.6 ppm is assigned to C3 since this is the only carbon without hydrogen (which is part of the aromatic ring and connected to the $C_4H_7NCH_3$ group) therefore it does not appear in the ^{13}C DEPT spectrum.

The ^{13}C DEPT spectrum clearly shows that the peaks at δ 143.8, 143.8, 143.8, 128.1 and 66.7 ppm are due to CH groups. The resonances between δ 144 and 128 ppm are assigned to C6, C2, C4 and C5 because they are part of the aromatic ring, therefore appear at relatively high frequency in the ^{13}C NMR spectrum.

The remaining signal at δ 66.7 ppm is assigned to C2′ because this is the only non-aromatic CH thus appears at relatively low frequency. Therefore the signal due to H2′ can be easily assigned from the analysis of two dimensional ^{13}C-^{1}H correlation spectrum (Fig 3.12) which appears with integration one at δ 3.50 ppm.

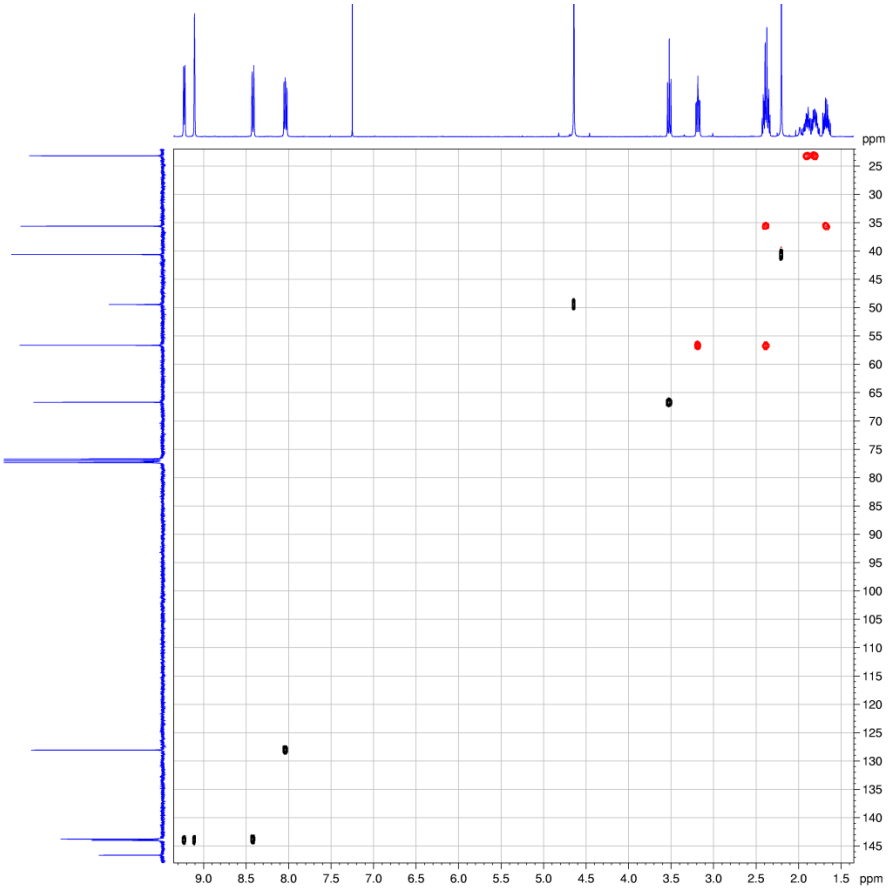

Fig 3.12 ^{13}C-^{1}H HSQC spectroscopy of salt 10

From the ^{1}H NMR spectrum it is clear that the doublet at δ 9.25 ppm is due to H6 since this proton is more deshielded because of the neighbouring $^{+}N1CH_3$ group than H4 which appears as doublet at δ 8.40 ppm. The singlet at δ 9.10 ppm is assigned to H2 because this is the only aromatic proton present without any neighbouring CH group. Therefore we can assign the ^{13}C signals of the carbons C6, C2 and C4 (which all appear at δ 143.8 ppm by coincidence) from the two dimensional ^{13}C-^{1}H correlation spectrum.

The triplet at δ 8.10 ppm in the ^{1}H NMR spectrum is assigned to H5 since this is the only proton adjacent to H6 and H4. Therefore from the analysis of the two dimensional ^{13}C-^{1}H correlation spectrum the ^{13}C NMR signal at δ 128.1 ppm is assigned to C5.

The ^{13}C signals at δ 56.6, 35.6 and 23.2 ppm are assigned to CH_2 groups because in the ^{13}C DEPT NMR spectrum these signals appear opposite to the CH_3 and CH signals. The resonance at δ 56.6 ppm is assigned to C5′ because it is adjacent to –N1′CH_3 therefore relatively more deshielded, and the remaining lower frequency signals at δ 35.6, 23.2 ppm are assigned to C3′ and C4′ respectively because these two positions are relatively shielded.

The ^{1}H NMR signals with integration three which appear as singlets at δ 4.65 and 2.15 ppm are assigned to CH_3 groups attached to $^{+}$N1 and N1′ respectively with the CH_3 group attached to $^{+}$N1 the more deshielded. The signals at δ 49.4 and 40.6 ppm in the ^{13}C NMR spectrum are assigned from the analysis of the two dimensional ^{13}C-^{1}H HSQC spectrum to the CH_3 groups attached to $^{+}$N1 and N1′ respectively.

In the two dimensional ^{13}C-^{1}H correlation spectrum the ^{1}H NMR signals at δ 3.15 and 2.35 ppm correlate with the ^{13}C NMR signal at δ 56.6 ppm which corresponds to C5′. Therefore the above ^{1}H NMR signals are assigned to H5′A and H5′B. Similarly the ^{1}H NMR signals at δ 2.35 and 1.65 ppm are assigned to H3′A and H3′B. The multiplet centered on δ 1.80 ppm is assigned to H4′A and H4′B.

The ^{1}H NMR results published using deuterated nicotine analogues by J. F. Whidby and co-workers[9] shows that the resonances at δ 3.15 and 2.35 ppm are assigned to H5′A and H5′B respectively and the resonances at δ 2.35 and 1.65 ppm are assigned to H3′B and H3′A respectively

The weighted average chemical shifts, $<\delta^{11}B>$, of compounds **11-15** are at higher frequencies compared to the equivalent value in 1,1′-bis(*o*-carborane) which means that the boron atoms in 12-vertex/12-vertex metallacarborane/metallacarborane species are more deshielded (Table 3.2).

Compounds	**<δ^{11}B>**
1,1′-bis(*o*-carborane)	-9.1
8-(1′-1′,2′-*closo*-$C_2B_{10}H_{11}$)-2-(η-C_5H_5)-2,1,8-*closo*-$CoC_2B_9H_{10}$ (**8**)[7]	-8.5
8-(8′-2′-(η-C_5H_5)-2′,1′,8′-*closo*-$CoC_2B_9H_{10}$)-2-(η-C_5H_5)-2,1,8-*closo*-$CoC_2B_9H_{10}$ (**11**)	-8.0
1-(1′-1′,2′-*closo*-$C_2B_{10}H_{11}$)-3-(η-C_5H_5)-3,1,2-*closo*-$CoC_2B_9H_{10}$ (**3**)[7]	-7.8
8-(8′-2′-(η-C_5H_5)-2′,1′,8′-*closo*-$CoC_2B_9H_{10}$)-3-(η-C_5H_5)-3,1,2-*closo*-$CoC_2B_9H_{10}$ (**12**)	-6.6
8-(8′-2′-(η-C_5H_5)-2′,1′,8′-*closo*-$CoC_2B_9H_{10}$)-3-(η-C_5H_5)-3,1,2-*closo*-$CoC_2B_9H_{10}$ (**13**)	-6.7
1-(1′-1′,2′-$C_2B_{10}H_{11}$)-3-(η-$C_{10}H_{14}$)-3,1,2-*closo*-$RuC_2B_9H_{10}$ (**1**)[7]	-8.9
8-(8′-2′-(η-$C_{10}H_{14}$)-2′,1′,8′-*closo*-$RuC_2B_9H_{10}$)-3-(η-$C_{10}H_{14}$)-3,1,2-*closo*-$RuC_2B_9H_{10}$ (**14**)	-8.6
8-(8′-2′-(η-$C_{10}H_{14}$)-2′,1′,8′-*closo*-$RuC_2B_9H_{10}$)-3-(η-$C_{10}H_{14}$)-3,1,2-*closo*-$RuC_2B_9H_{10}$ (**15**)	-8.8

Table 3.2 <δ^{11}B> for compounds 11-15 in ppm

The weighted average chemical shift of compound **11** is moved to higher frequency by ca. 0.5 ppm when replacing a boron vertex of the 1′,2′-$C_2B_{10}H_{11}$ cage in compound **8** by a {2′,1′,8′-CpCo} fragment. Similarly to compound **11**, <δ^{11}B> of compounds **12** and **13** are also shifted to higher frequencies by ca. 2 ppm, when replacing a boron atom of the 1′,2′-$C_2B_{10}H_{11}$ cage in compound **8** by a {3,1,2-CpCo}fragment.

Compounds **12** and **13** can also be considered to be formed by replacing a boron vertex of the 1′,2′-$C_2B_{10}H_{11}$ cage in compound **3** with a {2′,1′,8′-CpCo} fragment, and this causes <δ^{11}B> to move to higher frequency by ca. 1.2 ppm. The weighted average ^{11}B chemical shifts of compounds **14** and **15** also shift to higher frequency when replacing a boron atom of the 1′,2′-$C_2B_{10}H_{11}$ cage in compound **1** with {2′,1′,8′-(*p*-cymene)Ru} but the change is not large.

3.7.2 *X*-ray diffraction studies

X-ray diffraction studies of compounds, 8-(8′-2′-(η-C_5H_5)-2′,1′,8′-*closo*-$CoC_2B_9H_{10}$)-3-(η-C_5H_5)-3,1,2-*closo*-$CoC_2B_9H_{10}$ (**12** and **13**, α-form and β-form, respectively) and 8-(8′-2′-(η-$C_{10}H_{14}$)-2′,1′,8′-*closo*-$RuC_2B_9H_{10}$)-3-(η-$C_{10}H_{14}$)-3,1,2-*closo*-$RuC_2B_9H_{10}$ (**14** and **15**, α-form and β-form, respectively) confirmed that the two cages are different and that in all four compounds the ligand attached to the metal in the 3,1,2- cage is bent away from the 2′,1′,8′- cage with respect to 3-L-3,1,2-*closo*-$MC_2B_9H_{11}$[10] to avoid steric crowding (Fig 3.13).

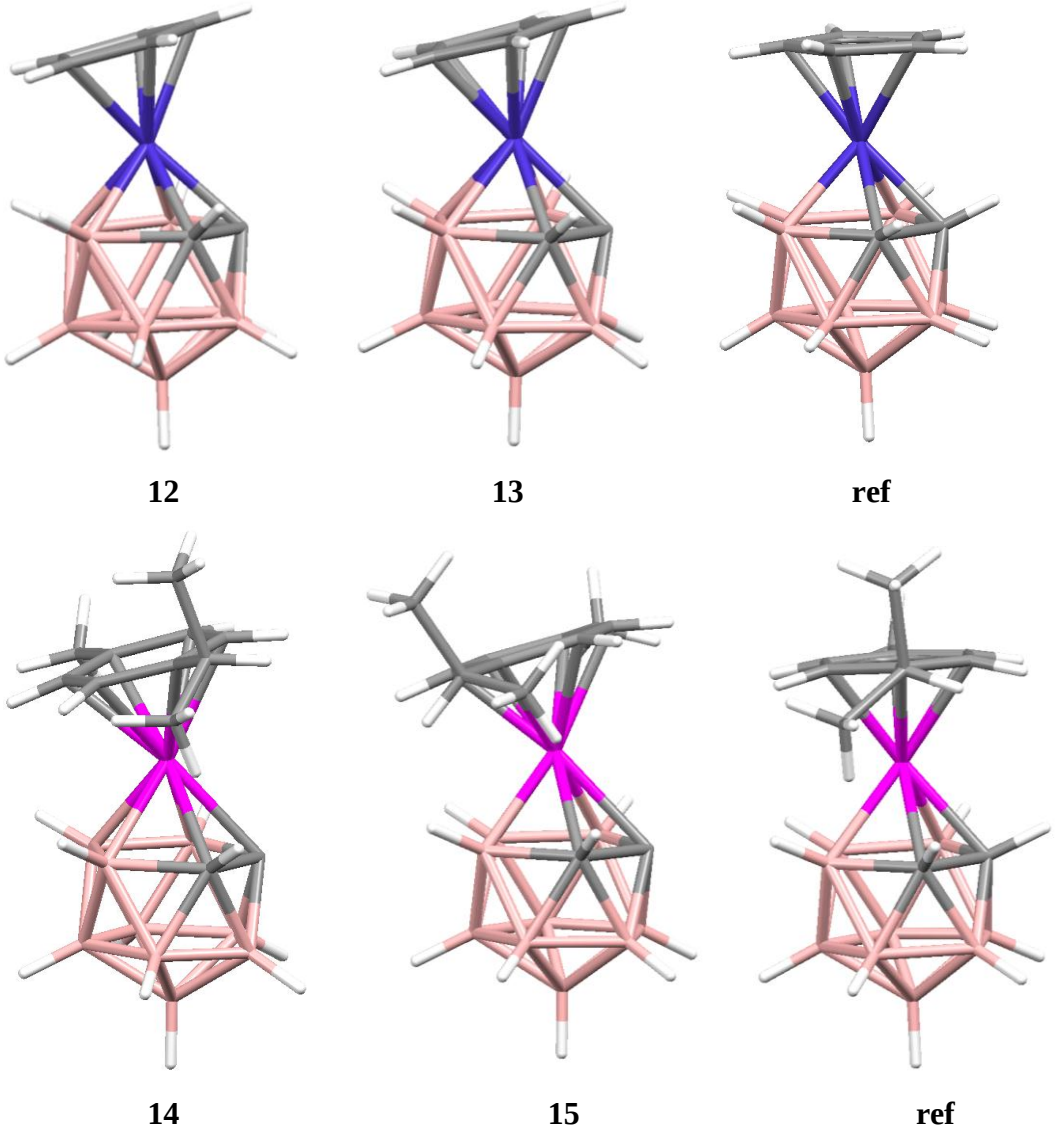

Fig 3.13 **Structures of 3-L-3,1,2-*closo*-$MC_2B_9H_{10}$ fragments (M=Co, compounds 12 and 13) and M=Ru, compounds 14 and 15) and 3-L-3,1,2-*closo*-$MC_2B_9H_{11}$ reference compounds**

Table 3.3 shows how much the ligand attached to the metal is bent away from the other cage with respect to the lower pentagonal belt. In 3,1,2- cages the angle θ is measured with respect to the B_5 face whereas in 2′,1′,8′- cages it is measured with respect to the CB_4 face.

	θ	
Compound	**{3,1,2-MC_2B_9}**	**{2′,1′,8′-MC_2B_9}**
Compound **12**	13.57	1.54
Compound **13**	15.46	2.40
Compound **14**	17.27	2.10
Compound **15**	17.16	3.04

Table 3.3 Dihedral angle θ (degrees) in 3,1,2-MC_2B_9 and 2′,1′,8′-MC_2B_9 cages of compounds 12-15

In all four compounds, **12**, **13**, **14** and **15**, the dihedral angle in the 3,1,2-MC_2B_9 cage is much larger than in the corresponding 2′,1′,8′-MC_2B_9 cage due to the fact that in the 3,1,2- cage a sterically demanding metallacarborane cage is attached at the C1 position whereas in the 2′,1′,8′- cage the metallacarborane cage is moved to the C8 position.

Table 3.4 shows by how much each atom in the 3,1,2-MC_2B_9 cages of compounds **12**, **13**, **14** and **15** has deviated with respect to the parent compounds[10]. The overall deviation is larger in {RuC_2B_9} fragments than in {CoC_2B_9} fragments. In these {MC_2B_9} fragments atoms C1 and M3 deviate more than the other atoms because H on C1 is replaced by a sterically bulky {2′,1′,8′-MC_2B_9 } fragment which also causes the tilting of the ligand attached to M3.

Compound **12**		Compound **13**	
{3,1,2-CoC_2B_9	dev.	{3,1,2-CoC_2B_9}	dev.
C1	0.094	C1	0.086
C2	0.037	C2	0.049
Co3	0.080	Co3	0.093
B4	0.023	B4	0.022
B5	0.008	B5	0.019
B6	0.042	B6	0.040
B7	0.010	B7	0.010
B8	0.016	B8	0.013
B9	0.012	B9	0.005
B10	0.022	B10	0.029
B11	0.007	B11	0.010
B12	0.028	B12	0.021
overall	0.042	overall	0.043

Compound **14**		Compound **15**	
{3,1,2-RuC_2B_9}	dev.	{3,1,2-RuC_2B_9}	dev.
C1	0.086	C1	0.077
C2	0.048	C2	0.058
Ru3	0.108	Ru3	0.106
B4	0.040	B4	0.067
B5	0.027	B5	0.024
B6	0.031	B6	0.042
B7	0.013	B7	0.031
B8	0.013	B8	0.017
B9	0.007	B9	0.025
B10	0.031	B10	0.031
B11	0.012	B11	0.023
B12	0.008	B12	0.023
overall	0.047	overall	0.051

Table 3.4 **Rms deviations (Å) between the {3,1,2-MC_2B_9} "component" of compounds 12-15 and these fragments in single cage reference compounds**

3.7.3 Cage connectivities

Cage connectivites of compounds **12** and **13** are tabulated in table 3.5. In compound **12** the C1-C2 distance in the 3,1,2-CoC_2B_9 cage is 1.652(5) Å, and cobalt to carbon distances are 2.128(3) and 2.041(3) Å. The Co3-B4, Co3-B8 and Co3-B7 distances are 2.065(4), 2.083(4) and 2.068(4) Å respectively. In compound **13** the C1-C2 distances in the 3,1,2-CoC_2B_9 cage is 1.635(5) Å whereas the cobalt to carbon distances are 2.137(4) and 2.054(4) Å. The Co3-B4, Co3-B8 and Co3-B7 distances are 2.081 (4) Å, 2.093 (4) Å and 2.055 (4) Å respectively.

In compound **12** C1′ and C8′ in the 2′,1′,8′-CoC_2B_9 cage are separated by 2.670 Å whereas in compound **13** they are separated by 2.673 Å. The Co2′ to C1′ distance is 2.022 (3) Å in compound **12** and 2.015(4) Å in compound **13**. The Co2′-B3′, Co2′-B7′, Co2′-B11′ and Co2′-B6′ distances in compound **12** are 2.026(4), 2.071(4), 2.079(4) and 2.065 (4) Å respectively, whereas in compound **13** they are 2.015 (4) Å, 2.057 (4) Å, 2.071 (4) Å and 2.056 (5) Å respectively.

Therefore the Co3-C and Co3-B distances in compound **13** are longer than in compound **12** except for Co3-B7 which is shorter, whereas Co2′-C1′ and Co2′-B′ distances are all longer in compound **12** than in compound **13**.

When cobalt atoms are replaced by ruthenium atoms the cage connectivity distances between metal and C_2B_3 face (2.186(9)-2.292(7) Å for compound **14** and 2.175(7)-2.303(6) Å for compound **15**) in the 3,1,2-RuC_2B_9 cage and CB_4 face in the 2′,1′,8′-RuC_2B_9 cage (2.140(9)-2.209(8) for compound **14** and 2.170(7)-2.210(7) Å for compound **15**) increase because the first row transition metals in compounds **12** and **13** are replaced by second row transition metals in compounds **14** and **15** (Table 3.6).

	12	**13**		**12**	**13**
Co3-C1	2.128(3)	2.137(4)	Co2′-C1′	2.022(3)	2.015(4)
Co3-C2	2.041(3)	2.054(4)	Co2′-B3′	2.026(4)	2.015(4)
Co3-B4	2.065(4)	2.081(4)	Co2′-B6′	2.065(4)	2.056(5)
Co3-B7	2.068(4)	2.055(4)	Co2′-B7′	2.071(4)	2.057(4)
Co3-B8	2.083(4)	2.093(4)	Co2′-B11′	2.079(4)	2.071(4)
C1-C2	1.652(5)	1.635(5)	C1′-B3′	1.699(5)	1.706(6)
C1-B4	1.742(5)	1.740(5)	C1′-B4′	1.685(5)	1.693(5)
C1-B5	1.724(5)	1.732(5)	C1′-B5′	1.714(5)	1.707(6)
C1-B6	1.758(5)	1.761(5)	C1′-B6′	1.724(6)	1.739(5)
C1-C8′	1.552(5)	1.559(5)	C8′-B3′	1.726(5)	1.727(5)
C2-B6	1.735(5)	1.735(5)	C8′-B4′	1.726(5)	1.720(5)
C2-B7	1.731(5)	1.744(6)	C8′-B7′	1.756(5)	1.764(5)
C2-B11	1.718(5)	1.724(5)	C8′-B9′	1.758(5)	1.741(5)
B4-B5	1.806(5)	1.798(6)	C8′-B12′	1.736(5)	1.758(5)
B4-B8	1.830(6)	1.818(7)	B3′-B4′	1.783(5)	1.803(6)
B4-B9	1.800(5)	1.801(6)	B3′-B7′	1.835(5)	1.813(5)
B5-B6	1.761(6)	1.775(6)	B4′-B5′	1.756(6)	1.753(6)
B5-B9	1.768(5)	1.758(6)	B4′-B9′	1.772(5)	1.764(6)
B5-B10	1.786(5)	1.761(6)	B5′-B6′	1.794(5)	1.779(6)
B6-B10	1.749(6)	1.776(6)	B5′-B9′	1.753(5)	1.771(6)
B6-B11	1.741(6)	1.747(6)	B5′-B10′	1.767(6)	1.770(6)
B7-B8	1.808(6)	1.806(6)	B6′-B10′	1.786(5)	1.786(6)
B7-B11	1.785(5)	1.778(6)	B6′-B11′	1.819(5)	1.813(6)
B7-B12	1.785(5)	1.776(6)	B7′-B11′	1.784(5)	1.777(6)
B8-B9	1.778(5)	1.772(6)	B7′-B12′	1.770(5)	1.775(6)
B8-B12	1.778(5)	1.782(6)	B9′-B10′	1.765(6)	1.775(6)
B9-B10	1.780(5)	1.751(6)	B9′-B12′	1.771(5)	1.780(6)
B9-B12	1.783(6)	1.784(6)	B10′-B11′	1.801(5)	1.800(6)
B10-B11	1.779(6)	1.788(6)	B10′-B12′	1.796(5)	1.772(6)
B10-B12	1.789(5)	1.766(6)	B11′-B12′	1.791(5)	1.766(6)
B11-B12	1.789(6)	1.781(6)			

Table 3.5 Cage connectivity distances in compounds 12 and 13

	14	**15**		**14**	**15**
Ru3-C1	2.292(7)	2.303(6)	Ru2′-C1′	2.181(7)	2.177(6)
Ru3-C2	2.204(8)	2.200(6)	Ru2′-B3′	2.140(9)	2.170(7)
Ru3-B4	2.214(9)	2.226(7)	Ru2′-B6′	2.202(7)	2.188(7)
Ru3-B7	2.186(9)	2.175(7)	Ru2′-B7′	2.187(8)	2.177(7)
Ru3-B8	2.186(9)	2.194(7)	Ru2′-B11′	2.209(8)	2.210(7)
C1-C2	1.631(10)	1.652(9)	C1′-B3′	1.725(10)	1.739(9)
C1-B4	1.724(13)	1.740(9)	C1′-B4′	1.693(12)	1.688(9)
C1-B5	1.734(11)	1.730(9)	C1′-B5′	1.719(10)	1.738(9)
C1-B6	1.742(10)	1.756(9)	C1′-B6′	1.754(11)	1.738(10)
C1-C8′	1.561(10)	1.546(8)	C8′-B3′	1.747(11)	1.733(9)
C2-B6	1.739(11)	1.740(9)	C8′-B4′	1.717(10)	1.696(9)
C2-B7	1.768(12)	1.747(9)	C8′-B7′	1.773(11)	1.791(9)
C2-B11	1.730(11)	1.738(9)	C8′-B9′	1.730(9)	1.725(9)
B4-B5	1.751(12)	1.795(10)	C8′-B12′	1.729(10)	1.753(9)
B4-B8	1.809(13)	1.824(10)	B3′-B4′	1.784(11)	1.783(10)
B4-B9	1.760(12)	1.785(10)	B3′-B7′	1.821(12)	1.834(10)
B5-B6	1.758(12)	1.753(10)	B4′-B5′	1.770(11)	1.770(10)
B5-B9	1.748(13)	1.767(10)	B4′-B9′	1.762(12)	1.786(10)
B5-B10	1.784(11)	1.776(10)	B5′-B6′	1.781(13)	1.802(10)
B6-B10	1.740(12)	1.765(10)	B5′-B9′	1.754(12)	1.774(10)
B6-B11	1.742(12)	1.765(10)	B5′-B10′	1.767(13)	1.780(11)
B7-B8	1.845(14)	1.825(10)	B6′-B10′	1.767(12)	1.799(10)
B7-B11	1.789(13)	1.782(10)	B6′-B11′	1.802(11)	1.822(10)
B7-B12	1.804(14)	1.779(10)	B7′-B11′	1.784(11)	1.805(10)
B8-B9	1.796(13)	1.790(10)	B7′-B12′	1.791(11)	1.781(10)
B8-B12	1.774(12)	1.797(10)	B9′-B10′	1.760(13)	1.763(10)
B9-B10	1.798(12)	1.785(10)	B9′-B12′	1.766(12)	1.780(10)
B9-B12	1.805(13)	1.787(10)	B10′-B11′	1.774(11)	1.775(10)
B10-B11	1.757(14)	1.774(10)	B10′-B12′	1.769(11)	1.783(10)
B10-B12	1.781(13)	1.774(10)	B11′-B12′	1.758(12)	1.765(10)

Table 3.6 Cage connectivity distances in compounds 14 and 15

3.8 Summary

Decapitation of 1,1′-bis(*o*-carborane) with 30 equivalents of KOH in EtOH yielded [7-(7′-7′,8′-*nido*-$C_2B_{10}H_{11}$)-7,8-*nido*-$C_2B_9H_{11}$]$^{2-}$ which is isolated as [BTMA]$_2$[7-(7′-7′,8′-*nido*-$C_2B_9H_{11}$)-7,8-*nido*-$C_2B_9H_{11}$] (**8**), [$HNMe_3$]$_2$[7-(7′-7′,8′-*nido*-$C_2B_9H_{11}$)-7,8-*nido*-$C_2B_9H_{11}$] (**9**) and [(*S*)-$CH_3NC_5H_4$-$C_4H_7NCH_3$]$_2$[7-(7′-7′,8′-*nido*-$C_2B_9H_{11}$)-7,8-*nido*-$C_2B_9H_{11}$] (**10**) individually in good yields. All three compounds were characterised by microanalysis and NMR spectroscopies.

$^{11}B\{^1H\}$ NMR spectroscopy of salts **8**, **9** and **10** clearly shows the presence of diastereoisomers. Salt **8** was characterised by *X*-ray crystallography and proved to be the *meso* diastereoisomer. However, NMR spectroscopy of crystalline material showed both diastereoisomers present (crystals of both forms appear to have only one habit and therefore cannot be separated). Therefore salt **10** was synthesised in which the cation has a chiral centre. We hoped that *racemic* and *meso* diastereoisomers would be separated during crystallisation but unfortunately crystallisation of the salt failed to yield diffraction-quality crystals.

Deprotonation and metallation of [$HNMe_3$]$_2$[7-(7′-7′,8′-*nido*-$C_2B_{10}H_{11}$)-7,8-*nido*-$C_2B_9H_{11}$] *racemic*/*meso* mixtures at room temperature affords a mixture of products. Metallation with {CpCo} fragments resulted in 3,1,2-metallacarborane/2′,1′,8′-metallacarborane and 2,1,8-metallacarborane/2′,1′,8′-metallacarborane whereas with {(*p*-cymene)Ru} fragments only 3,1,2-metallacarborane/2′,1′,8′-metallacarborane resulted. {CpCo} once again proved that it is more flexible than {(*p*-cymene)Ru} with respect to isomerisation.

3.9 References

3.1. R. A. Wiesboeck and M. F. Hawthorne, *J. Am. Chem. Soc*., 1964, **86**, 1642.

3.2. D. A. Owen, J. W. Wiggins and M. F. Hawthorne, *Inorg. Chem*., 1971, **10**, 1304.

3.3. P. E. Behnken, T. B. Marder, R. T. Baker, C. B. Knobler, M. R. Thompson and M. F. Hawthorne, *J. Am. Chem. Soc*., 1985, **107**, 933.

3.4. D. C. Young, P. A. Wegner and M. F. Hawthorne, *J. Am. Chem. Soc*., 1965, **87**, 1818.

3.5. S. Ren and Z. Xie, *Organometallics*, 2008, **27**, 5167.

3.6. G. Sivasubramanian, D. Ellis, D. McKay, S. A. Macgregor, L. Jourdan, G. M. Rosair and A. J. Welch, *Dalton Trans*., in preparation

3.7. (a) D. Ellis, M. E. Lopez, R. McIntosh, G. M. Rosair, A. J. Welch and R. Quenardelle, *Chem. Commun*., 2005, 1348; (b) S. Zlatogorsky, D. Ellis, G. M. Rosair and A. J. Welch, *Chem. Commun.*, 2007, 2178.

3.8. J. I. Seeman and J. F. Whidby, *J. Org. Chem.*, 1976, **41**, 3824.

3.9. T. P. Pitner, W. B. Edwards, R. L. Bassfield and J. F. Whidby, *J. Am. Chem. Soc*., 1978, **100**, 246.

3.10. (a) M. E. Lopez, M. J. Edie, D. Ellis, A. Horneber, S. A. Macgregor, G. M. Rosair and A. J. Welch, *Chem. Commun.*, 2007, 2243; (b) D. E. Smith and A. J. Welch, *Organometallics*, 1986, **5**, 760.

CHAPTER 4

Metallation of 1,1′-bis(*o*-carborane) and 2,2′-$(CH_3)_2$-1,1′-bis(*o*-carborane) with Ni(dmpe)Cl_2

4.1 Introduction

Since the first single cage icosahedral metallacarborane was synthesised in 1965 by Hawthorne[1] very many icosahedral metallacarboranes have been prepared. Most of them are of 3,1,2-*closo*-$MC_2B_9H_{11}$ geometry. As noted in chapter 2 the general route to synthesise 3,1,2-icosahedral metallacarborane is by the addition of ethanolic KOH to 1,2-*closo*-$C_2B_{10}H_{12}$ and heating under reflux to yield [7,8-*nido*-$C_2B_9H_{11}$]$^{2-}$ which is then metallated with a suitable metal fragments (Fig 4.1).

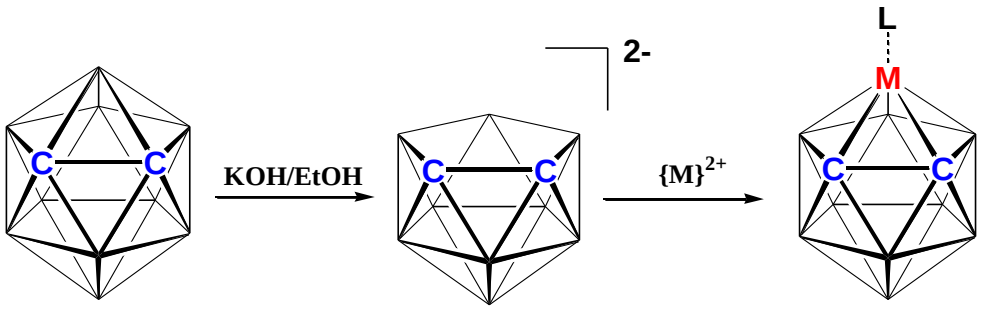

Fig 4.1 Decapitation of 1,2-*closo*-$C_2B_{10}H_{12}$ followed by metallation

Metallacarboranes can be categorised into three classes based on how the metal is bonded to the cage. In class 1 metallacarboranes the metal is incorporated as a cluster vertex whereas in class 2 the metal is bridged over the edge of the cluster and in class 3 metallacarboranes the metal is bonded to the cluster through an exopolyhedral covalent bond (Fig 4.2).

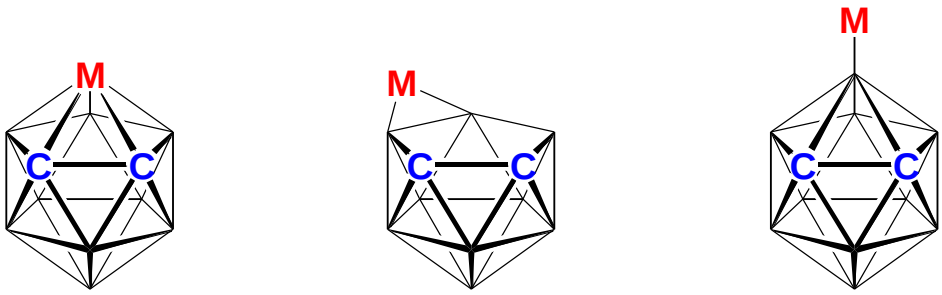

1 2 3

Fig 4.2 Different classes of metallacarboranes

Similarly to 12-vertex metallacarboranes the class categorisation is possible for metallated derivatives of 1,1′-bis(*o*-carborane). The class 1 and class 3 types have been published by Hawthorne and co-workers. A class 1[2] type of metallacarborane was synthesised by the addition of [Rh(COD)(PEt_3)Cl] to a THF solution of Cs_2[7-(7′-7′,8′-*nido*-$C_2B_9H_{11}$)-*nido*-7,8-$C_2B_9H_{11}$] and heating under reflux for two days. A class 3[3] type of metallacarborane was prepared by the addition of a diethyl ether solution of metal halide to a slurry of 2,2′-dilithiobiscarborane and stirring for 3 hrs at reflux temperature (Fig 4.3). The work presented in this thesis is about class 1 types of metallacarborane with 1,1′-bis(*o*-carborane) as the starting material.

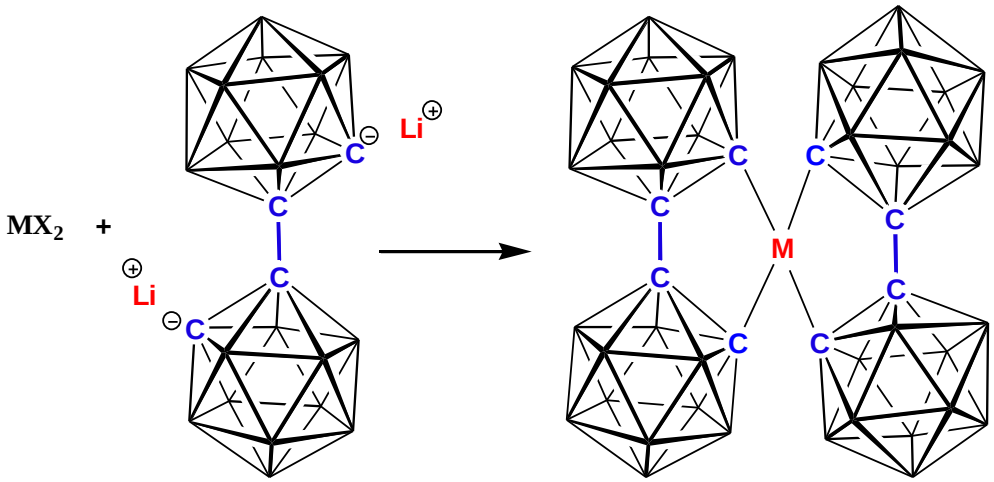

Fig 4.3 Structural representation of class 3 type of metallacarborane (M stands for Co(II), Ni(II), Cu(II) and Cu(III) and X stands for Cl and Br)

There are a few examples published so far for the metallation of [7,8-*nido*-$C_2B_9H_{11}$]$^{2-}$ with {LNi} fragments (L= phosphine)[4] by stirring the appropriate bis(phosphine)nickel dichloride complex and thallous dicarbollide in a suitable solvent yielding 3-L-3,1,2-*closo*-$NiC_2B_9H_{11}$, however metallation of 1,1′-bis(*o*-carborane) with {LNi} fragments is not reported.

It has been already noted that at room temperature 1,2-Ph_2-3-L-3,1,2-*closo*-$NiC_2B_9H_9$ readily isomerises to 1,2-Ph_2-4-L-4,1,2-*closo*-$NiC_2B_9H_9$ due to steric overcrowding[5].

This chapter discusses the syntheses and the complete characterisation of the compounds, 1-(1′-3′-(dmpe)-3′,1′,2′-*closo*-$NiC_2B_9H_{10}$)-3-(dmpe)-3,1,2-*closo*-$NiC_2B_9H_{10}$ (*racemic* and *meso*), 2,2′-$(CH_3)_2$-1,1′-bis(*o*-carborane) and 1-(1′-1′,2′-*closo*-$C_2B_{10}H_{10}$-2′-CH_3)-2-(dmpe)-7-CH_3-2,1,7-*closo*-$NiC_2B_9H_9$.

4.2 Preparation of 12-v/12-v nickelacarborane/nickelacarborane (16 and 17) species from the deprotonation and metallation of [7-(7′-7′,8′-*nido*-$C_2B_9H_{11}$)-7,8-*nido*-$C_2B_9H_{11}$]$^{2-}$

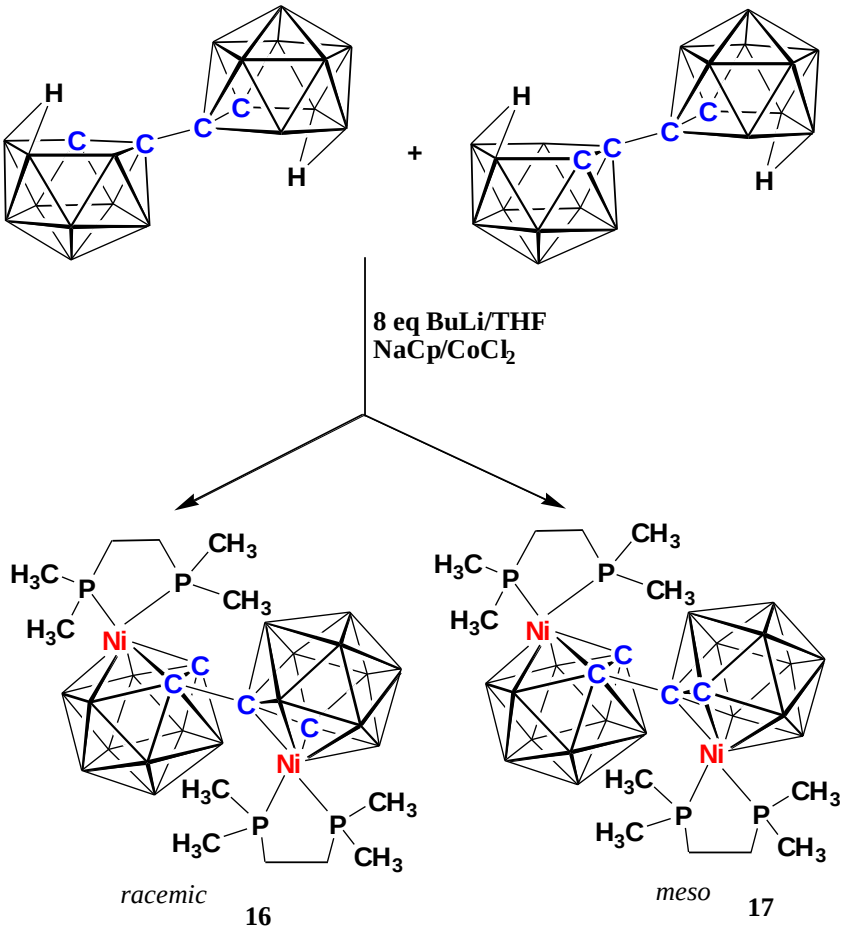

Deprotonation was carried out by the dropwise addition of 8 equivalents of BuLi to a THF solution of [$HNMe_3$]$_2$[7-(7′-7′,8′-*nido*-$C_2B_9H_{11}$)-7,8-*nido*-$C_2B_9H_{11}$] at 0^0C and the reaction mixture was then heated to reflux for 4 hrs. The colourless solution was then cooled to room temperature. Two equivalents of Ni(dmpe)Cl_2 were added to the reaction mixture while cooling to 0^oC and resulted in a dark green suspension which was then stirred overnight.

The resultant mixture was filtered through silica and THF was removed under reduced pressure. The remaining dark green solid was dissolved in DCM, filtered through Celite® and purified by TLC. Preparative TLC with a mixed eluent of DCM and petroleum ether (40-60^{o}C) (3:1) yielded two green bands (compounds **16** and **17**) with R_f 0.60 and 0.45 in 14.8% and 20% yields respectively.

Compound **16** was fully characterized by microanalysis, ^{31}P and ^{11}B NMR spectroscopies and *X*-ray crystallography. Elemental analysis gave close results to the calculated values for $C_{16}H_{52}B_{18}Ni_2P_4$.

The ^{1}H NMR spectrum of compound **16** clearly shows two singlets of intensity one at δ 2.45 and 2.35 ppm. The only possibility for these resonances is the protons of the cages. However both cages are chemically and magnetically equivalent and therefore should give only one CH_{cage} signal. The signals due to CH_2 and CH_3 groups in the dimethylphosphinoethane ligands are difficult to assign. ^{13}C DEPT NMR spectroscopy was attempted in order to identify the signals due to CH_2 and CH_3 groups but compound **16** is only partially soluble and therefore only a very weak spectrum was obtained.

^{31}P NMR spectroscopy of compound **16** shows two doublets at δ 43.55 and 33.55 ppm because in both cages one of the phosphorous atom is trans to carbon whereas the other phosphorus is trans to boron.

$^{11}B\{^{1}H\}$ NMR spectroscopy of compound **16** revealed seven resonances at δ -2.64, -3.93, -7.39, -12.02, -13.38, -15.76 and -21.14 ppm in the relative ratio 3:3:2:1:1:4:4.

X-ray quality green crystals of compound **16** were grown by vapour diffusion of a DCM solution and 40-60 petroleum ether at room temperature and the diffraction study confirmed that compound **16** is 1-(1′-3′-(dmpe)-3′,1′,2′-*closo*-$NiC_2B_9H_{10}$)-3-(dmpe)-3,1,2-*closo*-$NiC_2B_9H_{10}$ (Fig 4.4). In this compound both cages are identical but the molecule does not have internal mirror plane and therefore we can conclude that compound **16** is a *racemic* diastereoisomer.

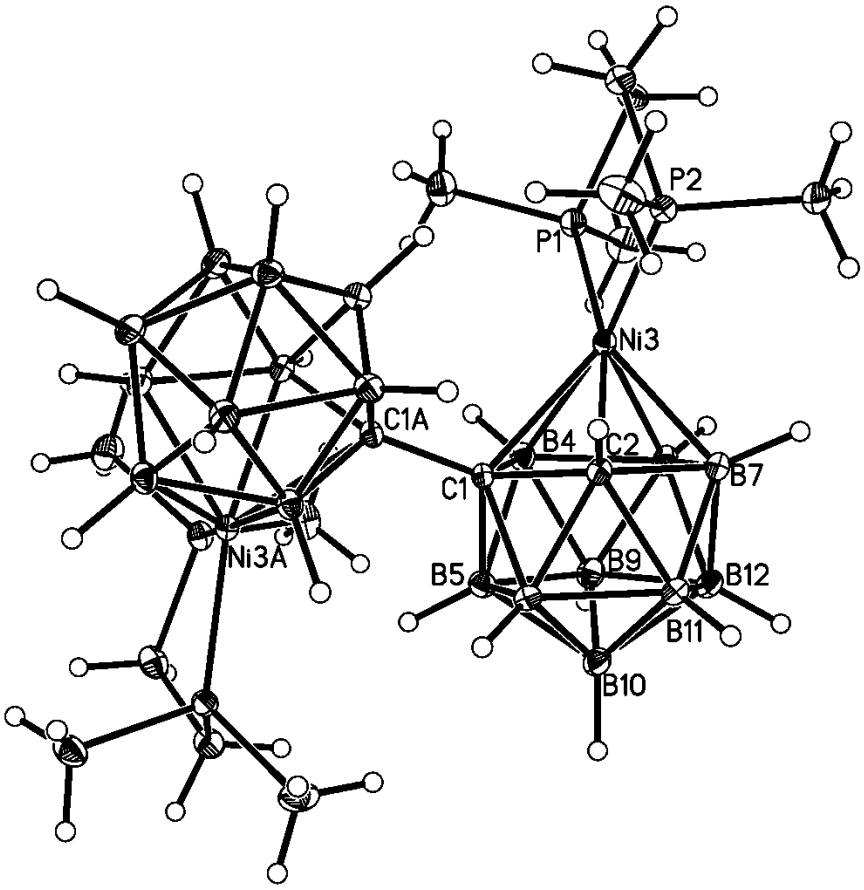

Fig 4.4 Molecular structure of the *racemic* form of 1-(1′-3′-(dmpe)-3′,1′,2′-*closo*-$NiC_2B_9H_{10}$)-3-(dmpe)-3,1,2-*closo*-$NiC_2B_9H_{10}$ (16)

Compound **17** was fully characterized by microanalysis, ^{31}P and ^{11}B NMR spectroscopies and *X*-ray crystallography. Unfortunately elemental analysis never gave results very close to the calculated values for $C_{16}H_{52}B_{18}Ni_2P_4$ even using a crystalline sample.

In the ^{1}H NMR spectrum of compound **17** the singlets with intensity one at δ 2.40 and 2.35 ppm are assigned to CH_{cage}. This is due to the fact that both cages are chemically equivalent but magnetically inequivalent. The signals due to CH_2 and CH_3 groups in the dimethylphosphinoethane ligands in **17** are difficult to assign but clearly indicate that **17** is different to **16**. ^{13}C DEPT NMR spectroscopy was attempted to identify the signals due to CH_2 and CH_3 groups but, as was the same with compound **16**, compound **17** is also poorly soluble therefore only a very weak spectrum was obtained.

Similarly to compound **16** the ^{31}P NMR spectrum of compound **17** shows two doublets (at δ 43.89 and 34.10 ppm) because the phosphorous atoms in the cage are different (one phosphorous is trans to carbon and the other phosphorus is trans to boron).

$^{11}B\{^{1}H\}$ NMR spectroscopy of compound **17** revealed seven resonances at δ -1.35, -3.79, -10.46, -11.76, -14.38, -15.82 and -20.51 ppm with integrals in the relative ratio 2:2:2:2:4:4:2. Although the frequencies are comparable for *racemic* and *meso* diastereoisomers[6] the values for compound **17** differ from those for compound **16.**

X-ray quality green crystals of compound **17** were grown by vapour diffusion of a DCM solution and 40-60 petroleum ether at room temperature and the structural study confirmed that compound **17** is 1-(1′-3′-(dmpe)-3′,1′,2′-*closo*-$NiC_2B_9H_{10}$)-3-(dmpe)-3,1,2-*closo*-$NiC_2B_9H_{10}$ (Fig 4.5). The *X*-ray diffraction study clearly shows that compound **17** is the *meso* diastereoisomer since it has an internal mirror plane of symmetry.

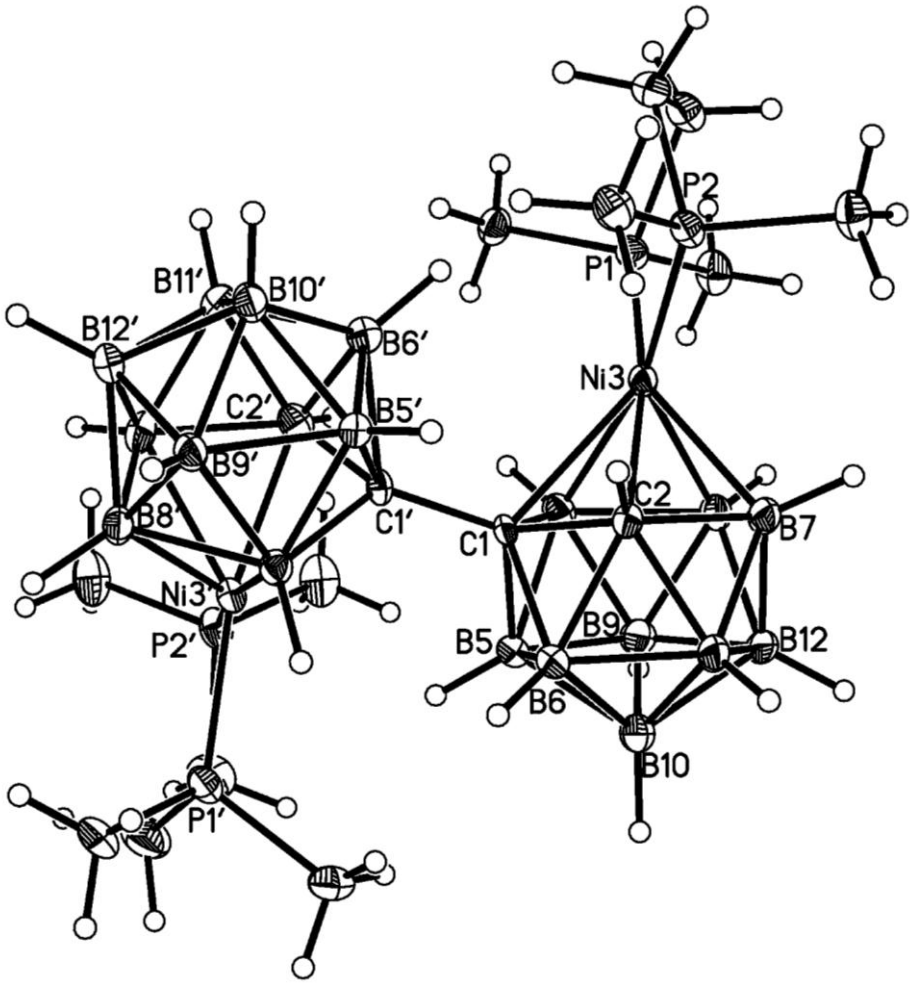

Fig 4.5 Molecular structure of the *meso* form of 1-(1′-3′-(dmpe)-3′,1′,2′-*closo*-$NiC_2B_9H_{10}$)-3-(dmpe)-3,1,2-*closo*-$NiC_2B_9H_{10}$ (17)

4.3 Preparation of 2,2′-$(CH_3)_2$-1,1′-bis-(*o*-carborane) (18)

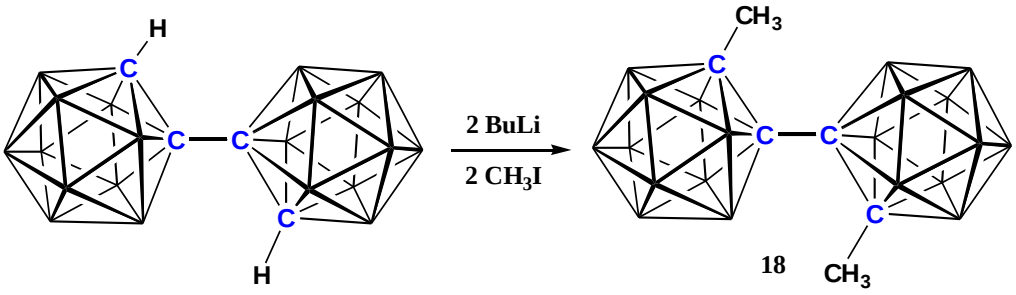

Methylation of 1,1′-bis-(*o*-carborane) was first performed by Hawthorne in 1964[7] but complete characterisation of the product was not reported. Methylation of 1,1′-bis-(*o*-carborane) was carried out by the dropwise addition of 2.2 equivalents of BuLi to a di-ethyl ether solution of 1,1′-bis-(*o*-carborane) while cooling at 0^0C.

The colourless solution was stirred overnight and 2.2 equivalents of CH_3I were added. The solution turned to red and was then heated to reflux for 4 hrs. The mixture was cooled to room temperature. The diethyl ether layer was dried with $MgSO_4$, filtered and the solvent was removed on a rotary evaporator to yield white solid (compound **18**).

Compound **18** was fully characterised by mass spectrometry, elemental analysis, ^{1}H NMR spectroscopy, ^{11}B{^{1}H} NMR spectroscopy and *X*-ray crystallography.

Mass spectrometry of compound **18** shows the parent ion to have a mass of 314.4 which is consistent with $C_6H_{26}B_{20}$ and a broad heteroborane envelope from 308.4 to 317.4 whilst elemental analysis was in good agreement with the values expected.

^{1}H NMR spectroscopy of compound **18** shows a singlet at δ 2.85 ppm which corresponds to the C*H*$_3$ group attached to the carbon atoms in both cages. ^{11}B{^{1}H} NMR spectroscopy reveals four resonances at δ -0.88, -5.00, -8.19 and -9.21 ppm in the relative ratio 2:2:12:4.

X-ray diffraction quality colourless crystals of compound **18** were grown by vapour diffusion of a DCM solution and 40-60 petroleum ether at room temperature and the structural study confirmed compound **18** is 2,2′-$(CH_3)_2$-1,1′-bis-(*o*-carborane) (Fig 4.6).

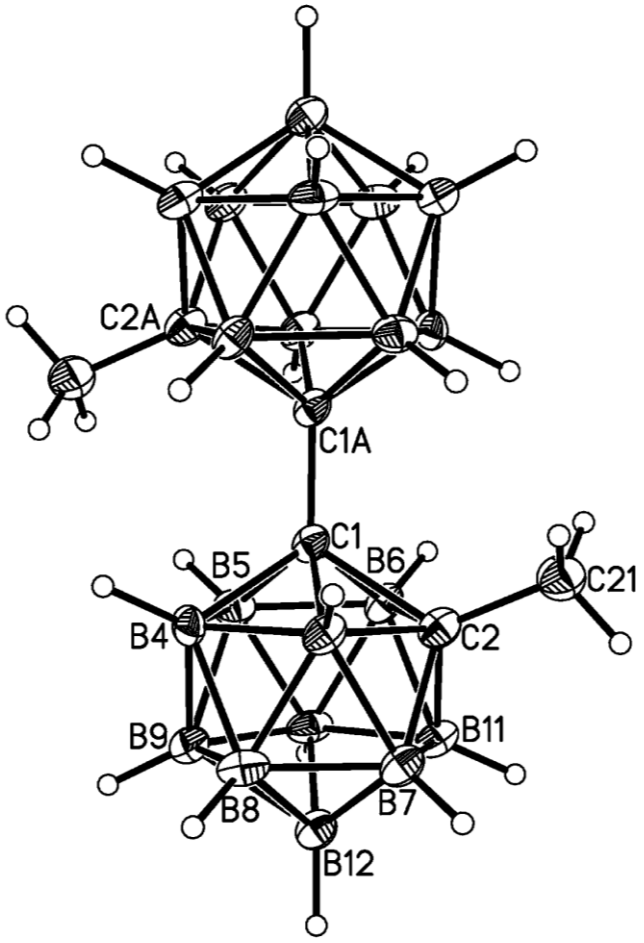

Fig 4.6 Molecular structure of 2,2′-$(CH_3)_2$-1,1′-bis-(*o*-carborane) (18)

The carborane cages are connected through C1 and C1A with a C-C distance of 1.577(8) Å which is significantly longer than the corresponding distance of 1,1′-bis-(*o*-carborane) (1.530(3) Å)[8]. The C2-C1-C1A-C2A torsion angle is 180^0 which is required since there is a center of inversion present in the middle of C1and C1A.

4.4 Preparation of 1-(1′-1′,2′-*closo*-$C_2B_{10}H_{10}$-2′-CH_3)-2-(dmpe)-7-CH_3-2,1,7-*closo*-$NiC_2B_9H_9$ (19)

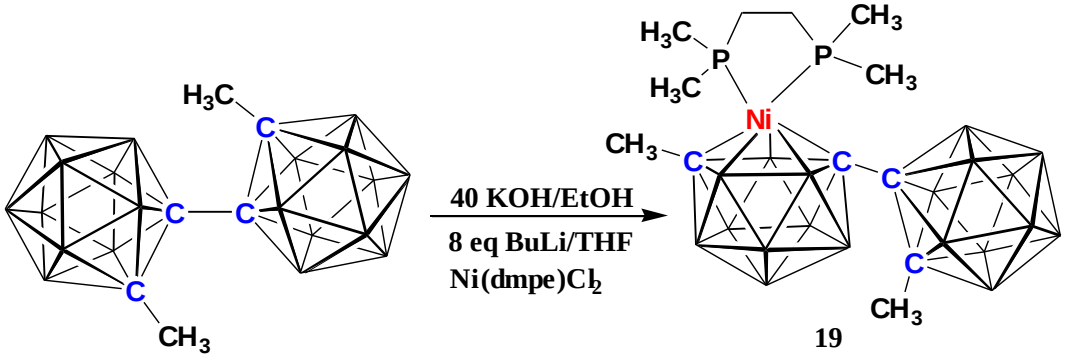

As noted in **4.2** the double decapitation of 1,1′-bis(*o*-carborane) followed by metallation with Ni(dmpe)Cl_2 resulted in formation of the *racemic* and *meso* forms of 3′1′2′-NiC_2B_9/3,1,2-NiC_2B_9 species. Therefore the decapitation and metallation of 2,2′-$(CH_3)_2$-1,1′-bis-(*o*-carborane) was carried out in order to see if isomerization would occur.

The decapitation was carried out by the addition of 40 equivalents of KOH to an EtOH solution of 2,2′-$(CH_3)_2$-1,1′-bis-(*o*-carborane) which was then heated to reflux for 48 hrs. The reaction mixture was then cooled to room temperature and $CO_{2(g)}$ was passed through the solution. The resulting white precipitate was filtered off and solvent was removed from the filtrate under reduced pressure to yield an oil.

The oil was dissolved in THF and four equivalents of BuLi was added dropwise while cooling the mixture which was then heated to reflux for 4 hrs. The reaction mixture was cooled again and Ni(dmpe)Cl_2 was added and the mixture stirred overnight. The dark brown solution was filtered through silica and the solvent was removed under reduced pressure. The resulting solid was dissolved in DCM, filtered through Celite® and purified by thin layer chromatography to yield an orange compound (**19**).

Compound **19** was characterised by microanalysis, ^{31}P NMR and $^{11}B\{^1H\}$ NMR spectroscopies and *X*-ray diffraction studies. Elemental analysis was in good agreement with the values expected for $C_{12}H_{41}B_{19}NiP_2$.

^{1}H NMR spectroscopy of compound **19** was attempted but the resonances were difficult to assign due to their complexity. However ^{31}P NMR spectroscopy consists of two broad resonances of intensity one at δ 37.17 and 24.10 ppm which implies that the two phosphorous atoms are in different environments.

^{11}B{^{1}H} NMR spectroscopy of compound **19** revealed seven resonances at δ -3.30, -5.35, -6.60, -9.08, -12.03, -17.55 and -18.37ppm in the relative ratio 1:1:2:10:1:2:2.

X-ray diffraction quality orange crystals of compound **18** were grown by vapour diffusion of a DCM solution and 40-60 petroleum ether at room temperature and the structural study confirmed compound **18** to be 1-(1′-1′,2′-*closo*-$C_2B_{10}H_{10}$-2′-CH_3)-2-(dmpe)-7-CH_3-2,1,7-*closo*-$NiC_2B_9H_9$ (Fig 4.7). The diffraction study shows that the metallacarborane cage is ordered whereas in the carborane cage the non-linking carbon atom is disordered between positions 2′ and 3′.

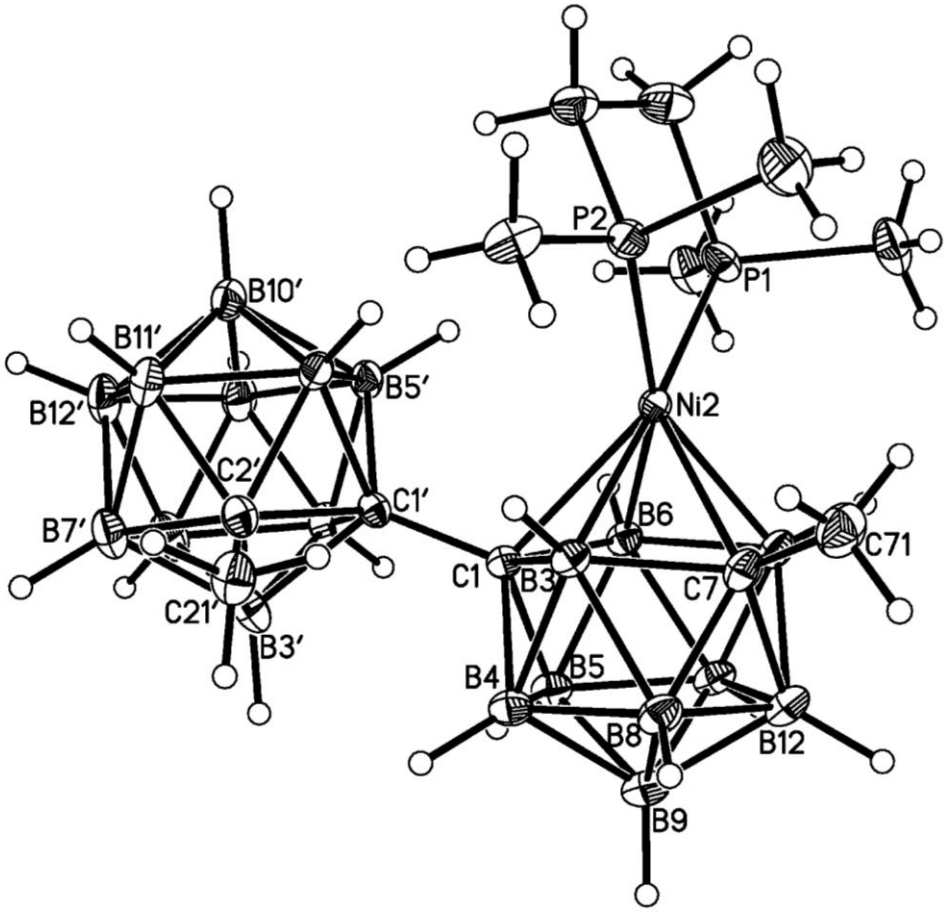

Fig 4.7 Molecular structure of 1-(1′-1′,2′-*closo*-$C_2B_{10}H_{10}$-2′-CH_3)-2-(dmpe)-7-CH_3-2,1,7-*closo*-$NiC_2B_9H_9$ (19)

4.5 Discussion

The compounds 1-(1′-3′-(dmpe)-3′,1′,2′-*closo*-$NiC_2B_9H_{10}$)-3-(dmpe)-3,1,2-*closo*-$NiC_2B_9H_{10}$ (**16** and **17**) were synthesised by deprotonation of $[HNMe_3]_2$[7-(7′-7′,8′-*nido*-$C_2B_9H_{11}$)-7,8-*nido*-$C_2B_9H_{11}$] with BuLi in THF followed by metallation with Ni(dmpe)Cl_2 at room temperature. The compounds **16** and **17** were fully characterised by elemental analysis, ^{31}P NMR spectroscopy, ^{11}B NMR spectroscopy and *X*-ray diffraction studies.

^{31}P NMR spectroscopy shows only slight variations for compounds **16** and **17** but ^{1}H NMR spectroscopy, ^{11}B NMR spectroscopy and *X*-ray diffraction studies confirmed that the two compounds are different although the ^{1}H resonances are very difficult to assign.

4.5.1 *X*-ray diffraction studies

As noted in chapter 3 double decapitation of 1,1′-bis(*o*-carborane) followed by metathesis separately with [BTMA]Cl, $[HNMe_3]$Cl and [(*S*)-$CH_3NC_5H_4$-$C_4H_7NCH_3$]I yielded diastereoisomers. In all three salts, **8**, **9** and **10** the presence of diasteroisomers was only confirmed by ^{11}B NMR spectroscopy. The ionic diastereoisomers cannot be separated to continue deprotonation followed by metallation individually. Therefore the deprotonation and metallation with {(*p*-cymene)Ru} and {CpCo} fragments was carried out for the mixture of *racemic* and *meso* diastereoisomers. Interestingly, with both metal fragments we obtained at least two products with one cage the same and the other cage enantiomerically related.

However, metallation of [7-(7′-7′,8′-*nido*-$C_2B_9H_{11}$)-7,8-*nido*-$C_2B_9H_{11}$]$^{4-}$ with {(dmpe)Ni}$^{2+}$ fragments revealed that both cages are identical with a 3,1,2-NiC_2B_9/3′,1′,2′-NiC_2B_9 geometry. From these two products, undoubtedly, compound **16** is *racemic* whereas compound **17** is *meso* (Fig 4.8). This is the first example of *racemic* and *meso* isomers identified for 12-vertex/12-vertex bismetallacarborane species.

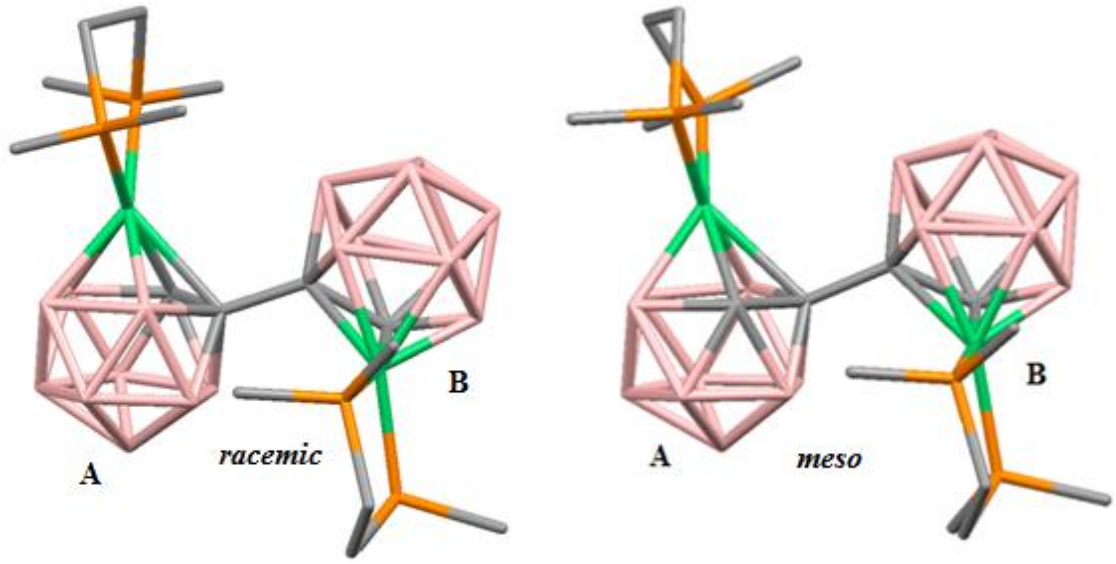

Fig 4.8 Relationship between compounds 16 (*racemic*) and 17 (*meso*) diastereoisomers

As noted in the introduction (**4.1**) at room temperature 1,2-Ph_2-3-L-3,1,2-*closo*-$NiC_2B_9H_9$ species can isomerise to 1,2-Ph_2-4-L-4,1,2-*closo*-$NiC_2B_9H_9$ because the molecule is severely crowded[5] (Fig 4.9).

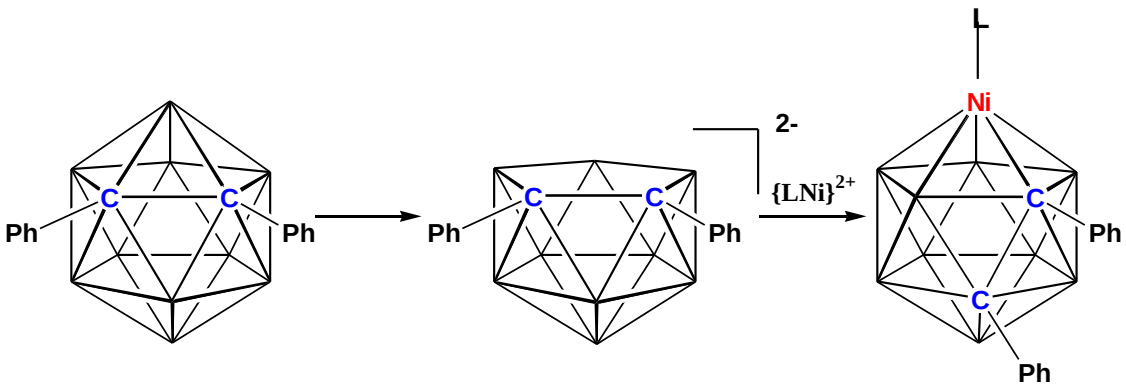

Fig 4.9 Isomerisation in nickelacarborane

To investigate if carbon atom substitution in 1,1′-bis(*o*-carborane) would also lead to isomerisation in nickel metallacarborane derivatives 1,1′-bis(*o*-carborane) was first methylated at both the carbon atoms before decapitation followed by metallation with the {(dmpe)Ni} fragment. Methylation was carried out by the addition of methyl iodide to a diethyl ether solution of 1,1′-bis(*o*-carborane). The compound, 2,2′-$(CH_3)_2$-1,1′-bis(*o*-carborane) (**18**) was fully characterised by mass spectroscopy, elemental analysis, ^{1}H NMR spectroscopy, ^{11}B NMR spectroscopy and *X*-ray diffraction studies.

The decapitation of compound **18** was carried out by heating to reflux with 40 equivalents of KOH in EtOH then deprotonation with BuLi in THF followed by metallation with Ni(dmpe)Cl_2 at room temperature. Compound **19** was isolated and characterised by elemental analysis, ^{31}P NMR spectroscopy, ^{11}B NMR spectroscopy and an *X*-ray diffraction study.

Interestingly, elemental analysis and the *X*-ray diffraction study confirmed that the isolated product is a single cage metallated species, 1-(1′-1′,2′-*closo*-$C_2B_{10}H_{10}$-2′-CH_3)-2-(dmpe)-7-CH_3-2,1,7-*closo*-$NiC_2B_9H_9$ and not the bismetallated species. As noted in **4.4** the *X*-ray diffraction study shows that the metallacarborane cage is ordered whereas in the carborane cage the non-linking carbon atom is disordered between positions 2′ and 3′.

Generally, 2,1,7-*closo*-MC_2B_9 species are synthesised by decapitation of 1,7-*closo*-C_2B_{10} followed by metallation[9]. However, in 1972 Hawthorne reported that 3-C_5H_5-3,1,2-*closo*-$CoC_2B_9H_{11}$ and 3-C_5H_5-1,2-$(CH_3)_2$-3,1,2-*closo*-$CoC_2B_9H_9$ can isomerise at 400-600^{0}C to 2-C_5H_5-2,1,7-*closo*-$CoC_2B_9H_{11}$ and 2-C_5H_5-1,7-$(CH_3)_2$-2,1,7-*closo*-$CoC_2B_9H_9$ respectively[10].

As far as we aware there are no 2-L-2,1,7-*closo*-NiC_2B_9 species reported so far. Compound **19** is the first example of a 12-vertex/12-vertex metallacarborane/carborane synthesised from 2,2′-$(CH_3)_2$-1,1′-bis(*o*-carborane). The unexpected isomerisation at room temperature may be due to the bulkiness of the cage itself.

4.5.2 NMR spectroscopy

In chapter 3 the $^{11}B\{^{1}H\}$ NMR spectra for the mixture of diasterioisomers of salts $[BTMA]_2[7\text{-}(7'\text{-}7',8'\text{-}\textit{nido}\text{-}C_2B_9H_{11})\text{-}7,8\text{-}\textit{nido}\text{-}C_2B_9H_{11}]$ (**8**), $[HNMe_3]_2[7\text{-}(7'\text{-}7',8'\text{-}\textit{nido}\text{-}C_2B_9H_{11})\text{-}7,8\text{-}\textit{nido}\text{-}C_2B_9H_{11}]$ (**9**) and $[(S)\text{-}CH_3NC_5H_4\text{-}C_4H_7NCH_3]_2[7\text{-}(7'\text{-}7',8'\text{-}\textit{nido}\text{-}C_2B_9H_{11})\text{-}7,8\text{-}\textit{nido}\text{-}C_2B_9H_{11}]$ (**10**) were reported but the individual resonances due to *racemic* and *meso* forms were not reported. The integrals clearly show that one form of diasteroisomer is major and the other form is minor. Therefore from the % yields of compounds **16** and **17** we can suggest the $^{11}B\{^{1}H\}$ NMR resonances due to *meso* and *racemic* diastereoisomers for salts **8**, **9** and **10**.

Compound **16** was isolated in 14.8% yield whereas compound **17** was isolated in 20% yield. Therefore compound **17** is the major product and is *meso*. It is therefore tentatively proposed that in salts **8**, **9** and **10** the *meso* diastereoisomer is the major component. From the $^{11}B\{^{1}H\}$ NMR spectrum, the resonances due to *meso* form in salts **8** and **10** can be assigned (Fig 4.10).

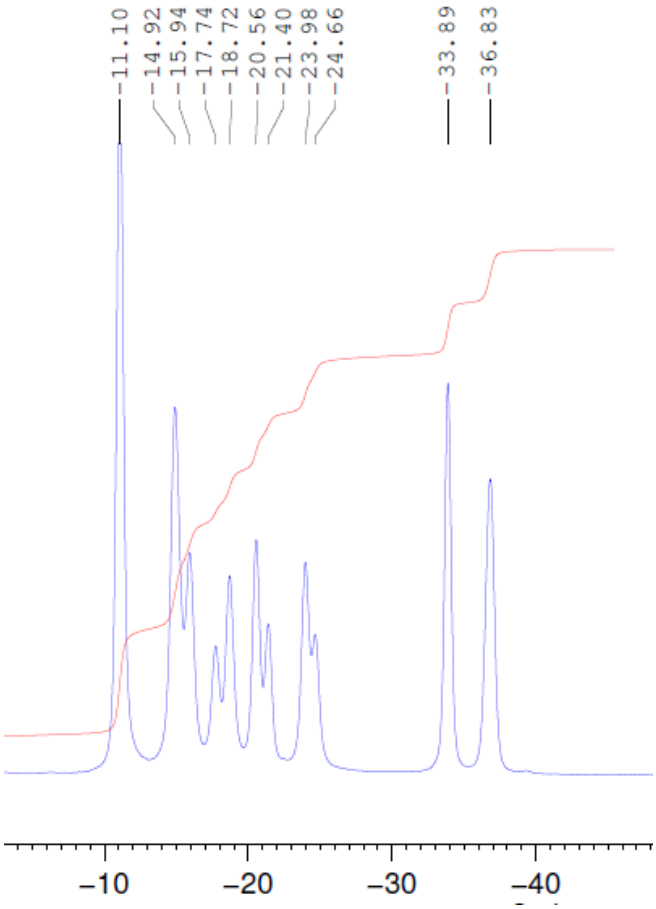

Fig 4.10 $^{11}B\{^{1}H\}$ NMR spectrum of $[7\text{-}(7'\text{-}7',8'\text{-}\textit{nido}\text{-}C_2B_9H_{11})\text{-}7,8\text{-}\textit{nido}\text{-}C_2B_9H_{11}]^{2-}$

The resonances at δ -11.04, -14.88, -18.69, -20.50, -23.96, -33.85 and -36.79 ppm in the relative ratio 2:2:1:1:1:1:1 arise from *meso* whereas the signals for *racemic* can be seen at δ -11.04, -15.90, -17.69, -21.39, -24.66, -33.85 and -36.79 ppm in the relative ratio 2:2:1:1:1:1:1. There are coincidences present in three places, δ -11.04, -33.85 and -36.79 ppm.

Similarly to salts **8** and **10** the individual resonances for *meso* and *racemic* isomers in salt **9** can be assigned. The signals at δ -11.10, -14.92, -18.72, -20.56, -23.98, -33.89 and -36.83 ppm in the relative ratio 2:2:1:1:1:1:1 correspond to *meso* and for *racemic* the signals appear at δ -11.10, -15.94, -17.74, -21.40, -24.66, -33.89 and -36.83 ppm in the relative ratio 2:2:1:1:1:1:1.

The weighted average ^{11}B chemical shifts, $<\delta^{11}B>$, of 1,1′-bis(*o*-carborane) and compounds **16**, **17**, **18** and **19** are given in table 4.1.

Compound	**$<\delta^{11}B>$**
1,1′-bis(*o*-carborane)	-9.1
Compound **16**	-12.0
Compound **17**	-11.5
Compound **18**	-7.3
Compound **19**	-10.3

Table 4.1 $<\delta^{11}B>$ values for 1,1′-bis(*o*-carborane) and compounds 16, 17, 18 and 19

Unlike the compounds reported in chapters 2 and 3 the weighted average chemical shifts of compounds **16** and **17** move to lower frequency by ca. 2.5-3.0 ppm when replacing a boron atom in each cage of 1,1′-bis(*o*-carborane) with {(dmpe)Ni} fragments. Similar results were obtained when replacing a boron vertex of 1,2-*closo*-$C_2B_{10}H_{12}$ with $\{(PPh_3)_2Ni\}$ and $\{(PEt_3)_2Ni\}$ fragments[4b] ($<\delta^{11}B>$, moves from δ -10.9 to -12.2 and -11.9 ppm respectively).

The weighted average chemical shifts of 2,2′-$(CH_3)_2$-1,1′-bis(*o*-carborane) (**18**) moves to higher frequency by ca. 1.8 ppm when replacing the H atoms attached to carbon atoms by CH_3 groups. Similarly to compounds **16** and **17**, $<\delta^{11}B>$ of compound **19** is shifted to lower frequency by ca. 3.0 ppm when replacing a boron atom of 2,2′-$(CH_3)_2$-1,1′-bis(*o*-carborane) (**18**) by a {(dmpe)Ni} fragment.

4.5.3 Cage connectivities

The cage connectivity distances of 1-(1′-3′-(dmpe)-3′,1′,2′-*closo*-$NiC_2B_9H_{10}$)-3-(dmpe)-3,1,2-*closo*-$NiC_2B_9H_{10}$ (**16** and **17**) are listed in table 4.2. The metallated biscages of compounds **16** and **17** are icosahedral with Ni3 capping the upper belt and in both compounds in both cages the carbon atoms and the metal atoms are adjacent to each other.

The intercage C-C distance in compound **16** is 1.546(3) Å and in compound **17** it is 1.545(3) Å. These values are higher than the corresponding distance in 1,1′-bis(*o*-carborane) (1.530(3) Å) recorded by Xie[8] which implies that these compounds are more sterically crowded than 1,1′-bis(*o*-carborane).

The cage connectivity distances in both cages are same for compound **16** since there is a crystallographic C_2 axis bisecting the C-C bond. The longest B-B connectivity in the nickellacarborane cages is 1.849(3) Å between B4-B8 while the shortest one is between B5-B6 with a length of 1.750(3) Å. The nickel to carbon distances are 2.298(18) Å to C1 and 2.069(2) Å to C2 and Ni3-B4, Ni3-B7 and Ni-B8 distances are 2.101(2), 2.107(2) and 2.132(2) Å respectively.

The longest B-B connectivity in compound **17** for one cage is 1.835(6) Å between B4-B8 whereas for the other cage it is 1.829(6) Å between B4′-B8′ while the shortest one is between B6-B10 with a length of 1.752(6) Å in one cage and between B6′-B10′ with a distance of 1.743(6) Å in the other cage. The nickel to carbon distance in one cage is 2.328(3) Å to C1 and 2.071(4) Å to C2 and in the other cage the distances are 2.300(3) and 2.105(4) Å respectively.

The intracage C-C distances in both cages of compound **16** are 1.639(3) Å whereas the distances in compound **17** are 1.647(5) and 1.618(5) Å. The corresponding distance in 3,1,2-*closo*-$MC_2B_9H_{11}$ species is around 1.64 Å[11].

	16	**17**		**16**	**17**
Ni3-C1	2.298 (18)	2.328(3)	Ni3′-C1′	2.298 (18)	2.300(3)
Ni3-C2	2.069(2)	2.071(4)	Ni3′-C2′	2.069(2)	2.105(4)
Ni3-B4	2.101(2)	2.127(4)	Ni3′-B4′	2.101(2)	2.077(4)
Ni3-B7	2.107(2)	2.096(4)	Ni3′-B7′	2.107(2)	2.119(4)
Ni3-B8	2.132(2)	2.123(4)	Ni3′-B8′	2.132(2)	2.119(4)
C1-C2	1.639(3)	1.647(5)	C1′-C2′	1.639(3)	1.618(5)
C1-B4	1.711(3)	1.697(6)	C1′-B4′	1.711(3)	1.732(5)
C1-B5	1.688(3)	1.703(6)	C1′-B5′	1.688(3)	1.686(5)
C1-B6	1.707(3)	1.702(5)	C1′-B6′	1.707(3)	1.692(5)
C1-C1′	1.546(3)	1.545(5)	C2′-B6′	1.757(3)	1.749(6)
C2-B6	1.757(3)	1.762(5)	C2′-B7′	1.748(3)	1.775(6)
C2-B7	1.748(3)	1.747(5)	C2′-B11′	1.731(3)	1.742(6)
C2-B11	1.731(3)	1.733(6)	B4′-B5′	1.810(3)	1.786(6)
B4-B5	1.810(3)	1.804(6)	B4′-B8′	1.849(3)	1.829(6)
B4-B8	1.849(3)	1.835(6)	B4′-B9′	1.812(3)	1.777(6)
B4-B9	1.812(3)	1.787(6)	B5′-B6′	1.750(3)	1.749(6)
B5-B6	1.750(3)	1.755(6)	B5′-B9′	1.776(3)	1.784(6)
B5-B9	1.776(3)	1.760(6)	B5′-B10′	1.768(3)	1.770(6)
B5-B10	1.768(3)	1.754(6)	B6′-B10′	1.766(3)	1.743(6)
B6-B10	1.766(3)	1.752(6)	B6′-B11′	1.784(3)	1.766(6)
B6-B11	1.784(3)	1.763(6)	B7′-B8′	1.768(3)	1.753(6)
B7-B8	1.768(3)	1.773(6)	B7′-B11′	1.765(3)	1.762(6)
B7-B11	1.765(3)	1.764(6)	B7′-B12′	1.777(3)	1.776(6)
B7-B12	1.777(3)	1.774(7)	B8′-B9′	1.775(3)	1.771(6)
B8-B9	1.775(3)	1.755(6)	B8′-B12′	1.793(3)	1.765(6)
B8-B12	1.793(3)	1.786(6)	B9′-B10′	1.804(3)	1.796(6)
B9-B10	1.804(3)	1.804(7)	B9′-B12′	1.787(3)	1.768(6)
B9-B12	1.787(3)	1.776(7)	B10′-B11′	1.794(3)	1.796(6)
B10-B11	1.794(3)	1.786(7)	B10′-B12′	1.780(3)	1.774(6)
B10-B12	1.780(3)	1.770(6)	B11′-B12′	1.769(3)	1.774(6)
B11-B12	1.769(3)	1.766(7)			

Table 4.2 Cage connectivity distances in compounds 16 and 17

4.6 Summary

Deprotonation of a *racemic*/*meso* mixture of $[HNMe_3]_2$[7-(7′-7′,8′-*nido*-$C_2B_9H_{11}$)-7,8-*nido*-$C_2B_9H_{11}$] with BuLi in THF followed by metallation with {(dmpe)Ni} fragments yielded 1-(1′-3′-(dmpe)-3′,1′,2′-*closo*-$NiC_2B_9H_{10}$)-3-(dmpe)-3,1,2-*closo*-$NiC_2B_9H_{10}$ (**16** and **17**). *X*-ray diffraction studies clearly show that the products obtained are 12-vertex/12-vertex 3′,1′,2′-NiC_2B_9/3,1,2-NiC_2B_9 species and confirmed that compound **16** is *racemic* whereas compound **17** is *meso*.

Since, compared to the products of chapter 3, no isomerisation occurred in **16** and **17**, the dimethyl bis(carborane) 2,2′-$(CH_3)_2$-1,1′-bis(*o*-carborane) (**18**) was synthesised by the addition of methyl iodide to the diethylether solution of 1,1′-bis(*o*-carborane). We planned to double decapitate and then metallate this to see if the steric bulk of the methyl groups would cause isomerisation.

The decapitation of 2,2′-$(CH_3)_2$-1,1′-bis(*o*-carborane) (**18**) with KOH in EtOH followed by metallation with {(dmpe)Ni} fragments surprisingly yielded 1-(1′-1′,2′-$C_2B_{10}H_{10}$-2′-CH_3)-2-(dmpe)-7-CH_3-2,1,7-$NiC_2B_9H_9$ (**19**). *X*-ray diffraction study clearly shows that the product obtained is a single cage metallated product and also shows an unprecedented 12-vertex/12-vertex 2,1,7-metallacarborane/1′,2′-carborane.

4.7 References

4.1. D. C. Young, P. A. Wegner and M. F. Hawthorne, *J. Am. Chem. Soc.*, 1965, **87**, 1818.

4.2. P. E. Behnken, T. B. Marder, R. T. Baker, C. B. Knobler, M. R. Thompson and M. F. Hawthorne, *J. Am. Chem. Soc.*, 1985, **107**, 933.

4.3. (a) D. A. Owen and M. F. Hawthorne, *J. Am. Chem. Soc.*, 1970, **92**, 3194; (b) D. A. Owen and M. F. Hawthorne, *J. Am. Chem. Soc.*, 1971, **93**, 873; (c) D. A. Harwell, J. McMillan, C. B. Knobler and M. F. Hawthorne, *Inorg. Chem.*, 1997, **36**, 5951.

4.4. (a) S. B. Miller and M. F. Hawthorne, *J. Chem. Soc., Chem. Commun*. 1976, 786; (b) R. E. King III, S. B. Miller, C. B. Knobler and M. F. Hawthorne, *Inorg. Chem.*, 1983, **22**, 3548.

4.5. R. M. Garrioch, P. Kuballa, K. S. Low, G. M. Rosair and A. J. Welch, *J. Organometal. Chem.*, 1999, **575**, 57.

4.6. D. Ellis, G. M. Rosair and A. J. Welch, *Chem. Commun.*, 2010, **46**, 7394.

4.7. J. A. Dupont and M. F. Hawthorne, *J. Am. Chem. Soc.*, 1964, **86**, 1643.

4.8. S. Ren and Z. Xie, *Organometallics.*, 2008, **27**, 5167.

4.9. M. E. Lopez, D. Ellis, P. R. Murray, G. M. Rosair, A. J. Welch and L. J. Yellowless, *Collect. Czech. Chem. Commun.*, 2010, **75**, 853.

4.10. M. K. Kaloustain, R. J. Wiersema and M. F. Hawthorne, *J. Am. Chem. Soc.*, 1972, **94**, 6679.

4.11. (a) M. E. Lopez, M. J. Edie, D. Ellis, A. Horneber, S. A. Macgregor, G. M. Rosair and A. J. Welch, *Chem. Commun.*, 2007, 2243; (b) D. E. Smith and A. J. Welch, *Organometallics.*, 1986, **5**, 760.

Overall Conclusions

Currently, metallacarboranes derived from biscarboranes are unknown, in large measure because the traditional synthesis of bis(carboranes) is inefficient. However, in 2008 Xie reported an improved synthesis of 1,1′-bis(*o*-carborane), opening up the possibility of exploring the derivative chemistry of this molecule.

Attempted stoichiometric two electron reduction/metallation of 1,1′-bis(*o*-carborane) affords, surprisingly, linked 12-vertex/12-vertex 3,1,2-MC_2B_9/1′,2′-C_2B_{10} species and not the anticipated 13-vertex/12-vertex 4,1,6-MC_2B_{10}/1′,2′-C_2B_{10}. Therefore polyhedral expansion is not possible with only two electrons. The ligand attached to the metal in the 3,1,2-MC_2B_9 cage is bent away from the 1′,2′-C_2B_{10} cage by around 16^0 to avoid steric crowding.

These molecules can be deliberately prepared in higher yields by deboronation/metallation. Deboronation followed by metallation with {(arene)Ru} fragments resulted the same products as reduction/metallation and the yields are improved but not by as much as we expected. However metallation with a {CpCo} fragment resulted additionally in a 12-vertex/12-vertex 2,1,8-CoC_2B_9/1′,2′-C_2B_{10} species. To investigate if this came from isomerisation of 3,1,2-CoC_2B_9/1′,2′-C_2B_{10} the later was heated under toluene reflux for 48 hrs however only starting material was isolated.

^{11}B-^{11}B correlation spectra were analysed in order to identify the resonances due to carborane and metallacarborane cages in the above species. When conjoining two 1,2-*closo*-carboranes to produce 1,1′-bis(*o*-carborane) $<\delta^{11}B>$ moves to high frequency. Similarly in all compounds above $<\delta^{11}B>$ moves to higher frequencies with respect to the single cage components. This is because a H atom is replaced by a carborane or metallacarborane cage, both of which are more electron withdrawing than H.

Double decapitation of 1,1′-bis(*o*-carborane) afforded both *racemic* and *meso* diastereoisomers of linked $C_2B_{\mathbf{9}}$-$C_2B_{\mathbf{9}}$ anions but as salts these cannot be separated. Therefore metallation was carried on the mixture of diastereoisomers.

Metallation with {CpCo} fragments of the double decapitated 1,1′-bis(*o*-carborane) resulted in diastereomerically related 3,1,2-CoC_2B_9/2′,1′,8′-CoC_2B_9 and 2,1,8-CoC_2B_9/2′,1′,8′-CoC_2B_9 products which were separated by thin layer chromatography. However the 2,1,8-CoC_2B_9/2′,1′,8′-CoC_2B_9 products could not be separated by TLC and co-crystallised together. Single cage and double cage isomerisation occurred with {CpCo} fragments at room temperature due.

Similarly metallation with {(arene)Ru} fragments resulted in diastereomerically related 12-vertex/12-vertex 3,1,2-RuC_2B_9/2′,1′,8′-RuC_2B_9 products. The unprecedented 3,1,2 to 2,1,8 isomerisation at room temperature presumably resulted from steric crowding.

Metallation of double decapitated 1,1′-bis(*o*-carborane) with {(dmpe)Ni} resulted in diastereomeric *racemic* and *meso* 3,1,2-NiC_2B_9/3′,1′,2′-NiC_2B_9 products. To see if isomerisation could be induced methylation was first carried out on the carbon atoms of 1,1′-bis(*o*-carborane) to make the cage more crowded. Decapitation followed by deprotonation and metallation with {(dmpe)Ni} resulted in only a single cage metallated product which showed an unprecedented 3,1,2- to 2,1,7- isomerisation at room temperature.

CHAPTER 5

Experimental

5.1 General Experimental

Syntheses

Unless otherwise stated, all experiments were carried out under an atmosphere of dry, oxygen-free, nitrogen, using Schlenk-line techniques, with some work-ups being completed in the open laboratory. Most of the compounds reported are stable in air both as solids and as solutions. All solvents used were dried with the appropriate drying agents immediately before use [CH_2Cl_2 and CH_3CN, CaH_2; tetrahydrofuran (THF) and diethyl ether, sodium wire-benzophenone; toluene and light petroleum (b.p. 40-60 and 60-80 ^oC), sodium-wire] under nitrogen. Preparative TLC employed 20×20cm Kieselgel 60 F_{254} glass plates.

Physical measurements

NMR spectroscopy was carried out on Bruker AVIII-400 (^{11}B at 128.4 MHz and ^1H at 400.1 MHz) and AVIII-300 (^{11}B at 96.3 MHz, ^1H at 300.1 MHz and ^{31}P at 162.0 MHz) spectrometers. Proton chemical shifts are reported relative to $SiMe_4$, boron chemical shifts relative to $BF_3.OEt_2$ and phosphorus chemical shifts relative to phosphoric acid. NMR spectra were obtained from $(CD_3)_2CO$ solutions at 298K. Electron impact mass spectrometry was carried out using a Finnigan LCQ classic ion trap mass spectrometer at the University of Edinburgh. Elemental analyses were carried out using an Exeter CE-440 elemental analyser by the departmental service at Heriot-Watt.

Hazards

Standard principles of safe handling and good general laboratory practice were followed, including the wearing of protective clothing and safety glasses. Extra care and attention was employed when handling flammable solvents, sodium, toxic heteroboranes and other hazardous materials.

Standard Preparations

The starting materials 1,1′-bis(*o*-carborane)[1], [Ru(*p*-cymene)Cl_2]$_2$[2], [Ru(C_6H_6)Cl_2]$_2$[3], *N*-methylnicotinium iodide[4] and [Ni(dmpe)Cl_2]$_2$[5] were prepared using literature methods or slight variants thereof. All other reagents and solvents were supplied commercially.

Crystallographic data collections

Single crystals suitable for *X*-ray diffraction were mounted in inert oil on a glass fibre and cooled to 100K by an Oxford Cryosystems Cryostream. All measurements were made on a Bruker X8 APEX2 diffractometer[6], employing graphite-monochromated Mo-Kα *X*-radiation (λ=0.71069Å) and were corrected for absorption semi-empirically from symmetry-equivalent and repeated reflections. Structures were solved by direct and Fourier methods and refined by full-matrix least squares[7], against F^2. Refinement was completed with all non-hydrogen atoms assigned anisotropic displacement parameters.

5.2 Preparation of 1-(1′-1′,2′-*closo*-$C_2B_{10}H_{11}$)-3-(η-cymene)-3,1,2-*closo*-$RuC_2B_9H_{10}$ (1)

A degassed THF (20 ml) solution of naphthalene (0.13 g, 1.1 mmol) and excess sodium was stirred until the solution changed the colour to green. The reduced sodium naphthalenide solution was transferred through cannula to a solution of 1,1′-bis(*o*-carborane) (0.15 g, 0.52 mmol) in degassed THF (30 ml) and stirred overnight at room temperature. The orange solution was transferred through a cannula to a third Schlenk tube containing [Ru(*p*-cymene)Cl_2]$_2$ (0.16 g, 0.26 mmol), partially dissolved in THF (10 ml) at -78 ^oC and stirred overnight at room temperature. This resulted in a brown suspension which was filtered through Celite® and the solvent removed *in vacuo*. The resulting brown solid was dissolved in DCM and filtered through silica. Preparative TLC with a mixed eluent of CH_2Cl_2/40-60 petroleum ether (1:1) revealed a single mobile yellow band with R_f = 0.68 in 2.3% yield (6 mg, 0.01 mmol).

Compound 1	**1-(1′-1′,2′-*closo*-$C_2B_{10}H_{11}$)-3-(η-cymene)-3,1,2-*closo*-$RuC_2B_9H_{10}$**	
MS (low. Res. EI)	m/z 510.3 (M^+)	
CHN	Calculated for $C_{14}H_{35}B_{19}Ru$:	C 33.0%, H 6.92%
	Found	C 32.1%, H 6.93%
^{1}H NMR	δ 6.45 - 6.25 (m, 4H, C_6H_4), 4.65 (s, 1H, CH_{cage}), 4.30 (s, 1H, CH_{cage}), 3.05 (app. septet, 1H, $CH(CH_3)_2$), 2.50 (s, 3H, CH_3), 1.40 (m, 6H, $CH(CH_3)_2$)	
^{11}B{^{1}H} NMR	δ 2.07 (1B), -0.42 (1B), -3.19 (1B), -3.94 (1B), -4.86 (1B), -7.92 (3B), -8.75 (sh., 2B), -9.66 (2B), -11.05 (2B), -13.21 (2B), -14.58 (1B), -17.79 (2B)	

X-ray quality yellow crystals were grown by vapour diffusion of a DCM solution and 40-60 petroleum ether at room temperature.

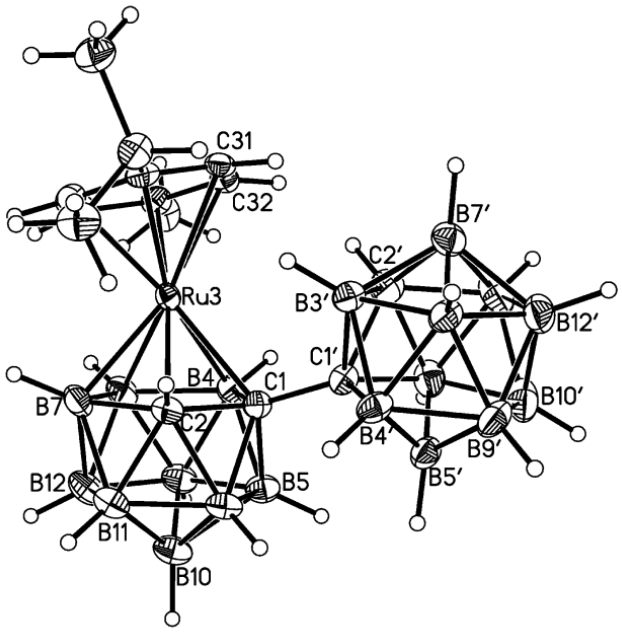

5.3 Preparation of 1-(1′-1′,2′-*closo*-$C_2B_{10}H_{11}$)-3-(η-benzene)-3,1,2-*closo*-$RuC_2B_9H_{10}$ (2)

A degassed solution of THF (30 ml) and 1,1′-bis(*o*-carborane) (0.30 g, 1.05 mmol) were stirred overnight with naphthalene (0.27 g, 2.11 mmol) and excess sodium at room temperature. The resulting orange solution was transferred *via* cannula to a second Schlenk tube containing $[Ru(C_6H_6)Cl_2]_2$ (0.26 g, 0.52 mmol), partially dissolved in THF (20 ml) at -78 ^oC. The reagents were stirred overnight, resulting in a brown suspension which was filtered through Celite® and the solvent removed *in vacuo*. The resulting brown solid was dissolved in DCM, filtered through silica and purified by TLC [CH_2Cl_2/40-60 petroleum ether (1:1)] to afford compound **2** with R_f = 0.70 as a yellow solid in 2.9% yield (14 mg, 0.03 mmol).

Compound 2	**1-(1′-1′,2′-*closo*-$C_2B_{10}H_{11}$)-3-(η-benzene)-3,1,2-*closo*-$RuC_2B_9H_{10}$**	
MS (low. Res. EI)	m/z 454.3 (M^+)	
CHN	Calculated for $C_{10}H_{27}B_{19}Ru$:	C 26.5%, H 6.00%
	Found	C 27.1%, H 6.67%
^{1}H NMR	δ 6.60 (s, 6H, C_6H_6), 4.65 (s, 1H, CH_{cage}), 4.60 (s, 1H, CH_{cage})	
^{11}B{^{1}H} NMR	δ 1.67 (1B), 0.09 (1B), -3.17 (1B), -3.85 (1B), -6.28 (1B), -7.83 (3B), -8.79 (2B), -9.25 (sh., 2B), -11.13 (2B), -13.19 (2B), -14.67 (1B), -17.83 (2B)	

X- ray quality yellow single crystals were grown by solvent diffusion of a $CDCl_3$ and 40-60 petroleum ether at room temperature.

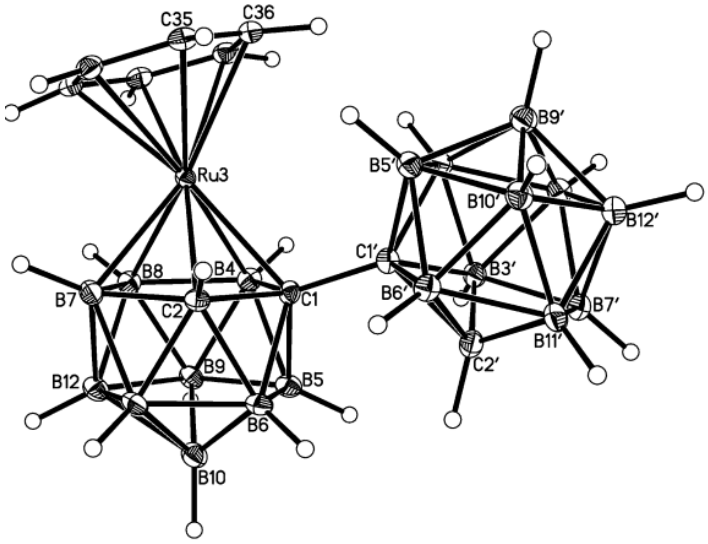

5.4 Preparation of 1-(1′-1′,2′-*closo*-$C_2B_{10}H_{11}$)-3-(η-C_5H_5)-3,1,2-*closo*-$CoC_2B_9H_{10}$ (3)

A degassed THF (20 ml) solution of naphthalene (0.13 g, 1.1 mmol) and excess sodium was stirred until the solution changed colour to green. The reduced sodium naphthalenide solution was transferred through cannula to a solution of 1,1′-bis(*o*-carborane) (0.15 g, 0.52 mmol) in degassed THF (20 ml) at -78 ^{o}C and the reaction mixture was stirred for 4 hrs at room temperature. NaCp (0.79 ml of 2.0M solution, 1.6 mmol) and $CoCl_2$ (0.25 g, 1.9 mmol) were added to the cooled reaction mixture. Then the reaction mixture was left to warm to room temperature with stirring overnight. The resultant brown suspension was subjected to aerial oxidation for an hour followed by filtration through silica and THF was removed on the vacuum line. The crude mixture was dissolved in DCM and filtered through Celite®. The brown residue was purified by TLC with a mixed eluent of CH_2Cl_2/40-60 petroleum ether (1:1) to reveal a mobile band with R_f 0.76 in 3.8% yield (8 mg, 0.02 mmol).

Compound 3	**1-(1′-1′,2′-*closo*-$C_2B_{10}H_{11}$)-3-(η-C_5H_5)-3,1,2-*closo*-$CoC_2B_9H_{10}$**	
MS (low. Res. EI)	m/z 399.2 (M^+)	
CHN	Calculated for $C_9H_{26}B_{19}Co$:	C 27.1%, H 6.57%
	Found	C 25.2%, H 6.76%
^{1}H NMR	δ 6.10 (s, 5H, C_5H_5), 4.75 (s, 1H, CH_{cage}), 4.65 (s, 1H, CH_{cage})	
^{11}B{^{1}H} NMR	δ 5.28 (1B), 0.87 (1B), -2.50 (sh., 1B), -3.51 (2B), -4.21 (1B), -5.32 (1B), -8.40 (2B), -9.60 (3B), -10.44 (2B), -11.75 (1B), -12.86 (2B), -15.07 (1B), -16.41 (1B)	

X-ray quality orange crystals were grown by vapour diffusion of a DCM solution and 40-60 petroleum ether at room temperature.

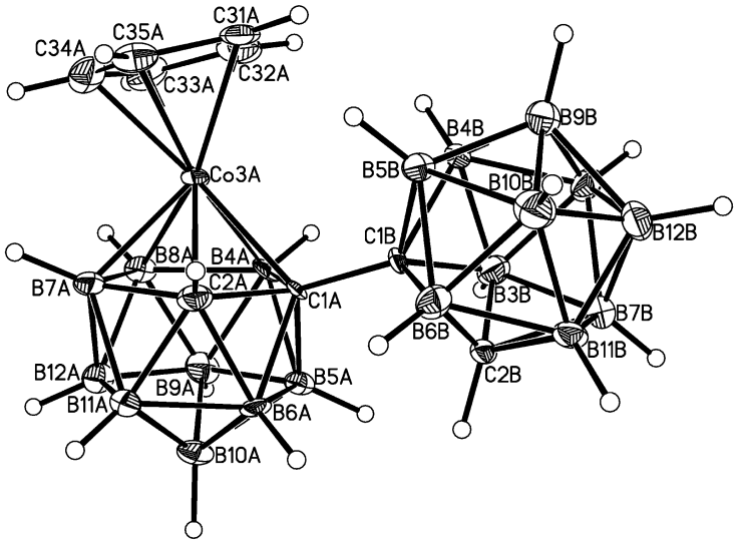

5.5 Preparation of [BTMA][7-(1′-1′,2′-*closo*-$C_2B_{10}H_{11}$)-7,8-*nido*-$C_2B_9H_{11}$] (4)

Deboronation of 1,1′-bis(*o*-carborane) was achieved by heating to reflux an EtOH (50 ml) solution of 1,1′-bis(*o*-carborane) (0.5 g, 1.8 mmol) with KOH (0.2 g, 3.6 mmol) for 4 hrs. The reaction mixture was then allowed to cool to room temperature, and CO_2 (g) was passed through to remove the excess KOH as K_2CO_3. The white solid was filtered off and the EtOH was evaporated under reduced pressure to yield an oil. Water was added to the oil yielding a clear solution and then [BTMA]Cl (0.32 g, 1.8 mmol) was added as an aqueous solution. Immediately precipitation of white solid occured and the solid was collected by filtration, then washed with water and dried *in vacuo* to yield [BTMA][7-(1′-1′,2′-*closo*-$C_2B_{10}H_{11}$)-7,8-*nido*-$C_2B_9H_{11}$] (**5**) (0.55 g, 1.3 mmol) in 74% yield.

Salt 4	**[BTMA][7-(1′-1′,2′-*closo*-$C_2B_{10}H_{11}$)-7,8-*nido*-$C_2B_9H_{11}$]**
CHN	Calculated for $C_{14}H_{38}B_{19}N$: C 39.5%, H 8.99%, N 3.29% Found C 41.5%, H 9.15%, N 3.25%
^{1}H NMR	δ 7.75-7.45 (m, 5H, C_6H_5), 4.75 (s, 2H, CH_2), 4.35 (s, 1H, CH_{cage}), 3.35 (s, 9H, $N(CH_3)_3$), 1.95 (s, 1H, CH_{cage})
^{11}B{^{1}H} NMR	δ -4.18 (1B), -6.24 (1B), -9.03 (1B), -10.64 (5B), -11.50 (sh., 2B), -13.77 (3B), -17.01 (2B), -19.24 (1B), -22.82 (1B), -33.15 (1B), -35.50 (1B)

X-ray quality colourless single crystals were grown by vapour diffusion of a DCM solution and 40-60 petroleum ether at room temperature.

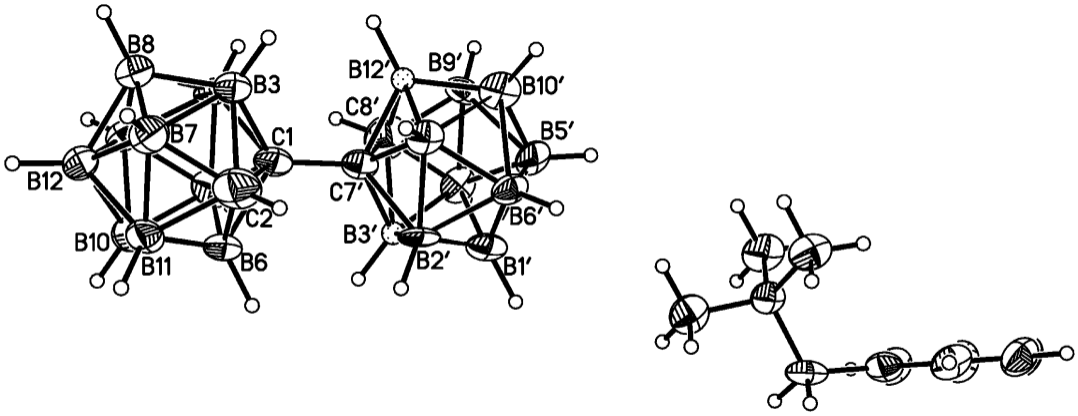

5.6 Preparation of [$HNMe_3$][7-(1′-1′,2′-*closo*-$C_2B_{10}H_{11}$)-7,8-*nido*-$C_2B_9H_{11}$] (5)

1,1′-bis(*o*-carborane) (0.50 g, 1.8 mmol) and KOH (0.2 g, 3.6 mmol) were dissolved in EtOH (50 ml). The mixture was heated under reflux for 4 hrs and then left to cool to room temperature. CO_2(g) was passed through the reaction mixture for half an hour and the solid then filtered off. EtOH was evaporated under reduced pressure to yield an oil which was then dissolved in water to yield a clear solution to which [$HNMe_3$]Cl (0.17 g, 1.8 mmol) was added as an aqueous solution. Immediately precipitation of a white solid occurred. The solid was collected by filtration and then washed with water and dried under reduced pressure to afford [$HNMe_3$][7-(1′-1′,2′-*closo*-$C_2B_{10}H_{11}$)-7,8-*nido*-$C_2B_9H_{11}$] (**5**) (0.46 g, 1.4 mmol) in 79.1% yield.

Salt 5	**[HNMe$_3$][7-(1′-1′,2′-*closo*-C$_2$B$_{10}$H$_{11}$)-7,8-*nido*-C$_2$B$_9$H$_{11}$]**
CHN	Calculated for $C_7H_{32}B_{19}N$: C 25.0%, H 9.63%, N 4.17% Found C 25.3%, H 9.27%, N 3.99%
^{1}H NMR	δ 4.35 (s, 1H, C*H*$_{cage}$), 3.15 (s, 9H, N(C*H*$_3$)$_3$), 1.95 (s, 1H, C*H*$_{cage}$)
^{11}B{^{1}H} NMR	δ -4.18 (1B), -6.23 (1B), -9.03 (1B), -10.63 (5B), -11.51 (sh., 2B), -13.73 (3B), -17.00 (2B), -19.23 (1B), -22.90 (1B), -33.12 (1B), -35.49 (1B)

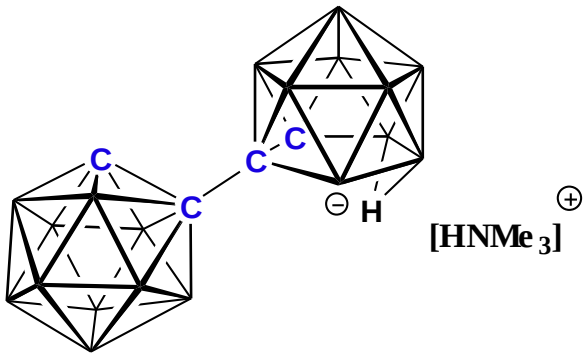

5.7 Preparation of 1-(1′-1′,2′-*closo*-$C_2B_{10}H_{11}$)-3-(η-cymene)-3,1,2-*closo*-$RuC_2B_9H_{10}$ (1) by deprotonation and metallation

[$HNMe_3$][7-(1′-1′,2′-*closo*-$C_2B_{10}H_{11}$)-7,8-*nido*-$C_2B_9H_{11}$] (0.1 g, 0.30 mmol) was dissolved in THF (20 ml). The solution was cooled to 0^oC and BuLi (0.24 ml of 2.5M solution, 0.60 mmol) was added dropwise. The colourless solution was then heated under reflux for 4 hrs. [Ru(*p*-cymene)Cl_2]$_2$ (0.09 g, 0.15 mmol) was added to the reaction mixture at 0^oC and then the reaction mixture was left to warm to room temperature with continuous stirring overnight. The THF was removed on the vacuum line and the crude mixture was dissolved in DCM and filtered through Celite®. The remaining brown solution was purified by TLC with a mixed eluent of CH_2Cl_2/40-60 petroleum ether (1:1) to reveal a yellow mobile band with R_f 0.68 (12 mg, 0.02 mmol) in 7.9 % yield.

5.8 Preparation of 1-(1′-1′,2′-*closo*-$C_2B_{10}H_{11}$)-3-(η-benzene)-3,1,2-*closo*-$RuC_2B_9H_{10}$ (2) by deprotonation and metallation

[$HNMe_3$][7-(1′-1′,2′-*closo*-$C_2B_{10}H_{11}$)-7,8-*nido*-$C_2B_9H_{11}$] (0.1 g, 0.30 mmol) was dissolved in 20 ml of THF. The solution was cooled to 0^{o}C and BuLi (0.24 ml of 2.5M solution, 0.60 mmol) was added dropwise and the colourless solution was then heated under reflux for 4 hrs. [$Ru(C_6H_6)Cl_2]_2$ (0.08 g, 0.15 mmol) was added to the reaction mixture at 0^{o}C then the reaction mixture was left to warm to room temperature with continuous stirring overnight. The THF solution was removed on the vacuum line and the crude mixture was dissolved in DCM and filtered through Celite®. Following removal of solvent the brown residue was purified by TLC with a mixed eluent of CH_2Cl_2/40-60 petroleum ether (1:1) to reveal a yellow mobile band with R_f 0.7 (12 mg, 0.03 mmol) in 8.8 % yield.

5.9 Preparation of 8-(1′-1′,2′-*closo*-$C_2B_{10}H_{11}$)-2-(η-C_5H_5)-2,1,8-*closo*-$CoC_2B_9H_{10}$ (6) and [Cp_2Co][7-(1′-1′,2′-*closo*-$C_2B_{10}H_{11}$)-7,8-*nido*-$C_2B_9H_{11}$] (7)

[$HNMe_3$][7-(1′-1′,2′-*closo*-$C_2B_{10}H_{11}$)-7,8-*nido*-$C_2B_9H_{11}$] (0.25 g, 0.74 mmol) was dissolved in 20 ml of THF. BuLi (0.60 ml of 2.5M solution, 1.5 mmol) was added dropwise while cooling to 0^oC and the mixture was then heated under reflux for 4 hrs. NaCp (1.12 ml of 2.0M solution, 2.24 mmol) and $CoCl_2$ (0.36 g, 2.8 mmol) were added to the reaction mixture while cooling then the reaction mixture was left to warm to room temperature with continuous stirring overnight. The resultant dark green suspension was subjected to aerial oxidation for an hour followed by filtration through silica. THF was removed on the vacuum line. The crude mixture was dissolved in DCM and filtered through Celite®. The brown residue was purified by TLC with a mixed eluent of CH_2Cl_2/40-60 petroleum ether (1:1) to reveal two mobile band, with R_f 0.7 and 0.1 which are 8-(1′-1′,2′-*closo*-$C_2B_{10}H_{11}$)-2-(η-C_5H_5)-2,1,8-*closo*-$CoC_2B_9H_{10}$ (**6**) (95 mg, 0.23 mmol) and [Cp_2Co][7-(1′-1′,2′-*closo*-$C_2B_{10}H_{11}$)-7,8-*nido*-$C_2B_9H_{11}$] (**7**) (45 mg, 0.10 mmol) in yields of 32% and 13% respectively.

Compound 6	**8-(1′-1′,2′-*closo*-$C_2B_{10}H_{11}$)-2-(η-C_5H_5)-2,1,8-*closo*-$CoC_2B_9H_{10}$**	
MS (low. Res. EI)	m/z 399.3 (M+)	
CHN	Calculated for $C_9H_{26}B_{19}Co$:	C 27.1%, H 6.57%
	Found	C 27.1%, H 6.65%
^{1}H NMR	δ 5.75 (s, 5H, C_5H_5), 4.45 (s, 1H, CH_{cage}), 3.15 (s, 1H, CH_{cage})	
^{11}B{^{1}H} NMR	δ 1.11 (1B), -0.67 (2B), -1.78 (1B), -3.36 (1B), -4.46 (1B), -6.36 (1B), -7.00 (sh., 1B), -10.46 (6B), -12.78 (1B), -13.36 (2B), -17.48 (1B), -18.36 (1B)	

X-ray quality yellow single crystals were grown by vapour diffusion of a DCM solution and 40-60 petroleum ether at room temperature.

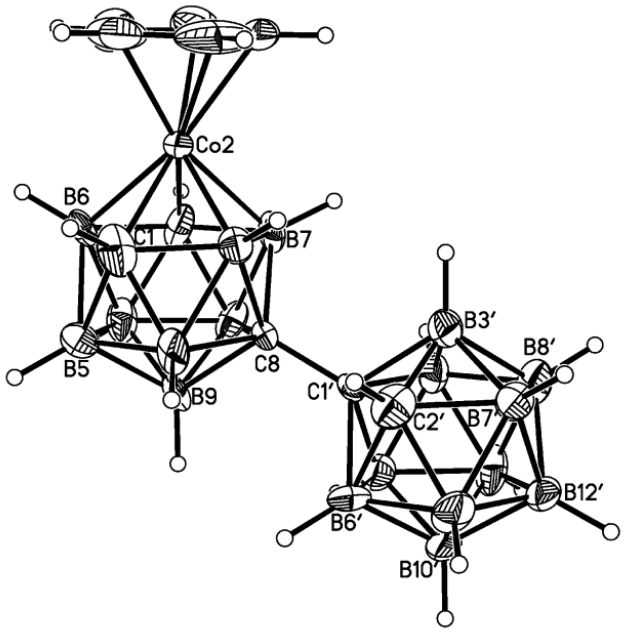

Salt 7	**[Cp_2Co][7-(1′-1′,2′-*closo*-$C_2B_{10}H_{11}$)-7,8-*nido*-$C_2B_9H_{11}$]**
CHN	Calculated for $C_{14}H_{32}B_{19}Co$: C 36.2%, H 6.94% Found C 35.3%, H 6.72%
^{1}H NMR	δ 5.85 (s, 10H, $2C_5H_5$), 4.35 (s, 1H, CH_{cage}), 1.95 (s, 1H, CH_{cage})
^{11}B{^{1}H} NMR	δ -4.18 (1B), -6.23 (1B), -9.03 (1B), -10.63 (5B), -11.51 (sh., 2B), -13.73 (3B), -17.00 (2B), -19.22 (1B), -22.90 (1B), -33.12 (1B), -35.49 (1B)

X-ray quality pale green crystals were grown by vapour diffusion of a DCM solution and 40-60 petroleum ether at room temperature.

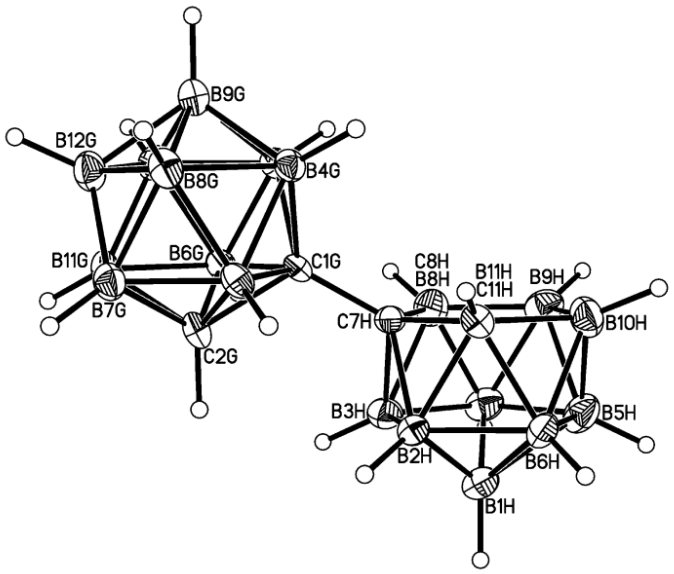

5.10 Preparation of [BTMA]$_2$[7-(7′-7′,8′-*nido*-$C_2B_9H_{11}$)-7,8-*nido*-$C_2B_9H_{11}$] (8)

1,1′-bis(*o*-carborane) (0.5 g, 1.8 mmol) and KOH (2.94 g, 52.4 mmol) were dissolved in EtOH (50 ml) and the mixture heated under reflux for 48 hrs then left to cool to room temperature. CO_2(g) was passed through the reaction mixture which was then filtered. The solution was evaporated under reduced pressure and the oily product obtained dissolved in water to give a clear solution which was filtered. [BTMA]Cl (0.65 g, 3.5 mmol) was added to the filtrate as an aqueous solution to yield [BTMA]$_2$[7-(7′-7′,8′-*nido*-$C_2B_9H_{11}$)-7,8-*nido*-$C_2B_9H_{11}$] (0.74 g, 1.33 mmol) in 75.2% yield.

Salt 8	**$[BTMA]_2[7\text{-}(7'\text{-}7',8'\text{-}nido\text{-}C_2B_9H_{11})\text{-}7,8\text{-}nido\text{-}C_2B_9H_{11}]$**
CHN	Calculated for $C_{24}H_{54}B_{18}N_2$: C 50.1%, H 9.63%, N 4.96% Found C 48.8%, H 9.60%, N 4.43%
^{1}H NMR	δ 7.65-7.50 (m, 10H, $2C_6H_5$), 4.75 (s, 4H, $2CH_2$), 3.30 (s, 9H, $N(CH_3)_3$)
^{11}B{^{1}H} NMR	δ -11.04, -14.88, -15.90, -17.69, -18.69, -20.50, -21.39, - 23.96, -24.66, -33.85, -36.79

X-ray quality colourless crystals were grown by vapour diffusion of a THF solution and 40-60 petroleum ether at room temperature.

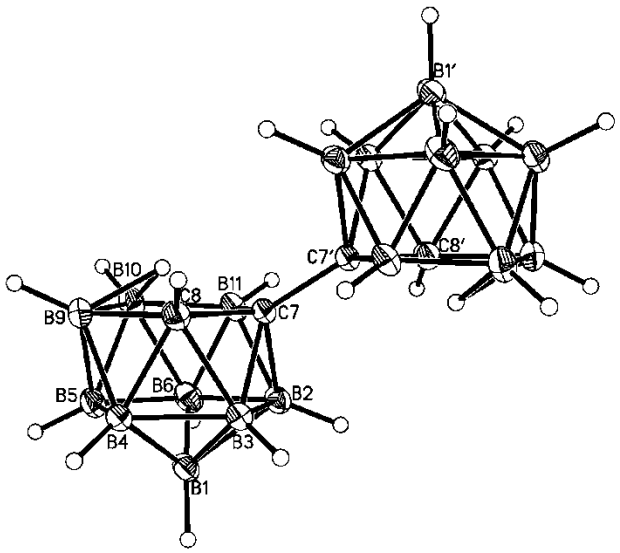

5.11 Preparation of $[HNMe_3]_2[7\text{-}(7'\text{-}7',8'\text{-}nido\text{-}C_2B_9H_{11})\text{-}7,8\text{-}nido\text{-}C_2B_9H_{11}]$ (9)

Double decapitation of 1,1′-bis(*o*-carborane) was carried out by heating to reflux an EtOH (50 ml) solution of 1,1′-bis(*o*-carborane) (0.5 g, 1.8 mmol) with KOH (2.94 g, 52.4 mmol) for 48 hrs. The reaction mixture was then allowed to cool to room temperature, and CO_2 (g) was passed through it to remove the excess KOH. The white solid was filtered off and the EtOH was evaporated under reduced pressure to yield an oil. Water was added to the oil yielding a clear solution to which $[HNMe_3]Cl$ (0.33 g, 3.5 mmol) was added as an aqueous solution. Immediately precipitation of white crystalline solid occurred and the solid was collected by filtration, then washed with water and dried under reduced pressure to yield $[HNMe_3]_2[7\text{-}(7'\text{-}7',8'\text{-}nido\text{-}C_2B_{10}H_{11})\text{-}7,8\text{-}nido\text{-}C_2B_9H_{11}]$ (**9**) (0.47 g, 1.23 mmol) in 70% yield.

Salt 9	**$[HNMe_3]_2[7\text{-}(7'\text{-}7',8'\text{-}nido\text{-}C_2B_9H_{11})\text{-}7,8\text{-}nido\text{-}C_2B_9H_{11}]$**
CHN	Calculated for $C_{10}H_{42}B_{18}N_2$: C 31.2%, H 10.99%, N 7.28% Found C 31.0%, H 11.08%, N 7.37%
$^{11}B\{^1H\}$ NMR	δ -11.10, -14.92, -15.94, -17.74, -18.72, -20.56, -21.40, -23.98, -24.66, -33.89, -36.83

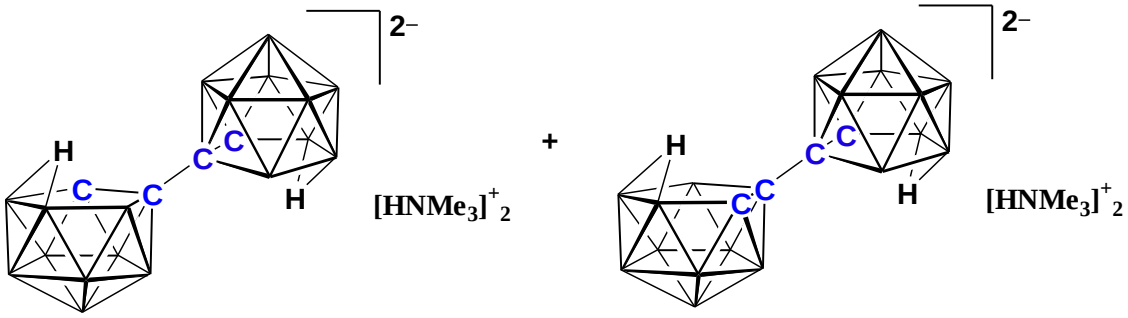

5.12 Preparation of [(*S*)-$CH_3NC_5H_4$-$C_4H_7NCH_3$]$_2$[7-(7′-7′,8′-*nido*-$C_2B_9H_{11}$)-7,8-*nido*-$C_2B_9H_{11}$] (10)

1,1′-bis(*o*-carborane) (0.5 g, 1.8 mmol) and KOH (2.94 g, 52.4 mmol) were dissolved in EtOH (50 ml) and the reaction mixture was heated under reflux for 48 hrs. The reaction mixture was then allowed to cool to room temperature, and CO_2 (g) was passed through for half an hour to remove the excess KOH. The white solid was filtered off and the EtOH was evaporated under reduced pressure to yield an oil. To the colourless oil water was added yielding a clear solution to which [(*S*)-$CH_3NC_5H_4$-$C_4H_7NCH_3$]I (1.1 g, 3.5 mmol) was added as an aqueous solution. The pale yellow solid which precipitated was collected by filtration, then washed with water and dried under reduced pressure to yield [(*S*)-$CH_3NC_5H_4$-$C_4H_7NCH_3$][7-(7′-7′,8′-*nido*-$C_2B_{10}H_{11}$)-7,8-*nido*-$C_2B_9H_{11}$] (**10**) (0.8 g, 1.3 mmol) in 74% yield.

Salt 10	**[(*S*)-$CH_3NC_5H_4$-$C_4H_7NCH_3$]$_2$[7-(7′-7′,8′-*nido*-$C_2B_9H_{11}$)-7,8-*nido*-$C_2B_9H_{11}$]**
CHN	Calculated for $C_{26}H_{56}B_{18}N_4$: C 50.4%, H 9.11%, N 9.05% Found C 48.3%, H 9.18%, N 8.44%
^{1}H NMR	δ 8.95 (s, 2H, 2C_5H_4), 8.85 (d, 2H, 2C_5H_4), 8.55 (d, 2H, 2C_5H_4), 8.05 (t, 2H, 2C_5H_4), 4.50 (s, 6H, 2NCH_3), 3.50 (t, 2H, 2C_4H_7), 3.20 (t, 2H, 2C_4H_7), 2.25 (m, 4H, 2C_4H_7), 2.10 (s, 6H, 2NCH_3), 1.80 (m, 4H, 2C_4H_7), 1.60 (m, 2H, 2C_4H_7)
^{11}B{^{1}H} NMR	δ -11.04, -14.88, -15.90, -17.69, -18.69, -20.55, -21.39, -23.96, -24.66, -33.85, -36.79

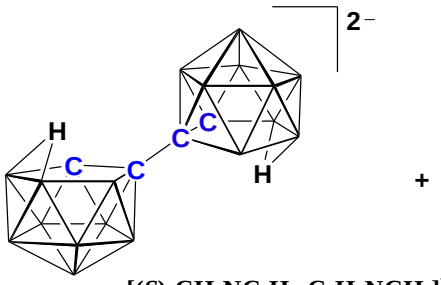

[(*S*)-$CH_3NC_5H_4$-$C_4H_7NCH_3$]$^+_2$

+

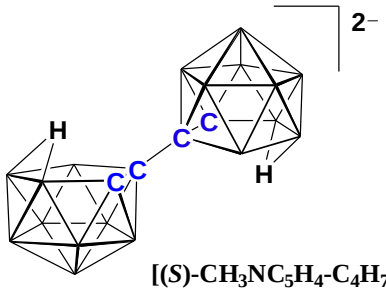

[(*S*)-$CH_3NC_5H_4$-$C_4H_7NCH_3$]$^+_2$

5.13 Preparation of 12-v/12-v cobaltacarborane/cobaltacarborane from the deprotonation and metallation of [7-(7′-7′,8′-*nido*-$C_2B_9H_{11}$)-7,8-*nido*-$C_2B_9H_{11}$]$^{2-}$ (11, 12 and 13)

$[HNMe_3]_2$[7-(7′-7′,8′-*nido*-$C_2B_9H_{11}$)-7,8-nido-$C_2B_9H_{11}$] (0.30 g, 0.78 mmol) was dissolved in THF (50 ml) in a Schlenk tube and cooled to 0^{o}C. To this, BuLi (2.5 ml of 2.5M solution, 6.24 mmol) was added dropwise and the mixture was heated under reflux for 4 hrs. NaCp (2.35 ml, 4.70 mmol) and $CoCl_2$ (0.75 g, 5.80 mmol) were added to the reaction mixture while cooling at 0^{o}C then the reaction mixture was left to warm to room temperature with stirring overnight. The resultant brown suspension was subjected to aerial oxidation for an hour followed by filtration through silica and THF was removed on the vacuum line. The crude mixture was dissolved in DCM and filtered through Celite®. Following removal of solvent the brown residue was purified by TLC with a mixed eluent of CH_2Cl_2/40-60 petroleum ether (1:1) to reveal three compounds **11** (R_f 0.62), **12** (R_f 0.56) and **13** (R_f 0.51) as yellow, orange and orange in 3.7% (15 mg, 0.03 mmol), 2% (8 mg, 0.02 mmol) and 5% (18 mg, 0.04 mmol) yields respectively.

Compound 11	**8-(8′-2′-(η-C_5H_5)-2′,1′,8′-*closo*-$CoC_2B_9H_{10}$)-2-(η-C_5H_5)-*closo*-2,1,8-$CoC_2B_9H_{10}$**
MS (low. Res. EI)	m/z 510.3 (M^+)
CHN	Calculated for $C_{14}H_{30}B_{18}Co_2$: C 32.9%, H 5.92% Found C 32.2%, H 5.86%
$^{11}B\{^1H\}$ NMR	δ 0.22 (3B), -1.75 (2B), -2.61 (1B), -3.15 (1B), -6.22 (2B), -9.83 (2B), -10.49 (1B), -12.80 (2B), -13.81 (1B), -17.40 (2B), -18.67 (1B)

X-ray quality yellow crystals were grown by vapour diffusion of a DCM solution and 40-60 petroleum ether at room temperature.

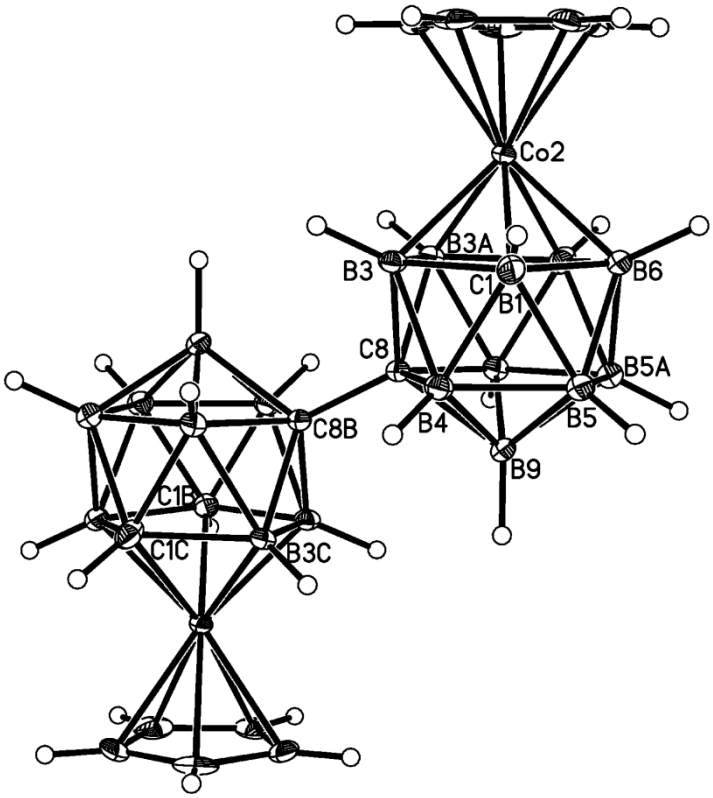

Compound 12	**1-(8′-2′-(η-C_5H_5)-2′,1′,8′-*closo*-$CoC_2B_9H_{10}$)-3-(η-C_5H_5)-*closo*-3,1,2-$CoC_2B_9H_{10}$ (form α)**
MS (low. Res. EI**)**	m/z 510.3 (M^+)
CHN	Calculated for $C_{14}H_{30}B_{18}Co_2$: C 32.9%, H 5.92% Found C 34.2%, H 5.98%
^{1}H NMR	δ 6.00 (s, 5H, C_5H_5), 5.70 (s, 5H, C_5H_5), 4.35 (s, 1H, CH_{cage}), 3.05 (s, 1H, CH_{cage})
^{11}B{^{1}H} NMR	δ 4.68 (1B), -1.25 (4B), -1.62 (1B), -4.61 (5B), -8.63 (1B), -10.64 (1B), -12.50 (2B), -15.18 (1B), -15.79 (1B), -18.27 (1B)

X-ray quality orange crystals were grown by vapour diffusion of a DCM solution and 40-60 petroleum ether at room temperature.

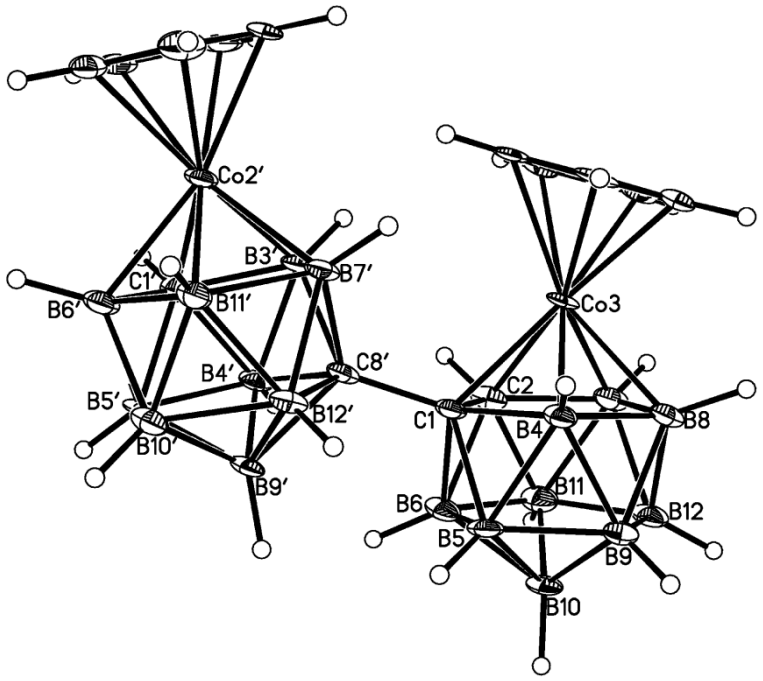

Compound 13	**1-(8′-2′-(η-C_5H_5)-2′,1′,8′-*closo*-$CoC_2B_9H_{10}$)-3-(η-C_5H_5)-*closo*-3,1,2-$CoC_2B_9H_{10}$ (form β)**
MS (low. Res. EI)	m/z 510.3 (M^+)
CHN	Calculated for $C_{14}H_{30}B_{18}Co_2$: C 32.9%, H 5.92% Found C 33.3%, H 6.31%
^{1}H NMR	δ 6.05 (s, 5H, C_5H_5), 5.70 (s, 5H, C_5H_5), 4.35 (s, 1H, CH_{cage}), 3.05 (s, 1H, CH_{cage})
^{11}B{^{1}H} NMR	δ 4.67 (1B), -1.30 (4B), -1.62 (1B), -4.60 (5B), -8.54 (1B), -10.83 (1B), -12.10 (1B), -15.28 (3B), -18.08 (1B)

X-ray quality orange crystals were grown by vapour diffusion of a DCM solution and 40-60 petroleum ether at room temperature.

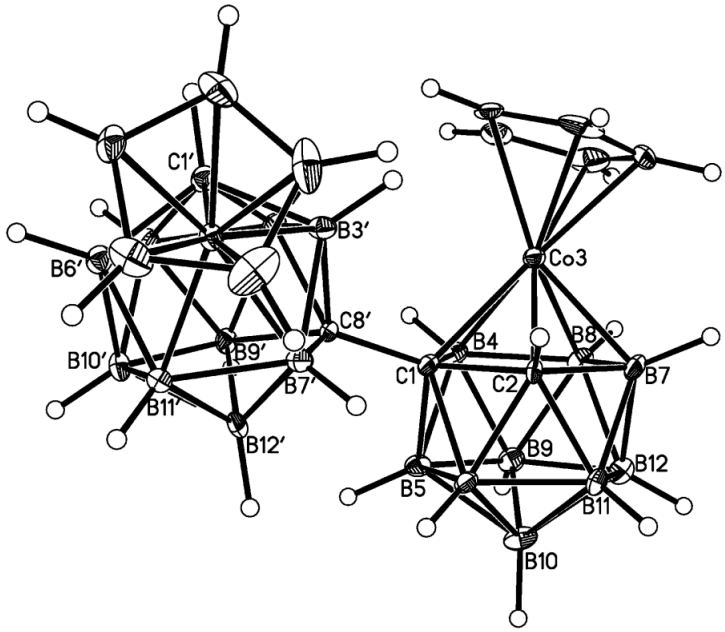

5.14 Preparation of 12-v/12-v ruthenacarborane/ruthenacarborane from deprotonation and metallation of [7-(7′-7′,8′-*nido*-$C_2B_9H_{11}$)-7,8-*nido*-$C_2B_9H_{11}$]$^{2-}$ (14 and 15)

$[HNMe_3]_2$[7-(7′-7′,8′-*nido*-$C_2B_9H_{11}$)-7,8-*nido*-$C_2B_9H_{11}$] (0.30 g, 0.78 mmol) was dissolved in THF (40 ml) in a Schlenk tube and cooled to 0^{o}C. To this, BuLi (2.5 ml of 2.5M solution, 6.24 mmol) was added dropwise, and the mixture was heated under reflux for 4 hrs. On cooling, the solution was transferred through a cannula to a freshly prepared suspension of [Ru(*p*-cymene)Cl_2]$_2$ (0.48 g, 0.78 mmol) in THF (20 ml) and stirred overnight. The mixture was then filtered through silica and the solvent was removed under reduced pressure. The resulted brown suspension was then dissolved in DCM, filtered through Celite® and purified by TLC eluting with DCM/40-60 petroleum ether (1:1) to reveal compounds **14 (**R_f 0.45**)** and **15** (R_f 0.40) in 2.1% (10 mg, 0.01 mmol) and 10.4% (50 mg, 0.07 mmol) yields respectively.

Compound 14	**1-(8′-2′-(η-$C_{10}H_{14}$)-2′,1′,8′-*closo*-$RuC_2B_9H_{10}$)-3-(η-$C_{10}H_{14}$)-*closo*-3,1,2-$RuC_2B_9H_{10}$ (form α)**
MS (low. Res. EI**)**	m/z 734.3 (M^+)
CHN	Calculated for $C_{24}H_{48}B_{18}Ru_2$: C 39.3%, H 6.60% Found C 40.8%, H 7.06%
^{1}H NMR	δ 6.25-6.05 (m, 8H, 2C_6H_4), 3.75 (s, 1H, CH_{cage}), 3.10 (septet, 1H, CH(CH_3)$_2$), 2.85 (m, 4H, CH(CH_3)$_2$ and CH_3), 2.75 (s, 1H, CH_{cage}), 2.45 (s, 3H, CH_3), 1.30 (m, 12H, 2CH(CH_3)$_2$)
^{11}B{^{1}H} NMR	δ 1.33 (1B), -0.58 (3B), -1.39 (1B), -4.15 (2B), -8.16 (5B), -13.34 (1B), -17.09 (3B), -18.01 (1B), -21.27 (1B)

X-ray quality yellow crystals were grown by vapour diffusion of a DCM solution and 40-60 petroleum ether at room temperature.

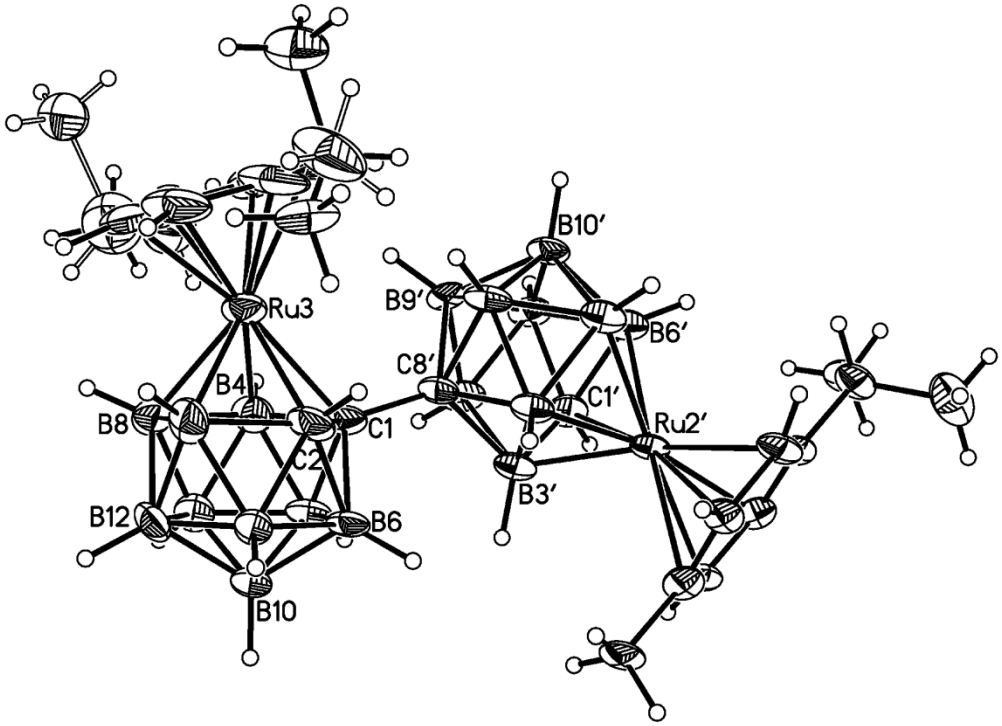

Compound 15	**1-(8′-2′-(η-$C_{10}H_{14}$)-2′,1′,8′-*closo*-$RuC_2B_9H_{10}$)-3-(η-$C_{10}H_{14}$)-*closo*-3,1,2-$RuC_2B_9H_{10}$ (form β)**
MS (low. Res. EI**)**	m/z 734.3 (M^+)
CHN	Calculated for $C_{24}H_{48}B_{18}Ru_2$: C 39.3%, H 6.60% Found C 39.3%, H 6.86%
^{1}H NMR	δ 6.25-6.05 (m, 8H, 2C_6H_4), 3.95 (s, 1H, CH_{cage}), 3.05 (septet, 1H, CH(CH_3)$_2$), 2.85 (m, 4H, CH(CH_3)$_2$ and CH_3), 2.70 (s, 1H, CH_{cage}), 2.45 (s, 3H, CH_3), 1.30 (m, 12H, 2CH(CH_3)$_2$)
^{11}B{^{1}H} NMR	δ 1.38 (1B), -0.50 (3B), -1.33 (1B), -4.42 (1B), -5.26 (1B), -8.20 (5B), -13.56 (1B), -16.98 (1B), -17.98 (3B), -21.03 (1B)

X-ray quality yellow crystals were grown from d_6-acetone by solvent evaporation at room temperature.

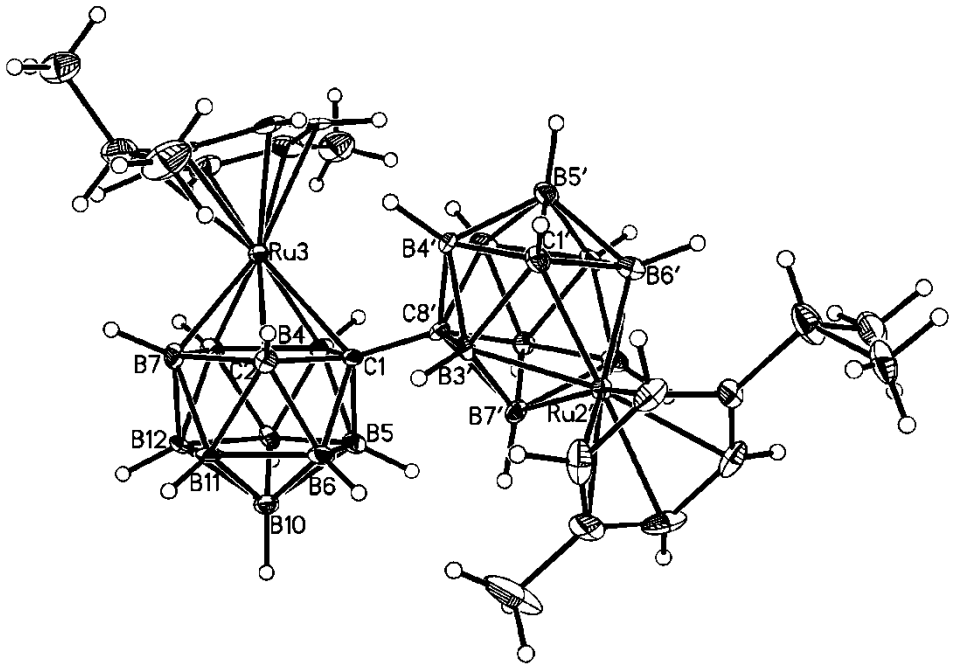

5.15 Preparation of 12-v/12-v nickelacarborane/nickelacarborane species from the deprotonation and metallation of [7-(7′-7′,8′-*nido*-$C_2B_9H_{11}$)-7,8-*nido*-$C_2B_9H_{11}$]$^{2-}$ (16 and 17)

$[HNMe_3]_2$[7-(7′-7′,8′-*nido*-$C_2B_9H_{11}$)-7,8-*nido*-$C_2B_9H_{11}$] (0.25 g, 0.65 mmol) was dissolved in THF (20 ml) and cooled to 0˚C. BuLi (2.1 ml of 2.5M solution, 5.2 mmol) was added to the reaction mixture which was then heated under reflux for 4 hrs. Then the reaction mixture was left to cool to room temperature. Ni(dmpe)Cl_2 (0.36 g, 1.3 mmol) was added at 0°C and the mixture stirred overnight. The resulting dark green suspension was filtered through silica and THF was removed on the vacuum line. The remaining solid was dissolved in DCM and filtered through Celite®. The dark green residue was purified by TLC with a mixed eluent of CH_2Cl_2/40-60 petroleum ether (3:1) to reveal two green mobile bands with R_f 0.60 and 0.45, *racemic* (**16**) and *meso* (**17**) forms of 1-(1′-3′-(dmpe)-3′,1′,2′-*closo*-$NiC_2B_9H_{10}$)-3-(dmpe)-3,1,2-*closo*-$NiC_2B_9H_{10}$ in yields of 14.8% (65 mg, 0.1 mmol) and 20% (88 mg, 0.13 mmol) respectively.

Compound 16	**1-(1′-3′-(dmpe)-3′,1′,2′-*closo*-$NiC_2B_9H_{10}$)-3-(dmpe)-3,1,2-*closo*-$NiC_2B_9H_{10}$ (*racemic*)**	
CHN	Calculated for $C_{16}H_{52}B_{18}Ni_2P_4$:	C 28.2%, H 7.70%
	Found	C 26.7%, H 7.69%
^{1}H NMR	δ 2.45 (s, 1H, CH_{cage}), 2.35 (s, 1H, CH_{cage})	
^{31}P NMR	δ 43.55 (d, 2P), 33.55 (d, 2P)	
^{11}B{^{1}H} NMR	δ -2.64 (3B), -3.93 (3B), -7.39 (2B), -12.02 (1B), -13.38 (1B), -15.76 (4B), -21.14 (4B)	

X-ray quality dark green crystals were grown by vapour diffusion of a DCM solution and 40-60 petroleum ether at room temperature.

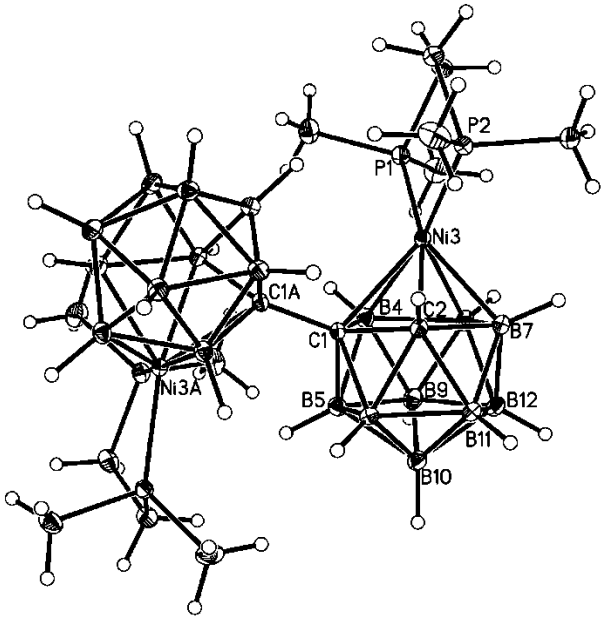

Compound 17	**1-(1′-3′-(dmpe)-3′,1′,2′-*closo*-$NiC_2B_9H_{10}$)-3-(dmpe)-3,1,2-*closo*-$NiC_2B_9H_{10}$ (*meso*)**
CHN	Calculated for $C_{16}H_{52}B_{18}Ni_2P_4$: C 28.2%, H 7.70% Found C 26.0%, H 7.87%
^{1}H NMR	δ 2.40 (s, 1H, C*H*$_{cage}$), 2.35 (s, 1H, C*H*$_{cage}$)
^{31}P NMR	δ 43.89 (d, 2P), 34.10 (d, 2P)
^{11}B{^{1}H} NMR	δ -1.35 (2B), -3.79 (2B), -10.46 (2B), -11.76 (2B), -14.38 (4B), -15.82(4B), -20.51 (2B)

X-ray quality dark green crystals were grown by vapour diffusion of a DCM solution and 40-60 petroleum ether at room temperature.

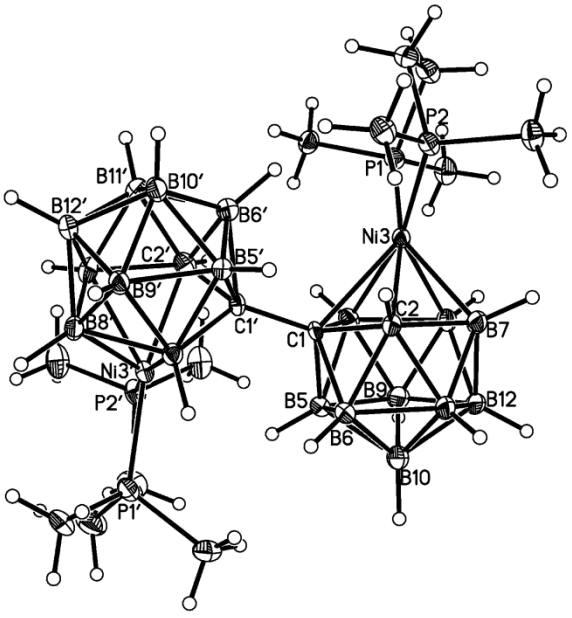

5.16 Preparation of 2,2′-$(CH_3)_2$-1,1′-bis-(*o*-carborane) (18)

1,1′-bis-(*o*-carborane) (0.25 g, 0.87 mmol) was dissolved in diethyl ether (25 ml) in a Schlenk tube and cooled to 0^0C. BuLi (0.80 ml of 2.5M solution, 1.92 mmol) was then added dropwise and the mixture was stirred overnight. CH_3I (0.12 ml, 1.92 mmol) was added to the colourless solution which turned to red and the mixture was then heated to reflux for 4 hrs. Then the reaction mixture was cooled to room temperature and washed with H_2O (75 ml). The diethyl ether layer was separated and dried with anhydrous $MgSO_4$. After filtration the solvent was removed on a rotary evaporator to yield a white solid in 94.5% yield (0.26 g, 0.83 mmol).

Compound 18	**2,2′-$(CH_3)_2$-(1,1′-bis-*o*-carborane)**	
MS (low. Res. EI)	m/z 314.4 (M^+)	
CHN	Calculated for $C_6H_{26}B_{20}$:	C 22.9%, H 8.33%
	Found	C 21.7%, H 8.55%
^{1}H NMR	δ 2.85 (s, 6H, 2C*H*$_3$)	
^{11}B{^{1}H} NMR	δ -0.88 (2B), -5.00 (2B), -8.19 (12B), -9.21 (4B)	

X-ray quality colourless crystals were grown by vapour diffusion of a DCM solution and 40-60 petroleum ether at room temperature.

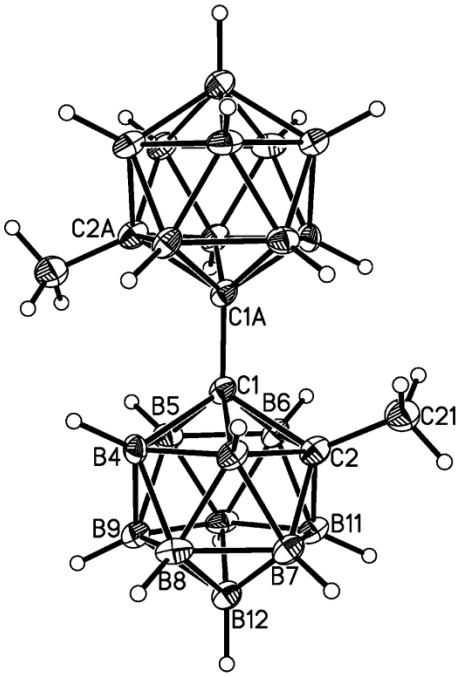

5.17 Preparation of 1-(1′-1′,2′-*closo*-$C_2B_{10}H_{11}$-2′-CH_3)-2-(dmpe)-7-CH_3-2,1,7-*closo*-$NiC_2B_9H_{10}$ (19)

2,2′-$(CH_3)_2$-1,1′-bis(*o*-carborane) (0.30 g, 0.95 mmol) and KOH (2.14 g, 0.04 mol) were dissolved in EtOH (50 ml). The colourless mixture was then heated to reflux for 48 hrs and left to cool to room temperature. CO_2(g) was passed through the reaction mixture for half an hour and the resulting white precipitate was filtered off. EtOH was evaporated from the filtrate under reduced pressure to yield an oil which was then dissolved in THF (30 ml). BuLi (1.5 ml of 2.5M solution, 3.8 mmol) was added dropwise while cooling at 0°C and then the mixture was heated to reflux for 4 hrs. The reaction mixture was then cooled to 0°C and Ni(dmpe)Cl_2 (0.27 g, 0.95 mmol) was added followed by stirring overnight. The resulting suspension was filtered through silica and the THF was removed on the vacuum line. The remaining solid was dissolved in DCM, filtered through Celite® and purified by TLC with a mixed eluent of CH_2Cl_2/40-60 petroleum ether (1:1) to reveal an orange mobile band with R_f 0.45 in 21.7% yield (0.11 g, 0.2 mmol).

Compound 19	**1-(1′-1′,2′-*closo*-$C_2B_{10}H_{10}$-2′-CH_3)-2-(dmpe)-7-CH_3-2,1,7-*closo*-$NiC_2B_9H_9$**
CHN	Calculated for $C_{12}H_{41}B_{19}NiP_2$: C 30.5%, H 7.97% Found C 28.7%, H 8.23%
^{31}P NMR	δ 37.17 (br. s, 1P), 24.10 (br. s, 1P)
^{11}B{^{1}H} NMR	δ -3.30 (1B), -5.35 (1B), -6.60 (2B), -9.08 (10B), -12.03 (1B), -17.55 (2B), -18.37 (2B)

X-ray quality orange crystals were grown by vapour diffusion of a DCM solution and 40-60 petroleum ether at room temperature.

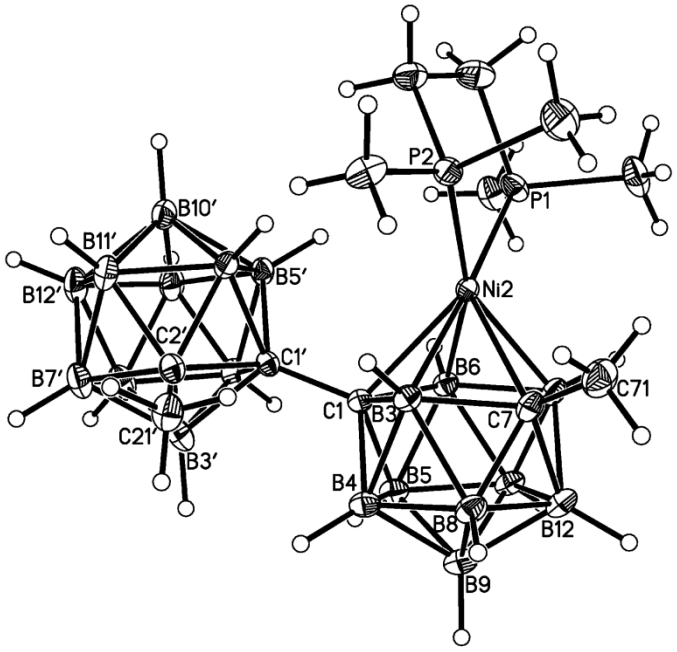

5.18 References

5.1. S. Ren and Z. Xie, *Organometallics.*, 2008, **27**, 5167.

5.2. M. A. Bennett, T.-N. Huang, T. W. Matheson and A. K. Smith, *Inorg. Synth*., 1982, **21**, 74.

5.3. M. A. Bennett and A. K. Smith, *J. Chem. Soc., Dalton Trans*., 1974, 233.

5.4. J. I. Seeman and J. F. Whidby, *J. Org. Chem.*, 1976, **41**, 3824.

5.5. G. Booth and J. Chatt, *J. Chem. Soc*., 1965, 3238.

5.6. Bruker AXS APEX 2, version 1.0-8; Bruker AXS Inc., Madison, WI, USA, 2003.

5.7. G. M. Sheldrick, SHELXTL, version 5.1; Bruker AXS Inc., Madison, WI, USA, 1999.

Appendix 1

Crystal data and structure refinement

Crystal data and structure refinement for compound **1**

Identification code	x82820
Empirical formula	C14 H35 B19 Ru
Formula weight	509.88
Temperature	100(2) K
Wavelength	0.71073 Å
Crystal system	Monoclinic
Space group	P2(1)/n
Unit cell dimensions	a = 11.5653(7) Å α= 90°. b = 14.1222(9) Å β= 91.611(4)°. c = 15.1116(10) Åγ = 90°.
Volume	2467.2(3) $Å^3$
Z	4
Density (calculated)	1.373 Mg/m^3
Absorption coefficient	0.640 mm^{-1}
F(000)	1032
Crystal size	0.42 x 0.38 x 0.10 mm^3
Theta range for data collection	1.97 to 27.47°.
Index ranges	-14<=h<=14, -18<=k<=18, -19<=l<=19
Reflections collected	34686
Independent reflections	5604 [R(int) = 0.0431]
Completeness to theta = 25.00°	99.9 %
Absorption correction	Semi-empirical from equivalents
Max. and min. transmission	0.9387 and 0.7748
Refinement method	Full-matrix least-squares on F^2
Data / restraints / parameters	5604 / 0 / 310
Goodness-of-fit on F^2	1.042
Final R indices [I>2sigma(I)]	R1 = 0.0325, wR2 = 0.0784
R indices (all data)	R1 = 0.0509, wR2 = 0.0871
Largest diff. peak and hole	0.895 and -0.727 $e.Å^{-3}$

Crystal data and structure refinement for compound **2**

Identification code	x82815
Empirical formula	C11 H28 B19 Cl3 Ru
Formula weight	573.14
Temperature	100(2) K
Wavelength	0.71073 Å
Crystal system	Orthorhombic
Space group	Pbca
Unit cell dimensions	a = 9.2654(19) Å α= 90°. b = 22.545(5) Å β= 90°. c = 23.720(5) Å γ = 90°.
Volume	4954.9(17) $Å^3$
Z	8
Density (calculated)	1.537 Mg/m^3
Absorption coefficient	0.960 mm^{-1}
F(000)	2272
Crystal size	0.78 x 0.28 x 0.12 mm^3
Theta range for data collection	2.49 to 30.46°.
Index ranges	-12<=h<=13, -32<=k<=32, -33<=l<=33
Reflections collected	118311
Independent reflections	7478 [R(int) = 0.0705]
Completeness to theta = 25.00°	99.9 %
Absorption correction	Semi-empirical from equivalents
Max. and min. transmission	0.8935 and 0.5215
Refinement method	Full-matrix least-squares on F^2
Data / restraints / parameters	7478 / 0 / 307
Goodness-of-fit on F^2	1.000
Final R indices [I>2sigma(I)]	R1 = 0.0321, wR2 = 0.0684
R indices (all data)	R1 = 0.0552, wR2 = 0.0763
Largest diff. peak and hole	0.642 and -0.631 $e.Å^{-3}$

Crystal data and structure refinement for compound **3**

Identification code	x83845a
Empirical formula	C9 H26 B19 Co
Formula weight	398.62
Temperature	100(2) K
Wavelength	0.71073 Å
Crystal system	Triclinic
Space group	P-1
Unit cell dimensions	a = 6.7920(18) Å α= 89.93(2)°. b = 14.478(5) Å β= 85.594(13)°. c = 20.361(5) Å γ = 89.838(14)°.
Volume	1996.2(10) $Å^3$
Z	4
Density (calculated)	1.326 Mg/m^3
Absorption coefficient	0.853 mm^{-1}
F(000)	808
Crystal size	0.22 x 0.12 x 0.10 mm^3
Theta range for data collection	1.00 to 27.63°.
Index ranges	-8<=h<=7, -18<=k<=17, -26<=l<=23
Reflections collected	27973
Independent reflections	8820 [R(int) = 0.1074]
Completeness to theta = 25.00°	99.5 %
Absorption correction	Semi-empirical from equivalents
Max. and min. transmission	0.9196 and 0.8346
Refinement method	Full-matrix least-squares on F^2
Data / restraints / parameters	8820 / 78 / 523
Goodness-of-fit on F^2	1.132
Final R indices [I>2sigma(I)]	R1 = 0.1641, wR2 = 0.3847
R indices (all data)	R1 = 0.2003, wR2 = 0.4005
Largest diff. peak and hole	4.340 and -2.855 $e.Å^{-3}$

Crystal data and structure refinement for salt **4**

Identification code	x82895m
Empirical formula	C14 H38 B19 N
Formula weight	425.84
Temperature	100(2) K
Wavelength	0.71073 Å
Crystal system	Monoclinic
Space group	P2(1)/c
Unit cell dimensions	a = 18.851(9) Å α= 90°. b = 10.072(4) Å β= 97.068(13)°. c = 13.477(6) Å γ = 90°.
Volume	2540(2) $Å^3$
Z	4
Density (calculated)	1.114 Mg/m^3
Absorption coefficient	0.052 mm^{-1}
F(000)	896
Crystal size	0.28 x 0.08 x 0.04 mm^3
Theta range for data collection	1.09 to 20.84°.
Index ranges	-18<=h<=18, -8<=k<=10, -13<=l<=13
Reflections collected	14879
Independent reflections	2651 [R(int) = 0.2172]
Completeness to theta = 20.84°	99.6 %
Absorption correction	Semi-empirical from equivalents
Max. and min. transmission	0.998 and 0.980
Refinement method	Full-matrix least-squares on F^2
Data / restraints / parameters	2651 / 12 / 320
Goodness-of-fit on F^2	1.000
Final R indices [I>2sigma(I)]	R1 = 0.0862, wR2 = 0.1904
R indices (all data)	R1 = 0.2019, wR2 = 0.2424
Largest diff. peak and hole	0.236 and -0.243 $e.Å^{-3}$

Crystal data and structure refinement for compound **6**

Identification code	x82888
Empirical formula	C9 H26 B19 Co
Formula weight	398.62
Temperature	100(2) K
Wavelength	0.71073 Å
Crystal system	Monoclinic
Space group	P2(1)/c
Unit cell dimensions	a = 7.055(4) Å α= 90°. b = 11.927(5) Å β= 97.854(19)°. c = 24.209(10) Å γ = 90°.
Volume	2017.9(16) $Å^3$
Z	4
Density (calculated)	1.312 Mg/m^3
Absorption coefficient	0.844 mm^{-1}
F(000)	808
Crystal size	0.35 x 0.14 x 0.06 mm^3
Theta range for data collection	1.70 to 24.72°.
Index ranges	-5<=h<=8, -14<=k<=13, -28<=l<=27
Reflections collected	25070
Independent reflections	3428 [R(int) = 0.0902]
Completeness to theta = 24.72°	99.5 %
Absorption correction	Semi-empirical from equivalents
Max. and min. transmission	0.951 and 0.766
Refinement method	Full-matrix least-squares on F^2
Data / restraints / parameters	3428 / 0 / 272
Goodness-of-fit on F^2	1.239
Final R indices [I>2sigma(I)]	R1 = 0.1453, wR2 = 0.3718
R indices (all data)	R1 = 0.1705, wR2 = 0.3825
Largest diff. peak and hole	1.089 and -2.102 $e.Å^{-3}$

Crystal data and structure refinement for salt **7**

Identification code	x82865
Empirical formula	C14 H32 B19 Co
Formula weight	464.72
Temperature	100(2) K
Wavelength	0.71073 Å
Crystal system	Triclinic
Space group	P-1
Unit cell dimensions	a = 13.2154(10) Åα= 97.249(4)°. b = 13.9115(10) Åβ= 90.142(4)°. c = 29.969(2) Å γ = 116.058(3)°.
Volume	4899.6(6) $Å^3$
Z	8
Density (calculated)	1.260 Mg/m^3
Absorption coefficient	0.705 mm^{-1}
F(000)	1904
Crystal size	0.44 x 0.28 x 0.06 mm^3
Theta range for data collection	0.69 to 24.40°.
Index ranges	-15<=h<=15, -15<=k<=14, -34<=l<=34
Reflections collected	88924
Independent reflections	15717 [R(int) = 0.0741]
Completeness to theta = 24.40°	97.4 %
Absorption correction	Semi-empirical from equivalents
Max. and min. transmission	0.9589 and 0.7468
Refinement method	Full-matrix least-squares on F^2
Data / restraints / parameters	15717 / 5 / 1276
Goodness-of-fit on F^2	1.088
Final R indices [I>2sigma(I)]	R1 = 0.0512, wR2 = 0.1200
R indices (all data)	R1 = 0.0842, wR2 = 0.1400
Largest diff. peak and hole	1.170 and -1.071 $e.Å^{-3}$

Crystal data and structure refinement for salt **8**

Identification code	229a
Empirical formula	C24 H54 B18 N2
Formula weight	565.27
Temperature	100(2) K
Wavelength	0.71073 Å
Crystal system	Triclinic
Space group	P-1
Unit cell dimensions	a = 8.8436(12) Å α= 116.225(6)°. b = 10.5897(11) Åβ= 101.483(7)°. c = 11.103(2) Å γ = 104.113(5)°.
Volume	846.5(2) $Å^3$
Z	1
Density (calculated)	1.109 Mg/m^3
Absorption coefficient	0.055 mm^{-1}
F(000)	302
Crystal size	0.42 x 0.28 x 0.04 mm^3
Theta range for data collection	2.19 to 28.33°.
Index ranges	-11<=h<=11, -14<=k<=13, -14<=l<=14
Reflections collected	11069
Independent reflections	4082 [R(int) = 0.0332]
Completeness to theta = 25.00°	98.4 %
Absorption correction	Semi-empirical from equivalents
Max. and min. transmission	0.9978 and 0.9772
Refinement method	Full-matrix least-squares on F^2
Data / restraints / parameters	4082 / 9 / 227
Goodness-of-fit on F^2	1.030
Final R indices [I>2sigma(I)]	R1 = 0.0541, wR2 = 0.1422
R indices (all data)	R1 = 0.0822, wR2 = 0.1595
Largest diff. peak and hole	0.297 and -0.381 $e.Å^{-3}$

Crystal data and structure refinement for compound **11**

Identification code	3077oc
Empirical formula	C14 H30 B18 Co2
Formula weight	510.82
Temperature	100(2) K
Wavelength	0.71073 Å
Crystal system	Orthorhombic
Space group	Cmca
Unit cell dimensions	a = 11.6947(5) Å α= 90°. b = 13.8249(6) Å β= 90°. c = 14.5031(6) Å γ = 90°.
Volume	2344.83(17) $Å^3$
Z	4
Density (calculated)	1.447 Mg/m^3
Absorption coefficient	1.419 mm^{-1}
F(000)	1032
Crystal size	0.22 x 0.18 x 0.12 mm^3
Theta range for data collection	2.68 to 27.14°.
Index ranges	-14<=h<=14, -17<=k<=17, -18<=l<=18
Reflections collected	19428
Independent reflections	1365 [R(int) = 0.0458]
Completeness to theta = 25.00°	100.0 %
Absorption correction	Semi-empirical from equivalents
Max. and min. transmission	0.8482 and 0.7454
Refinement method	Full-matrix least-squares on F^2
Data / restraints / parameters	1365 / 0 / 85
Goodness-of-fit on F^2	1.019
Final R indices [I>2sigma(I)]	R1 = 0.0241, wR2 = 0.0579
R indices (all data)	R1 = 0.0298, wR2 = 0.0606
Largest diff. peak and hole	0.341 and -0.276 $e.Å^{-3}$

Crystal data and structure refinement for compound **12**

Identification code	x83132
Empirical formula	C14 H30 B18 Co2
Formula weight	510.82
Temperature	100(2) K
Wavelength	0.71073 Å
Crystal system	Monoclinic
Space group	P2(1)/c
Unit cell dimensions	a = 11.6962(13) Å α= 90°. b = 15.9743(17) Å β= 109.935(4)°. c = 12.9143(13) Å γ = 90°.
Volume	2268.3(4) $Å^3$
Z	4
Density (calculated)	1.496 Mg/m^3
Absorption coefficient	1.467 mm^{-1}
F(000)	1032
Crystal size	0.78 x 0.12 x 0.04 mm^3
Theta range for data collection	2.25 to 25.99°.
Index ranges	-14<=h<=13, -19<=k<=19, -12<=l<=15
Reflections collected	19160
Independent reflections	4434 [R(int) = 0.0757]
Completeness to theta = 25.00°	99.8 %
Absorption correction	Semi-empirical from equivalents
Max. and min. transmission	0.9437 and 0.3941
Refinement method	Full-matrix least-squares on F^2
Data / restraints / parameters	4434 / 22 / 307
Goodness-of-fit on F^2	1.032
Final R indices [I>2sigma(I)]	R1 = 0.0467, wR2 = 0.1156
R indices (all data)	R1 = 0.0672, wR2 = 0.1273
Largest diff. peak and hole	1.031 and -1.028 $e.Å^{-3}$

Crystal data and structure refinement for compound **13**

Identification code	x83114
Empirical formula	C14 H30 B18 Co2
Formula weight	510.82
Temperature	100(2) K
Wavelength	0.71073 Å
Crystal system	Monoclinic
Space group	P21/c
Unit cell dimensions	a = 7.5233(8) Å α= 90°. b = 14.3413(15) β= 96.904(5)°. c = 21.528(2) Å γ = 90°.
Volume	2306.0(4) $Å^3$
Z	4
Density (calculated)	1.471 Mg/m^3
Absorption coefficient	1.443 mm^{-1}
F(000)	1032
Crystal size	0.62 x 0.14 x 0.06 mm^3
Theta range for data collection	1.71 to 28.30°.
Index ranges	-9<=h<=9, -19<=k<=0, -8<=l<=28
Reflections collected	23483
Independent reflections	5267 [R(int) = 0.0517]
Completeness to theta = 25.00°	95.6 %
Absorption correction	Semi-empirical from equivalents
Max. and min. transmission	0.9184 and 0.4682
Refinement method	Full-matrix least-squares on F^2
Data / restraints / parameters	5267 / 0 / 308
Goodness-of-fit on F^2	1.510
Final R indices [I>2sigma(I)]	R1 = 0.0436, wR2 = 0.1063
R indices (all data)	R1 = 0.0555, wR2 = 0.1091
Largest diff. peak and hole	0.672 and -0.538 $e.Å^{-3}$

Crystal data and structure refinement for compound **14**

Identification code	3146m
Empirical formula	C24 H48 B18 Ru2
Formula weight	733.34
Temperature	100(2) K
Wavelength	0.71073 Å
Crystal system	Monoclinic
Space group	P2(1)/c
Unit cell dimensions	a = 19.190(2) Å α= 90°. b = 10.7869(11) Å β= 116.289(4)°. c = 17.9357(17) Å γ = 90°.
Volume	3328.8(6) $Å^3$
Z	4
Density (calculated)	1.463 Mg/m^3
Absorption coefficient	0.926 mm^{-1}
F(000)	1480
Crystal size	0.46 x 0.08 x 0.04 mm^3
Theta range for data collection	2.23 to 26.15°.
Index ranges	-18<=h<=23, -13<=k<=13, -22<=l<=17
Reflections collected	42726
Independent reflections	6592 [R(int) = 0.1180]
Completeness to theta = 25.00°	100.0 %
Absorption correction	Semi-empirical from equivalents
Max. and min. transmission	0.9639 and 0.6754
Refinement method	Full-matrix least-squares on F^2
Data / restraints / parameters	6592 / 27 / 422
Goodness-of-fit on F^2	1.025
Final R indices [I>2sigma(I)]	R1 = 0.0632, wR2 = 0.1488
R indices (all data)	R1 = 0.1184, wR2 = 0.1768
Largest diff. peak and hole	1.505 and -1.881 $e.Å^{-3}$

Crystal data and structure refinement for compound **15**

Identification code	gos0169t
Empirical formula	C24 H48 B18 Ru2
Formula weight	733.34
Temperature	120(2) K
Wavelength	0.71073 Å
Crystal system	Monoclinic
Space group	P2(1)/n
Unit cell dimensions	a = 9.3011(6) Å α= 90°. b = 41.899(3) Å β= 113.751(2)°. c = 9.3950(6) Å γ = 90°.
Volume	3351.2(4) $Å^3$
Z	4
Density (calculated)	1.454 Mg/m^3
Absorption coefficient	0.920 mm^{-1}
F(000)	1480
Crystal size	0.08 x 0.06 x 0.03 mm^3
Theta range for data collection	3.06 to 25.68°.
Index ranges	-11<=h<=10, 0<=k<=51, 0<=l<=11
Reflections collected	6370
Independent reflections	6370 [R(int) = 0.0000]
Completeness to theta = 25.00°	99.7 %
Absorption correction	Analytical
Max. and min. transmission	0.9729 and 0.9301
Refinement method	Full-matrix least-squares on F^2
Data / restraints / parameters	6370 / 105 / 415
Goodness-of-fit on F^2	1.346
Final R indices [I>2sigma(I)]	R1 = 0.0663, wR2 = 0.1234
R indices (all data)	R1 = 0.0776, wR2 = 0.1309
Largest diff. peak and hole	1.195 and -1.177 $e.Å^{-3}$

Crystal data and structure refinement for compound **16**

Identification code	3636n
Empirical formula	C16 H52 B18 Ni2 P4
Formula weight	680.46
Temperature	100(2) K
Wavelength	0.71073 Å
Crystal system	Monoclinic
Space group	P2/n
Unit cell dimensions	a = 13.6195(9) Å α= 90°. b = 8.7239(5) Å β= 100.316(3)°. c = 14.3241(9) Å γ = 90°.
Volume	1674.41(18) $Å^3$
Z	2
Density (calculated)	1.350 Mg/m^3
Absorption coefficient	1.328 mm^{-1}
F(000)	708
Crystal size	0.38 x 0.36 x 0.20 mm^3
Theta range for data collection	2.79 to 26.37°.
Index ranges	-17<=h<=16, 0<=k<=10, 0<=l<=17
Reflections collected	3411
Independent reflections	3482 [R(int) = 0.0000]
Completeness to theta = 25.00°	99.7 %
Absorption correction	Semi-empirical from equivalents
Max. and min. transmission	0.7771 and 0.6324
Refinement method	Full-matrix least-squares on F^2
Data / restraints / parameters	3482 / 0 / 186
Goodness-of-fit on F^2	0.960
Final R indices [I>2sigma(I)]	R1 = 0.0237, wR2 = 0.0558
R indices (all data)	R1 = 0.0272, wR2 = 0.0574
Largest diff. peak and hole	0.307 and -0.305 e.$Å^{-3}$

Crystal data and structure refinement for compound **17**

Identification code	x83603
Empirical formula	C9.50 H29 B9 Cl3 Ni P2
Formula weight	467.62
Temperature	100(2) K
Wavelength	0.71073 Å
Crystal system	Triclinic
Space group	P-1
Unit cell dimensions	a = 11.4867(6) Å α= 96.986(3)°. b = 12.5327(6) Å β= 90.037(3)°. c = 15.0938(8) Å γ = 91.277(2)°.
Volume	2156.21(19) $Å^3$
Z	4
Density (calculated)	1.440 Mg/m^3
Absorption coefficient	1.412 mm^{-1}
F(000)	960
Crystal size	0.62 x 0.20 x 0.06 mm^3
Theta range for data collection	2.23 to 26.10°.
Index ranges	-14<=h<=14, -15<=k<=15, -18<=l<=18
Reflections collected	29045
Independent reflections	8280 [R(int) = 0.0517]
Completeness to theta = 25.00°	98.4 %
Absorption correction	Semi-empirical from equivalents
Max. and min. transmission	0.9201 and 0.4748
Refinement method	Full-matrix least-squares on F^2
Data / restraints / parameters	8280 / 0 / 450
Goodness-of-fit on F^2	1.031
Final R indices [I>2sigma(I)]	R1 = 0.0442, wR2 = 0.0971
R indices (all data)	R1 = 0.0767, wR2 = 0.1084
Largest diff. peak and hole	1.190 and -0.785 e.$Å^{-3}$

Crystal data and structure refinement for compound **18**

Identification code	x83154
Empirical formula	C6 H26 B20
Formula weight	314.47
Temperature	100(2) K
Wavelength	0.71073 Å
Crystal system	Monoclinic
Space group	P2(1)/n
Unit cell dimensions	a = 7.577(3) Å α= 90°. b = 9.391(3) Å β= 96.256(15)°. c = 12.939(4) Å γ = 90°.
Volume	915.2(5) $Å^3$
Z	2
Density (calculated)	1.141 Mg/m^3
Absorption coefficient	0.048 mm^{-1}
F(000)	324
Crystal size	0.36 x 0.18 x 0.06 mm^3
Theta range for data collection	2.69 to 25.04°.
Index ranges	-8<=h<=8, 0<=k<=11, 0<=l<=15
Reflections collected	8954
Independent reflections	1432 [R(int) = 0.0871]
Completeness to theta = 25.00°	87.9 %
Absorption correction	Semi-empirical from equivalents
Max. and min. transmission	0.9972 and 0.9831
Refinement method	Full-matrix least-squares on F^2
Data / restraints / parameters	1432 / 0 / 120
Goodness-of-fit on F^2	1.040
Final R indices [I>2sigma(I)]	R1 = 0.0845, wR2 = 0.2120
R indices (all data)	R1 = 0.1461, wR2 = 0.2555
Largest diff. peak and hole	0.349 and -0.290 e.$Å^{-3}$

Crystal data and structure refinement for compound **19**

Identification code	x83781
Empirical formula	C12 H41 B19 Ni P2
Formula weight	511.47
Temperature	100(2) K
Wavelength	0.71073 Å
Crystal system	Monoclinic
Space group	P21/n
Unit cell dimensions	a = 10.6579(5) Å α= 90°. b = 16.2781(7) Å β= 93.819(2)°. c = 15.8191(7) Å γ = 90°.
Volume	2738.4(2) $Å^3$
Z	4
Density (calculated)	1.238 Mg/m^3
Absorption coefficient	0.829 mm^{-1}
F(000)	1060
Crystal size	0.56 x 0.28 x 0.20 mm^3
Theta range for data collection	2.50 to 30.95°.
Index ranges	-15<=h<=15, -23<=k<=22, -20<=l<=22
Reflections collected	56288
Independent reflections	8586 [R(int) = 0.0420]
Completeness to theta = 25.00°	99.9 %
Absorption correction	Semi-empirical from equivalents
Max. and min. transmission	0.8517 and 0.6538
Refinement method	Full-matrix least-squares on F^2
Data / restraints / parameters	8586 / 0 / 324
Goodness-of-fit on F^2	0.974
Final R indices [I>2sigma(I)]	R1 = 0.0400, wR2 = 0.0936
R indices (all data)	R1 = 0.0577, wR2 = 0.1009
Largest diff. peak and hole	0.884 and -0.591 e.$Å^{-3}$